

University of Strathclyde

Strathclyde Institute of Pharmacy and Biomedical
Sciences,
University of Strathclyde,
Glasgow, G4 0RE

**Analysis of LmxMPK2 and
LmxGSK3- β , two protein kinases
important for the survival of
Leishmania mexicana.**

A thesis submitted in fulfilment of the
requirements for the degree of Doctor of
Philosophy

Laura Anne Munro

Glasgow, Scotland, September 2013

This thesis is the result of the author's original research. It has been composed by the author and has not been previously submitted for examination that has led to the award of a degree.

The copyright of this thesis belongs to the author under the terms of the United Kingdom Copyright Acts as qualified by University of Strathclyde Regulation 3.50. Due acknowledgement must always be made of the use of any material contained in, or derived from, this thesis.

Signed:

Date:

In all science, error precedes the truth, and it is better it should go first than last.

-Hugh Walpole, 1884-1941

Abstract

Leishmaniasis is a tropical disease affecting around 12 million people worldwide with a further 350 million people at risk. Two million new cases are identified every year with an estimated 60,000 fatalities. Treatments have changed little in the past century and often patients are treated with increasingly ineffective and highly toxic drugs, thus highlighting the requirement for safer and more effective medication. Protein kinases have attracted a lot of attention as potential targets for treating a variety of human diseases, including leishmaniasis.

LmxMPK2 is a mitogen-activated protein (MAP) kinase homologue in *Leishmania mexicana* that is expressed in both the amastigote and promastigote life stages. Generation of homozygous gene knock out mutants revealed a reduction in cell proliferation and a range of morphological alterations with cells showing multiple flagella, kinetoplasts and nuclei, lobed cell bodies, spiked posterior ends and division furrow ingression from the posterior end. Localisation studies using GFP-tagged LmxMPK2 revealed localisation at both poles of the cell. LmxMPK2 might play a role in the organisation of microtubules influencing cell shape and cytokinesis. Recombinant expression of LmxMPK2 resulted in an active enzyme already phosphorylated on tyrosine and threonine which is able to phosphorylate myelin basic protein (MBP) despite the absence of activation by a MAP kinase kinase. Co-expression with different phosphatases led to LmxMPK2 being dephosphorylated on tyrosine but not threonine residues, yet retaining the ability of tyrosine autophosphorylation maintaining equal levels of MBP phosphorylation. This suggests that LmxMPK2 is an unusual MAP kinase which is able to autophosphorylate on threonine and tyrosine residues of unknown localisation without affecting the activity of the enzyme.

Investigations to determine whether a relationship existed between LmxMPK2 and LmxDIP13 (Deflagellation Inducible Protein), a protein shown to associate with microtubules and likely to be involved in cell division, were undertaken. N-terminally GFP-tagged LmxDIP13 was expressed in promastigotes of wild type and

LmxMPK2 null mutant *Leishmania*. Localisation was punctate and found in singular or multiple spots following a discrete line throughout the cell. An increased percentage of null mutant promastigotes with an anterior localisation of GFP*LmxDIP13* suggested a functional link between *LmxDIP13* and *LmxMPK2*.

Glycogen Synthase Kinase 3 (*LmxGSK3-β*) was investigated as a potential drug target. The phosphatase co-expression system was applied to recombinant *LmxGSK3-β*. However, it was not possible to fully dephosphorylate *LmxGSK3-β* on either threonine or tyrosine. Activity of *LmxGSK3-β* was discovered to be similar to that of human *GSK3-β*. Natural compounds Malabaricone B and C were isolated from *Myristica* plants and used for screening against *LmxGSK3-β*. Both compounds were identified as inhibitors of *LmxGSK3-β* and possess potent anti-leishmanial activity.

Abbreviations

-/-	double-allele deletion
+/-	single-allele deletion
× g	times gravity
°C	degree Celsius
1NA	1-naphthyl-pyrazolo[3,4 <i>d</i>]pyrimidine
A	ampère
aa	amino acids
ADP	adenosine diphosphate
Amp	ampicillin
AP	alkaline phosphatase
APS	ammonium persulfate
ATP	adenosine triphosphate
<i>BLE</i>	phleomycin resistance marker gene
bp	base pairs
BSA	bovine serum albumin
<i>C. elegans</i>	<i>Caenorhabditis elegans</i>
<i>C. reinhardtii</i>	<i>Chlamydomonas reinhardtii</i>
cDNA	complementary DNA
CL	cutaneous leishmaniasis
DAPI	4',6-diamidino-2-phenylindole dilactate
DB	database
DCL	diffuse cutaneous leishmaniasis

ddH ₂ O	double distilled water
DMSO	dimethyl sulfoxide
DNA	deoxyribonucleic acid
dNTP	deoxyribonucleotide triphosphate
DTT	1,4-dithiothreitol
<i>E. coli</i>	<i>Escherichia coli</i>
EDTA	ethylenediamine tetraacetic acid
ER	endoplasmic reticulum
ERK	extracellular signal-related kinase
EtBr	ethidium bromide
FCS	fetal calf serum
g	gramme
gDNA	genomic DNA
GFP	green fluorescent protein
GSK	glycogensynthase kinase
GST	glutathione-S-transferase
h	hours
HCl	hydrochloric acid
HEPES	N-2-hydroxyethylpiperazine-N'-2-ethanesulfonic acid
His	histidine
HRP	horse radish peroxidase
<i>HYG</i>	hygromycin B resistance marker gene
iFCS	heat-inactivated fetal calf serum
IgG	immunoglobulin G

iNOS	inducible nitric oxide synthase
InsP	Inositol phosphate
InsP3	inositol 1,4,5-triphosphate
IPS	<i>myo</i> -inositol-1-phosphate synthase
IPTG	isopropyl- β -D-thiogalactopyranoside
JNK	c-Jun N-terminal kinase
kb	kilo base pairs
kDa	kilo Dalton
kDNA	kinetoplast DNA
l	litres
<i>L.</i>	<i>Leishmania</i>
LB	Luria-Bertani (broth)
LPG	lipophosphoglycan
M	molar
MAP	mitogen-activated protein
MAP2K	MAP kinase kinase
MAP3K	MAP kinase kinase kinase
MAPK	MAP kinase
MAPKAPK	MAPK-activated protein kinase
MBP	myelin basic protein
MCL	mucocutaneous leishmaniasis
MOPS	morpholinopropane sulfonic acid
mRNA	messenger RNA
MS	mass spectrometry

MS/MS	tandem MS
NaCl	sodium chloride
NaOH	sodium hydroxide
<i>NEO</i>	neomycin resistance marker gene
OD	optical density
ORF	open reading frame
<i>PAC</i>	puromycin resistance marker gene
PBS	phosphate-buffered saline
PCR	polymerase chain reaction
PhD	<i>Philosophiae Doctor</i>
<i>PHLEO</i>	phleomycin resistance marker gene
PKA	protein kinase A
PKDL	post kala-azar dermal leishmaniasis
PM	peritrophic membrane
PMSF	phenylmethyl sulfonyl fluoride
PSG	promastigote secretory gel
PtdIns	phosphatidylinositol
PtdInsP	phosphatidylinositol phosphate
PV	parasitophorous vacuoles
PVDF	polyvinylidene difluoride
RNA	ribonucleic acid
RNAi	RNA interference
rpm	revolutions per minute
rRNA	ribosomal RNA

RT	room temperature
RT	reverse transcriptase
RTK	receptor tyrosine kinases
s	seconds
SAP	shrimp alkaline phosphatase
SDS	sodium dodecyl sulphate
SDS-PA	SDS-polyacrylamide
SDS-PAGE	SDS-PA gel electrophoresis
SH	Src homology
<i>T.</i>	<i>Trypanosoma</i>
TBS	Tris-buffered saline
TEM	transmission electron microscopy
TEMED	N,N,N',N'-tetramethylethylenediamine
TLCK	N α -tosyl-L-lysine chloromethyl ketone hydrochloride
Tris	tris(hydroxymethyl)aminomethane
U	units
UV	ultraviolet
V	volt
v/v	volume per volume
VL	visceral leishmaniasis
w/v	weight per volume
WHO	World Health Organisation
X-Gal	5-Bromo-4-chloro-3-indolyl- β -D-galactopyranoside

Table of Contents

1.	Introduction	1
1.1	<i>Leishmania</i> and leishmaniasis	1
1.1.1	Taxonomy.....	1
1.1.2	Epidemiology and clinical manifestations.....	2
1.1.3	Treatment and prevention of leishmaniasis.....	8
1.1.4	Life cycle of <i>Leishmania</i>	10
1.2	Signal transduction in Eukaryotes.....	16
1.2.1	Signalling pathways in higher eukaryotes	16
1.2.2	Protein kinases	18
1.2.3	MAP kinases	21
1.3	Signal transduction in Trypanosomatids	25
1.3.1	Trypanosomatid MAP kinases	29
1.4	State of knowledge and research objectives.....	35
1.4.1	LmxMPK2 and LmxDIP13	35
1.4.2	LmxGSK3- β	40
2.	Materials and Methods.....	43
2.1	Materials.....	43
2.1.1	Laboratory Equipment	43
2.1.2	Glassware and consumables.....	45
2.1.3	Chemicals.....	46
2.1.4	Media and Buffers	49
2.1.5	Bacterial Strains	53
2.1.6	<i>Leishmania</i> strain	53
2.1.7	Oligonucleotides.....	54
2.1.8	DNA vectors and plasmid constructs	54
2.1.9	Antibodies.....	55
2.1.10	Enzymes.....	56
2.1.11	Molecular biology kits	56
2.1.12	DNA and protein molecular weight markers	56
2.2	Methods	57
2.2.1	Cell biology methods	57
2.2.2	Culturing of <i>E. coli</i>	57
2.2.3	Culturing of <i>Leishmania</i>	57
2.2.4	Mouse footpad infection studies	59
2.2.5	Molecular biology methods	60
2.2.6	Protein Biochemistry.....	64
2.2.7	Preparation of <i>E. coli</i> cell lysates for protein purification	65
2.2.8	Affinity purification of recombinant proteins.....	65
2.2.9	Determination of protein concentrations using Bradford assay	66
2.2.10	Preparation of <i>Leishmania</i> lysates for immunoblot.....	66
2.2.11	Discontinuous SDS polyacrylamide gel electrophoresis (SDS-PAGE) 67	
2.2.12	Coomassie staining of SDS-PA gels.....	67
2.2.13	Silver staining of SDS-PA gels.....	67
2.2.14	Drying of SDS-PA gels	68
2.2.15	Immunoblot analysis	68
2.2.16	Stripping- off antibodies from an immunoblot.....	69
2.2.17	<i>In vitro</i> kinase assays	69
2.2.18	Microscopy techniques	69
2.2.19	Inhibitor screening	70
2.2.20	Statistical Analysis.....	71

Chapter 3.....	72
Phenotypic characterisation of the <i>LmxMPK2</i> and its relationship with <i>LmxDIP13</i>	72
3.1 Introduction	72
3.2 Results	74
3.2.1 Phenotypic analysis of <i>LmxMPK2</i> null mutant parasites	74
3.2.2 Proliferation analysis of <i>LmxMPK2</i> mutants.....	78
3.2.3 Measurement of flagellar length of <i>LmxMPK2</i> mutants.....	80
3.2.4 Analysis of the <i>in vivo</i> localisation of <i>LmxMPK2</i> using GFP-tagged mutants.....	83
3.2.5 <i>LmxMPK2</i> and <i>LmxDIP13</i>	91
3.3 Discussion.....	100
3.3.1 The Phenotype of <i>LmxMPK2</i> null mutants and <i>LmxMPK2</i> add back mutants.....	100
3.3.2 Morphology and proliferation	100
3.3.3 <i>In vivo</i> analysis of GFP-tagged <i>LmxMPK2</i>	103
3.4 Summary of Phenotypic analysis of <i>LmxMPK2</i> null mutants and <i>LmxDIP13</i>	107
Chapter 4.....	109
Characterisation of recombinant <i>LmxMPK2</i>	109
4.1 Introduction	109
4.2 Results	110
4.2.1 Generation of <i>LmxMPK2</i> expression plasmids	110
4.2.2 Recombinant co-expression and affinity purification of <i>LmxMPK2</i>	110
4.2.3 Evaluation of <i>LmxMPK2</i> bands on SDS-PA gels	112
4.2.4 Optimisation of kinase assay conditions	114
4.2.5 Assessment of <i>LmxMPK2</i> activity	126
4.3 Discussion.....	139
4.3.2 <i>LmxDIP13</i> subcellular localisation	148
4.3.3 Summary.....	150
Chapter 5.....	151
Characterisation of recombinant <i>LmxGSK3-β</i>	151
5.1 Introduction	151
5.2 Results	153
5.2.1 Generation of various <i>LmxGSK3-β</i> expression plasmids	153
5.2.2 Assessment of <i>LmxGSK3-β</i> activity.....	153
5.2.3 Screening of novel compounds.....	162
5.3 Discussion.....	177
5.3.1 <i>LmxGSK3-β</i> by co-expression with phosphatases and analysis of kinase activity.....	177
5.3.2 Effects of novel compounds on <i>LmxGSK3-β</i> and <i>Leishmania</i> parasites	179
5.3.3 Summary.....	183
Chapter 6.....	184
6.1 General Discussion	184
7. References.....	188
8. Appendix.....	200
8.1 <i>LmxMPK2</i>	200
8.1.1 Genetic sequence of <i>LmxMPK2</i> (Genbank: CAC07956).....	200
8.1.2 Amino acid sequence <i>LmxMPK2</i>	200
8.2 <i>LmxDIP13</i>	201
8.2.1 Genetic sequence of <i>LmxDIP13</i> (Acc No: LmxM.33.4540)	201
8.2.2 Amino acid sequence of <i>LmxDIP13</i>	201

8.3	LmxGSK3- β	201
8.3.1	Genetic sequence of <i>LmxGSK3-β</i> (Acc No: LmxM.18.0270)	201
8.3.2	Amino acid sequence of LmxGSK3- β	202
8.4	Phosphatases.....	202
8.4.1	Genetic sequence of PTP1B (Acc no. M33689).....	202
8.4.2	Amino acid sequence of PTP1B	203
8.4.3	Genetic sequence of λ -phosphatase (Acc No: J02459, ORF: 43224-43889 bp).....	203
8.4.4	Amino acid sequence of λ -phosphatase	203
8.5	Plasmid maps.....	204
	Acknowledgments.....	207

1. Introduction

1.1 *Leishmania* and leishmaniasis

In 1898, a Soviet surgeon identified the causative agent for oriental sore (now known as cutaneous leishmaniasis) by examining sections of tissue from an early stage sore under a microscope. He described oval bodies with a nucleus usually found within host cells and attributed these to protozoa. His findings were published in a Russian medical-military journal but due to the publication being in Russian, it was not until much later his work was recognised (Hoarse, C. A., 1938). Five years later, William Leishman, a Doctor from Glasgow serving in the British army in India developed one of the earliest stains for identifying malaria and other parasites. While examining samples from a patient suffering from “Dum-Dum fever” (Kala Azar), he identified oval bodies in the liver and spleen and published his findings in the British Medical Journal (Leishman, W. B., 1903). In the same year an Irish physician, Charles Donovan, made the same findings from a smear taken from a patient in Madras. His account was also published in the British Medical Journal (Donovan, C., 1903). It was recognised that the two findings described the same parasite and were later named *Leishmania donovani*. Since 1903, many more species of the genus *Leishmania* have been identified and are responsible for a wide range of diseases collectively known as leishmaniasis.

1.1.1 Taxonomy

Leishmania belong to the Kinetoplastida class of organisms. The class is recognised by the presence of a single mitochondrion, a cellular structure that contains minicircles and maxicircles of densely coiled DNA which form the kinetoplast, which is closely associated to the flagella pocket. There are two orders within the Kinetoplastida; Trypanosomatidae which possess a single flagellum and are obligatory parasites and Bodonidae which possess two flagella and can be either free-living or parasitic. Trypanosomatidae is divided into ten genera (one extinct). While most infect plants, insects or reptiles as their main hosts, *Trypanosoma*, *Leishmania* and *Endotrypanum* infect mammals. Due to the impact on human, animal and plant health *Leishmania*,

Trypanosoma and *Crithidia* are of most interest for research. *Leishmania* can be further divided into two sub-genera; *L. Leishmania* and *L. Viannia*. Classification of the sub-genera is due to the additional developmental phase in the hindgut of the sand fly by *L. Viannia* as *L. Leishmania* exclusively develops in the midgut and foregut of the sand fly (Lainson *et al.*, 1987). More recently, *L. Leishmania* has been shown to have lost genes and activity associated with RNA interference pathways while *L. Viannia* has retained the components necessary for activity (Lye *et al.*, 2010). *L. mexicana* is a member of the *L. Leishmania* sub-genus and the species of interest for the purpose of these investigations, and therefore incapable of being studied using RNAi techniques.

1.1.2 Epidemiology and clinical manifestations

There are approximately 30 species of *Leishmania* parasites, of which around 20 are suggested to be human pathogens. The obligate parasites are transmitted to the host through the bite of female sand flies of the *Phlebotomus* genus in the Old World (Africa, Asia and Europe) and *Lutzomyia* genus in the New World (America) (Pavli *et al.*, 2010). The distribution of leishmaniasis is therefore closely related to the natural habitat of the sand fly vector and is endemic in over 88 countries, of which at least 72 are developing nations (Kelly and Baudry, 2012; Desjeux, 2004). Until recently, the only continents not affected by leishmaniasis were Antarctica and Australia. However, *Leishmania* have recently been found to infect red Kangaroos (*Macropus rufus*) (among other native animals) in Australia (Dougall *et al.*, 2011; Rose *et al.*, 2004). It is estimated that 12 million people are currently infected with a further 350 million people at risk. Every year 2 million new cases are identified (approximately 1.5 million cutaneous leishmaniasis and 0.5 million visceral), with fatalities estimated around 60,000 per year (Neuber, 2008). The incidence may be higher as many people in endemic regions often have sub-clinical infections (Murray *et al.*, 2005), and leishmaniasis is a reportable disease in only 33 of the 88 endemic countries (Desjeux, 2004). There are three main forms of leishmaniasis: cutaneous leishmaniasis, mucocutaneous and visceral. Morbidity and mortality are largely dependent upon the species responsible.

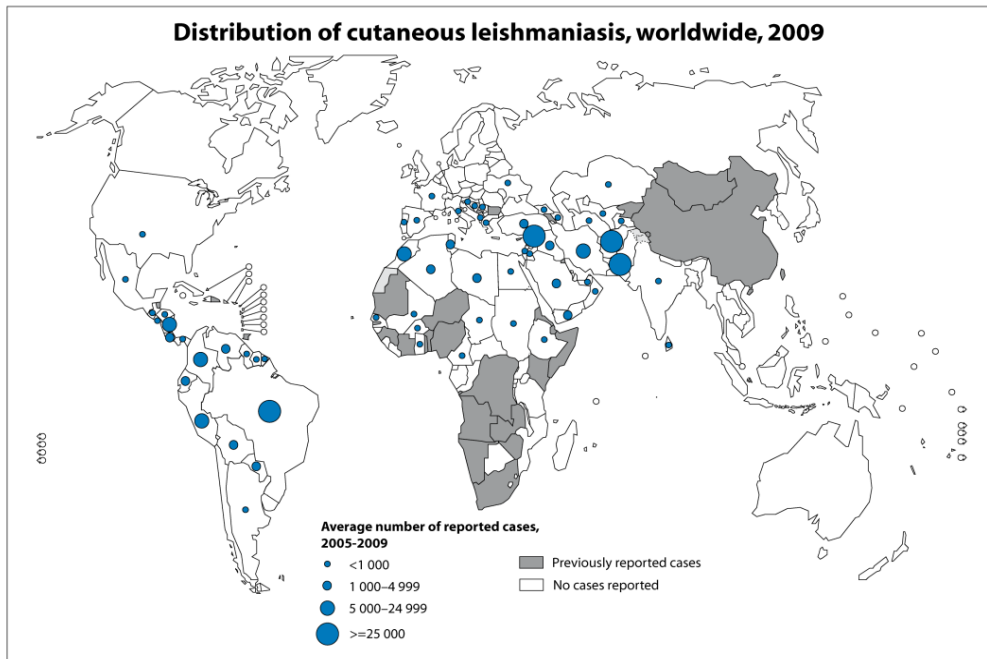
Cutaneous Leishmaniasis (CL)

Cutaneous leishmaniasis accounts for around 75% of new leishmaniasis infections, with 90% of these occurring in Afghanistan, Algeria, Brazil, Iran, Peru, Saudi Arabia and Syria. It is the mildest form of leishmaniasis. *L. aethiopica*, *L. major*, *L. infantum* and *L. tropica* are the causative agents of CL in the Old World. In the new world, cutaneous leishmaniasis is caused by *L. mexicana*, *L. venezuelensis* and *L. amazonensis* (Berzunza-Cruz *et al.*, 2008). Initially, CL is indistinguishable from a common reaction to an insect bite, presenting as an area of redness and swelling at the site of the sand fly bite, typically on exposed skin such as arms, legs and face (Neuber, 2008). After an incubation period of one week to three months (depending on species, immunocompetency of an individual etc.) the bite develops into a painless ulcer. A seropurulent discharge develops and later dries forming a crust – removal of which reveals the most common characteristic of cutaneous leishmaniasis, a shallow crater (Salman *et al.*, 1999). CL will often spontaneously resolve in an immunocompetent host, often leaving a scar and significant disfiguration. A more severe form of CL is diffuse cutaneous leishmaniasis (DCL) largely caused by *L. mexicana* and *L. amazonensis*. This is more severe as the lesions disseminate, causing papules to form in other areas of the skin which do not self-heal and respond poorly to treatment (Desjeux, 2004). Countries affected by cutaneous leishmaniasis are shown in figure 1.1A.

A dramatic increase in the number of leishmaniasis cases in recent years has been observed. There are many contributing factors such as migration and industrialisation, large-scale movement of people who lack pre-existing immunity to endemic *Leishmania* species is ideal for disease transmission (Desjeux, 2004). However, there is also a huge increase in global travel and thus an increase in the number of imported leishmaniasis cases reported in non endemic countries. Cutaneous leishmaniasis is responsible for more than 80% of cases, and is ranked one of the top ten most common diseases reported by tourists returning from tropical regions (Kelly & Baudry, 2012).

Mucocutaneous Leishmaniasis (ML)

Mucocutaneous leishmaniasis (also known as Espundia) is a severe form of cutaneous leishmaniasis caused by *L. braziliensis* and *L. guyanensis*. The parasites migrate from the original cutaneous lesion to the mucous membranes notably the nose, mouth and throat (and less commonly the trachea and genital mucosal membranes) via lymphatic and blood vessels (Neuber, 2005; Desjeux, 2004). The infection causes massive tissue destruction leaving the patient with major disfiguration and vulnerability to potentially life-threatening secondary infections (Neuber, 2005).

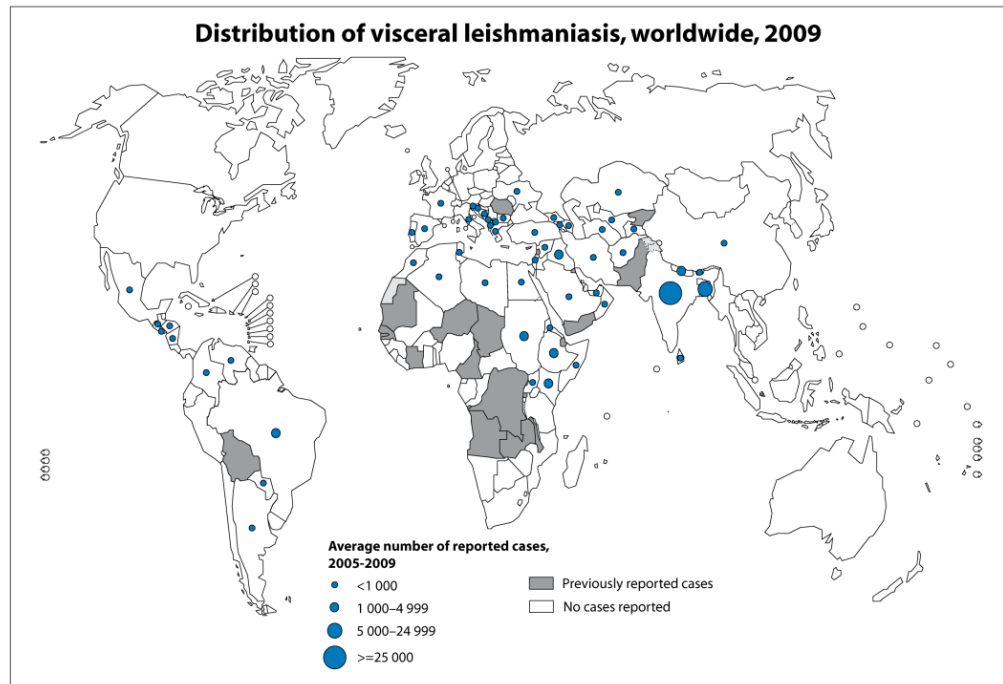


The boundaries and names shown and the designations used on this map do not imply the expression of any opinion whatsoever on the part of the World Health Organization concerning the legal status of any country, territory, city or area or of its authorities, or concerning the delimitation of its frontiers or boundaries. Dotted lines on maps represent approximate border lines for which there may not yet be full agreement. © WHO 2010. All rights reserved

Data Source: World Health Organization
Map Production: Control of Neglected Tropical Diseases (NTD)
World Health Organization



A



The boundaries and names shown and the designations used on this map do not imply the expression of any opinion whatsoever on the part of the World Health Organization concerning the legal status of any country, territory, city or area or of its authorities, or concerning the delimitation of its frontiers or boundaries. Dotted lines on maps represent approximate border lines for which there may not yet be full agreement. © WHO 2010. All rights reserved

Data Source: World Health Organization
Map Production: Control of Neglected Tropical Diseases (NTD)
World Health Organization



B

Figure 1.1: Countries affected by leishmaniasis.
A, Countries affected by cutaneous leishmaniasis; B, Countries affected by visceral leishmaniasis.

(Source for both maps: WHO (<http://gamapservr.who.int/mapLibrary/>))

Visceral leishmaniasis (VL)

Visceral leishmaniasis (also known as Kala Azar), is the most severe form of leishmaniasis, cases are less distributed than CL as shown in figure 1.1B but more than 90% occurs in just five countries; Bangladesh, India, Nepal, Sudan and Brazil (Tiuman *et al.*, 2011; Singh *et al.*, 2011). Visceral leishmaniasis is most commonly associated with *L. donovani*, *L. chagasi* and *L. infantum* (Murray *et al.*, 2005). The effects of visceral leishmaniasis can range from no symptoms (sub-clinical disease), oligosymptomatic (which may spontaneously resolve but could also progress to Kala Azar) to fully established Kala Azar (Murray *et al.*, 2005). After a bite from a sand fly a papule forms, which can be mistaken for CL in the early stages, however, after infection the parasites then disseminate to internal organs. Fully established infections are characterised by undulating fever, anaemia and weight loss as well as hepatomegaly (enlargement of the liver) and splenomegaly (enlargement of the spleen) (Murray *et al.*, 2005; Desjeux, 2004). Left untreated VL results in susceptibility to secondary infection and/or haemorrhaging followed by death of the host within two years (Murray *et al.*, 2005).



Figure 1.2: Clinical manifestations of leishmaniasis

A, cutaneous leishmaniasis; B, mucocutaneous leishmaniasis; C, visceral leishmaniasis.

Sources;

A, <http://www.stanford.edu/class/humbio103/ParaSites2006/Leishmaniasis/images/Hand.jpg>;

B, <http://tmcr.usuhs.mil/tmcr/chapter46/large46/46-18.jpg>;

C, <http://www.icp.ucl.ac.be/~opperd/parasites/images/WHO1.jpg>

1.1.3 Treatment and prevention of leishmaniasis

Currently there are several drugs available for the treatment of leishmaniasis, treatment varies through different countries and depends upon several factors such as access to treatment, financial situation and time. Determination of the causative species is important in selecting the correct drug; this can be difficult as many endemic countries have several concurrent species of *Leishmania*. The form in which the disease presents itself is also a factor for consideration. It is not always necessary to treat cutaneous leishmaniasis as most lesions are self healing and resolve within a couple of months (Murray *et al.*, 2005). The patient's ability to pay may be one of the most important considerations as many of the endemic countries are regarded as less developed countries with high levels of poverty. The cost of treatment is not limited to the drug which in itself can be costly but also the cost of hospitalisation and length of treatment and time away from earning money (Alvar *et al.*, 2006).

For the past 60 years, antimonial drugs such as sodium stibogluconate (Pentostam®) and meglumine antimonate (Glucantime®) have been used as the “first line” treatment, which kill *Leishmania* by DNA fragmentation (although the exact mechanism of action is unknown) (Singh *et al.*, 2012). Treatment for cutaneous leishmaniasis would normally be administered for large, persistent or multiple lesions. The World Health Organisation recommends intra-lesional antimony, where the drug is injected around the edge of the lesion every 2-7 days for up to 30 days (depending on the chosen antimony) (Minodier & Parola, 2007).

The extended parenteral administration, toxicity and increasing resistance to antimony has led to several “second line” treatments being introduced. Amphotericin B (Fungizone®) is selective against ergosterol (the predominant sterol in *Leishmania*) and is a highly effective polyene antifungal used against VL and ML. Due to the adverse side effects, several liposomal Amphotericin B (AmBisome®) formulations were developed and showed reduced toxicity. Unfortunately, its high cost limits its use as an anti-leishmanial drug (Singh *et al.*, 2012; Croft and Coombs, 2003).

Miltefosine (Impavido®) is an oral anti-tumour agent that interferes with cell signal transduction pathways and inhibits phospholipids and sterol biosynthesis (Minodier & Parola, 2007). It was the first effective oral treatment used against visceral leishmaniasis, and also showed effectiveness against strains shown to be resistant to antimonial drugs (Murray *et al.*, 2005). It is now commonly used in India where almost half of all visceral leishmaniasis occurs. Due to teratogenicity it cannot be administered to women of child bearing age (Croft and Coombs, 2003). Paromomycin (Humatin®) is an aminoglycoside-amino-cyclitol antibiotic used to treat VL and CL, which is administered either topically or parenterally. The side effects are limited but inadequate availability restricts its use in endemic regions.

Drug resistance is fast becoming a problem in the treatment of leishmaniasis. The toxicity to the patient, cost and resistance to currently available drugs are representative of the need to develop new, safe and effective drugs and/or a vaccine (that are also cost effective) against leishmaniasis. Studies by Croft *et al.*, 2006 using *L. donovani* to investigate resistance to standard antimonial drugs showed that resistance is easily generated in promastigotes, and more recently axenic amastigotes. Results suggested that the resistance could be overcome by increasing the dose of the drug. Unfortunately the current dose required produces unacceptable toxicity and further increase would jeopardise the safety of the patient (Croft *et al.*, 2006). These problems demonstrate the urgency for new and safer drugs.

In addition to drugs, there are several measures which could reduce the burden of disease. Sand fly control measures such as residual insecticidal house spraying (RIHS) would reduce the vector population and alleviate the disease burden. The cost and frequency of spraying insecticide makes this method difficult to maintain. Insecticide impregnated bed nets would provide some protection from the disease as sand flies are most active between dusk and dawn. Although bed nets are a cheaper alternative to RIHS, they are still poorly implemented and financially out of reach for the majority of the population in endemic regions (Alvar *et al.*, 2006; Desjeux, 2004). Covering exposed skin is the simplest prophylactic measure and is not restricted by cost;

however, due to the climate in endemic regions it could be impractical for this to become common practice.

1.1.4 Life cycle of *Leishmania*

Leishmania have a digenetic life cycle consisting of two principle morphologies. The uniflagellate motile promastigote replicates within the sand fly vector. In the mammalian host *Leishmania* live as obligate intracellular amastigotes, oval non-motile cells with a flagellum that does not protrude past the flagellar pocket. Figure 1.3 shows the life cycle of *Leishmania* spp.

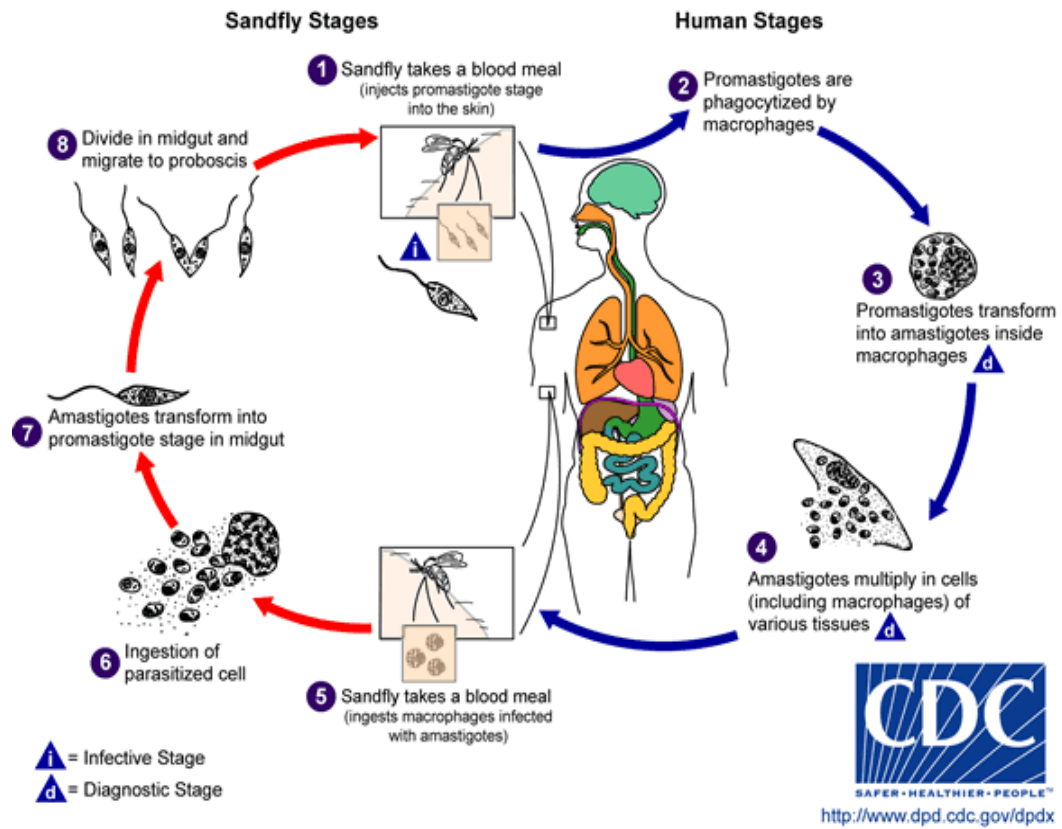


Figure 1.3: Life cycle of *Leishmania*

(Source: http://dpd.cdc.gov/dpdx/html/imageLibrary/Leishmaniasis_il.asp?body=G-L/Leishmaniasis/body_Leishmaniasis_il_th.htm)

There is evidence for transmission of *Leishmania* through blood transfusion and needle sharing between intravenous drug users (Cruz *et al.*, 2006). However, the primary vector for *Leishmania* transmission is the female phlebotomine sand fly, a subfamily of Psychodidae (of the order Diptera). Of the approximately 1000 species of phlebotomine sand flies, only 70 are implicated as vectors for *Leishmania* (Bates 2008). These encompass all known vectors of *Leishmania* except *L. enriettii* (recently discovered to infect red kangaroos in Australia), which is suggested to be transmitted by a midge (*Forcipomyia (lasiohelea)* spp.) (also of the Order Diptera) (Dougall *et al.*, 2011). In the Old World, sand flies of the genus *Phlebotomus* are responsible for the spread of leishmaniasis, while in the New World it is the genus *Lutzomyia* (Bates, 2008). *L. olmecaolmecca* is the natural vector for *L. mexicana*.

Sand flies typically feed upon sugar sources, however, during egg production the female sand fly takes a blood meal to obtain additional nutrients. The parasites are taken up (in macrophages) with the blood meal from an infected mammalian host which passes to the posterior abdominal midgut. The change in environment prompts the ovoid amastigotes to differentiate into several distinct developmental stages as they migrate through the sand fly gut culminating in the infective metacyclic promastigotes (Kamhawi, 2006). Within 12 hours, a meshwork of protein, proteoglycans and chitin secreted by the midgut epithelium called the peritrophic membrane (PM) encloses the blood meal and therefore the parasites. This type I PM is secreted as a direct response to distension of the midgut caused by blood feeding (Sadlova and Volf, 2009). The peritrophic membrane is semi-permeable which allows the inward diffusion of sand fly digestive enzymes and outward diffusion of nutrients. This is important in the early stages of development of the parasites as it limits the amount of digestive enzymes passing through the membrane. Within 48 hours after the blood meal, the amastigotes have differentiated to short, weakly motile procyclic promastigotes which are highly replicative within the PM. In the following 24 hours replication slows and the procyclic promastigotes differentiate into elongated motile nectomonad promastigotes which escape the PM through the action of parasite and sand fly secretory chitinase. They then attach between microvilli of the epithelium facilitated by the surface glycoconjugate lipophosphoglycan (LPG) to avoid expulsion from the midgut during digestion (Bates,

2007; Kamhawi, 2006). The nectomonads then begin to migrate toward the anterior thoracic midgut, when they reach the stomodeal valve (SV) they differentiate to the shorter form leptomonad promastigotes and undergo another round of replication. The leptomonads are responsible for the production of the promastigote secretory gel (PSG). The PSG, primarily composed of filamentous proteophosphoglycan (fPPG), a mucin-like glycoprotein unique to *Leishmania*, fills the lumen contributing to the 'blocked fly' effect (Kamhawi, 2006; Rogers *et al.*, 2004). Around five days after infection the leptomonads differentiate into the mammalian infective, rapidly motile metacyclic promastigotes. In addition to the metacyclics, some of the leptomonads attach to the cuticle-lined surface of the stomodeal valve and transform into haptomonads which form a parasite plug aided by the disc-like expansion of the flagellar tip (Bates, 2007). The haptomonads attached to the SV produce chitinases which degrade the chitinous lining of the valve, resulting in the need for more probing and prolonged feeds. This, along with the need to clear the PSG by regurgitation deposits the infective parasite into the host's skin and contributes to the transmission of the disease. The different forms in which promastigotes are found within the phlebotomine fly are detailed in figure 1.4.

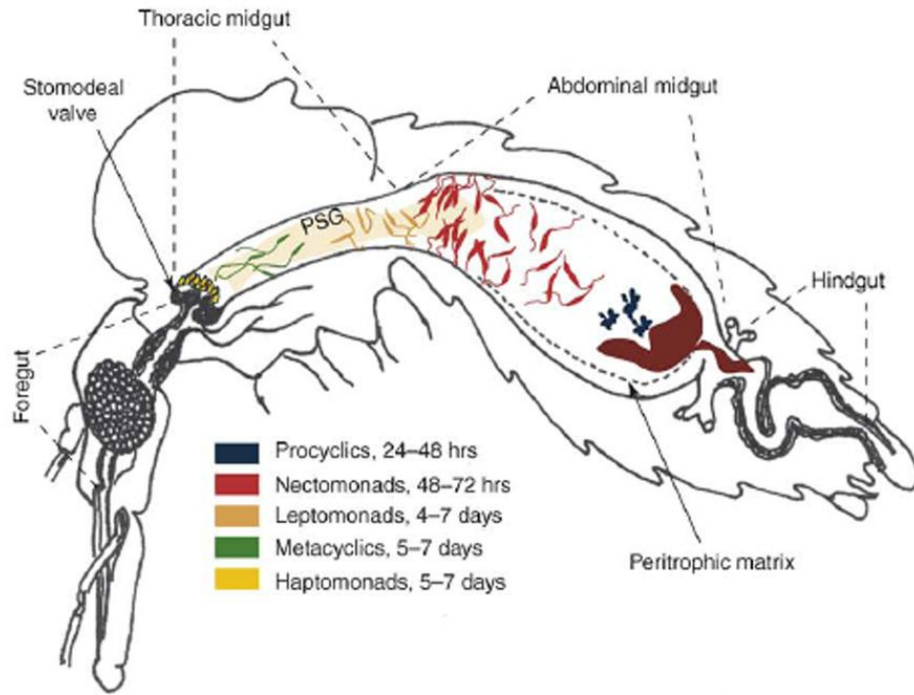


Figure 1.4: The different *Leishmania* promastigote forms in the phlebotomine sand fly vector (Kamhawi, S. 2006).

Several differences exist between the forms of promastigotes, such as various proteins are found at differing concentrations (Alexander *et al.*, 1992). Enzymes involved in cell division such as Elongation Factor 2 and RNA helicase are found at higher levels in the procyclic promastigote (the replicative form) (Mojtahedi *et al.*, 2008), whereas α -tubulin, β -tubulin and other proteins involved in cell motility are found in higher levels in metacyclic promastigotes (Mojtahedi *et al.*, 2008).

Depending on the causative *Leishmania* species, leishmaniasis can be anthroponotic (transmitted solely between humans) or zoonotic (also infects animals as reservoir hosts). The increased probing and prolonged feeding of the sand fly increases the opportunity to transmit the parasite to the host's skin, depositing a mixture of saliva, PSG and up to 1000 parasites per feed (Rogers *et al.*, 2004). Once the metacyclic promastigotes have been transferred into the skin they need to manipulate and evade the innate immune system but ensure phagocytosis by macrophages. Lipophosphoglycan (LPG) is an important surface molecule of metacyclic promastigotes. It inhibits protein kinase C (PKC) activity by binding the regulatory domain of PKC, reducing the generation of O_2^- (Shio *et al.*, 2012). Additionally, LPG blocks the attachment of C5b-C9 subunits of the complement complex which mediates cellular lysis (Olivier and Gregory, 2005). Other means of evading the complement system include secretion of a serine/threonine kinase (LPK-1) by metacyclics leading to the inactivation of C3, C5 and C9 (Hermoso, 1991). However, the parasites depend upon complement-mediated phagocytosis to enter the host macrophages. This is achieved through activity of the surface molecule gp63. To prevent the activation and recruitment of other complement components, gp63 rapidly converts C3 to iC3b which favours phagocytic clearance rather than lytic (Olivier and Gregory, 2005). Parasite opsonisation with iC3b binds the complement receptors CR1 and CR3 and prevents the oxidative burst, which is advantageous to the survival of *Leishmania* within the macrophage (Oliver and Gregory, 2005; Alexander *et al.*, 1999). Receptors for mannose-fucose and fibronectin which bind LPG and gp63 also facilitate the phagocytosis of *Leishmania* (Solbach and Laskay, 2000). In addition to macrophages, there are other phagocytic cells involved in the uptake of *Leishmania* such as dendritic cells and polymorphonuclear neutrophil

granulocytes, however, the latter are considered to be temporary host cells (Liu *et al.*, 2012; Sarkar *et al.*, 2012).

Once phagocytosed, the *Leishmania*-containing phagosomes fuse with lysosomes (containing acid hydrolases) creating the parasitophorous vacuole (PV). Depending on the *Leishmania* species, PVs may envelope all parasites together as with *L. mexicana* and *L. amazonensis*, whereas, *L. major* and *L. donovani* have separate vacuoles for each cell (Antoine *et al.*, 1998). The low pH of the vacuole and higher temperature in the mammalian host induces the differentiation of promastigotes to amastigotes. The amastigotes are small spherical cells (about 4-5 μm), with a short flagellum that does not extend past the flagellar pocket. Differentiation to amastigotes can take up to five days, subsequent proliferation of the amastigotes leads to the rupture of macrophages and release of *Leishmania* back into the blood where further infection of macrophages occurs (Wiese, 2007; Alexander *et al.*, 1999).

Several mechanisms allow *Leishmania* to modulate the host immune system to its own benefit. The sand fly saliva contains a peptide, maxadilan, which is a selective agonist of the pituitary adenylate-cyclase activating polypeptide type 1 receptor. This inhibits the production of TNF- α by lipopolysaccharide-stimulated macrophages, reducing their ability to produce NO and kill *Leishmania*, and exacerbating lesion development (Alexander *et al.*, 1999). Also gp63 activates the host tyrosine phosphatase SHP-1, which negatively regulates the ERK1/2 and JAK/STAT1 pathways. This causes a decrease in pro-inflammatory cytokines leading to a non-healing response by the host (Shio *et al.*, 2012).

1.2 Signal transduction in Eukaryotes

1.2.1 Signalling pathways in higher eukaryotes

It is essential for all eukaryotic cells to be able to react to changes in their environment. This involves recognition, relay and conversion of extracellular signals. In multicellular organisms, homeostasis, growth and response to pathogens are induced and regulated in large part by the endocrine signalling, while in unicellular organisms such as

Leishmania, differentiation is controlled by discreet signalling events. The signalling pathways within cells utilise phosphorylations, ubiquitinylations, acetylations and phosphoinositides to relay extracellular signals (Pearson *et al.*, 2001). Signalling receptors can be divided into two main types depending on their location in the cell; intracellular and extracellular. The three most important extracellular receptors are the ligand-gated ion channels, G-protein coupled receptors (GPCR) and the receptors with enzymatic activity.

Ligand-gated ion channels are transmembrane ion channels that change conformation upon binding a ligand, e.g. acetylcholine. This mediates a rapid influx of ions changing the membrane potential and influences the transmission of the signal. In the case of ligand-gated ion channels on the myoceptor of skeletal muscle, the binding of acetylcholine causes an influx of cations which polarises the membrane and leads to muscle contraction.

G-protein coupled receptors (GPCR) (also called serpentine receptors) are integral membrane proteins with seven transmembrane domains. GPCRs are activated by the binding of hormones or neurotransmitters following which they undergo a conformational change of the G-protein (Parsons and Ruben, 2000). This allows for the exchange of bound GDP on the $G\alpha$ subunit for GTP which stimulates cAMP signalling or the phosphatidylinositol pathway. The G-protein can be activated repeatedly as the GPCR remains active as long as the signal is bound (Parsons and Ruben, 2000).

Receptors with their own enzymatic activity include receptor tyrosine kinases (RTKs), tyrosine phosphatases and guanylate cyclases. RTKs are the most common receptors with enzymatic activity. They are composed of an intracellular domain with tyrosine kinase activity. Binding of a ligand such as growth factors and insulin induces oligomerisation or the re-orientation of oligomer subunits which directly enables the kinase domains to activate each other via autophosphorylation. This allows the binding of other proteins (usually characterised by highly conserved domains such as Src-homology region or phosphotyrosine binding) to form a signalling complex (Kim *et al.*, 2010).

Intracellular receptors can be localised in the nucleus or in the cytoplasm and bind signalling molecules which are either soluble or capable of diffusing through the plasma membrane. The intracellular signals are differentiated by the distance and type of elicitor cells. The soluble gas nitric oxide (NO) activates cytosolic guanylate cyclase which leads to the production of cyclic guanosine monophosphate (cGMP) (Francis *et al.*, 2010). Diffusion of lipophilic steroid hormones into a cell activates cytosolic receptors, causing translocation to the nucleus. Binding of hormone receptor complexes to hormone response elements (HREs) in the nucleus regulates transcription of certain genes (Francis *et al.*, 2010).

1.2.2 Protein kinases

Protein kinases are a class of enzymes that are key regulatory molecules, along with their antagonists – the protein phosphatases, forming complex networks of mutually activating and silencing molecules in all eukaryotic cells. They act by transferring the γ -phosphate of ATP to a hydroxyl group in a kinase substrate. Phosphorylation is a common post-translational modification, which can induce conformational changes in proteins generating or masking binding motifs. These changes can modulate the activity of an enzyme, binding properties, protein stability or change the subcellular localisation of a protein. Protein kinases are important components of cell signalling, regulating several major cellular processes such as proliferation, differentiation, metabolism, and gene expression. Their importance is further demonstrated by 1.5-2.5% of eukaryotic genomes encoding protein kinases (Hanks, 2003; Manning *et al.*, 2002a).

Protein kinases can be divided into two main groups; the eukaryotic protein kinases (ePKs) which share a highly conserved catalytic domain and the atypical protein kinases which lack sequence identity to ePKs but have been shown to possess biochemical kinase activity (Manning *et al.*, 2002b). The majority of protein kinases belong to the ePK group with many organisms having only one aPK. The ePK group can be further divided into Ca^{2+} /calmodulin-dependent kinases (CAMK), protein kinases A, G and C (AGC), homologues of yeast sterile kinases 7, 11 and 20 (STE), tyrosine kinases (TK), tyrosine kinase-like kinases (TKL) and the CMGC group (consisting of cyclin-

dependent kinases, MAP kinases, GSK3 and CDK-like kinases) (Manning *et al.*, 2002b). Alternatively, they can be subdivided according to the amino acid residue being phosphorylated; serine/threonine kinases, tyrosine kinases and dual-specificity kinases (accept serine, threonine and tyrosine residues). The occurrence of phosphorylation of serine, threonine and tyrosine differs greatly with ratio of 1800:200:1 (Johnson and Hunter, 2005; Hubbard & Cohen, 1993). *T. brucei* was found to show a slightly lower serine phosphorylation and greater phosphorylation of threonine residues - more similar to prokaryotes than higher eukaryotes (Nett *et al.*, 2009a).

The structure of protein kinases is highly conserved and is composed of two domains linked by a hinge region (figure 1.5a). The smaller N-terminal lobe (top of figure 1.5a) consists of five beta-sheets ($\beta 1$ - $\beta 5$) and one alpha helix (αC). The C-terminal lobe is larger and consists primarily of alpha-helices. The hinge region includes the ATP and substrate binding domains (Krupa *et al.*, 2004). The N-terminal lobe and hinge region are mainly responsible for the binding and orientation of ATP, whereas the C-terminal lobe is responsible for the binding and orientation of substrates (Hanks & Hunter, 1995).

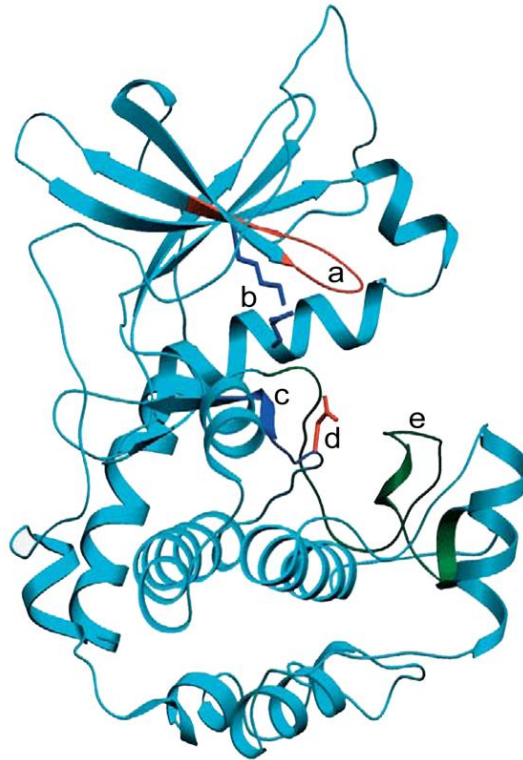


Figure 1.5a: The three-dimensional structure of the catalytic domain of an exemplary serine/threonine kinase.

Key functional elements are labelled with lower case letters; a, phosphate anchor ribbon; b, lysine-glutamate salt bridge; c, catalytic loop; d, catalytic base; e, activation segment (Krupa *et al.*, 2004).

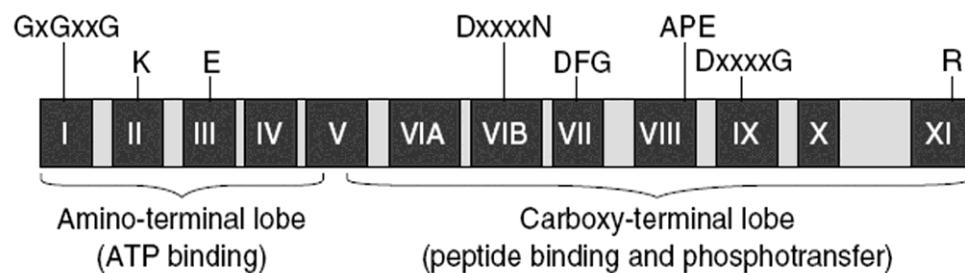


Figure 1.5b: The conserved catalytic domain of eukaryotic protein kinases.

The conserved subdomains are numbered with Roman numerals and highly conserved amino acid motifs are displayed above their position in the subdomains (x: arbitrary amino acid); the common amino-terminal and carboxy-terminal lobe as identified by crystal structures are indicated below the subdomains (Hanks, 2003).

The structure of protein kinases can be further divided into twelve subdomains separated by amino acid inserts of variable length. The N-terminal lobe encompasses subdomains I-IV while the C-terminal lobe includes subdomains VIA to XI (figure 1.5b). Subdomain I contains the phosphate-anchor ribbon, a glycine-rich loop defined by the GxGxxG motif. Subdomains II and III are linked by a salt bridge between a critical lysine in subdomain II and a glutamate in subdomain III. This stabilises the interaction of the kinase with α - and β -phosphates of ATP (Hanks & Hunter, 1995). Mutation of the critical lysine renders the kinase inactive as it is no longer able to correctly orientate the ATP into position, thus preventing phosphotransfer (Gibbs & Zoller, 1991). The catalytic loop is found in subdomain VIB and is defined by the invariant DxxxxN motif. The aspartic acid (D) acts as the catalytic base by accepting a proton from the attacking substrate hydroxyl group during phosphotransfer. The DFG motif in subdomain VII assists in orientating the ATP correctly, while both the APE motif of subdomain VIII and DxxxxG of subdomain IX stabilise the C-terminal lobe. The activation lip is found in subdomain VIII (from the conserved DFG until the conserved APE motif). Phosphorylation of the activation lip found in subdomain VIII residues activates the kinase leading to conformational changes which allow for substrate recognition (Hanks & Hunter, 1995).

1.2.3 MAP kinases

Mitogen-activated Protein Kinases are a family of enzymes involved in cellular signal transduction. They are part of the CMGC group of kinases and are essential in all eukaryotes, with the single exception of *Encephalitozoon cuniculi* (Miranda-Saavedra *et al.*, 2007), although *Plasmodium falciparum* encodes only two MAP kinases, it also lacks a MAP Kinase kinase orthologue and therefore the traditional cascade (Brumlik *et al.*, 2011; Dorin-Sembalt *et al.*, 2007). The MAP kinase cascade forms an important part of cell signalling, influencing essential processes such as proliferation, differentiation, stress response and apoptosis (Avruch, 2007). In mammals, at least four distinct classes of MAP kinases have been identified; ERK (extracellular signal-related kinase) 1/2, JNK (c-Jun N-terminal kinase) 1/2/3, the p38 proteins (α , β , γ , δ) and ERK5. Signalling cascades involving the ERKs are mainly associated with proliferation

and differentiation, while JNK and p38 proteins play key roles in stress and immune responses, respectively.

The MAP kinase cascade is conserved between the distinct MAP kinase families among all eukaryotes. In higher eukaryotes a signal (often hormone or cytokine) is transmitted via cell membrane receptors, which activates a MAP kinase kinase kinase (MAP3K). The activated MAP3K phosphorylates (and thus activates) a MAP kinase kinase (MAP2K) which in turn phosphorylates a MAP kinase (MAPK). In higher eukaryotes the signal often terminates with the activation of a transcription factor or phosphorylation of another protein by the MAP kinase might occur (figure 1.6a).

The serine/threonine kinase MAP3Ks are activated by phosphorylation by Ste20-like kinases or by interaction with small GTP-binding proteins of the Ras or Rho family (Avruch, 2007; Pearson *et al.*, 2001). The MAP3K then phosphorylates one or a few dual-specificity MAP2K on two serine and/or threonine residues thereby activating it. The N-terminus of MAP2Ks often contains a docking site (D-site), which binds the common docking or CD-domain of the MAP kinase it is activating. The D-site with a consensus motif [K/R]₂₋₃-X₋₁₋₆-[L/I]-X-[L/I] has been found in most eukaryotic MAP2Ks. The CD-domain consensus sequence is simpler DXXDE (Pearson *et al.*, 2001). The MAP2Ks phosphorylate one or very few MAPKs on the threonine and the tyrosine residue of the highly conserved TXY motif located on the activation loop in subdomain VIII (figure 1.6b). The unusual dual phosphorylation on both threonine and tyrosine residues within the activation loop is characteristic of typical MAP kinases. MAPKs are serine/threonine kinases that can phosphorylate many different substrates within the cytoplasm and nucleus with a consensus sequence P-X-[S/T]-P, although some identified substrates occur only with a condensed consensus sequence of [S/T]-P (Davis, 1993). Substrates include transcription factors, cytosolic proteins such as heat shock proteins and MAPKAPKs (MAPK-activated protein kinases). Activation of atypical kinases is less well documented as they do not share the typical mechanisms or classical three tiered cascade as conventional MAP kinases and often do not require the dual phosphorylation of the activation loop (Cargnello *et al.*, 2011). MAPK inactivation is by dephosphorylation of one or both residues of the TXY motif on the activation lip

by a MAP kinase phosphatase (MKP), which is often a dual-specificity phosphatase (DUSP) (Jeffrey *et al.*, 2007). To date, a total of 22 MAPKs, 7 MAP2Ks and 20 MAP3Ks have been identified in mammals (Pearson *et al.*, 2001).

The proper regulation of MAP kinases within signal transduction pathways is key to eukaryotic cell welfare, the breakdown of which is ultimately responsible for diseases such as Alzheimer's disease, Parkinson's disease and various cancers (Kim *et al.*, 2010). Consequently, MAP kinases are promising targets for the development of new drugs. At present there are ten inhibitors of protein kinases approved for treatment of different cancers (Cohen, 2009).

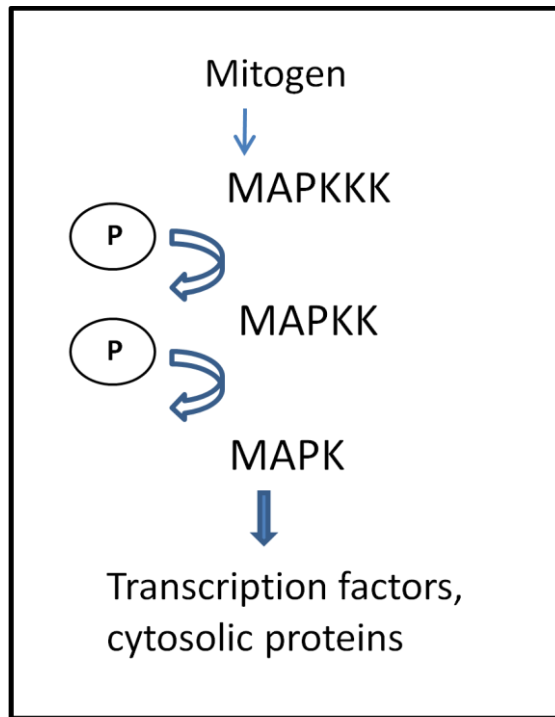


Figure 1.6a: A typical MAP kinase cascade schematic

The activation of a MAPKKK by a ‘mitogen’ triggers the phosphorylation of the following MAP kinases in the MAP kinase cascade.

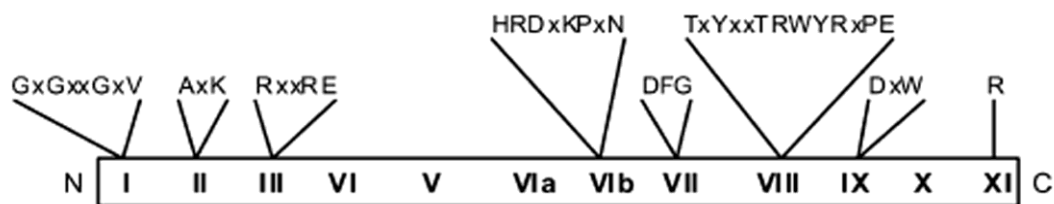


Figure 1.6b: The conserved catalytic domain of mitogen-activated protein kinases.

The Roman numerals denote the twelve conserved subdomains; conserved consensus motifs are indicated above (Wiese *et al.*, 2003).

1.3 Signal transduction in Trypanosomatids

As *Leishmania* pass through their digenetic life cycle they have to adapt to the changing environments as they move between hosts. The biochemical and morphological changes observed during the life cycle are a result of changes in gene expression likely regulated by signal transduction. Furthermore, the presence of a large number of protein kinases encoded within the Kinetoplastid genome suggests phosphorylations play an important role in signalling processes (Parsons *et al.*, 2005). Signalling pathways are very well documented in higher eukaryotic cells, however, very little is currently known about signalling in *Leishmania*. Application of signalling knowledge in higher eukaryotes to *Leishmania* is limited for several reasons. For example, only some of the signalling pathways are present in both higher eukaryotes and *Leishmania*, other pathways are found to be lacking in *Leishmania* (figure 1.7). The functions of these pathways are currently undetermined (Parsons and Ruben, 2000). In addition to unexplored pathways, the external stimuli that initiate signal transduction pathways in trypanosomatids are largely unknown. Growth factors and cytokines have been shown to have an effect on trypanosomes and secreted proteins from the host or parasite may play a role in signal transduction (Gomes *et al.*, 1998; Barcinski *et al.*, 1992).

The activation mechanism of trypanosomatid signalling cascades is unclear. In mammals, receptor tyrosine kinases are the most common receptors of extracellular signals which activate intracellular signalling cascades (Manning *et al.*, 2002b). Interestingly, all plant receptors are serine/threonine kinases (Shui *et al.*, 2004) and trypanosomatids may use similar methods in environmental sensing. No tyrosine kinases or phosphatases have been identified in trypanosomatids. It had been suggested tyrosine phosphorylation may be carried out by serine/threonine kinases or atypical kinases such as Wee1 (Parsons *et al.*, 2005).

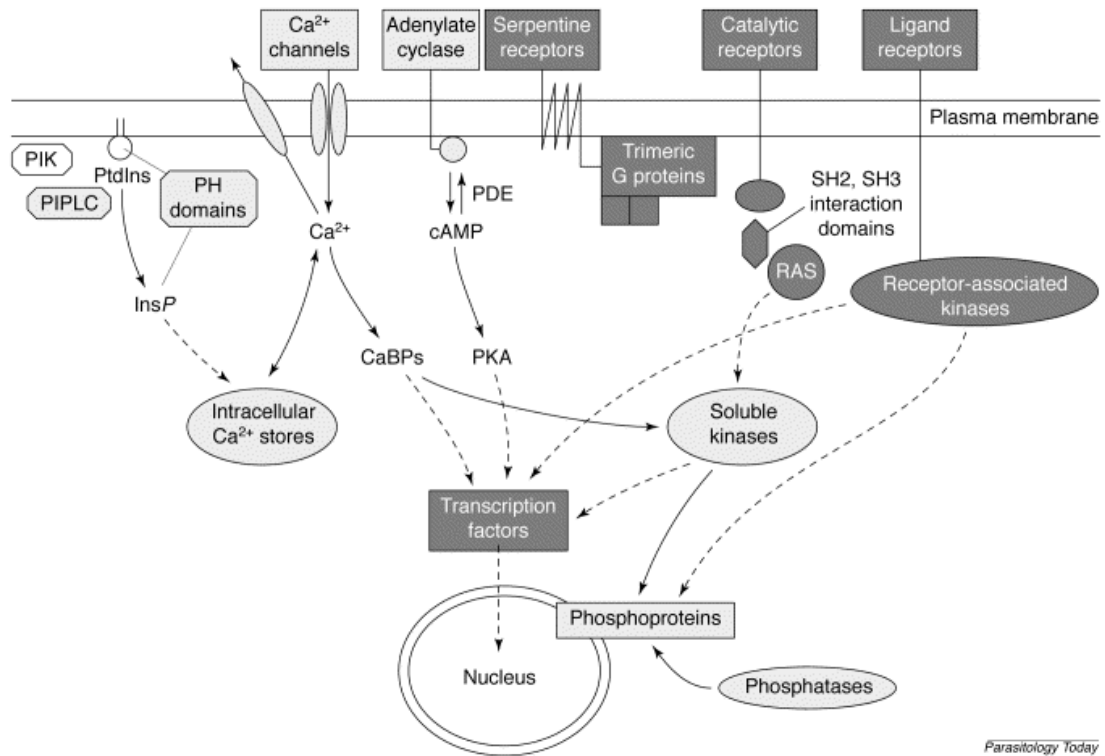
Ca^{2+} is an important signalling molecule in all eukaryotic cells. In higher eukaryotes, the transport system of Ca^{2+} is well documented whereas in comparison, little is known of these systems in trypanosomatids. Ca^{2+} homeostasis within trypanosomatids is maintained in part by energy-dependent transport by the endoplasmic reticulum (ER), plasma membrane and acidocalcisomes, however, the external stimuli leading to an influx of Ca^{2+} ions is unknown (Parsons and Ruben, 2000; Nolan *et al.*, 1994).

Response of the cell to Ca^{2+} is determined by Ca^{2+} -binding proteins (CaBP) which convert the Ca^{2+} signal into a physiological outcome. The specific process regulated by Ca^{2+} and CaBPs are as yet unknown in trypanosomatids. Molecules of the phosphoinositol cascade, one of the major pathways inducing proliferation in higher eukaryotes, has been identified in kinetoplasts. This cascade involves the phosphorylation of membrane-bound phosphatidylinositols (PtsIns) by phosphatidylinositol 3-kinase (PI3K). Phosphatidylinositol phosphates (PtdInsPs) bind intracellular proteins with PH (pleckstrin homology) domains to signal complexes which then relay the signal of growth factors. Although genes for these molecules have been identified in *T. brucei* and *T. cruzi* (Nozaki *et al.*, 1999; Bringaud *et al.*, 1998), the consequent release of Ca^{2+} does not take place in trypanosomes as it does in higher eukaryotes (Parsons *et al.*, 2000)

Adenylyl cyclases (ACs) are integral membrane proteins and thus far the only known transmembrane receptor in trypanosomatids. They consist of a transmembrane domain which links with a putative ligand-binding domain and a highly conserved cytoplasmic adenylate cyclase domain (Seebeck *et al.*, 2001). Kinetoplastids feature a comparatively large number of adenylyl cyclases (AC), most of which are integral membrane proteins and differ considerably in structure from their mammalian counterparts, as they belong to class II cyclases which are exclusive to protozoa (Laxman, S. *et al.* 2007). ACs are encoded by a multigene family in *Leishmania* and *T. brucei*. The extracellular domain differs between family members suggesting an interaction with different ligands to regulate adenylate cyclase activity. Activation of ACs appears to require dimerisation, however, unlike in mammals, this occurs independently of G-proteins (homodimerisation) (Naula *et al.*, 2001). Cyclic adenosine monophosphate (cAMP) is an important “second messenger” mainly involved in the activation of protein kinase A (PKA). Although cAMP signalling is not fully elucidated in trypanosomatids, there is strong evidence to suggest it is involved in regulation of proliferation and differentiation (Naula *et al.*, 2001). As previously discussed, the primary signal receptors in higher eukaryotes (receptor tyrosine kinases) do not exist in trypanosomatids. Due to the abundance (approximately 10 times more ACs encoded in the trypanosomatid genome

than in higher eukaryotes) and diversity, adenylyl cyclases are proposed to be the primary signal receptors in trypanosomatids (Naula *et al.*, 2001; Seebeck *et al.*, 2001).

Another fundamental difference between higher eukaryotes and trypanosomatids is the signalling pathways in higher eukaryotes often terminate with the activation of transcription factors leading to a change in transcription of particular genes. The apparent absence of transcription factors and the polycistronic transcription of mRNA in trypanosomatids suggest that regulation of signalling cascades is exerted at a post-transcriptional level occurring at the mRNA stage (Parsons *et al.*, 2005; Wiese *et al.*, 2003).



Parasitology Today

Figure 1.7: Differences between major signalling pathways in Trypanosomatids and higher eukaryotes.

Components shown in light grey are present in both; those shown in a darker grey are only present in higher eukaryotes; dotted lines show unknowns of the trypanosomatid pathway. PDE, cAMP phosphodiesterase; PIK, phosphatidylinositol kinases; PIPLC, phosphoinositides phospholipase C; PKA, cAMP-dependent protein kinase; PtdIns, phosphatidylinositol; SH2, SRC homology region 2 (Parsons and Ruben, 2000).

1.3.1 Trypanosomatid MAP kinases

Leishmania MAP kinases have the same general structure as other MAP kinases, composed of a large kinase domain which is further divided into twelve kinase subdomains. The activation site, a Threonine-any amino acid- Tyrosine (TXY) motif, is located on the activation lip, which when phosphorylated leads to a conformational change in the kinase structure. This enables it to transfer a phosphate group from a molecule of ATP to the kinase substrate. In higher eukaryotes, the cascade culminates with the activation of transcription factors or phosphorylation of another protein by a MAPK. *Leishmania* lack transcription factors, thus *Leishmania* MAP kinase substrates are currently unknown (Wiese, 2007).

The *Leishmania* genome encodes all three levels of the MAP kinase cascade. To date, 15 MAP kinases have been identified in *Leishmania* with a further two MAP kinase-like kinases described (Morales *et al.*, 2007), some of which are genetically implicated in parasite virulence and flagellar biogenesis (Wiese, 2007). Despite this there is still very little to no information available on the (specific) activity of the endogenous MAPKs, their substrates and downstream regulated target proteins (Naula *et al.*, 2005). Eight MAP kinase kinase (MAPKK) homologues, all members of the STE7 family of protein kinases have been identified through sequence homology analysis (Parsons *et al.*, 2005), two of which have been shown to be activators of MAPKs; LmxMKK activates LmxMPK3 (Erdmann *et al.*, 2006) and LmxMKK5 activates LmxMPK4 (John von Freyend *et al.*, 2010a). Bioinformatics also identified 23 potential MAP3K homologues (members of the STE11 family), the need to artificially activate MAPKKs *in vitro* supports the existence of MAP3K homologues in trypanosomes (Parsons *et al.*, 2005; Wiese, 2003). In mammals, MAP3Ks belong to the STE20 family, only one MAP3K homologue belonging to this family has been analysed in *L. major* so far. LmjMRK1 is suggested to be essential in *L. major* as all attempts to delete the gene from the genome failed (Agron *et al.*, 2005). An overview of the *Leishmania* MAP kinases is detailed in figure 1.8a.

Many of the 15 MAP kinases have been investigated within our laboratory, of which several have been shown to be essential or important in *Leishmania*. Three of these have been validated as drug targets. LmxMPK1, the first MAP kinase identified in *Leishmania* is essential for the survival of amastigotes in macrophages (Wiese, 1998). The *T. brucei* homologue, TbKFR1 was shown to be essential in procyclics in the insect host (Hua *et al.*, 1997). LmxMPK2 and LmxMPK4 were also shown to be essential for the survival of amastigotes in mammalian hosts through the use of deletion analysis (Wiese, 2007; John von Freyend *et al.*, 2010a). A further five MAPKs were shown to be of no value as a drug target (3, 9, 11, 12 and 13). While LmxMPK11 and LmxMPK12 were shown not to be essential for survival of *Leishmania* at any stage nor affect the normal infectivity in Balb/c mice, LmxMPK3, LmxMPK9 and LmxMPK13 were all shown to affect flagellum length. It has been suggested that the flagellum acts as a sensory organ in *Leishmania* via MAP kinase signalling (Rotureau *et al.*, 2009). LmxMPK5 deletion mutants retain infectivity and persist at the site of infection but are unable to cause lesions rendering it unsuitable as a drug target (Wiese, 2007). The homologue of LmxMPK5 in *T. brucei*, TbMAPK5, is not essential in procyclics in the insect host, however it regulates the differentiation of bloodstream forms in the mammalian host (Domenicali *et al.*, 2006). There is evidence to suggest LmxMPK6 may be essential in the promastigote stage (and possibly amastigotes too), as attempts to generate a deletion mutant failed (John von Freyend, 2010b). LmxMPK7 and LmxMPK8 are the only *Leishmania* MAPKs without a *Trypanosoma* homologue, suggesting they may be important in the intracellular stage of the life cycle. Attempts to generate an LmaMPK7 null mutant were unsuccessful in the absence of an external copy of the gene (i.e. on a plasmid) further supporting the importance of LmaMPK7 in the survival of *Leishmania* (in both life stages) (Morales *et al.*, 2010). LmaMPK10 may be a regulator of parasite differentiation and play a role for survival in the mammalian host. Thus it is a potential drug target, and has already been shown to be sensitive to a p38 specific inhibitor (Horjales *et al.*, 2012). LmaMPK10 is also the first trypanosomatid MAP kinase to have its 3D crystal structure elucidated (figure 1.8b) (Horjales *et al.*, 2012), and is only one of two protein kinase crystal structures reported in *Leishmania*, the other being LmaGSK3 (Ojo *et al.*, 2011). The structure is similar to the human orthologue p38, however several differences were noted. One key difference

observed was the $\alpha 1$ helix replaces the typical two-stranded β -sheet found in most MAP kinases – this could be a feature common to trypanosomatid protein kinases as it is also found in the LmaGSK3 3D model (Horjales *et al.*, 2012).

MAP kinase	Phosphorylation motif	Estimated molecular weight (kDa)	Activator or substrate identified?	Potential drug target	Published Observations
LmxMPK 1	TDY	41.0	No	Yes	Essential for intracellular survival. Wiese, 1998
LmxMPK 2	TDY	50.5	No	Yes	Essential for intracellular survival. Wiese, 2007.
LmxMPK 3	TDY	43.7	Activator: LmxMKK	No	Involved in flagella length regulation. Activated by LmxMKK Erdmann et al., 2006
LmxMPK 4	TQY	41.5	Activator: LmxMKK 5	Yes	Essential to both life stages. Activated by LmxMKK5. John von Freyend et al., 2010
LmxMPK 5	TDY	43.9	No	No	Potential attenuation in virulence. Wiese, 2007
LmxMPK 6	TDY	118.9	No	Yes	May be essential to both life stages. John von Freyend, PhD Thesis, 2010
LmxMPK 7	TDY	61.8	No	yes	Association with HSP70. Morales et al., 2007
LmxMPK 8	TNY	165.7	No	No	Displays long carboxy terminal region. Wiese, 2007.
LmxMPK 9	TEY	45.0	No	No	Role in flagellar length. Bengs et al., 2005
LmxMPK 10	THY	46.4	No	Yes	Amastigote specific phosphorylation and kinase activity. Crystal structure available. Horjales et al., 2012
LmxMPK 11	TDY	46.9	No	No	Not essential for either life stage. Wiese, 2007.
LmxMPK 12	TQY	46.4	No	No	Not essential for either life stage. Wiese, 2007.
LmxMPK 13	TEY	44.5	No	No	Highest homology to human MOK. Wiese, 2007.
LmxMPK 14	TDY	71.6	No	No	Shows homology to mouse male germ cell-associated kinase. Wiese, 2007.
LmxMPK 15	TIY	108.9	No	Unknown	Extended Carboxy terminal region. Wiese, 2007

Figure 1.8a: Overview of Leishmania MAP kinases discussed in this Thesis.

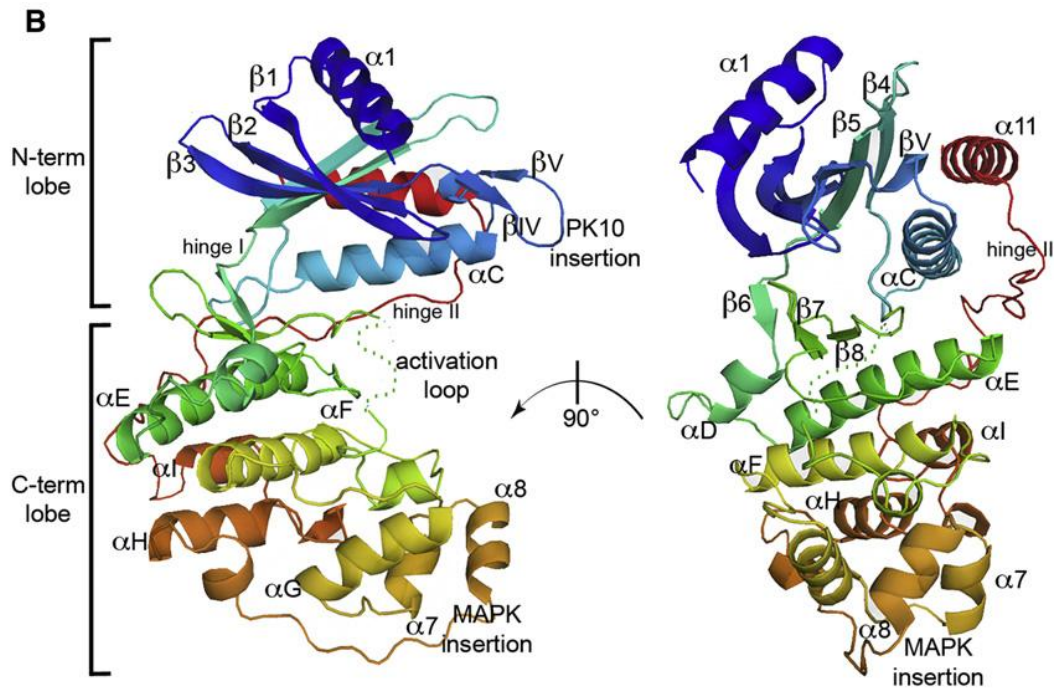


Figure 1.8b: The three-dimensional structure of LmaMPK10ΔC

Three-dimensional structure viewed from two orientations (90° rotation according to the vertical axis). Key functional elements and particular LmaMPK10-specific motifs are labelled (Horjales *et al.*, 2012).

The signalling pathways for MAP kinases have been determined for higher eukaryotes, however, there are several problems associated with applying this to *Leishmania*. The external stimuli (known as “mitogens”) that initiate the cascade are uncharacterised, although it is known that changes in pH, temperature and nutrient concentration trigger differentiation which is likely regulated by MAP kinases (Wiese, 2007). In addition to the external stimuli, the substrates of the *Leishmania* MAPKs are unknown. LmjAQP1, an aquaglyceroporin has been suggested as the substrate of LmjMPK2 as it shows altered activity in LmjMPK2 null mutant cells (Mandal *et al.*, 2012). However, there is no evidence that LmjMPK2 directly phosphorylates LmjAQP1, rather than an intermediary kinase.

The importance of MAP kinases in *Leishmania* cell signalling highlights their value as ideal drug targets in the search for new anti-leishmanial drugs and the need for further research.

1.4 State of knowledge and research objectives

1.4.1 LmxMPK2 and LmxDIP13

The *Leishmania mexicana* Mitogen-activated Protein Kinase 2 (LmxMPK2) was described in 2007 (Wiese, 2007). The gene encoding it was found to be 1,377 bp long, with a TDY (Threonine-Aspartic acid-Tyrosine) activation motif on the activation lip. The protein it encodes, LmxMPK2, is composed of 458 amino acids and has a molecular mass of 50.5 kDa.

The protein shows strong amino acid identity to homologues in other *Leishmania* species; *L. amazonensis* 98%, *L. tropica*, *L. major*, *L. aethiopica*, *L. donovani* and *L. infantum* 97%. However, it shares lower amino acid identity with other kinetoplastids; 63% identity with *Trypanosoma brucei* and *Trypanosoma cruzi*. The closest human homologue is MPK15 (ERK7/8), which still shows 50% sequence identity.

LmxMPK2 is a serine/threonine kinase expressed in both the promastigote and amastigote life stages of *Leishmania*. Previous work within the Wiese group had shown that it was possible to generate homozygous *LmxMPK2* deletion mutants (figure 1.9). The inability to persist in mammalian hosts suggested LmxMPK2 to be essential in amastigotes. In addition to this, several morphological abnormalities were noted, with cells showing multiple flagella, kinetoplasts and nuclei, lobed cell bodies, spiked posterior ends and division furrow ingression from the posterior end (figure 1.10b). The expression of *LmxMPK2* as a genomic add-back returned full function of the kinase and a normal phenotype in both life stages of the parasite.

Unpublished work within the laboratory suggests regulation of LmxMPK1 to be rather unusual. Phosphorylation of tyrosine (Y-178) appears to induce inactivation of the kinase whereas monophosphorylation of Threonine (T-176) leads to a fully activated kinase. As LmxMPK1 and LmxMPK2 comprise a subfamily of *Leishmania* MAPKs (figure 1.11) an understanding of the phosphorylation states and activation of LmxMPK2 would be beneficial.

Investigation into the localisation of LmxMPK2 within *Leishmania* could provide valuable information for the function of LmxMPK2. This could be achieved through GFP (green fluorescent protein) tagging, which has previously been used in similar studies using *L. major*, *L. donovani* (Rotureau *et al.*, 2009) and *L. mexicana* (Kuhn & Wiese, 2005)

LmxDIP13 (Deflagellation inducible protein 13) is a small coiled protein first described in 2003 (Pfannenschmid *et al.*, 2003). The gene encoding the *L. mexicana* (DIP13) was found to be 327 bp long. The protein it encodes, LmxDIP13, is composed of 108 amino acids and has a molecular mass of approximately 12 kDa.

DIP13 was first discovered in *Chlamydomonas reinhardtii* which has been shown to associate with microtubule structures and to be involved in cell division (Pfannenschmid *et al.*, 2003). DIP13 has been found to be absent from common eukaryotic model systems such as *Saccharomyces cerevisiae*, *Caenorhabditis elegans* and *Drosophila melanogaster*. However, it is encoded by the genomes of the flagellated green algae *Chlamydomonas reinhardtii*, trematode worms - *Schistosoma* spp. and protozoan parasites (Price *et al.*, 2012). The *T. brucei* orthologue shows only 33% amino acid identity with the *Chlamydomonas* protein. In a study by Price *et al.*, 2012, TbDIP13 was identified in only some stages of trypanosome cell cycle. It was hypothesised that LmxDIP13 may be a putative marker protein for cell division and could be used to identify different cell cycle stages in *Leishmania*. This led to the investigation into the localisation of LmxDIP13 in wild type *L. mexicana* and the LmxMPK2 null mutant using N-terminally GFP-tagged LmxDIP13.

I hypothesise that LmxMPK2 possesses an unusual activation mechanism and dephosphorylated LmxMPK2 will be capable of autophosphorylation (similar to LmxMPK1). It appears LmxMPK2 may influence microtubule dynamics and localisation within *L. mexicana* should clarify its role. Additionally, DIP13 associates with microtubules in *T. brucei*, a similar localisation will be observed in *L. mexicana*. Moreover, a relationship will exist between LmxMPK2 and LmxDIP13.

The aims of this project were:

- I. Characterise the phenotype of homozygous LmxMPK2 null mutants and the genomic add-backs
- II. Generate dephosphorylated recombinant kinase for use in kinase assays
- III. Assess activation mechanism of LmxMPK2 *in vitro*
- IV. Generate green fluorescent protein (GFP)-tagged LmxMPK2 and express in wild type *L. mexicana* promastigotes as well as *LmxMPK2* null mutant promastigotes. Assess *in vivo* localisation and elucidate the role of LmxMPK2
- V. Generate green fluorescent protein (GFP)-tagged LmxDIP13 and express in wild type *L. mexicana* promastigotes as well as *LmxMPK2* null mutant promastigotes. Assess the *in vivo* localisation of LmxDIP13, assess its potential as a cell cycle marker and ascertain its relationship with LmxMPK2

The results generated fulfilling aims (II) and (III) should also allow a conclusion to be made about the mechanism of activation and regulation of the activity of LmxMPK2.

I hypothesise that LmxMPK2 possesses an unusual activation mechanism and dephosphorylated LmxMPK2 will be capable of autophosphorylation (similar to LmxMPK1). LmxMPK2 may influence microtubule dynamics and localisation within *L. mexicana* will elucidate its role. Additionally, DIP13 associates with microtubules in *T. brucei*, a similar localisation will be observed in *L. mexicana*. Moreover, a relationship will exist between LmxMPK2 and LmxDIP13.

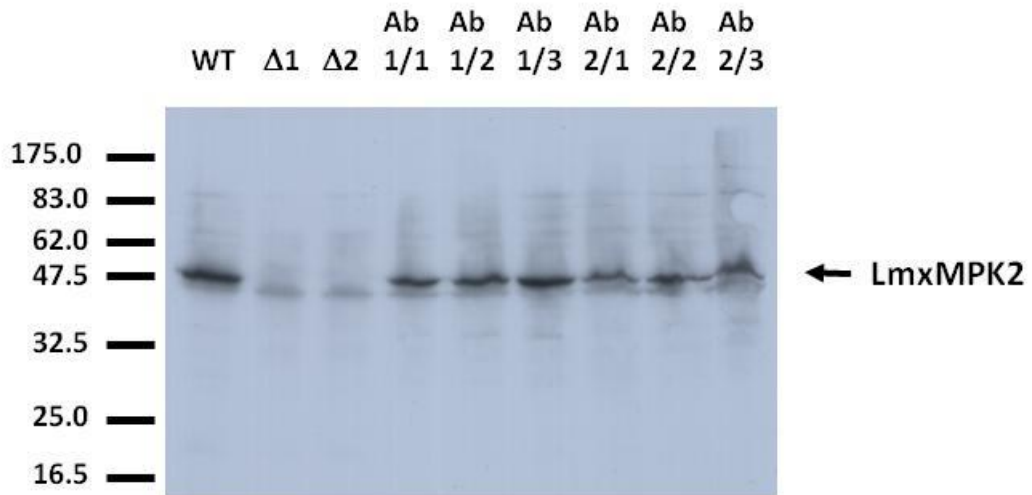


Figure 1.9: Immunoblot assessing presence of LmxMPK2 in total cell lysates

Total cell lysates at a concentration of 2×10^7 wild type (WT), $\Delta LmxMPK2^{-/-}$ ($\Delta 1$, $\Delta 2$) and $\Delta LmxMPK2^{-/-}$ + *gMPK2* promastigotes were subjected to immunoblot to confirm the presence or absence of LmxMPK2. (Mandal *et al.*, 2012).

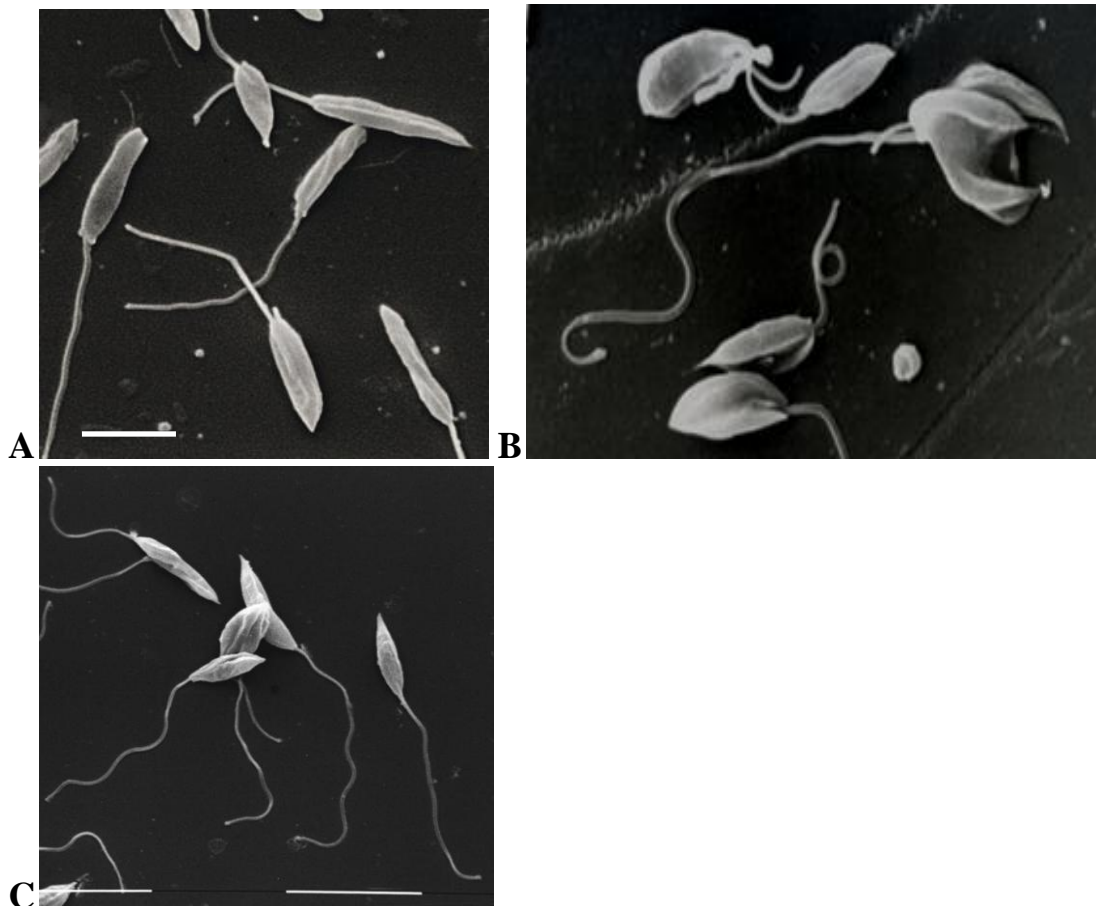


Figure 1.10: Scanning electron micrographs of *L. mexicana* promastigotes.

A, wild type; B, $\Delta LmxMPK2^{-/-}$; C, $\Delta LmxMPK2^{-/-}$ + *gMPK2*. Bar 10 μm (Wiese, unpublished)

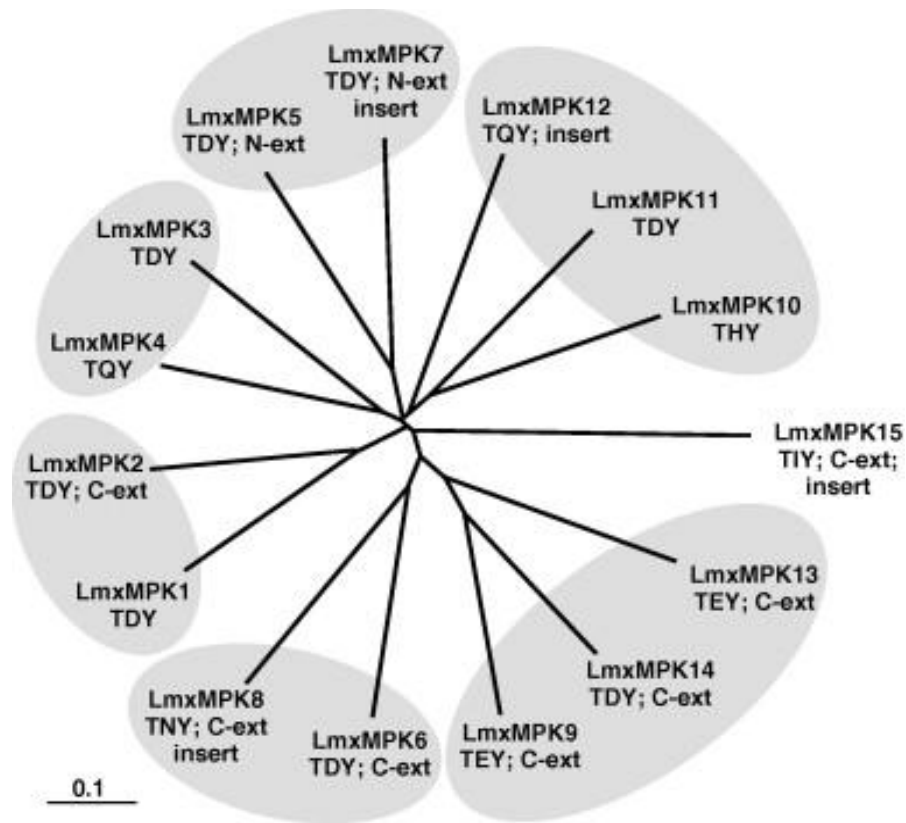


Figure 1.11: Phylogenetic tree of the *Leishmania mexicana* MAP kinases.

The residues of the TXY motif are indicated. N-ext, N-terminal extension longer than 40 amino acids; C-ext, C-terminal extension longer than 100 amino acids; insert, denotes the presence of insert(s) (Wiese, 2007).

1.4.2 LmxGSK3- β

Glycogen-synthase kinase 3- β (GSK3- β) is a ubiquitous protein and an important regulator of several cellular processes in eukaryotes. The gene encoding the *Leishmania mexicana* homologue was found to be 1,068 bp long. The protein it encodes, LmxGSK3- β , is composed of 355 amino acids and has a molecular mass of 40.7 kDa.

The protein shows strong amino acid identity to homologues in other *Leishmania* species; *L. infantum* 98%, *L. major* 97% and *L. braziliensis* 92%. However, it shares lower amino acid identity with other kinetoplastids; 68% identity with *Trypanosoma cruzi* and 65% identity with *Trypanosoma brucei*. The closest human homologue is HsGSK3- β which shows only 40.9% sequence identity.

GSK3- β is serine/threonine kinase which has been shown to be constitutively active under basal conditions in cells (Wang *et al.*, 2011). It is an important regulator of several cellular processes in eukaryotes including glycogen metabolism, cell proliferation, motility and apoptosis which has attracted attention as a potential drug target. It has been implicated in a wide variety of human illnesses such as diabetes mellitus, Alzheimer's dementia, osteoporosis and atherosclerosis (Phukan *et al.*, 2010) highlighting the importance and versatility of this kinase. It is therefore understandable that GSK3 has been the subject of a lot of research in human disease since the 1980's. More recently, it has been identified as a potential target for the treatment of human African trypanosomiasis and leishmaniasis (Xingi *et al.*, 2009; Ojo *et al.*, 2008). Although the catalytic domain is well conserved between the orthologues, they are sufficiently different to allow for the design of parasite specific inhibitors.

Although the activity of human GSK3- β is well documented, the activity of LmxGSK3- β is less well known. Since GSK3 possesses a highly conserved catalytic domain, LmxGSK3- β is likely to be constitutively active on a tyrosine residue. Previous work within the laboratory focused on generating LmxGSK3- β null mutants. All attempts to generate a null mutant by replacing the two alleles of *LmxGSK3- β* using resistance conferring genes using homologous recombination failed. However, when providing a

copy of the wild type *LmxGSK3-β* on a plasmid both alleles could be deleted. The $\Delta LmxGSK3-\beta$ $-/-$ + pLmxGSK3- β retained a normal phenotype. When used in mouse infection studies it was found that parasites expressing $\Delta LmxGSK3-\beta$ $-/-$ + pLmxGSK3- β had reduced infectivity and produced significantly less lesion development than wild type *L. mexicana* (figure 1.12). Promastigotes derived from amastigotes which had been isolated from mouse lesions 4 weeks post infection were used in a limited dilution study and cultivated in the absence of any antibiotic selection (Puromycin). Using polymerase chain reaction (PCR) we found the parasite was unable to lose the plasmid and therefore showed it to be essential in the promastigote stage (figure 1.13, unpublished data – representative of 98 samples). Having shown LmxGSK3- β as essential to both life stages of *L. mexicana* suggested it would be an ideal drug target.

The aims of this project were:

- I. Generate dephosphorylated recombinant kinase for use in kinase assays
- II. Characterise the phosphorylation states of LmxGSK3- β
- III. Test novel inhibitors against LmxGSK3- β

As a highly conserved kinase, I hypothesis that LmxGSK3- β will exhibit a similar activation mechanism to that of orthologues in higher eukaryotes. The Malabaricone inhibitors will possess potent anti-leishmania activity, as previously described (Sen *et al.*, 2007). Moreover, these inhibitors will be effective against LmxGSK3- β .

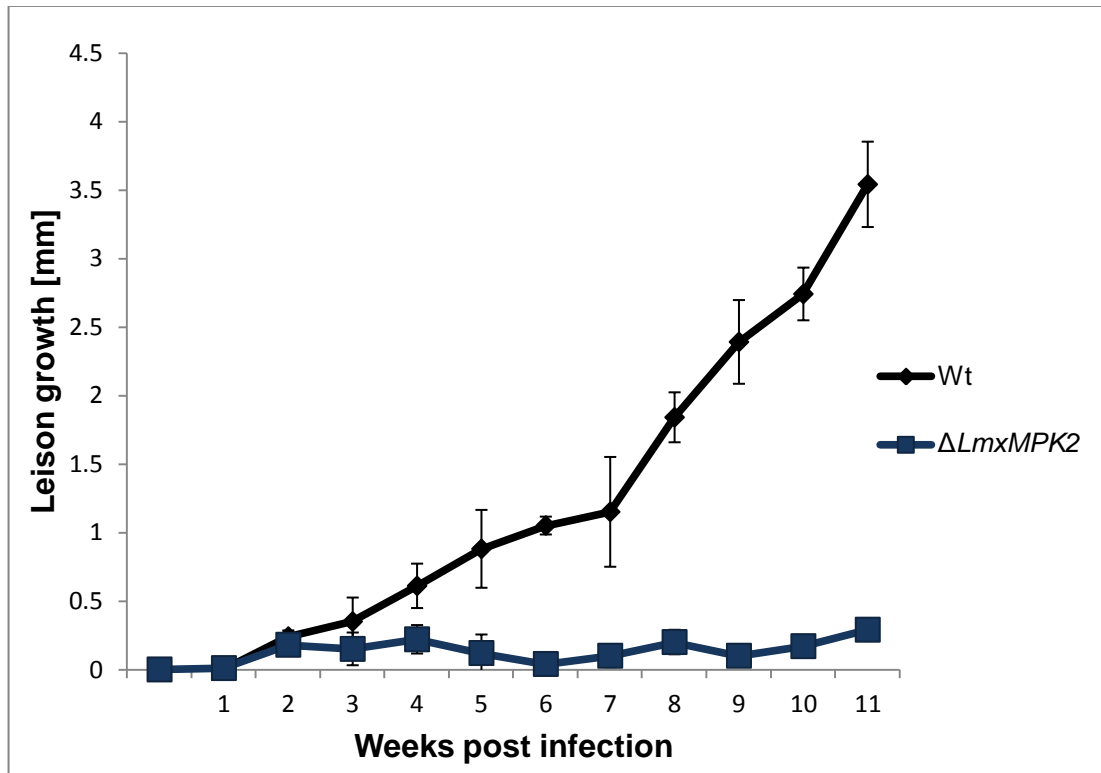


Figure 1.12: Growth of Balb/c footpad lesion caused by *L. mexicana* wild type and $\Delta LmxGSK3\text{-}\beta$ + pLmxGSK3- β promastigotes. (n=5). (Munro, 2009).

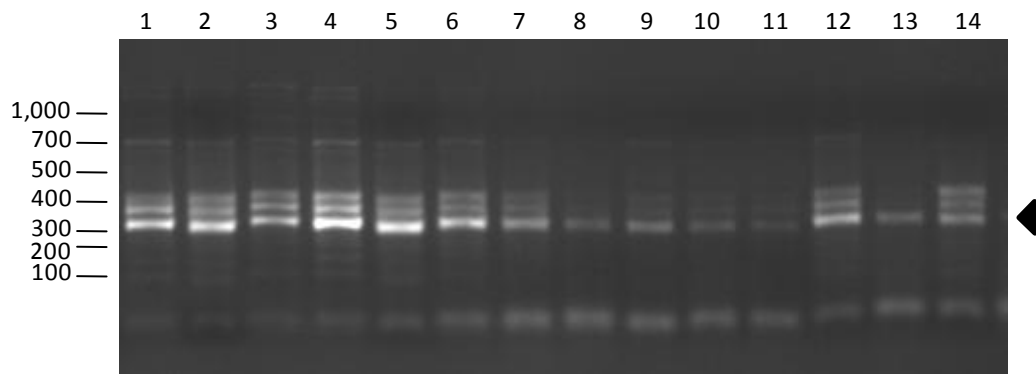


Figure 1.13: PCR assessing LmxGSK3- β plasmid retention in promastigotes derived from amastigotes (4 weeks in mouse)

Lanes 1-10, PCR samples amplifying LmxGSK3- β from cloned promastigotes derived from amastigotes after 4 week in Balb/c mouse cultivated in the absence of puromycin. Lanes 11-14 cloned promastigotes cultured in absence of puromycin (never introduced into mouse). Samples separated on a 1.2% agarose gel. Black arrow indicated LmxGSK3- β (representative of 98 samples). (Munro, 2009)

2. Materials and Methods

2.1 Materials

2.1.1 Laboratory Equipment

Centrifuges

Centrifuge 5424	Eppendorf, Hamburg, Germany
Centrifuge 5415R	Eppendorf, Hamburg, Germany
HERMLE Z 400 K	HermleLabortechnik, Wehingen, Germany

CO₂ incubator

BBK 6220	Kendro Laboratory Products, Hanau, Germany
----------	---

Electrophoresis equipment

Minigel (Twin) Tank	Biometra, Göttingen, Germany
Power supply: Consort E734	Consort, Turnhout, Belgium
Power supply: Gene Power Supply GPS 200/400	Amersham Biosciences, Freiburg, Germany

Immunoblotting equipment

Fastblot B33 / B34	Biometra, Göttingen, Germany
--------------------	------------------------------

In vivo imaging system

IVIS (<i>In vivo</i> Imaging System) 200 series	CaliperLifeScience, Runcorn, UK
---	---------------------------------

Heat block

Thermomixer comfort	Eppendorf, Cambridge, UK
---------------------	--------------------------

Microscopes

Axiovert 25	Carl Zeiss, Jena, Germany
Axiostar plus	Carl Zeiss, Jena, Germany
Nikon TE2000S (inverted, epifluorescent)	Nikon Instruments, Derby, UK
CFI Plan Fluor DLL-100X objective lens	
Camera: Hamamatsu Orca-285	

pH Meter

Digital-pH-Meter CG 820	Schott, Hofheim am Taunus, Germany
Microprocessor pH meter, HI 1221	Hannah instruments, UK

Photometer

BioPhotometer 6131	Eppendorf, Hamburg, Germany
Pharmacia LKB Ultrospec III	Pharmacia, Milton Keynes, UK

Shaking incubators

Innova 4230/4400 USA	New Brunswick Scientific, Edison, NJ,
-------------------------	---------------------------------------

Shaking water baths

GFL 1083	GFL, Burgwedel, Germany
mgw LAUDA M3	Heidolph Electro, Kehlheim, Germany

Sonicator

Branson Sonifier 250	Branson, Danbury, CT, USA
----------------------	---------------------------

Thermocyclers

Gene Amp PCR System 9700	PE Applied Biosystems, Weiterstadt, Germany
Gene Amp PCR System 2400	PE Applied Biosystems, Weiterstadt, Germany

Tissue Culture Hood

Thermo SAFE 2020, Class II Safety Cabinet

Fischer Scientific, Loughborough, UK

Transfactor

Nucleofector II

AmaxaBiosystems, Gaithersburg, MD, USA

Vortex

IKA-VIBRO-FIX VF2

IKA Labortechnik, Staufen, Germany

UV transilluminators

VWR Genosmart

VWR International, Lutterworth, UK

High Performance UV Transilluminator

UVP, Cambridge, UK

2.1.2 Glassware and consumables

Biodyne A nylon membrane

Pall, Dreieich, Germany

Complete EDTA-free protease inhibitor tablets

Roche Diagnostics, Burgess Hill, UK

Gel drying frames

Sigma-Aldrich, Gillingham, UK

Immobilon-P PVDF membrane

Millipore, Schwalbach, Germany

Neubauer counting chambers

VWR International, Darmstadt, Germany

Parafilm M

Brand GmbH, Wertheim, Germany

Plastic consumables`

Eppendorf, Cambridge, UK
Sarstedt, Leicester, UK
Greiner Bio-One, Solingen, Germany
Nunc, Langenselbold, Germany
VWR International, Lutterworth, UK

X-ray films

FotochemischeWerke, Berlin, Germany

2.1.3 Chemicals

[γ - ³² P]-ATP	Hartmann Analytics GmbH, Braunschweig, Germany
Acetic acid	Carl Roth, Karlsruhe, Germany
Acrylamide 30% (w/v) /Bis-acrylamide 0.8% (w/v)	VWR, Lutterworth, UK
Adenosine triphosphate (ATP)	Roche Diagnostics, Sussex, UK
Agar-Agar	Techmate Ltd, Milton Keynes, UK
Agarose (electrophoresis grade)	Techmate Ltd, Milton Keynes, UK
Ammonium chloride	Sigma-Aldrich, Steinheim, Germany
Ammonium persulfate (APS)	VWR, Lutterworth, UK
Ampicillin	Sigma-Aldrich, Steinheim, Germany
BactoTryptone	Becton Dickinson, Heidelberg, Germany
Boric acid	Techmate Ltd, Milton Keynes, UK
Bovine serum albumine (BSA)	Sigma-Aldrich, Steinheim, Germany
Bromophenol blue	Sigma-Aldrich, Steinheim, Germany
Calcium chloride	Techmate Ltd, Milton Keynes, UK
Chelating sepharose fast flow	GE Healthcare, Little Chalfont, UK
Chloroform	Techmate Ltd, Milton Keynes, UK
Cobalt chloride	Carl Roth, Karlsruhe, Germany
Coomassie Brilliant Blue G250	Techmate Ltd, Milton Keynes, UK
Coomassie Brilliant Blue R250	Techmate Ltd, Milton Keynes, UK
DABCO	Sigma-Aldrich, Steinheim, Germany
DAPI	Sigma-Aldrich, Steinheim, Germany
Disodium hydrogen phosphate dihydrate	Techmate Ltd, Milton Keynes, UK
DMSO	Techmate Ltd, Milton Keynes, UK
dNTP mix	Roche Diagnostics, Mannheim, Germany
DTT	Biomol, Hamburg, Germany
EDTA disodium dihydrate	Techmate Ltd, Milton Keynes, UK

EGTA	Techmate Ltd, Milton Keynes, UK
Ethanol	Techmate Ltd, Milton Keynes, UK
Ethidium bromide	Sigma-Aldrich, Steinheim, Germany
FCS	PAN Biotech, Aidenbach, Germany
Formaldehyde 37% (Formaline)	Carl Roth, Karlsruhe, Germany
Formamide	Techmate Ltd, Milton Keynes, UK
Glucose	Techmate Ltd, Milton Keynes, UK
Glutaraldehyde	Merck, Darmstadt, Germany
Glutathione, reduced	Sigma-Aldrich, Steinheim, Germany
Glutathione Sepharose 4B	GE Healthcare, UK
Glycerol	Techmate Ltd, Milton Keynes, UK
Glycine	Techmate Ltd, Milton Keynes, UK
Hemin	Sigma-Aldrich, Steinheim, Germany
HEPES	Techmate Ltd, Milton Keynes, UK
Hydrochloric acid	Techmate Ltd, Milton Keynes, UK
Hygromycin B	Merck Biosciences, Schwalbach, Germany
Imidazole	Techmate Ltd, Milton Keynes, UK
IPTG	GerbuBiochemicals, Gaiberg, Germany
Isoamyl alcohol	Techmate Ltd, Milton Keynes, UK
Isopropanol	Techmate Ltd, Milton Keynes, UK
Kanamycin sulfate	VWR, Lutterworth, UK
Leupeptin	Sigma-Aldrich, Steinheim, Germany
L-Glutamine	PAN Biotech, Aidenbach, Germany
Lithium chloride	Sigma-Aldrich, Steinheim, Germany
Luciferin solution	Calliper LifeScience, UK
Magnesium chloride hexahydrate	Techmate Ltd, Milton Keynes, UK
Magnesium sulfate	Merck, Darmstadt, Germany
Maleic acid	Techmate Ltd, Milton Keynes, UK
Manganese chloride	Merck, Darmstadt, Germany
MBP dephosphorylated	Millipore, UK
MES	Fischer Scientific, Loughborough, UK
Methanol	Carl Roth, Karlsruhe, Germany

Milk powder	Carl Roth, Karlsruhe, Germany
MOPS	Sigma-Aldrich, Gillingham, UK
Mowiol 4-88	Merck, Darmstadt, Germany
Neomycin (G418)	Roche Diagnostics, Mannheim, Germany
N-Lauroylsarcosine sodium salt	VWR, Lutterworth, UK
Okadaic acid	Merck, Darmstadt, Germany
ortho-Phenanthroline	Sigma-Aldrich, Steinheim, Germany
ortho-Phosphoric acid	Carl Roth, Karlsruhe, Germany
Paraformaldehyde	VWR, Lutterworth, UK
Penstrep (1000 U/ml Penicillin, 10 mg/ml Streptomycin)	Life Technologies, Carlsbad, USA
Phenol, equilibrated in TE buffer pH 7.5-8.0	Techmate Ltd, Milton Keynes, UK
Phleomycin (Bleomycin)	Merck Biosciences, Schwalbach, Germany
PMSF	Sigma-Aldrich, Steinheim, Germany
Poly-L-Lysine hydrobromide	Sigma-Aldrich, Steinheim, Germany
Potassium acetate	Techmate Ltd, Milton Keynes, UK
Potassium chloride	Sigma-Aldrich, Gillingham, UK
Potassium dihydrogen phosphate	Merck, Darmstadt, Germany
Puromycindihydrochloride	Techmate Ltd, Milton Keynes, UK
Rubidium chloride	Sigma-Aldrich, Gillingham, UK
Saponin	Carl Roth, Karlsruhe, Germany
Schneider's Drosophila medium	PAN Biotech, Aidenbach, Germany
SDM medium	Generon, Maidenhead, UK
Silver nitrate	Techmate Ltd, Milton Keynes, UK
Sodium acetate trihydrate	Techmate Ltd, Milton Keynes, UK
Sodium carbonate	Techmate Ltd, Milton Keynes, UK
Sodium chloride	Sigma-Aldrich, Gillingham, UK
Sodium dihydrogen phosphate	Merck, Darmstadt, Germany
Sodium dodecyl sulfate (SDS)	Fischer Scientific, Loughborough, UK
Sodium fluoride	Merck, Darmstadt, Germany
Sodium hydroxide	Techmate Ltd, Milton Keynes, UK

Sodium orthovanadate	Sigma-Aldrich, Steinheim, Germany
Sodium thiosulfate pentahydrate	Techmate Ltd, Milton Keynes, UK
TEMED	Sigma-Aldrich, Steinheim, Germany
Tetracycline	Sigma-Aldrich, Steinheim, Germany
Trisodium citrate	Techmate Ltd, Milton Keynes, UK
TLCK	Sigma-Aldrich, Steinheim, Germany
Triton X-100	Techmate Ltd, Milton Keynes, UK
Trizma	Sigma-Aldrich, Gillingham, UK
Tween 20	Techmate Ltd, Milton Keynes, UK
X-Gal	Roche Diagnostics, Mannheim, Germany
Xylenecyanol	Sigma-Aldrich, Steinheim, Germany
Yeast extract	Fluka, Gillingham, UK
β -mercaptoethanol	Techmate Ltd, Milton Keynes, UK

2.1.4 Media and Buffers

Agarose gel loading buffer (10 \times)	0.1 M EDTA pH 8.0 0.1% (w/v) bromophenol blue 0.1% (w/v) xylenecyanol 0.5 \times TBE 50% (v/v) glycerol
Ammonium Persulphate (10%)	10% (w/v) Ammonium Persulphate dissolved in ddH ₂ O
Bradford reagent	5% (v/v) ethanol 0.01% (w/v) Coomassie Brilliant Blue G250 10% (v/v) phosphoric acid Filtered, stored at 4°C, in opaque container
Complete EDTA-free protease inhibitor cocktail	1 tablet complete EDTA-free (Roche) in 2 ml PBS
Coomassie R250 destaining solution	30% (v/v) methanol 10% (v/v) acetic acid

Coomassie R250 staining solution	0.1% (w/v) Coomassie Brilliant Blue R250 40% (v/v) methanol 10% (v/v) acetic acid Filtered through fluted filter
Cryo medium for <i>Leishmania</i>	90% (v/v) iFCS 10% (v/v) DMSO
DAPI stock solution	160 µg/ml in methanol
Fixing solution for <i>Leishmania</i> cell counting	3.7% (w/v) formaldehyde in 1× PBS
Gel drying solution	20% (v/v) ethanol 10% (v/v) glycerol
GST elution buffer	10 mM reduced glutathione 50 mM Tris-HCl pH 8.0
Hemin stock solution	2.5 mg/ml in 50 mM NaOH
His-purification binding buffer	50 mM Tris-HCl pH 8.0 1 M NaCl 10% (v/v) glycerol 20 mM imidazole
His-purification elution buffer	50 mM Tris-HCl pH 8.0 300 mM NaCl 10% (v/v) glycerol 500 mM imidazole 1 mM PMSF
His-purification washing buffer	50 mM Tris-HCl pH 8.0 1 M NaCl 10% (v/v) glycerol 10 mM imidazole
iFCS	FCS inactivated for 45 min at 56°C, filter sterilised
Immunoblot blocking solution I	5% (w/v) milk powder 20 mM Tris-HCl pH 7.5 in 1 × PBST
Immunoblot blocking solution II	5% (w/v) BSA in 1 × TBST

Immunoblot stripping solution	62.5 mM Tris-HCl pH 6.7 2% (w/v) SDS 0.78% (v/v) 2-mercaptoethanol
Immunoblot transfer buffer	25 mM Trizma 150 mM glycine 10% (v/v) methanol
Kinase-Glo® buffer	40 mM Tris/HCl 10 mM MgCl ₂ 0.1 mg/ml BSA Adjusted to pH 7.4
Kinase reaction buffer LmxMPK2 (10 ×)	20 mM MnCl ₂ 500 mM Tris/HCl pH 7.0 1 M NaCl
Kinase reaction buffer standard (10 ×)	20 mM MnCl ₂ 100 mM MgCl ₂ 500 mM MOPS pH 7.2 1 M NaCl
LB agar	1.5% (w/v) agar-agar in LB medium autoclaved for sterilisation (if required, antibiotics were added after LB agar had cooled to ca. 50°C)
LB medium	1% (w/v) bactotryptone 0.5% (w/v) yeast extract 1% (w/v) NaCl Autoclaved for sterilisation (If required, antibiotics were added after LB medium had cooled to ca. 50°C)
<i>Leishmania</i> lysis buffer for immunoblot	1 × PBS 0.1 (w/v) SDS 50 mM DTT 1 × SDS-PAGE loading buffer 1 mM PMSF 50 µM leupeptin 10 mM ortho-phenantroline 25 µM TLCK
PBS (10 ×)	137 mM NaCl 2.7 mM KCl

	10.1 mM Na ₂ HPO ₄ 1.8 mM KH ₂ PO ₄
PBST (1 ×)	0.2% (v/v) Tween 20 in 1x PBS
RF1	100 mM RbCl 50 mM MnCl ₂ ·4H ₂ O 10 mM CaCl ₂ ·2H ₂ O 30 mM potassium acetate 15% (v/v) glycerol Adjusted to pH 5.8, filter-sterilised
RF2	10 mM RbCl 75 mM CaCl ₂ ·2H ₂ O 10 mM MOPS 15% (v/v) glycerol Adjusted to pH 6.8, filter-sterilised
Schneider's Drosophila medium	Complete 20% (v/v) iFCS (PAN) 1% (v/v) penstrep 1% (v/v) L-glutamine 3.9 mg/ml MES in Schneider's Drosophila medium Filter-sterilised
SDM medium complete	10% (v/v) iFCS 1% (v/v) penstrep 7.5 µg/ml hemin in SDM medium Filter-sterilised
SDS-PAGE electrophoresis buffer (10 ×)	0.25 M Trizma 1.92 M glycine 1% (w/v) SDS
SDS-PAGE sample buffer (5 ×)	62.5 mM Tris-HCl pH 6.8 20% (v/v) glycerol 2% (w/v) SDS 0.001% (w/v) bromophenol blue 200 mM DTT
SDS-PAGE resolving gel buffer (4 ×)	1.5 M Tris base 0.4% (w/v) SDS Adjusted to pH 8.8
SDS-PAGE stacking gel buffer (4 ×)	0.5 M Tris base 0.4% (w/v) SDS Adjusted to pH 6.8

Silver stain sensitizing solution	0.02% Na ₂ S ₂ O ₃ in ddH ₂ O
Silver stain solution	0.1% AgNO ₃ in ddH ₂ O
Silver stain developing solution	0.04% formalin 2% Na ₂ CO ₃ in ddH ₂ O
Silver stain stop solution	1% Acetic acid in ddH ₂ O
TBE (5 ×)	0.45 M Trizma 0.45 M boric acid 10 mM EDTA pH 8.0
TBS (10 ×)	200 mM Tris-HCl pH 7.5 150 mM NaCl
TBST (1 ×)	0.05% (v/v) Tween 20 in TBS
TENS	10 mM Tris-HCl pH 8.0 1 mM EDTA pH 8.0 100 mM NaOH 0.5% (w/v) SDS

2.1.5 Bacterial Strains

Description	Genotype	Source
BL21 (DE3) [pAPlacIQ]	B F ⁻ dcmompThsdS(r _B ⁻ m _B ⁻) gal λ(DE3) [pAPlacIQ]	Joachim Clos, Hamburg, Germany
XL1-Blue	ecAendA gyrA96 thi-1 hsdR17 supE44 rel A1 lac [F' proAB lac ^q ZΔM15 Tn10 (Tet ^R)]	Stratagene, La Jolla, CA, USA
BL21(DE3)	B F ⁻ dcmompThsdS(r _B ⁻ m _B ⁻) gal λ(DE3)	Stratagene, La Jolla, CA, USA

2.1.6 Leishmania strain

Leishmania mexicana mexicana MNYC/BZ/62/M379, clone 2

Δ*LmxMPK2* -/- K1

Mandal et al., 2012

$\Delta LmxMPK2$ -/- K2	Mandal et al., 2012
$\Delta LmxMPK2$ -/- K1 + g <i>LmxMPK2</i> K1	Weise, Unpublished
$\Delta LmxMPK2$ -/- K2 + g <i>LmxMPK2</i> K3	Wiese, Unpublished
$\Delta LmxMPK2$ -/- K1 + pXMPK2GFP	Munro, PhD Thesis, 2013
$\Delta LmxMPK2$ -/- K2 + pXMPK2GFP	Munro, PhD Thesis, 2013
$\Delta LmxMPK2$ -/- K1 + pXPACGFPDIP13	Munro, PhD Thesis, 2013
$\Delta LmxMPK2$ -/- K2 + pXPACGFPDIP13	Munro, PhD Thesis, 2013

2.1.7 Oligonucleotides

Description	Sequence
Mapkin22_5.for	5' GCC TCG CTG CGC CGT ATC T 3'
Mapkin22_5.rev	5' GAT GAT TCG TTG ACT CCA 3'
Mapkin22_1.for	5' CTG CTC GTA AAC AGC GAC T 3'
pXPHLEO anti	5' TCC CCG CGC GTT GGC CGA T 3'
pXPHLEO2	5' AAA CCG CTC GCG GTG TGT T 3'

2.1.8 DNA vectors and plasmid constructs

<u>Name</u>	<u>Source</u>
pJC-MPK2	Wiese, unpublished
pGEXKG17-mapkin22	Wiese, unpublished
pJC-MPK1PTP1B	McAler, PhD Thesis, 2012
pJC-MPK1- λ -phosphatase	McAler, PhD Thesis, 2012
pMK-RQMPK2	Mr Gene, Regensburg, Germany
pX2PACMPK2	Wiese, unpublished
pX63-MPK1sHAGFP	McAler, PhD Thesis, 2012
pXPolPACNcoI	Wiese, unpublished
pTHcGFPDIP13	Wiese, unpublished
pJC-GSK3 β	Wiese, unpublished
pJC-MPK2- λ	Munro, PhD Thesis, 2013
pJC-MPK2-PTP1B	Munro, PhD Thesis, 2013

pMK-PACMPK2	Munro, PhD Thesis, 2013
pXMPK2GFP	Munro, PhD Thesis, 2013
pXPACGFPDIP13	Munro, PhD Thesis, 2013
pJCGSK3PTP1B	Munro, PhD Thesis, 2013
pJCGSK3- λ	Munro, PhD Thesis, 2013

2.1.9 Antibodies

Primary antibodies

<u>Antigen / Name</u>	<u>Host</u>	<u>Dilution</u>	<u>Source</u>
Phosphotyrosine / 4G10 (hybridoma cell supernatant)	mouse	1:2500	Bernhard Fleischer, BNI, Hamburg
anti-mapkin 22	Rabbit	1:500	Wiese, 1998
anti-Phosphothreonine (72-8300)	Rabbit	1:2000	Invitrogen, UK

Secondary antibodies

<u>Antigen / Name</u>	<u>Host</u>	<u>Dilution</u>	<u>Source</u>
Mouse IgG (HRP-conjugated)	rabbit	1:2000	DAKO, Hamburg, Germany
Mouse IgG (HRP-conjugated)	Goat	1:20,000	Promega,
Rabbit IgG (HRP-conjugated)	swine	1:5000	DAKO, Hamburg, Germany

One-step antibody

<u>Antigen / Name</u>	<u>Host</u>	<u>Dilution</u>	<u>Source</u>
anti-GFP coupled directly to HRP	Mouse	1:1000	MiltenyiBiotec, Surrey, UK

2.1.10 Enzymes

Alkaline phosphatase, shrimp	Roche Diagnostics, Mannheim, Germany
Expand High Fidelity PCR System	Roche Diagnostics, Mannheim, Germany
Restriction endonucleases	New England Biolabs, Hitchin, UK
RNase A (bovine pancreas)	Roche Diagnostics, Mannheim, Germany
T4 DNA ligase	Roche Diagnostics, Mannheim, Germany
Basemuncher	Expedeon, Cambridge, UK

2.1.11 Molecular biology kits

Human T Cell Nucleofector Kit	Amata Biosystems, Gaithersburg, USA
M&N NucleoSpin Extract II Kit	Macherey& Nagel, Düren, Germany
M&N NucleoSpin Plasmid Kit	Macherey& Nagel, Düren, Germany
M&N NucleoBondXtra Midi Kit	Macherey& Nagel, Düren, Germany
SuperSignal West Pico	Pierce/Perbio Science, Bonn, Germany
Chemiluminescent Substrate Kit	

2.1.12 DNA and protein molecular weight markers

1kb DNA Ladder	Carl Roth, Karlsruhe, Germany
100bp DNA Ladder	New England Biolabs, Hitchin, UK
λ -DNA ladder	New England Biolabs, Hitchin, UK
PCR Marker	New England Biolabs, Hitchin, UK
Prestained Protein Marker, Broad Range	New England Biolabs, Hitchin, UK

2.2 Methods

2.2.1 Cell biology methods

2.2.2 Culturing of *E. coli*

2.2.2.1 Culturing on medium plates

A maximum volume of 200 µl transformed *E. coli* cells were evenly distributed on LB agar plates containing required antibiotics using a sterile spreader. Antibiotics were used to select positive clones at concentrations of 100 µg/ml (ampicillin), 50 µg/ml (kanamycin) and 20 µg/ml (tetracycline). The inoculated agar plates were incubated upside down over night at 37°C.

2.2.2.2 Culturing in liquid medium

A single colony of *E. coli*, taken with a sterile 100 µl pipette tip from freshly incubated agar plates, or an aliquot of a liquid pre-culture to a final concentration of no more than 1% (v/v) were used to inoculate an appropriate volume of LB medium. Antibiotics were, if required, added to the same concentrations as mentioned in 2.2.2.1 The cultures were incubated in a shaking incubator at 37°C and 220 rpm until they had reached the required optical density.

2.2.2.3 Preparation of glycerol stocks

500 µl was taken from an overnight culture and carefully mixed with 500 µl sterile glycerol in a sterile cryotube. The mixture was incubated for 10 minutes on ice and subsequently stored at -70°C.

2.2.3 Culturing of *Leishmania*

2.2.3.1 Culturing of *Leishmania mexicana* promastigotes

L. mexicana promastigotes were cultivated at 27°C in SDM medium (Brun, R. *et al.*, 1977), containing antibiotics if required. The antibiotics were used at a concentration of

5 µg/ml (phleomycin/bleomycin), 20 µg/ml (hygromycin B), 10 µg/ml (G418/neomycin) and 40 µM (puromycin). Cultures were passaged every 3-4 days (on reaching late log phase to early stationary phase) by inoculating a fresh culture with a ratio of 1:500 to 1:1,000 using a sterile disposable plastic pastette.

2.2.3.2 Preparation of *Leishmania cryostabilates*

Cryo medium (2 ml/culture) was prepared and chilled on ice. A standard 10 ml late log-phase promastigote culture ($2-3 \times 10^7$ cells/ml) was sedimented by centrifugation for 10 min at $5,200 \times g$, 4°C, the supernatant was removed and the cell pellet was resuspended in 2 ml of cryo medium, then distributed to four cryo tubes (500 µl/tube). The cryo tubes were placed in the gas phase of liquid nitrogen overnight and then submerged in the liquid phase for long-term storage.

2.2.3.3 Defrosting and re-culturing of *Leishmania stabilates*

Cryo tubes with frozen cells were removed from liquid nitrogen and rapidly defrosted in a water bath at 37°C then transferred to 10 ml of SDM medium containing antibiotics if required. The cultures were incubated overnight at 27°C then used to sub-cultured to a fresh 10 ml SDM medium.

2.2.3.4 *Leishmania* cell counting

10 µl of the *Leishmania* culture were diluted in fixing solution to the appropriate ratio and the cell suspension was loaded onto a Neubauer chamber (0.1 mm, 0.0025 mm²) for cell counting using a light microscope. The whole area (two large squares) was counted and the average value was used to calculate the cell density using the following formula: number of cells/ml = number of counted cells \times diluting factor $\times 10^4$.

2.2.3.5 Proliferation curve

Proliferation curves were performed on a 24-well plate, with each curve performed in quadruplicate. 1ml of SDM-79 (complete) was seeded with *Leishmania mexicana* cells at a density of 5×10^5 cells/ml. At each time point a sample was taken from each well and diluted in fixing solution at an appropriate dilution (ranging from 1:10 to 1:100) for up to 10 days. Each sample was counted as described in 2.2.3.4 and the average of each quadruplicate was taken as cell density.

2.2.4 Mouse footpad infection studies

All footpad infection studies were conducted with female 6-12 weeks old BALB/c mice. *Leishmania* promastigotes from a culture in late log-phase ($3-4 \times 10^7$ cells/ml) were harvested by centrifugation at $5,600 \times g$ for 20 s, washed with ice-cold PBS and resuspended in PBS to a final density of 3.3×10^8 cells/ml. Each mouse was infected into the left hind footpad with 30 μ l of the *Leishmania* cell suspension, equalling 1×10^7 cells. Both hind paws were measured regularly with the help of a calliper gauge to monitor lesion development.

2.2.4.1 Isolation of *L. mexicana* from mouse footpads

The severed footpads were sterilised with 70% ethanol, cut into pieces and transferred into 10 ml of ice-cold PBS. To disrupt tissues and liberate amastigotes from macrophages, the pieces were passed through a sterile metal grid. The resulting debris was collected in a sterile petri dish within the PBS used to rinse the grid. The suspension was transferred to sterile centrifugation tubes and cell debris was removed by centrifugation for 10 min at $150 \times g$ and 4°C . The supernatant was again centrifuged at $1,500 \times g$ at 4°C for 10 min to sediment amastigotes, which were subsequently resuspended in 10 ml ice-cold PBS.

2.2.5 Molecular biology methods

2.2.5.1 Preparation of competent *E. coli* cells

A disposable streak-loop was used to plate cells from the glycerol stock onto an LB agar plate, containing 20 µg/ml Tetracycline (XL1-Blue) or 10 µg/ml Kanamycin (BL21(DE3) [pA*PlacIQ*]). No antibiotics were required for the selection of BL21(DE3). The plate was incubated at 37°C overnight, a single colony was picked and used to inoculate a 2 ml LB culture containing required antibiotics then incubated overnight at 37°C in a shaking incubator at 220rpm. 500 µl of the pre-culture was used to inoculate 100 ml of LB medium containing 40 µg/ml Tetracycline (XL1-Blue), 10 µg/ml Kanamycin (BL21(DE3) [pA*PlacIQ*]). The culture was incubated at 37°C with 225 rpm agitation for 3-5 hours until it reached an OD₅₅₀ of 0.2. The culture was cooled on ice for 15 min then divided into two 50 ml tubes and centrifuged for 15 min at 4,000 × g and 4°C. Each cell pellet was resuspended in 16 ml of RF1, and left on ice for 90 min. The suspension was then centrifuged for 15 min at 4,000 × g and 4°C. The supernatant was discarded and the pellet was resuspended in 8 ml of RF2, left on ice for 15 min then 200 µl aliquots were made, which were quick frozen in liquid nitrogen and stored at -70°C.

2.2.5.2 Transformation of *E. coli*

Competent cells were thawed on ice and a maximum of 5 µl DNA were added to the cells (200 µl for XL1-Blue and BL21(DE3), 25 µl of BL21(DE3) [pA*PlacIQ*]), gently mixed then kept on ice for up to 45 min. The cells were then heat-shocked at 42°C in a water bath (pA*PlacIQ* cells for 45 seconds, the others for 90 seconds) then immediately placed on ice for 5 min. 800 µl of LB medium without antibiotics were added and the cells were incubated in a thermomixer for 1 hour at 37°C (600 rpm) before 100 µl and 200 µl were spread on agar plates containing the selective antibiotic(s). Plates were incubated upside down at 37°C overnight.

2.2.5.3 Transfection of *Leishmania*

Transfections were carried out using the *Amaxa* Human T Cell Nucleofector Kit. 3×10^7 late log phase promastigotes were harvested by centrifugation for 10 min at $5,600 \times g$ and 4°C then resuspended in 100 μl Human T Cell Nucleofector buffer, supplemented according to the manufacturer's instructions. DNA was added to the cell suspension at a concentration of 1-5 $\mu\text{g}/\text{ml}$ linearised DNA and 5 $\mu\text{g}/\text{ml}$ plasmid DNA and gently mixed then transferred into the provided cuvette that was pre-chilled on ice. The cells were electroporated in the *Amaxa* Nucleofector II using programme V-033 and subsequently incubated on ice for 10 min before being transferred into 10 ml SDM medium. The cells were incubated at 27°C for 24 hours after which, antibiotics were added according to the resistance gene of the transfected DNA, and the cultures were distributed to two 96-well plates (200 $\mu\text{l}/\text{well}$) in a 1:4 and 1:40 dilution. The plates were sealed with parafilm and incubated at 27°C until resistant cells grew (10-14 days).

2.2.5.4 Isolation of plasmid DNA from *E. coli*

2.2.5.4.1 Plasmid DNA mini-preparation (*TENS method, Zhou et al., 1990*)

3 ml of LB medium containing the appropriate antibiotic(s) was inoculated with a single colony from a spread LB plate of transformed *E. coli* and incubated overnight at 37°C with 220 rpm agitation. Approximately half (1.5 ml) of the culture was centrifuged for 30 s at $15,800 \times g$ at room temperature. The majority of the supernatant was decanted and the cell pellet was resuspended in the remaining ca. 100 μl by vortexing vigorously. 300 μl of TENS solution was added, the mixture was vortexed for 4 s then 150 μl of 3M sodium acetate (pH 5.2) was added and the solution was vortexed for 3 s (samples kept on ice until all had been processed). The mixture was then centrifuged at $15,800 \times g$, 4°C for 15 min. The particle-free supernatant was transferred to a fresh tube and the DNA was precipitated by the addition of 900 μl of ice-cold 100% ethanol. Following centrifugation under the same conditions as before, the pellet was washed with 1 ml of ice-cold 70% ethanol, centrifuged for 5 min at $15,800 \times g$, 4°C . The supernatant was discarded and the pellet was air-dried before being resuspended in 40 μl of ddH₂O.

2.2.5.4.2 Plasmid DNA midi-preparation using Macherey & Nagel Kits

100 ml of LB medium containing the appropriate antibiotic(s) was inoculated with a single colony from a spread LB plate of transformed *E. coli*. The culture was incubated at 37°C with 220 rpm agitation overnight. (A sterile glycerol culture, if required, was prepared as previously described 2.2.2.3) The overnight culture was centrifuged for 15 min at $4,000 \times g$, 4°C. Subsequent steps followed the instructions of the manufacturer's manual "Plasmid DNA Purification" in the chapter "High-copy plasmid purification" until the elution of the plasmid DNA. The eluate was distributed between six 1.5 ml Eppendorf tubes; 833 μ l of eluate was mixed with 583 μ l of isopropanol, before being centrifuged for 30 minutes at $15,800 \times g$ and 4°C. The supernatant was decanted and the DNA pellets were washed with 1 ml of 70% ice-cold ethanol then centrifuged for 10 min at $15,800 \times g$, 4°C. The pellets were air-dried and resuspended in a total volume of 120 μ l. The DNA was stored at -20°C

2.2.5.5 Determination of DNA concentration

The Nanodrop2000c (Thermo Scientific) was set up for nucleic acid measurement then blanked using ddH₂O. 1 μ l DNA solution was added directly to the micro-volume pedestal for concentration to be determined.

2.2.5.6 Reactions with DNA-modifying enzymes

2.2.5.6.1 Cleavage of DNA using type II restriction endonucleases

All restriction endonucleases were purchased from New England Biolabs and used according to the manufacturer's instructions with supplied buffers and BSA solution. Analytical digests of plasmid DNA were performed in a total volume of 15 μ l using 1 μ g of DNA and 5-10 U of enzyme and incubated for up to 3 h at the appropriate temperature. When using DNA isolated via the TENS method, 2 μ g of RNase A was also added. Preparative digests of plasmid DNA were performed in a total volume of 100 μ l using 10-20 μ g DNA and 30-60 U of enzyme and incubated for 3 hours.

2.2.5.6.2 Dephosphorylation of DNA 5'- ends

Linearised plasmid DNA showing compatible overhang or blunt ends were treated with shrimp alkaline phosphatase (SAP) to prevent re-ligation of the fragments. The ethanol precipitated DNA was dissolved in 25.5 µl ddH₂O. 3 µl of the provided 10 × SAP buffer and 1.5 U SAP were added, and incubated at 37°C for 2 hours. The enzyme was inactivated by heating the mixture to 65°C for 20 minutes.

2.2.5.6.3 Ligation of DNA fragments

50-100 ng vector DNA and three times more insert DNA were mixed with 1.5 µl of the provided 10 × T4 ligase buffer and 1 U T4 DNA ligase in a final volume of 15 µl. The reaction was then incubated overnight at 13°C in a thermocycler and subsequently used for bacterial transformation. Where blunt ends were used for ligation, 60 % (w/v) PEG 4000 was added to a final volume of 15%.

2.2.5.7 Agarose gel electrophoresis

0.8-1.2% (w/v) agarose gels were prepared with 0.5 × TBE and containing 0.3 µg/ml ethidium bromide. 1/10 volume of 10 × DNA loading buffer was added to the DNA samples then loaded into the gel pockets and separated at 1.4-10 V/cm in 0.5 × TBE. Nucleic acids were visualised by UV illumination with intercalated ethidium bromide, and photographed for analysis

2.2.5.8 DNA extraction from agarose gels using the NucleoSpin Extract II Kit by Macherey & Nagel

Agarose gel electrophoresis was carried out and DNA bands of interest were liberated under low intensity UV light ($\lambda = 365$ nm) using a clean scalpel. DNA was extracted according to the manufacturer's instructions. The DNA was eluted using 20-40 µl ddH₂O.

2.2.5.9 Polymerase Chain Reaction (PCR)

PCRs were conducted using the Expand High Fidelity PCR System from Roche. Reactions were set up to a final volume of 50 μ l in 200 μ l PCR tubes and contained approximately 30 ng template DNA, 1.5 μ l of each oligonucleotide primer solution (10 μ M), 5 μ l of the supplied PCR buffer that included 15 mM MgCl₂, 1 μ l of a 20 mM dNTP solution and 0.75 μ l of the supplied enzyme mix. The tubes were kept on ice during the set up and until the reaction was performed in a thermocycler. The program used depended largely on individual conditions. The annealing temperature was chosen as a few degrees under the mean melting temperature of the oligonucleotides, while the elongation time depended on the length of the amplified DNA fragment and equated roughly to 1 min per each 1.5 kb of the expected product. The overall used program was constituted like the following:

DNA denaturation	5 min	95°C	
DNA denaturation	1 min	95°C	} 25-32 cycles
Primer annealing	1 min	45-65°C	
DNA elongation	1-3 min	72°C (for products over 3 kb: 68°C)	
Final DNA elongation	7 min	72°C (for products over 3 kb: 68°C)	

2.2.6 Protein Biochemistry

2.2.6.1 Expression of recombinant proteins in *E. coli*

Competent *E. coli* cells were transformed with plasmids encoding the recombinant protein of interest as detailed in the previous section. The agar plates were incubated at 37°C overnight and the colonies harvested by washing the plates with 2 ml of sterile LB medium, which was then used to inoculate 100-200 ml of LB medium containing the appropriate antibiotic(s). The cultures were incubated at 37°C with 220 rpm agitation until it reached an optical density at 600nm (OD₆₀₀) of approximately 0.9. The cultures were cooled to 18°C and protein expression was induced by addition of Isopropyl β -D-

1-thiogalactopyranoside (IPTG) to a final concentration of 100 μ M. The cells were then incubated overnight at 18°C with 220 rpm agitation and subsequently sedimented by centrifugation at 3,500 \times g at 4°C for 15 min. Each pellet was washed in 10 ml 1 \times PBS, centrifuged as before and used in preparation of cell lysates (alternatively, the pellets could be stored at -20°C until required).

2.2.7 Preparation of *E. coli* cell lysates for protein purification

The centrifugation was repeated as before (3.3.1) and the pellet was resuspended in 5 ml cold 1 \times PBS/100ml original culture volume and kept on ice. The cells were then lysed (while still on ice) using a Branson sonifier fitted with a 6mm tip. Each sonication intensity was used three times for 20 s each, with increasing intensity from 2-4. 10% (v/v) Triton X-100 was added to each lysate to a final concentration of 1% and mixed by rotating at 4°C for 30 min before being centrifuged at 15,800 \times g and 4°C for 10 minutes to remove cell debris. The supernatants were immediately used for protein purification.

2.2.8 Affinity purification of recombinant proteins

2.2.8.1 Purification of GST-fusion proteins

Glutathione sepharose beads were prepared at the same time as centrifugation and wash steps. 200 μ l 50% (w/v) bead suspension per 100 ml original culture volume were centrifuged in a 1.5 ml micro centrifuge tube for 5 min at 1,000 \times g, 4°C. The supernatant was carefully removed and the beads were resuspended in 1 ml cold 1 \times PBS, vortexed briefly then centrifuged as before. The beads were washed a further three times with 1 ml of cold 1 \times PBS. The beads were transferred into a 15ml centrifuge tube, and centrifuged for 2 min at 1,000 \times g, 4°C.

The cell lysates were collected, mixed with an equal volume of 1 \times PBS, added to the sepharose and rotated at 4°C for 1 hour. The mixture was then centrifuged for 5 min at 11,000 \times g, 4°C, then washed with 6 ml cold 1 \times PBS, 1 ml cold 1 \times PBS and 1 ml cold 1 \times PBS by rotating for 10 min at 4°C then centrifuging as previously described. To

elute the protein from the beads 200 μ l GST-tag protein elution buffer was added and the suspension, rotated and centrifuged as previously described.

2.2.8.2 Purification of His-tag fusion proteins

Chelating sepharose beads were prepared at the same time as centrifugation and wash steps. 200 μ l 50% (w/v) bead suspension per 100 ml original culture volume were centrifuged in a 15 ml centrifuge tube for 2 min at $1,000 \times g$, 4°C . The supernatant was carefully removed and the beads were resuspended in 1 ml of ddH₂O, rotated at 4°C for 5 min then centrifuged as before. The beads were washed again in 1 ml ddH₂O, then 200 μ l 0.1 M CoCl₂ were added to each sample rotated for 10 min at 4°C and centrifuged as before. The beads were washed a further three times as previously described with 1 ml ddH₂O and finally with 200 μ l of binding buffer.

The cell lysates were collected, mixed with an equal volume of binding buffer, added to the sepharose and rotated at 4°C for 1 hour. The mixture was then centrifuged for 5 min at $11,000 \times g$, 4°C , then washed with 6 ml wash buffer, 1 ml binding buffer and 1 ml wash buffer by rotating for 10 min at 4°C then centrifuging for 5 min at $1,000 \times g$, 4°C . To elute the protein from the beads 200 μ l His-tag protein elution buffer was added and the suspension, rotated and centrifuged as previously described.

2.2.9 Determination of protein concentrations using Bradford assay

10 μ l eluted protein was added to 500 μ l Bradford solution in a cuvette and incubated for 2-3 min at room temperature. The protein concentration was determined using a calibrated BioPhotometer (Eppendorf) set to Bradford mode.

2.2.10 Preparation of *Leishmania* lysates for immunoblot

5×10^8 late log-phase promastigotes were harvested at $5,600 \times g$ for 10 min and resuspended in 5 ml $1 \times$ PBS. 1 ml aliquots were transferred into 1.5 ml centrifuge tubes before being centrifuged as previously described then resuspended in 500 μ l $1 \times$ PBS containing protease inhibitors (Complete EDTA-free protease inhibitor tablet (Roche) + o-phenanthroline). The cell suspension was centrifuged as before, the supernatant was

removed and the pellet was fast frozen in liquid nitrogen then stored at -70°C . The cells were resuspended in 100 μl *Leishmania* lysis buffer, incubated at 95°C for 10 min then chilled on ice.

2.2.11 Discontinuous SDS polyacrylamide gel electrophoresis (SDS-PAGE)

SDS-PA gels were used to separate proteins either as reaction mixtures or from total *Leishmania* cell lysate preparations. Gels were prepared at room temperature and consisted of 4% acrylamide stacking gels and resolving gels were typically 12% acrylamide. SDS sample buffer ($5 \times \text{SSB}$) was added to the sample and incubated at 95°C for 10 minutes to denature the proteins, then 25-30 μl was loaded into the gel pocket. The samples were separated at 20 mA in the stacking gel and 30 mA in the resolving gel until the dye reached the end of the gel. A pre-stained NEB protein molecular weight marker was used to estimate the molecular weight of separated proteins.

2.2.12 Coomassie staining of SDS-PA gels

Following SDS-PAGE and immunoblotting (if performed) the gel was placed in Coomassie R250 staining solution and agitated for approximately 10-30 min (depending upon whether the Coomassie solution was fresh or regenerated). The gel was subsequently washed with destaining solution, which was changed several times until the bands of protein were easily distinguished and the blue background was reduced. The gels were either dried or stored in ddH_2O .

2.2.13 Silver staining of SDS-PA gels

Following SDS-PAGE and immunoblotting (if performed) the gel was fixed using destaining solution then washed for a minimum of 1 hour in ddH_2O before being incubated in silver staining sensitising solution for 30 min at room temperature on a benchtop shaker (as with all future steps). The gel was subsequently washed twice with ddH_2O for 1 min each then incubated for 10 min with silver stain solution. This was followed by a further two 1 min washes with ddH_2O then incubation with developing

solution for no more than 5 min. When the gel bands were distinctly visible the developing solution was discarded and the reaction was stopped by the addition of silver stain stopping solution.

2.2.14 Drying of SDS-PA gels

Destained gels were agitated at room temperature for 30 minutes in gel drying solution. Cellophane sheets were soaked in water and the gels placed between the two sheets in a gel-drying frame without trapping air bubbles to ensure the gels did not crack. The assembled frame was placed in a fume hood for a minimum of 12 hours.

2.2.15 Immunoblot analysis

Proteins were separated by SDS-PAGE then transferred to an Immobilon-P Polyvinylidene Difluoride (PVDF) membrane by semi-dry electroblotting using the *BiometraFastblot* system at a current of 4 mA/cm² of gel for 30 min (1 gel) or 45 min (2 gels). Prior to setting up the electroblot six Whatman papers, cut to the size of the resolving gel, were soaked in transfer buffer then 3 layered on top of each other followed by the PVDF membrane (soaked in 100% methanol for 1 min, and subsequently washed in transfer buffer). The resolving gel was placed on top, then three more papers layered. A plastic serological pipette was carefully rolled over the assembled stack to remove air bubbles. Following blotting, the membrane was then incubated for one hour at 37°C in an appropriate blocking solution; this was then replaced with blocking solution containing the primary antibody and incubated overnight rotating at 4°C or for one hour with gentle agitation at 37°C. The membrane was then washed four times for 5 min with either 1 × TBST or 1 × PBST (depending on the antibody used) at room temperature. It was then incubated for one hour at 37°C with the secondary antibody diluted in blocking solution, washed three times for 5 min in 1 × TBST or 1 × PBST then twice for 5 min in 1 × TBS or 1 × PBS. The blot was developed by incubating the membrane with a 1:1 mix of Supersignal Peroxide solution and Signal Enhancer, then placed between two sheets of plastic in a radiographic cassette and exposing to X-ray film for times ranging from 1 sec to 1 hour.

2.2.16 Stripping- off antibodies from an immunoblot

Antibodies were removed from PVDF membranes that had been previously probed by incubation in 100 ml of immunoblot stripping solution at 65°C in a shaking water-bath for 30 min. The membrane was then washed twice with approximately 150 ml 1 × TBST or 1 × PBST at room temperature for 10 minutes before being re-blocked and probed with a different antibody.

2.2.17 *In vitro* kinase assays

Approximately 1 µg of recombinant protein was incubated rotating end-over-end (or shaking if eluted) at 34°C for up to 1 hour with 1 × kinase buffer, 5 µl 1mM ATP (either “cold” or 5 µCi γ -³²P ATP (6000 Ci/mmol)) and 5 µg MBP in a total volume of 50 µl. The reaction was stopped by addition of 12.5 µl SSB/DTT and heating to 95°C for 10 min then placing on ice. 25 µl of each reaction was separated by SDS-PAGE, using 12% SDS-PA gels. The radioactive gels were stained, destained and dried then exposed to X-ray film in a white background radiograph cassette at -70°C for several hours or days. Non-radioactive gels were immunoblotted as described in 2.2.15.

2.2.18 Microscopy techniques

2.2.18.1 Flagella length determination

A sample of a *Leishmania* culture (2×10^7 cells/ml) was diluted 1:20 in fixing solution (4% formaldehyde in PBS). 8 µl of this was loaded on a slide and the coverslip sealed. Cells were viewed using a Nikon fluorescence microscope equipped with a Hamamatsu digital camera. Several random images were taken where many parasites were present in the field of view and used to measure the flagellum of 500 parasites per culture. Flagella lengths were measured from the cell surface to the flagella tip, tracing the flagellum using the freehand tool of the IPLab software.

2.2.18.2 Hoechst staining of *Leishmania* cells

A final concentration of 1.6 µg/ml Hoechst stain was added to *Leishmania* cultures at a density of $2-4 \times 10^7$ cells per ml in fixing solution then incubated at room temperature for 10 minutes. The cells were loaded to a slide and the cover slip was sealed, random

images were taken where many parasites were present in the field of view and used to count the number of nuclei per cell.

2.2.19 Inhibitor screening

2.2.19.1 Inhibition of LmxGSK3- β by malabaricone inhibitors (KinaseGlo® assay)

Kinase-Glo® assays were performed in an assay buffer using black 96-well plates. 10 μ l of test compound dissolved in 1% DMSO (then diluted in advance in assay buffer to the desired concentration) and 10 μ l (~ 20 ng) of LmxGSK3- β were added to each well followed by 20 μ l of assay buffer containing 25 μ M substrate (MBP) and 1 μ M ATP. The final DMSO concentration in the reaction mixture did not exceed 1%. After 2 hour incubation (previously optimised) at 30°C the enzymatic reaction was stopped with 40 μ l of Kinase-Glo® reagent. Glow-type luminescence was recorded after 10 min incubation at room temperature using a spectramax plate reader. The inhibitory activities were calculated on the basis of maximal activities measured in the absence of inhibitor.

2.2.19.2 Susceptibility of promastigotes to malabaricone inhibitors (Alamar blue® assay)

Susceptibility of promastigotes to various inhibitors was determined by Alamar blue assay. 2×10^7 /ml stationary phase *L. mexicana* promastigotes were seeded into 96-well flat bottomed plates at a density of 2.5×10^6 /ml in 200 μ l medium without phenol red containing increasing concentration of pre-prepared inhibitor (or DMSO control), each in triplicate. The final concentration of DMSO was always less than 1%, and did not affect the growth of the parasites. Following inhibitor treatment (at 26°C) for 72 h, Alamar blue (20 μ l/well) was added and incubated for a further 18 h at 26°C. After incubation, colourimetric readings were performed. Plates were read at 550-590 nm using a spectrophotometer and analysed using Softmax Pro 2.0 software. Percentage suppression compared with control values were calculated using Microsoft Excel.

2.2.19.3 Susceptibility of intracellular amastigotes to malabaricone inhibitors

Susceptibility of intracellular amastigotes to various inhibitors was determined through the use of dose response assays against luminescent parasites. Macrophages in complete

RPMI were added to wells at a concentration of 0.5×10^5 cells/well in 24 and 96 well plates then made up to a final volume of 200 μ l and 100 μ l respectively with complete RPMI. For 96 well plates, the outer wells were filled with RPMI and not analysed as part of the experiment to account for “edge-effects” (carried out for both clear plates and black plates). Plates were incubated overnight at 37°C to allow macrophages to adhere to the bottom of wells. Parasites were added to plates of macrophages at a ratio of 1:40 (macrophage:parasites). The appropriate volume of parasites in complete RPMI was added to plates and incubated overnight at 37°C (*L. donovani*) or 34°C (*L. major* and *L. mexicana*), 5% CO₂ to allow parasites to invade macrophages. Following overnight incubation, unattached parasites and macrophages were removed and inhibitors or fresh medium (control) was added to appropriate wells and plates incubated for a further 72 hours at 37°C (*L. donovani*) or 34°C (*L. major* and *L. mexicana*), 5% CO₂. Luciferase amastigotes were tested for susceptibility to the various malabaricone fractions and pure compounds. 96 well plates were made up to a final volume 200 μ l and 24 well plates to 500 μ l to avoid evaporation. Bioluminescence of luciferase parasites was measured using the IVIS (*In vivo* Imaging System) 200 Series from Caliper LifeScience, Runcorn, UK. Light emission was measured in photons per second. In plates incubated with *L. donovani* carrying the luciferase plasmid supernatant was removed and 50-100 μ l of sterile 150 μ g/ml luciferin solution (Caliper LifeScience) in complete RPMI was added to all wells. Plates were imaged immediately after. A mean luminescence background value was obtained by reading wells containing only macrophages and luciferin solution. The background value was subtracted from all wells during analysis to produce a value of luminescence due to luciferase.

2.2.20 Statistical Analysis

Data was interpreted using GraphPad Prism Version 6.0 where all data are shown as a mean \pm SE where n=3. Significant differences were determined using students t-test or one way ANOVA (as appropriate) where p<0.05 was deemed significant.

Chapter 3

Phenotypic characterisation of the *LmxMPK2* and its relationship with *LmxDIP13*

3.1 Introduction

Gene deletion and RNA interference are invaluable tools in the investigation of the physiological function of a protein in Trypanosomatids. However, most *Leishmania* species, including *Leishmania mexicana* are not suited to RNA interference as they lack the required components for the RNAi pathway (Kolev *et al.*, 2011; Lye *et al.*, 2010). Generation of a null mutant by homologous recombination therefore provides an effective method of investigating the role of a protein in *L. mexicana*.

The introduction of a plasmid carrying *LmxMPK2* was necessary before it was possible to replace both alleles of *LmxMPK2* with different resistance markers in two consecutive rounds of electroporation. Clones acquired ($\Delta LmxMPK2$ *-/-* K1 and $\Delta LmxMPK2$ *-/-* K2) contained selective markers for hygromycin B and phleomycin, conferring resistance (as described by Mandal *et al.*, 2012). The ability of the *L. mexicana* *LmxMPK2* null mutants to lose the plasmid suggested it was not essential in promastigotes. However, the inability to persist in mammalian hosts suggested *LmxMPK2* to be essential in amastigotes. In order to demonstrate phenotypic differences were due to the deletion of *LmxMPK2*, the gene was re-introduced into the null background. The *LmxMPK2* add-back mutants also existed prior to this project ($\Delta LmxMPK2$ *-/-* + *gMPK2*). These were obtained by re-integrating *LmxMPK2* with a puromycin selection marker back into the original chromosomal gene locus through homologous recombination (Mandal *et al.*, 2012). Null mutant and add-back mutant clones were confirmed using both Southern blot and immunoblot analyses (immunoblot shown in figure 9). Wild type *L. mexicana* and the null mutant parasites were used in various investigations into growth and morphology to gain insight into the function of *LmxMPK2* and the implications of the deletion.

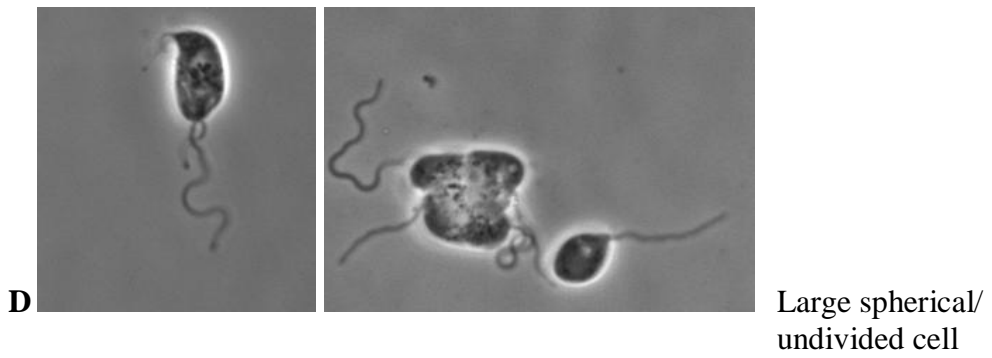
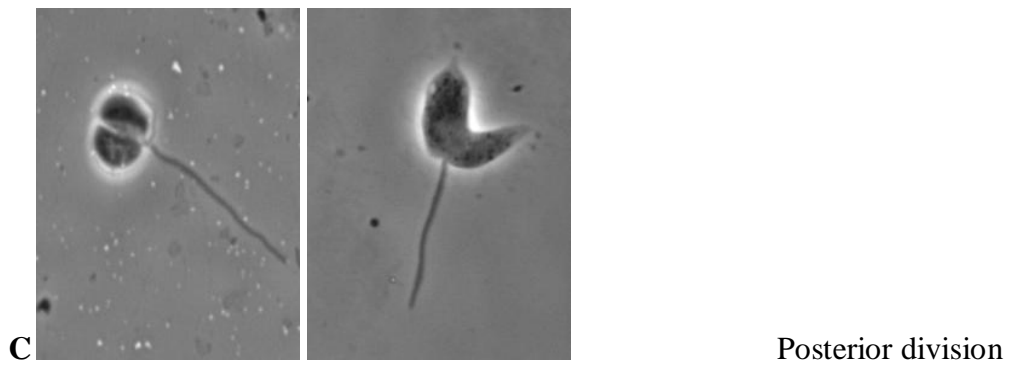
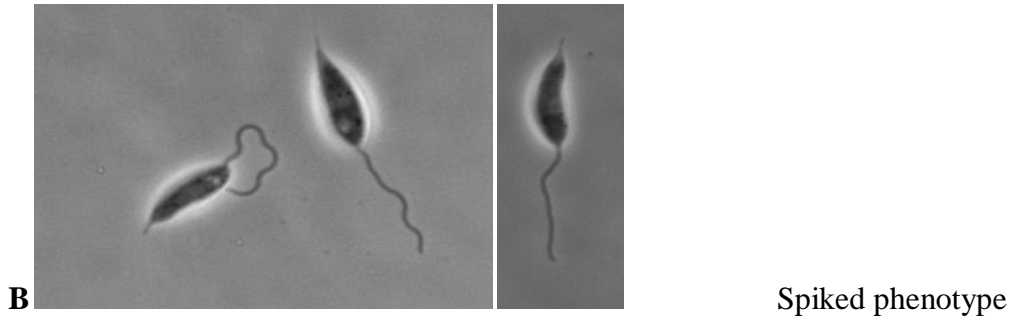
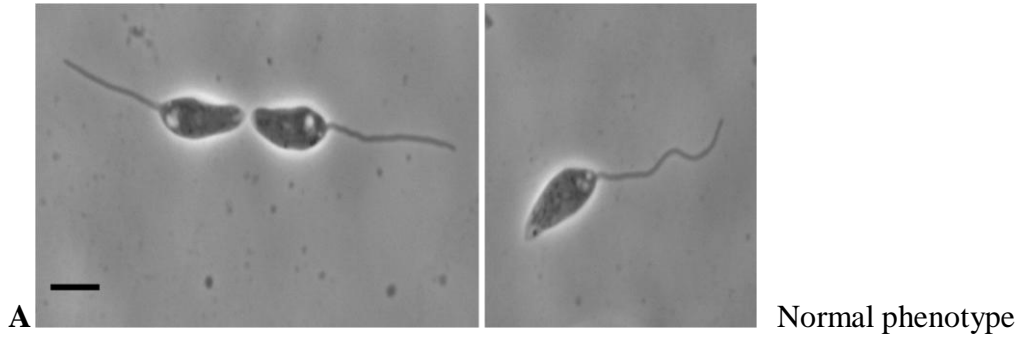
DIP13 (Deflagellation inducible protein 13) was first discovered in *Chlamydomonas reinhardtii* which has been shown to associate with microtubule structures and to be involved in cell division (Pfannenschmid *et al.*, 2003). DIP13 has been found to be absent from common eukaryotic model systems such as *Saccharomyces cerevisiae*, *Caenorhabditis elegans* and *Drosophila melanogaster*. However, it is encoded by the genomes of the flagellated green algae *Chlamydomonas reinhardtii*, trematode worms - *Schistosoma* spp. and protozoan parasites (Price *et al.*, 2012). The *T. brucei* orthologue shows only 33% amino acid identity with the *Chlamydomonas* protein.

In a study by Price *et al.*, 2012, TbDIP13 was identified in early mitosis of the trypanosome cell cycle. It was hypothesised that LmxDIP13 may be a putative marker protein for cell division and could be used to identify different cell cycle stages in *Leishmania*. Since LmxDIP13 was known to associate with microtubule structures and LmxMPK2 might also associate with microtubule structures, a second hypothesis suggesting a relationship existed between the two proteins was conceived. Both investigations were incorporated into one simply by transfecting GFP-LmxDIP13 in wild type and *LmxMPK2* null mutant *L. mexicana*. It was hoped that several different localisations (in line with different cell cycle stages) would be observed in wild type *L. mexicana*. Moreover, it was expected that the localisations would be different in *LmxMPK2* null *L. mexicana* to compensate for the loss of LmxMPK2.

3.2 Results

3.2.1 Phenotypic analysis of *LmxMPK2* null mutant parasites

Scanning electron microscopy had revealed several morphological abnormalities of the *LmxMPK2* null mutants including lobed cell bodies, spiked posterior ends, irregular length of flagella and cell division from the posterior end. These findings had not been further investigated, thus, the various phenotypes were quantified. The only phenotypic difference suggested between wild type *L. mexicana* and the *LmxMPK2* add-back mutants was the apparent increase in flagella length in the add-back mutants. Brightfield microscopy was performed. Images were captured using a Hamamatsu Orca-2885 firewire digital charge-coupled device camera and processed using ImageJ (NIH, USA).



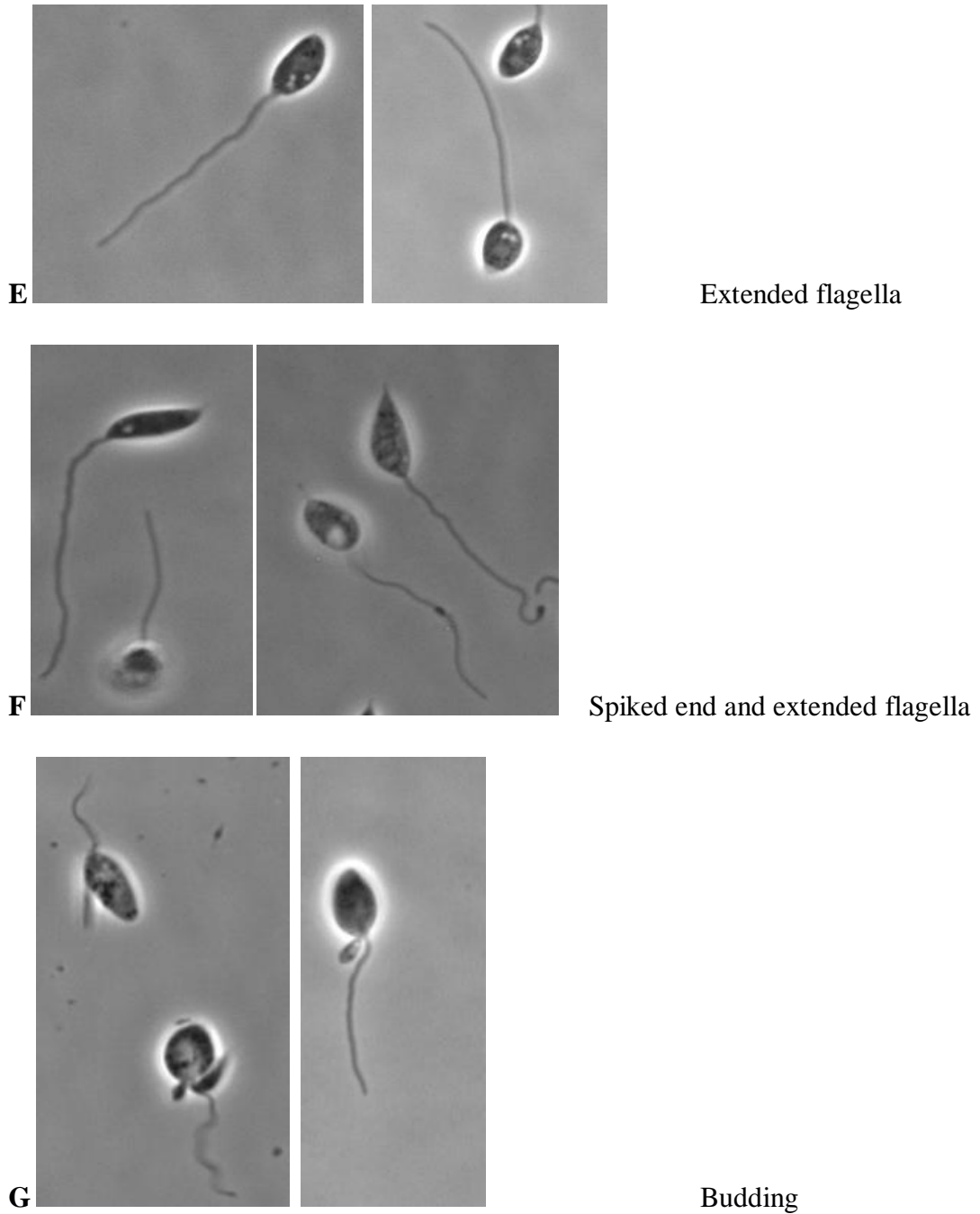


Figure 3.1 Brightfield images of various *L. mexicana* *LmxMPK2* null mutant phenotypes.

Overview of the various phenotypes observed in the *LmxMPK2* null mutants. (A) normal phenotype; (B) spiked phenotype; (C) posterior division; (D) large spherical/undivided cell; (E) extended flagella; (F) spiked end and extended flagella; (G) budding cell bodies. Same magnification used for all images; bar - 5 μ m.

	Normal phenotype	Spiked end	Posterior division	Large spherical bodies	Extended flagella	Spiked end and extended flagella	Budding bodies
$\Delta LmxMPK2$ -/- K1	42%	25%	8%	9%	8%	3%	5%
$\Delta LmxMPK2$ -/- K2	41%	27%	10%	8%	7%	3%	4%

Table 3.1 Overview of *LmxMPK2* null mutant phenotypes.

Figure 3.1 shows the different phenotypes in logarithmic phase ($2-3 \times 10^7$ cells/ml) *LmxMPK2* null mutant cultures. Table 1 summarises the observed phenotype as a percentage of each mutant culture.

Seven phenotypes were observed in the different log phase *LmxMPK2* null mutant cultures. These include a normal phenotype as found in wild type *L. mexicana* (figure 3.1 A); cell bodies with spiked posterior ends (figure 3.1 B); cells dividing from the posterior end - “wrong end division” (figure 3.1 C); large undivided cell bodies often with multiple flagella (figure 3.1 D); normal cell bodies with extended flagella (the absence of a second flagellum or beginning of second flagellum suggests it is not a dividing cell) (figure 3.1 E). A similar phenotype to figure 3.1 E was also found, however the cell body is also spiked (figure 3.1 F) and finally, cell bodies with one or multiple small “buds” or lobes (figure 3.1 G).

The percentage of each phenotype was determined for each null mutant; the percentage phenotype was consistent between the two independent mutant clones. The most common phenotype was a normal phenotype consisting of 41-42% of the cells in culture. The spiked cell bodies make up the second most abundant phenotype consisting of 25-27% of the cells. Cells dividing from the posterior end, large undivided cells and non-spiked bodies with extended flagella make up similar proportions of the cells at 7-10% each. This was followed by budding cell bodies, which constitute approximately 5% of the population, and finally the smallest phenotype group was the spiked bodies with extended flagella making up just 3% of the cells.

3.2.2 Proliferation analysis of *LmxMPK2* mutants

The effect of *LmxMPK2* deletion on *L. mexicana* proliferation and viability was investigated. Four parallel proliferation experiments were performed to test the effect of the *LmxMPK2* deletion and *LmxMPK2* re-introduction on *L. mexicana* promastigote growth in comparison to wild type *L. mexicana*. Samples for cell counting were taken at the same time each day from four independent cultures to determine cell density.

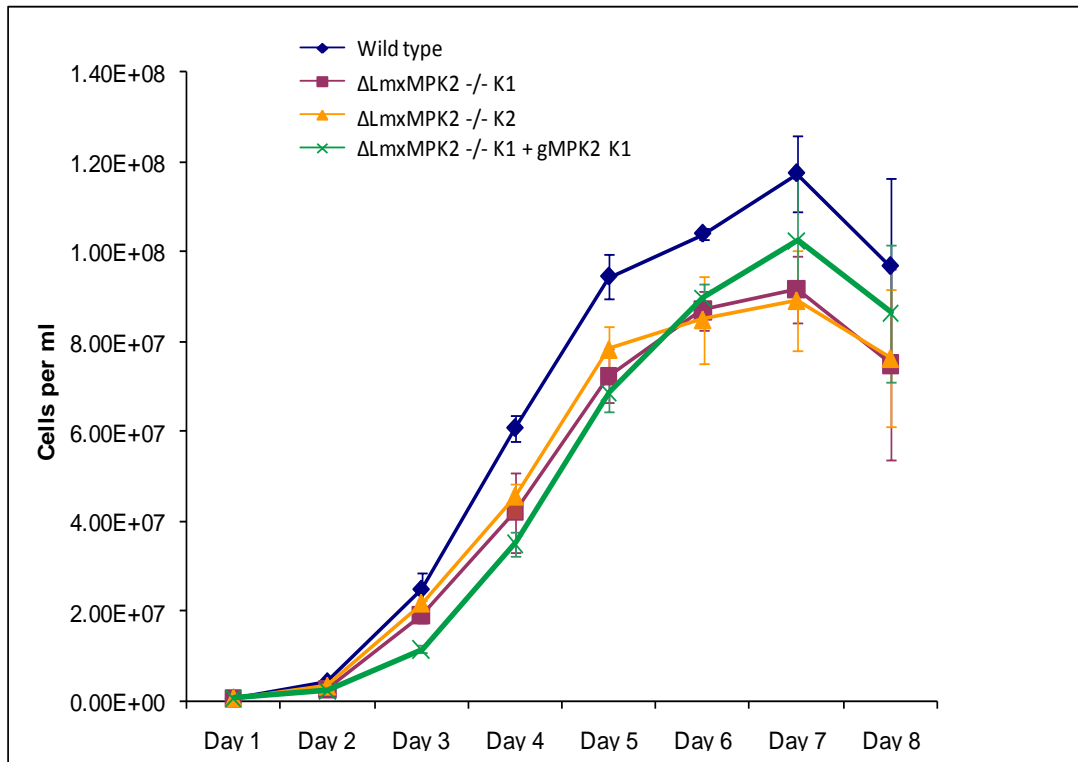


Figure 3.2. Proliferation analysis of *L. mexicana* wild type, *LmxMPK2* null mutants and *LmxMPK2* add-back mutant promastigotes.

Graph displays mean cell density (\pm SD) sampled daily from four independent cell culture preparations ($n=4$) per cell line.

Blue line with diamond marker - WT *L. mexicana*; pink line with square marker - $\Delta LmxMPK2$ -/- K1; orange line with triangle marker - $\Delta LmxMPK2$ -/- K2; green line with cross marker - $\Delta LmxMPK2$ -/- K1 + gMPK2 K1.

The proliferation of *L. mexicana* wild type, *LmxMPK2* null mutants and the *LmxMPK2* add-back mutant promastigotes was measured over the course of 8 days. The significance of the data was determined using an unpaired, two-tail T-test. Figure 3.2 shows the cell proliferation of *L. mexicana* wt, $\Delta LmxMPK2$ -/- K1, $\Delta LmxMPK2$ -/- K2 and $\Delta LmxMPK2$ -/- K1 + gMPK2 K1. Previous work on the add-back parasites showed good consistency between the clones and therefore only one clone was selected as a comparison to the effects of deletion of *LmxMPK2*.

All cell lines reached maximum stationary phase density on day 7, after which they entered death phase. $\Delta LmxMPK2$ -/- + gMPK2 showed a lower proliferation rate than wild type and null mutant promastigotes on days 1-4. However, the add-back mutant appeared to recover and increase proliferation rates to an almost normal level. By day 7 the add-back mutant reached a maximum density of 1.02×10^8 cells per ml, approximately 87% of the wild type maximum density of 1.17×10^8 cells per ml. The difference in growth between the add-back mutant and the wild type promastigotes was found to be not significant ($p > 0.05$).

Proliferation of the two null mutant promastigotes was concurrent, following the same general proliferation as the wild type but at a consistently lower density. At day 7 the null mutants reached a maximum density of 9.2×10^7 cells per ml, 78% of the wild type maximum density. Statistical analysis showed null mutant final cell density to be significantly lower than that of the wild type ($p < 0.05$).

3.2.3 Measurement of flagellar length of *LmxMPK2* mutants

Upon inspection of the electron micrographs (figure 1.10), it appeared that both the $\Delta LmxMPK2$ -/- and the add-back mutants may display elongated flagella. Microscopic analysis of the different cell lines was undertaken to demonstrate any difference. To confirm and quantify this observation, the flagellar lengths of *L. mexicana* wild type, $\Delta LmxMPK2$ -/- K1, $\Delta LmxMPK2$ -/- K2 and $\Delta LmxMPK2$ -/- K1 + gMPK2 K1 at a density of 2×10^7 cells per ml were measured. Images captured were used to measure the lengths of 200 cells per cell line using IPLab software.

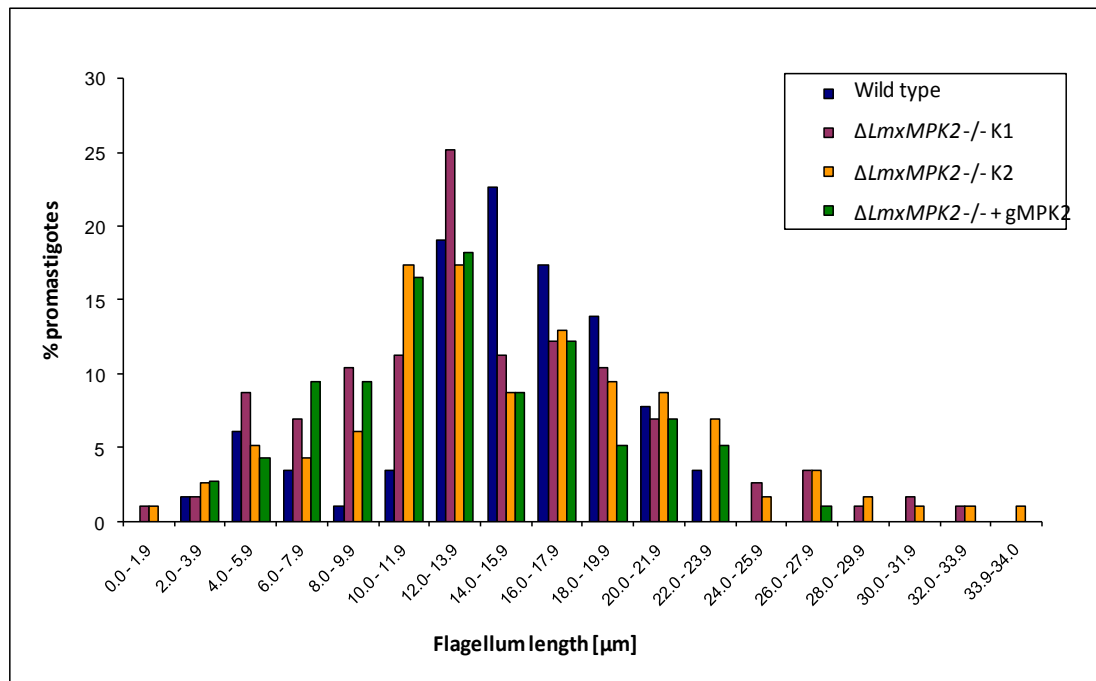


Figure 3.3. Histogram of flagellar lengths from *L. mexicana* wild type, *LmxMPK2* null mutants and *LmxMPK2* add-back mutant promastigotes.

Brightfield images captured for phenotype analysis were used to measure the flagella lengths of null mutants. Further images were captured for wild type and add back mutant promastigotes. 200 cells measured per cell line.

Blue bar - WT *L. mexicana*; pink bar - $\Delta LmxMPK2$ -/- K1; orange bar - $\Delta LmxMPK2$ -/- K2; green bar - $\Delta LmxMPK2$ -/- K1 + gMPK2 K1.

	Average flagellar length (μm)	Standard deviation (μm)	Minimal flagellar length (μm)	Maximal flagellar length (μm)
Wild type	14.9	4.4	4.0	23.6
$\Delta LmxMPK2$ -/- K1	13.8	5.9	1.5	32.2
$\Delta LmxMPK2$ -/- K2	15.3	6.8	1.7	42.7
$\Delta LmxMPK2$ -/- K1 + gMPK2 K1	13.2	4.9	2.9	23.6

Table 3.2. Overview of average, minimal and maximal flagellar lengths from the different *LmxMPK2* mutants.

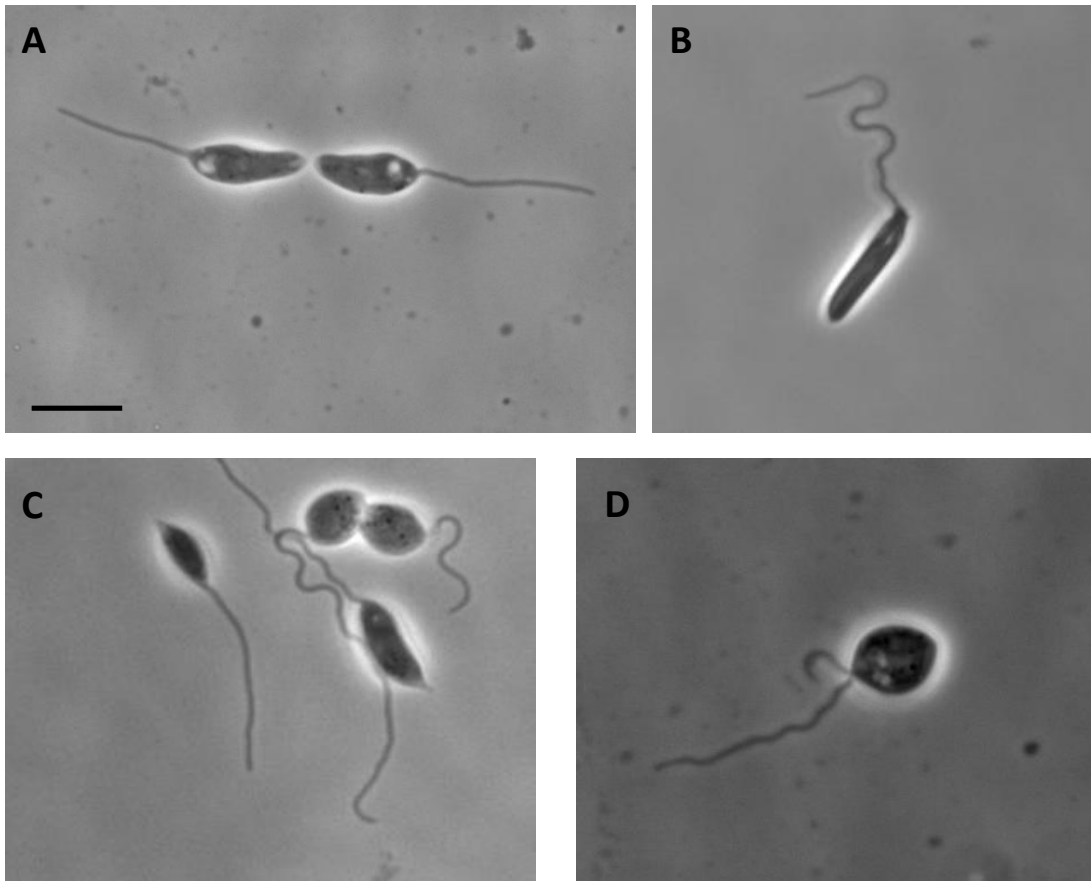


Figure 3.4. Overview of flagella lengths in *Leishmania*.

Brightfield images providing examples of the various flagellum lengths observed (A) Average flagella length found in wt, null mutant and add back; (B) Extended flagella length as found in *LmxMPK2* null mutants (~ 28 μm); (C) Maximal flagella length (42.7 μm) observed in Δ *LmxMPK2* $-/-$ K2 (slightly right of centre cell); (D) Short second flagella (due to dividing cell). Same magnification used for all images; bar, 10 μm .

A larger distribution of flagellar lengths for the null mutant (both larger and smaller values) and a return to the normal phenotype when *LmxMPK2* is re-expressed in the null background is displayed in figure 3.3. Table 3.1 summarises the key values of various measurements. The average length of a wild type *L. mexicana* promastigote flagellum is approximately 15 μm (usual range 10-20 μm). All groups fell within the normal average. However, compared to the wild type *L. mexicana* which ranged from 4.0 μm to 23.6 μm (table 3.1), the *LmxMPK2* null mutants $\Delta LmxMPK2$ *-/-* K1 and $\Delta LmxMPK2$ *-/-* K2 revealed minimal flagellar lengths of 1.5 μm and 1.7 μm and significantly larger maximal lengths ($p < 0.05$) of 31.3 μm and 42.8 μm , respectively (table 3.1). Generally, $\Delta LmxMPK2$ *-/-* K1 showed shorter flagella than $\Delta LmxMPK2$ *-/-* K2, however the 42.8 μm flagellum (shown in Figure 3.4 C) in the $\Delta LmxMPK2$ *-/-* K2 appeared to be exceptionally long with the next longest flagellum being 33.2 μm (figure 3.3). Although microscopy analysis suggested the add-back mutant $\Delta LmxMPK2$ *-/-* + *gMPK2* may produce elongated flagella, this was not reflected in the study; the average flagellar length was 13.3 μm with a maximum of 23.6 μm and a minimum of 2.9 μm (table 3.1), which is consistent with wild type *L. mexicana*. The short flagella reflect the beginning of a second flagella in dividing cells and not a shortening effect caused by the deletion of *LmxMPK2* (figure 3.4 D).

3.2.4 Analysis of the *in vivo* localisation of LmxMPK2 using GFP-tagged mutants

3.2.4.1 Generation of transfection construct

In order to identify the localisation of LmxMPK2, a green fluorescent protein (GFP) was tagged to LmxMPK2 for transfection into the *L. mexicana* $\Delta LmxMPK2$ *-/-* mutants and the wild type *L. mexicana*. Sequencing ensured correct plasmid.

3.2.4.2 Transfection and verification of clones

The plasmid carrying LmxMPK2-GFP was transfected into *L. mexicana* wild type and the *LmxMPK2* deletion mutant backgrounds. A minimum of three clones were selected

for each cell line and were selected for by continuous puromycin pressure. Protein expression was verified by fluorescent microscopy. Before localisation studies could begin, it was necessary to confirm fluorescence was due to LmxMPK2-GFP expression. To confirm this, an immunoblot was carried out using total cell lysates. The blots were developed using chemiluminescence.

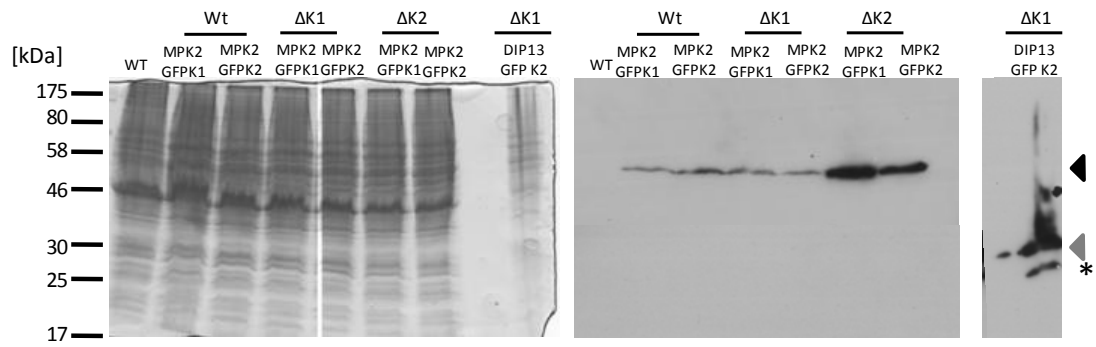


Figure 3.5. Immunoblot of *L. mexicana* cell lysates expressing GFP-tagged LmxMPK2

Expression of GFP fused to the C-terminus of LmxMPK2 and transfected into various *L. mexicana* parasites Immunoblot compares control cells, WT and Δ LmxMPK2 $-/-$ K1 + GFPDIP13 K1 with MPK2GFP expressing cells

Left panel - Coomassie-stained gels; right panel - immunoblot probed with the monoclonal anti-GFP-HRP antibody after 40 min exposure. (◄) GFP-tagged LmxMPK2. Molecular masses of standard proteins are indicated in kDa.

Figure 3.5 shows an immunoblot of whole cell lysates probed with an anti-GFP-HRP antibody.

A single band at the anticipated size of around 78 kDa is observed in all GFP-tagged LmxMPK2 transfected cells (lanes 2-7). Two bands were observed in the positive control (lane 9), the expected 38 kDa indicating GFP-tagged (26 kDa) LmxDIP13 (11.8 kDa) and a second band at 26 kDa - equivalent to the size of the GFP-tag alone. Additionally, no bands are observed for *L. mexicana* wild type whole cell lysates showing the specificity of the antibody and proving the absence of free GFP protein in these clones.

3.2.4.3 Localisation of LmxMPK2

Fluorescence was confirmed to be due to expression of LmxMPK2-GFP in the *L. mexicana* cultures. Localisation of the kinase was carried out through fluorescence microscopy using logarithmic cells ($2-4 \times 10^7$). Images were processed using ImageJ (NIH, USA). False colour was added using the lookup table setting. Images were taken over several days, top and bottom images are representative of two separate samples collected on different days to provide a true reflection of fluorescence within a culture.

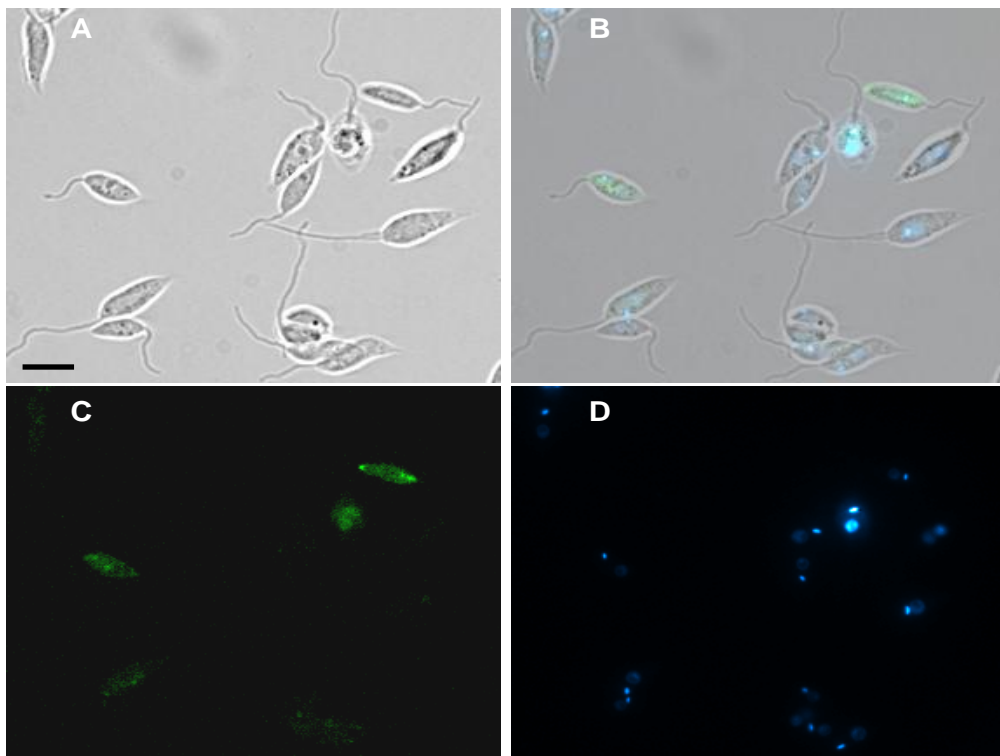
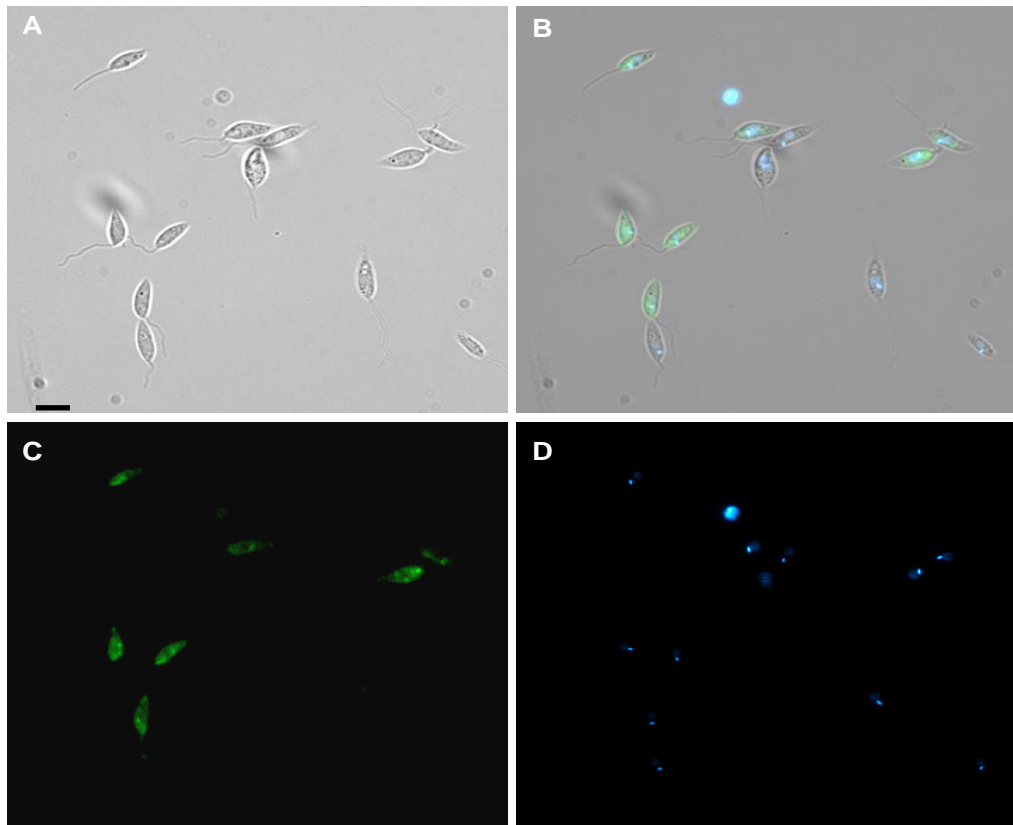


Figure 3.6. Wild type *L. mexicana* cells expressing GFP-tagged LmxMPK2. Fluorescent microscopy representative of Wt *L. mexicana* cells expressing GFP-tagged LmxMPK2. (A) Brightfield micrograph; (B) brightfield/GFP/Hoechst merge; (C) fluorescence (GFP) micrograph; (D) fluorescence (Hoechst) micrograph. Bar - 10 μ m

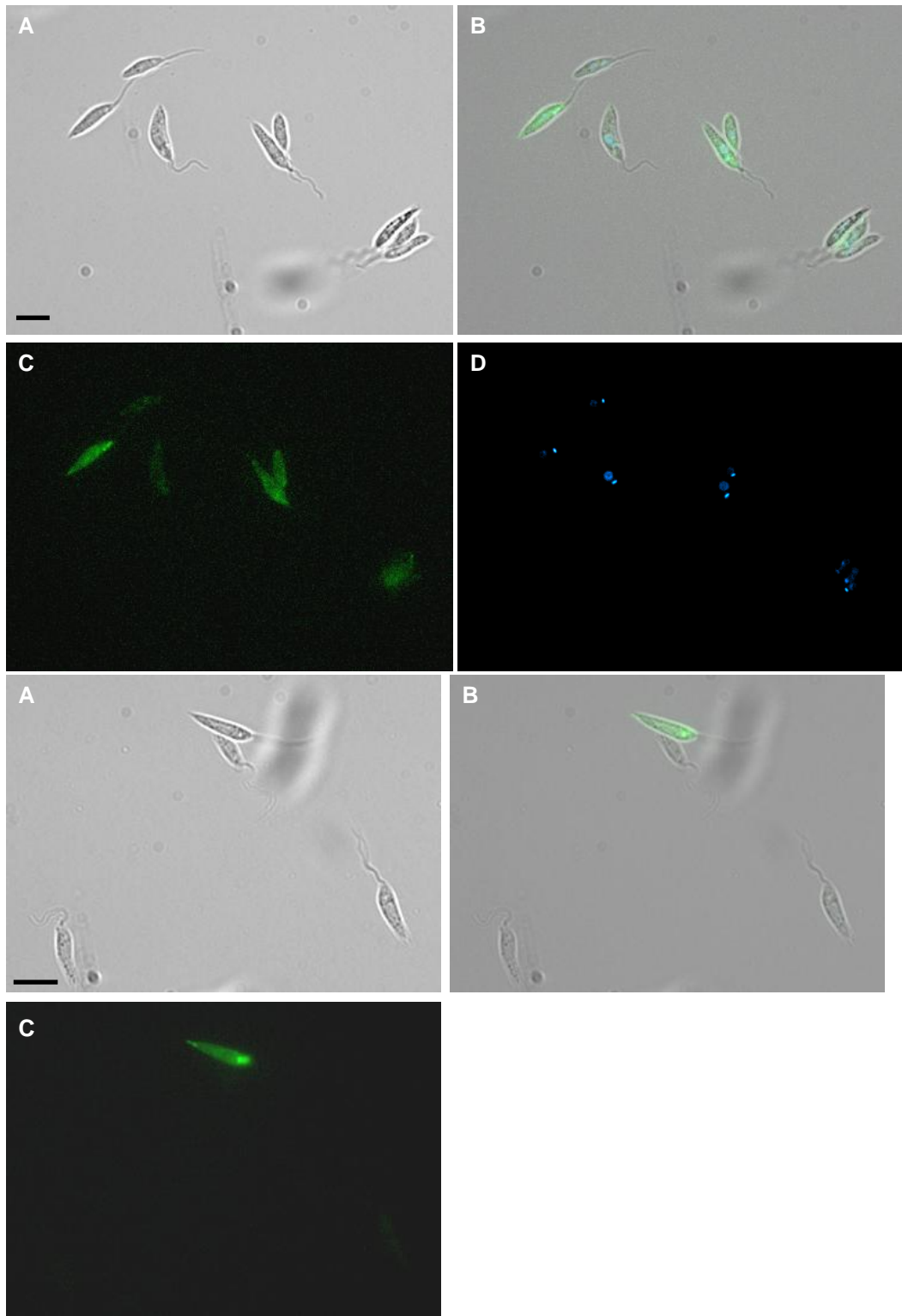


Figure 3.7. Δ LmxMPK2^{-/-} K1 *L. mexicana* cells expressing GFP-tagged LmxMPK2. Fluorescent microscopy representative of Δ LmxMPK2^{-/-} K1 *L. mexicana* cells expressing GFP-tagged LmxMPK2
 (A) Brightfield micrograph; (B) brightfield/GFP/Hoechst merge; (C) fluorescence (GFP) micrograph; (D) fluorescence (Hoechst) micrograph. Bar - 10 μ m

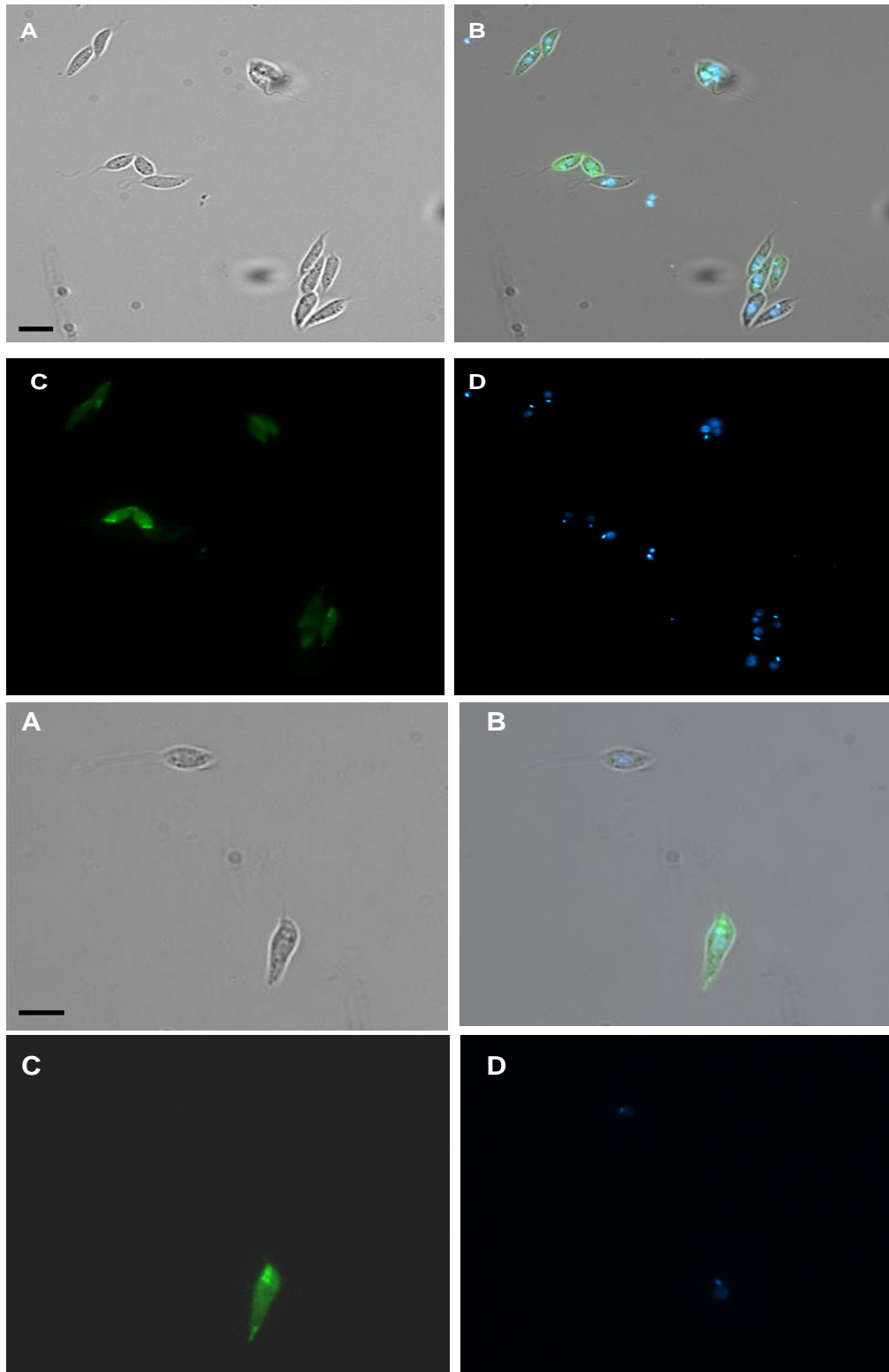


Figure 3.8. $\Delta LmxMPK2^{-/-}$ K2 *L. mexicana* cells expressing GFP-tagged LmxMPK2. Fluorescent microscopy representative of $\Delta LmxMPK2^{-/-}$ K2 *L. mexicana* cells expressing GFP-tagged LmxMPK2
 (A) Brightfield micrograph; (B) brightfield/GFP/Hoechst merge; (C) fluorescence (GFP) micrograph; (D) fluorescence (Hoechst) micrograph. Bar 10 μ m

Excellent consistency of localisation was observed between the wild type cells expressing LmxMPK2GFP (figure 3.6) and both null mutant clones expressing the tagged kinase (figure 3.7 and Figure 3.8). Although quantification was not carried out, it should be noted that only a small number of the cells showed any fluorescence.

GFP-tagged LmxMPK2 expressed in wild type *L. mexicana* exhibited a defined localisation around the anterior end of the cell body and posterior localisation also observed as shown in Figure 3.6. A small number of the cells exhibited anterior localization only but none showed posterior only. Although defined localisation was present some of the cells, they also exhibited diffuse fluorescence of the cell body. The nucleus and kinetoplast of the cells were stained using Hoechst. Overlay of the Hoechst-stained cells with the GFP-fluorescence suggests LmxMPK2 localisation at the anterior end to be between the kinetoplast and the end of the cell body.

GFP-tagged LmxMPK2 expressed in either *LmxMPK2* null mutant background showed the same localisation as that expressed in wild type cells - a defined spot localisation around the anterior end and a second localization at the posterior end localisation also visible as shown in figure 3.7 and 3.8. As with the wild type, a small number of cells showed localisation to the anterior end alone but not posterior. Although defined localisation was present in some of the cells they also exhibited diffuse localisation. Greater GFP fluorescence was observed in the $\Delta LmxMPK2$ $-/-$ K2 + LmxMPK2GFP clones. As previously described for the wild type background cells, GFP-tagged LmxMPK2 expressed in null mutant backgrounds were also stained with Hoechst. Images captured suggest the localisation to be between the kinetoplast and end of cell body as with the wild type background localisation. It was also noticed that almost all the $\Delta LmxMPK2$ $-/-$ + LmxMPK2GFP cells possessed a normal phenotype and correct number of kinetoplasts and nuclei.

3.2.5 LmxMPK2 and LmxDIP13

3.2.5.1 Generation of GFPDIP13 construct

To begin investigations into the relationship between LmxMPK2 and LmxDIP13 in *L. mexicana*, a GFP expressing LmxDIP13 construct was required. A construct containing a GFP-tagged LmxDIP13 had already been generated (Wiese, unpublished). However, this construct encoded a hygromycin resistance marker which was used in the deletion of one allele of *LmxMPK2* from *L. mexicana* in order to generate a null mutant. Therefore a new plasmid containing a puromycin resistance marker had to be generated.

3.2.5.2 Transfection and verification of clones

The plasmid was transfected into *L. mexicana* wild type and two independent LmxMPK2 deletion mutants, K1 and K2. A minimum of three clones were selected for each cell line and were selected for by continuous puromycin pressure at 40 μ M. Protein expression was verified by fluorescence microscopy. To confirm the expression of GFP-tagged LmxDIP13 immunoblot analysis using an HRP-conjugated anti-GFP monoclonal antibody was carried out using total cell lysates. 2×10^7 cells. Wild type *L. mexicana* lysates were included as a negative control.

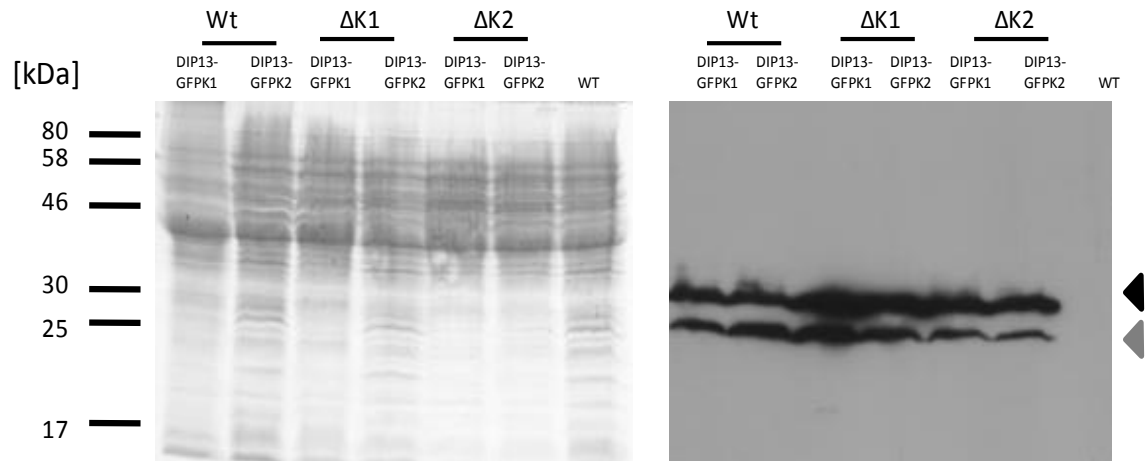


Figure 3.9. Immunoblot of *L. mexicana* promastigotes expressing N-terminally GFP-tagged LmxDIP13 in wild type and LmxMPK2 null mutants using an HRP-conjugated anti-GFP monoclonal antibody.

Expression of GFP fused to the N-terminus of LmxDIP13 and transfected into wild type *L. mexicana* and *LmxMPK2* null mutant parasites. Immunoblot compares control cells, WT *L. mexicana* with GFPDIP13 expressing cells. Left panel - Coomassie-stained gels; right panel - immunoblot probed with the monoclonal anti-GFP-HRP antibody after 2 min exposure. Representative of three independent repeats.

(◄) GFP-tagged DIP13; (◄) corresponds in size to GFP-tag. Molecular masses of standard proteins are indicated in kDa.

GFP expression was confirmed using immunoblot analysis of whole cell promastigote lysates probed with an HRP-conjugated anti-GFP monoclonal antibody (figure 3.9).

The expected band size of 38 kDa was observed in all GFP-tagged (26 kDa) LmxDIP13 (11.8 kDa) transfected cells (lanes 1-6). A second band at 26 kDa, which is equivalent to the size of the GFP-tag alone, was observed in all transfected samples (lanes 1-6). *L. mexicana* wild type whole cell lysates were included as a negative control (lane 7). As expected no bands were observed in lane 7, thus showing the anti-GFP antibody to be specific.

3.2.5.3 Localisation of LmxDIP13 within wild type and LmxMPK2 null mutants

Following transfection and verification of expression, localisation of LmxDIP13 in logarithmic promastigotes was carried out using fluorescence microscopy. Images were processed using ImageJ (NIH, USA). False colour was added using the lookup table setting.

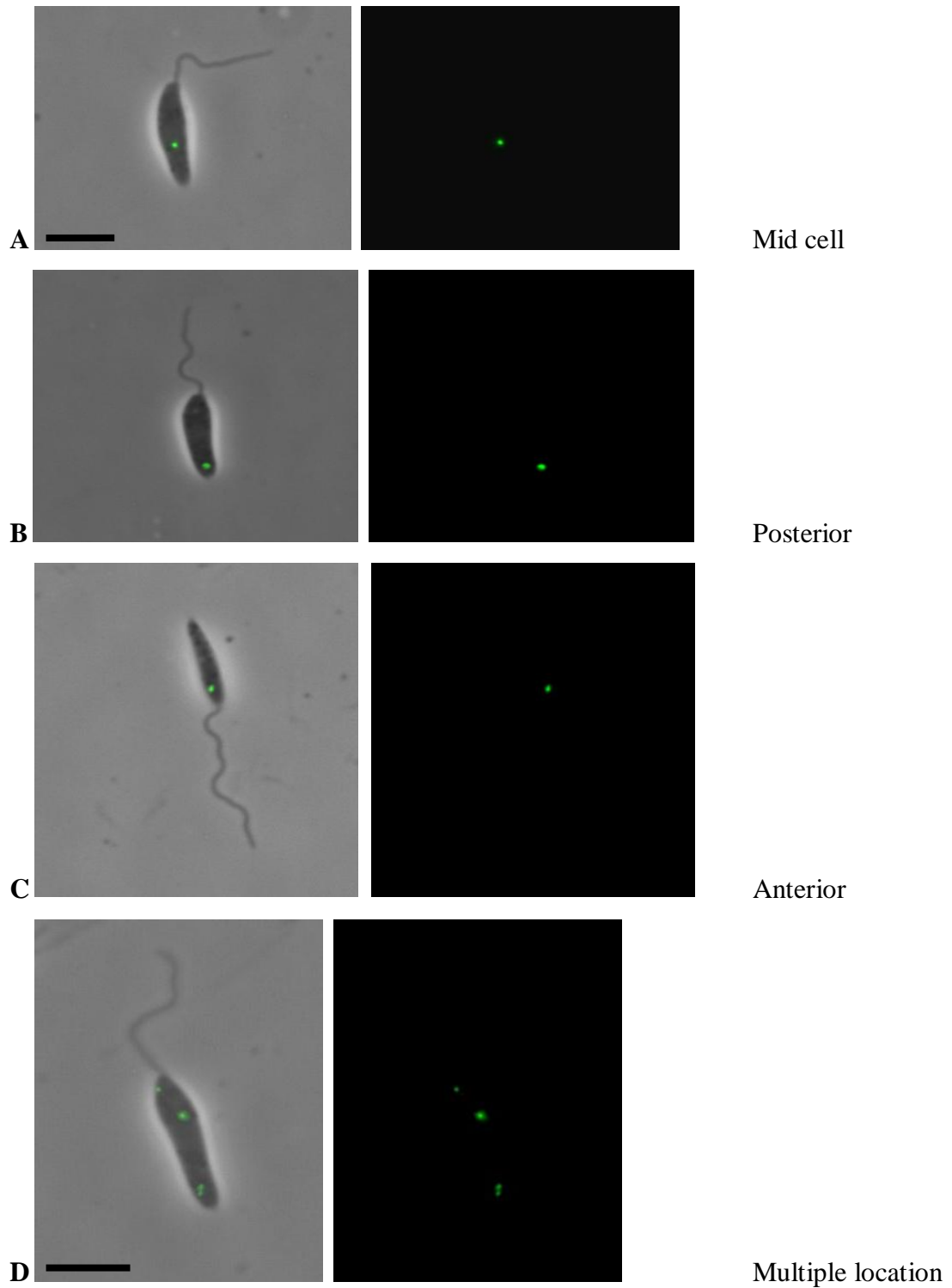
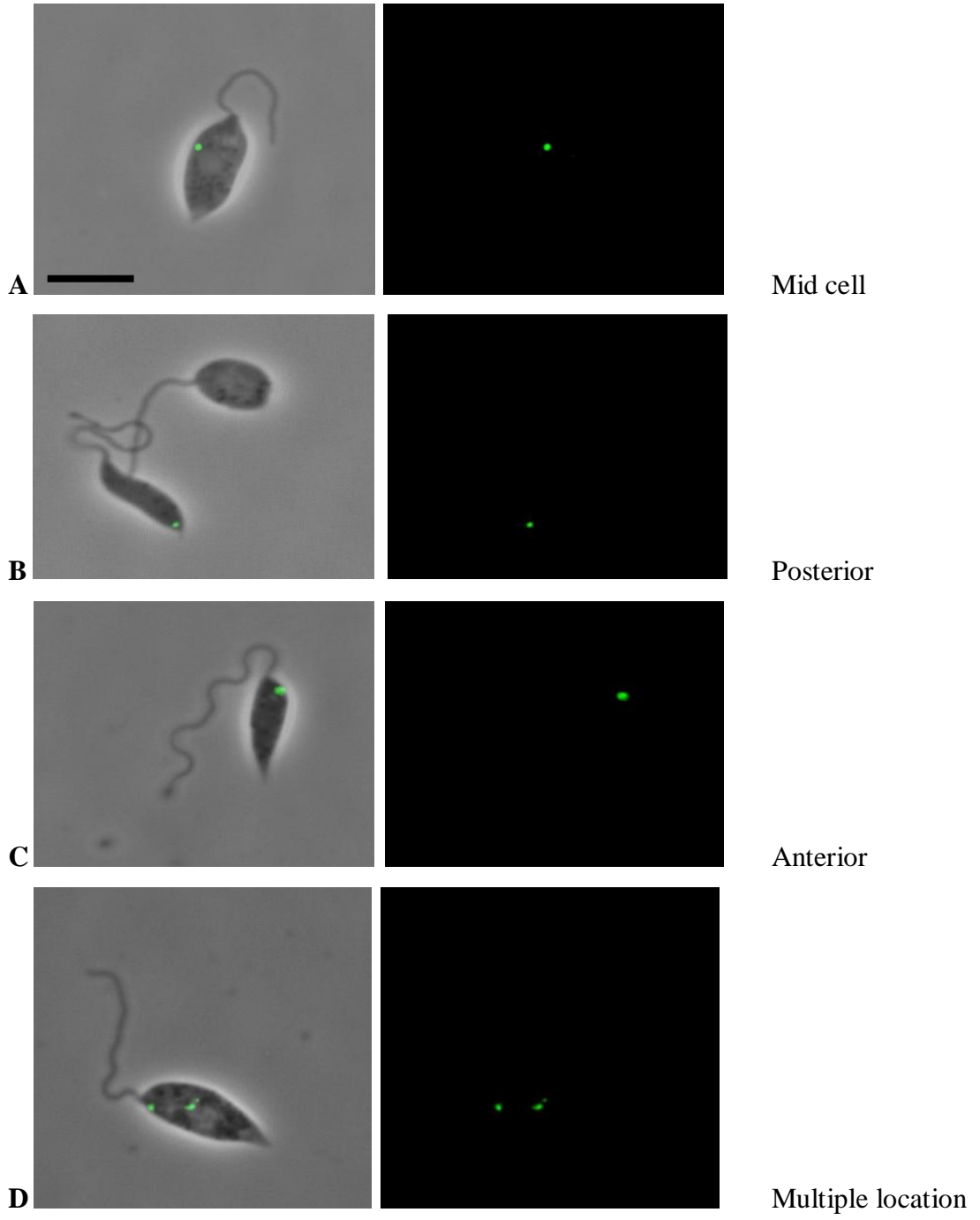


Figure 3.10. Fluorescence microscopy showing wild type *L. mexicana* cells expressing GFP-tagged LmxDIP13.

Fluorescent microscopy representative of wt *L. mexicana* cells expressing GFP-tagged LmxDIP13.

Left panel - brightfield/GFP merge; right panel – GFP image. (A) mid cell localisation; (B) posterior localisation; (C) anterior localisation; (D) multiple location localisations. Bar 10 μ m.



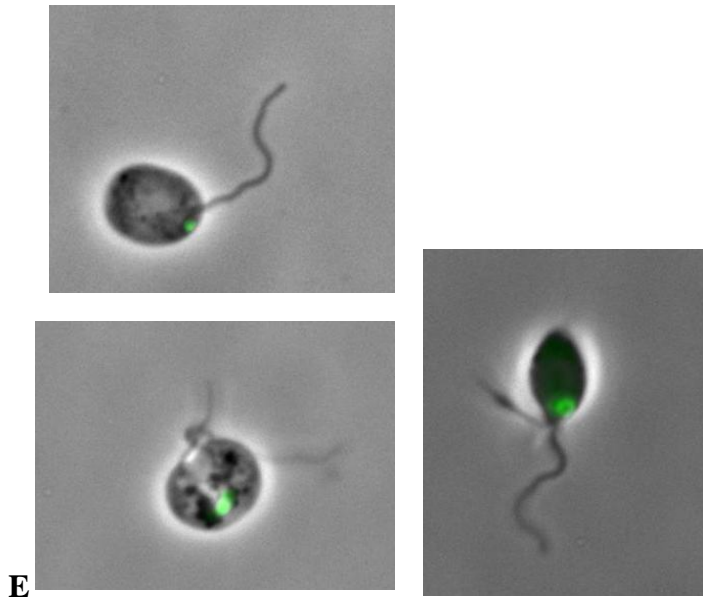


Figure 3.11. Fluorescence microscopy showing *LmxMPK2* null mutant *L. mexicana* cells expressing GFP-tagged LmxDIP13.

Fluorescent microscopy representative of $\Delta LmxMPK2$ $-/-$ K1 + GFPLmxDIP13 and $\Delta LmxMPK2$ $-/-$ K2 + GFPLmxDIP13.

Left panel shows brightfield/GFP merge; right panel shows GFP image. (A) mid cell localisation; (B) posterior localisation; (C) anterior localisation; (D) multiple location localisations; (E) GFP-LmxDIP13 shown in various *LmxMPK2* null mutant phenotypes. Bar, 10 μ m

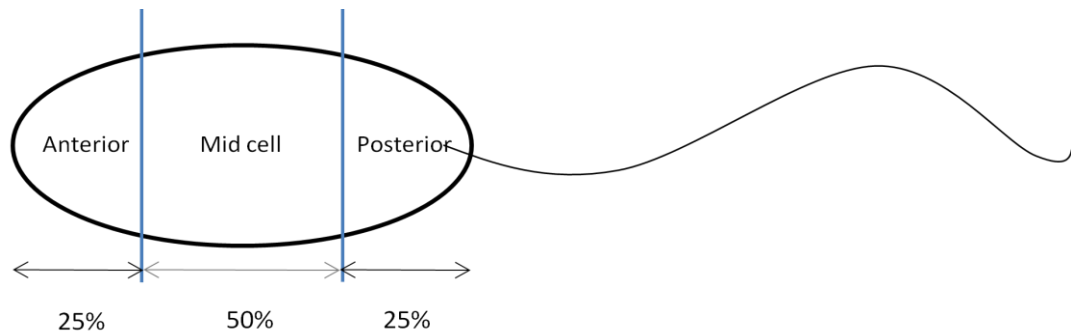


Figure 3.11A. Schematic showing localisation measurements

Schematic of *Leishmania* parasite showing determination of localisation for each GFP spot

	Mid cell	Posterior	Anterior	Multiple location
WT + GFP-LmxDIP13	33%	55%	6%	6%
Δ MPK2 -/- K1 + GFP-LmxDIP13	25%	42%	23%	10%
Δ MPK2 -/- K2 + GFP-LmxDIP13	33%	42%	20%	5%

Table 3.3. Overview of GFP-tagged LmxDIP13 localisation.

Overview of GFP spot location within *Leishmania*.

The different localisations of GFP-tagged LmxDIP13 expressed in wild type (figure 3.10) and *LmxMPK2* null mutant (figure 3.11) *L. mexicana* promastigotes are shown above. Not all cells exhibited fluorescence, with around a third expressing GFP. However, full quantification of the number of GFP expressing cells within each cell line was not carried out. An overview of the localisation and percentage of each found within the cells is described in Table 3.2.

GFP-tagged LmxDIP13 expressed in wild type *L. mexicana* exhibits four defined localisations; three individual localised spots and one where multiple localisations were present. The individual localisations found in various cells were identified in mid cell body (figure 3.10 A), posterior end of the cell (figure 3.10 B) and at the anterior end of the cell (figure 3.10 C). Some cells also exhibited multiple localisations (consisting of all previous individual localisations) at anterior, posterior and mid cell body (figure 3.10 D).

GFP-tagged LmxDIP13 expressed in *LmxMPK2* null mutant promastigotes displayed the same localisation as in the *L. mexicana* wild type cells - three individual localised spots and one where multiple localisations were present. Localisation at mid cell body (figure 3.11 A), the posterior end of the cell (figure 3.11 B), at the anterior end of the cell (figure 3.11 C) was observed. Some cells exhibited multiple localisations (consisting of previous individual localisations) at anterior, posterior and mid cell body (figure 3.11 D). The low frequency of some of the mutant phenotypes (described in figure 3.1) was reflected in this investigation, combined with the number of GFP expressing cells within the transfected culture resulted in a limited number of some of the imaged GFP mutant phenotypes. Figure 3.11 E was included to show GFP expression in the various phenotypes observed in the *LmxMPK2* null mutant promastigotes

The percentage of each different localisation was determined. The most common localisation was at the posterior end constituting 55% in wild type promastigotes and 42% in *LmxMPK2* null mutants. Localisation to mid cell made up 33% and 25% of wild

type and null mutant cells, respectively. GFP-LmxDIP13 localisation to the anterior end of the parasites and to multiple locations constituted similar proportions when expressed in the wild type. However, when expressed in the *LmxMPK2* null mutant localisation to the anterior end of the cell occurred significantly more frequently ($p < 0.05$) than localisation to multiple locations within the cell (Table 3.3). The results between $\Delta LmxMPK2$ -/- K1 and $\Delta LmxMPK2$ -/- K2 are similar and further support the consistency between the null mutants. No correlation between cell size and shape was observed for the specific localisation of LmxDIP13.

3.3 Discussion

3.3.1 The Phenotype of *LmxMPK2* null mutants and *LmxMPK2* add back mutants

Prior to the commencement of this work both *LmxMPK2* null mutants and genomic add back mutants had been generated. Two independent clones had been selected for each mutant – $\Delta LmxMPK2$ $-/-$ K1, $\Delta LmxMPK2$ $-/-$ K2, $\Delta LmxMPK2$ $-/-$ K1 + g*MPK2* K1 and $\Delta LmxMPK2$ $-/-$ K2 + g*MPK2* K3. These clones were used for all further analysis. Preliminary work showed *LmxMPK2* to be essential for the proliferation of amastigotes and therefore the kinase constitutes a potential drug target (Munro, Bachelors Thesis, 2009). Electron microscopy of the null mutants revealed several morphological abnormalities including lobed cell bodies, multiple flagella, spiked posterior ends and division from the posterior end. The add back mutants appeared to regain a normal phenotype, although some electron micrographs suggested they may have longer flagella than the wild type promastigotes. Here, several strategies have been applied to investigate the function of *LmxMPK2* in more detail.

3.3.2 Morphology and proliferation

Several phenotypes were observed in the *LmxMPK2* null mutant *L. mexicana*. It was expected that the *LmxMPK2* add back should reveal wild type morphology. However, scanning electron microscopy seemed to show a phenotypic difference between the wild type *L. mexicana* and the *LmxMPK2* add back mutants to be the apparent increase in flagellar length in the *LmxMPK2* add back mutant (figure 1.10). These non concordant findings were analysed and quantified using brightfield microscopy.

Both independent *LmxMPK2* null mutant clones were included to show consistency of results and to confirm that the phenotypes observed were due to the deletion of *LmxMPK2*. Seven distinct morphologies were observed, with the most common being an apparently normal phenotype making up 42% of the promastigotes (table 3.1). The other six phenotypes can be categorised into two sub groups; cosmetic abnormalities

and division abnormalities. The first group, cosmetic abnormalities, consists of spiked cell bodies, spiked cell bodies with extended flagella and normal cell bodies with extended flagella. These account for 25%, 3% and 8% of promastigotes, respectively (figure 3.1/table 3.1). The division abnormalities group consists of cells dividing from the posterior end, large spherical cells (often with multiple flagella) and cells which show budding cell bodies, making up 8%, 9% and 5% of the promastigotes, respectively (figure 3.1/table 3.1). The effect of the deletion of *LmxMPK2* on cell morphology and division suggests involvement in microtubule regulation. It is possible that the various abnormalities, at least in part, represent various stages of the cell cycle. The cells with a long flagellum may represent cells which have undergone several cycles (discussed later). Posterior dividing and budding cells would indicate cytokinesis, since approximately only 10-20% of cells are undergoing division at any given time, this would account for the low penetrance. Additionally, it is difficult to tell whether the large proportion of normal cells actually reflect cells lacking an abnormal phenotype. Since wild type cells were not included in this investigation, it is not clear if any of these abnormalities would be found within a wild type *L. mexicana* culture and what percent would exhibit abnormal cell morphology or division. Therefore conclusions drawn at this stage are limited and should be approached with caution.

As a proportion of the *LmxMPK2* null mutants exhibited division abnormalities, it was expected to find an impaired ability to proliferate. The *LmxMPK2* null mutant failed to reach the maximum stationary phase density of 1.17×10^8 cells/ml for wild type *L. mexicana* promastigotes only reaching 9.2×10^7 cells/ml (figure 3.2). This is 78% of the wild type maximum cell density, however *LmxMPK2* null mutants appeared to proliferate at a similar rate as the wild type during log phase growth (as shown by the growth trend). The *LmxMPK2* add back mutant reached a slightly lower maximum stationary phase density at 1.02×10^8 cells/ml than the wild type (figure 3.2). Statistical analysis found this not to be a significant difference ($p > 0.05$). Since the re-expression of *LmxMPK2* in the add back mutants showed growth comparable to that of the wild type, the lower final cell density of the $\Delta LmxMPK2$ *-/-* mutants must be an effect of the *LmxMPK2* deletion. This is also in accordance with the results of the phenotype quantification of the *LmxMPK2* null mutants (figure 3.1/table 3.1) where around 20% of

the cells exhibited division abnormalities. It is not clear whether the posterior dividing cells eventually produce a second flagellum. MAP kinases have been directly implicated in environmental sensing and regulation of the cell cycle (Rotureau *et al.*, 2009). For example, null mutants of *TbMAPK2*, the orthologue of *Leishmania* MPK4, proliferated normally in culture at the bloodstream stage but differentiated less efficiently at the procyclic blood stream stage. Null mutants of *TbMAPK4*, the orthologue of *Leishmania* MPK12, proliferated normally but were sensitive to an elevation in temperature (Rotureau *et al.*, 2009). It is possible that the deletion of *LmxMPK2* from *L. mexicana* interrupted the parasites ability to properly sense or utilise the nutrients in the media leading to the *LmxMPK2* null mutants entering stationary phase at a lower final cell density than the wild type.

Although *LmxMPK2* null mutants displayed an array of phenotypic abnormalities, electron micrographs of the *LmxMPK2* add back mutants suggested they had returned to a normal phenotype but may produce extended flagella. An investigation into the flagellar length of each cell line was carried out to confirm this observation. Measurements of the flagellar length of *LmxMPK2* null mutants and the *LmxMPK2* add back mutant revealed no significant difference in the average length compared to the wild type *L. mexicana* (figure 3.3). However, the *LmxMPK2* null mutants showed a greater distribution of flagellar lengths which vary from 1.5 μm to 42.7 μm compared to the wild type which ranges from 4.0 μm to 23.6 μm (table 3.2). The *LmxMPK2* add back mutant showed a similar distribution to the wild type. *Leishmania* cell division begins with the formation of the new flagellum (Wheeler *et al.*, 2011). All flagella measured in this study under 5 μm belonged to a dividing cell (or an *LmxMPK2* null mutant multiple flagella phenotype cell). The shorter flagella measured in each cell line indicated the beginning of cell division and not that deletion of *LmxMPK2* led to a shortening effect of the flagellum. However, second, third and (occasionally) fourth flagella observed in the *LmxMPK2* null mutants appeared to be reduced in length. Without following these cells through the cell cycle, it was not possible to determine whether they would reach a normal flagellar length or longer. It is possible that *LmxMPK2* is important in the correct signalling of cytokinesis or more likely indirectly blocking the correct signal being relayed – this will be discussed in more detail later.

Wheeler *et al.*, 2011 observed that the growth of the flagella extends over multiple cell cycles, growing progressively longer with each cycle, until a certain length when it began to disassemble at the tip. The growth rate of the flagella was inversely proportional to the length of the flagella, meaning the growth rate and slow disassembly eventually give rise to an equilibrium length (Wheeler *et al.*, 2011). Additionally, it was noted that disassembly of the flagella began with the growth of the second flagellum. A second flagellum was not always present in the dividing cells which could therefore give rise to cells with extended flagella. Especially, if cells start dividing from the posterior end without the formation of a new flagellum and accomplish cytokinesis the daughter with the flagellum will show an increase in flagellar length. This would also explain why the large cells in the *LmxMPK2* null mutant with multiple flagella have average or close to average flagella lengths. Differences in *LmxMPK2* null mutant flagellum length is therefore likely an effect of the *LmxMPK2* deletion.

3.3.3 *In vivo* analysis of GFP-tagged LmxMPK2

LmxMPK2 has been shown to affect cell morphology and may be involved in microtubule regulation. However, the exact mechanism is unknown. In order to gain insight into its function, green fluorescent protein was fused to the C-terminus of LmxMPK2, expressed in promastigotes and subsequently localised using fluorescence microscopy. This had the advantage of visualising the kinase *in situ* aiding elucidation of LmxMPK2 function and a convenient tag for purification in its natural state (Morales *et al.*, 2007). Viability and activity retention of C-terminally tagged LmxMPK1-GFP had previously been confirmed through infection of Balb/c mice with recombinant parasites (Wiese unpublished). Similarities between LmxMPK1 and LmxMPK2 suggested C-terminally tagged LmxMPK2GFP would also be functional.

Taking the sub-cellular localisation of LmxMPK2 and the various phenotypes of the *LmxMPK2* null mutant into account, it appears that LmxMPK2 may play a role in the regulation of microtubules. The sub-pellicular microtubules, which are essential for the maintenance of cell shape (Robinson *et al.*, 1995), are the most likely to be influenced

by LmxMPK2. The phenotypic abnormalities observed in the *LmxMPK2* null mutants all point toward an error in sub-pellicular microtubule organisation and indicate LmxMPK2 may be involved in their regulation (or at least co-regulation). As all the sub-pellicular microtubules exhibit the same polarity with the plus end at the posterior end of the cell (Robinson *et al.*, 1995), dysregulation may result in the continued polymerisation of individual or a small number of the microtubules resulting in the spiked posterior end.

Detergent extracted cytoskeletons of trypanosomatids retain cell shape due to the sub-pellicular corset of microtubules that are cross-linked to each other and the plasma membrane (Dagger *et al.*, 2013; Robinson *et al.*, 1995). Fluorescent labelling of the tubulin after detergent removal of the cytoskeleton revealed diffuse fluorescence throughout the cell with an accumulation at both the anterior and posterior ends (Dagger *et al.*, 2013). This was similar to the localisation of LmxMPK2 further supporting the notion of interaction between the two. Additionally, the inhibition of *L. mexicana* by the anti-microtubule drug ansamitocin P3 (AP3) revealed large spherical cells caused by impairment in the development of the sub-pellicular microtubules (Dagger *et al.*, 2013). This was similar to one of the *LmxMPK2* null mutant phenotypes. It would be interesting to see if there is a direct interaction of this inhibitor with LmxMPK2.

There have been several investigations into the cell cycle of trypanosomatids and *Leishmania*, yet still the mechanism of the furrowing of the membrane in preparation for cytokinesis remains obscure (Ambit *et al.*, 2011; Wheeler *et al.*, 2011; Hammarton *et al.*, 2006). As the main role of the sub-pellicular microtubules is to maintain the cell shape, it is not unreasonable to assume they are involved in the ingression furrow. If this is in part regulated by LmxMPK2, the *LmxMPK2* null mutant *L. mexicana* could result in ingression furrow errors. In the *LmxMPK2* null mutant the ingression furrow begins at the posterior end and not the accepted anterior end (Ambit *et al.*, 2011; Wheeler *et al.*, 2011). Indeed, around 20% of the cells exhibited localisation of LmxMPK2GFP at the posterior in addition to the anterior end which correlates with results discussed in chapter 4.1.1, where around 20% of the cells showed division abnormalities.

Recently, a relationship between LmxMPK2 and the aquaglyceroporin 1 was suggested by Mandal *et al.*, 2012. Over expression of LmjMPK2 in *Leishmania* affected the osmotic stress response and metalloid sensitivity of the parasite by positively regulating LmjAQP1. After confirming that all clones generated expressed GFP-LmxDIP13 (figure 3.9), an unexpected band was detected by the anti-GFP antibody in lanes 1-6 at 26 kDa – the approximate size of the GFP-tag. It is possible this additional band is observed due to cleavage of the tag. Although it is not clear how this might occur, it is not unique to this fusion protein. Similar results have been observed in fusion proteins such as GFP-PINK1 (Beilina *et al.*, 2005). It is also possible that association with microtubules may leave LmxDIP13 susceptible to regular degradation releasing free GFP into the cell.

The localisation of GFP-LmxDIP13 within the wild type *L. mexicana* and the LmxMPK2 null background *L. mexicana* was found to be similar, showing single spots (at the anterior, posterior or mid cell) or multiple spots (figure 3.3, Figure 3.4). It was initially thought the multiple spots consisted of the individual puncta found in the single localisations. On further analysis (illustrated in figure 3.11A), it was discovered that these spots were not confined to an individual localisation but appeared to form a non-continuous line through the cell. This line appears to be consistent with the single microtubule which forms an almost straight line through the interior of *Leishmania* (Weise *et al.*, 2000), suggesting GFP-LmxDIP13 co-localise to this microtubule. This is also a consistent pattern with the *T. brucei* homologue. TbDIP13 was found to have the ability to self-assemble into filaments when sufficient concentrations were reached. However, lower levels of the protein led to a punctate pattern partially co-localising with acetylated α -tubulin (Price *et al.*, 2012). In *C. reinhardtii*, the localisation of DIP13 was limited to the basal apparatus – associated to the flagella where the acetylated α -tubulin is found exclusively (Schoppmeier *et al.*, 2005). These observations suggest that LmxDIP13 also co-localises with acetylated α -tubulin (although acetylated α -tubulin appears not to be restricted to the flagella in trypanosomatids) which plays an important role in the regulation of microtubule assembly (Perdiz *et al.*, 2011). Although the localisation of LmxDIP13 appeared similar between the wild type and *LmxMPK2* null mutants, quantification revealed a clear shift in localisation. LmxDIP13 was locating more frequently to the anterior end in the *LmxMPK2* null mutants (Table 3.3). As

previously discussed in chapter 3.3.3, LmxMPK2 localises to the anterior end with occasional posterior localisation – possibly also the central microtubule. The similar localisations and LmxDIP13 localisation shift to the anterior end in the absence of LmxMPK2 suggests a relationship exists between the two. The actual nature of the relationship remains unclear. However, the deletion of DIP13 in the *T. brucei* homologue revealed no morphological abnormalities, yet deletion of *LmxMPK2* resulted in morphological alterations in *L. mexicana* promastigotes and a shift in the localisation of LmxDIP13 to the main LmxMPK2 localisation. There may be a secondary or compensatory role played by the LmxDIP13 in the regulation of the microtubules; this is suggested by the shift in LmxDIP13 localisation distribution to the anterior end of the *LmxMPK2* null mutants - which was found to be the localisation of LmxMPK2.

However, as a potential cell cycle marker, the size of the cell does not appear to play a role in the specific localisation of LmxDIP13 and therefore no determination of different cell cycle stages could be made. DIP13 is therefore not suitable as a cell cycle marker in *Leishmania*.

Although there is some consistency between the localisation of DIP13 in *L. mexicana* and *T. brucei*, detection of GFP by immunoblot analysis suggested that there could be free GFP within the cell contributing to the fluorescence. Therefore it cannot be definitively shown to be only the localisation of the GFP-LmxDIP13. However, studies using GFP only expression in various *Leishmania* species showed localisation to the whole cytosol (Costa *et al.*, 2011; Bolhassani *et al.*, 2011). Performing immunofluorescence using an anti-DIP13 antibody rather than GFP-tagging could corroborate this – although time and expense made this unfeasible. Overall, the similarities in the localisation to other models may suggest fluorescence on the whole is due to DIP13.

3.4 Summary of Phenotypic analysis of *LmxMPK2* null mutants and *LmxDIP13*

LmxMPK2 was previously found to be essential to the amastigote stage of the *Leishmania* life cycle (Wiese, 2007). Therefore, investigations into the role, localisation and activity of the kinase were carried out. Work in this section focused on the phenotypic analysis and localisation of the kinase in order to elucidate its role within *Leishmania*.

Prior to this project, homozygous gene deletion mutants for *LmxMPK2* had been generated. Initial investigations revealed morphological abnormalities of promastigotes including lobed cell bodies, spiked posterior ends and division from the posterior end (Wiese, unpublished). This study further catalogued the full extent of the abnormalities. Seven phenotypes were described; normal, spiked posterior ends, large spherical cells, non-spiked cells with extended flagella, spiked cells with extended flagella, and cells with budding cell bodies. Despite 60% of the cells showing an array of abnormal phenotypes, only 10-20% affected the proliferation of *L. mexicana* promastigotes.

To elucidate the localisation and role of *LmxMPK2* within *L. mexicana* C-terminally GFP-tagged *LmxMPK2* was expressed in wild type and *LmxMPK2* null mutant parasites. Fluorescence microscopy of promastigotes revealed localisation of *LmxMPK2*GFP to both poles of the cell. Taking the intracellular localisation of *LmxMPK2* and the various phenotypes of the *LmxMPK2* null mutant into account, it appears that *LmxMPK2* may play a role in the organisation of the microtubules influencing cell shape. Similar localisation of *LmxMPK2* and *LmjAQP1* suggests a link between the two. Ultimately, *LmxMPK2* appears to play an important role in the signalling and regulation of cytokinesis.

Investigations to determine whether co-localisation between *LmxMPK2* and *LmxDIP13* (Deflagellation Inducible Protein), a protein shown to associate with microtubules, occurred or whether *LmxDIP13* would be suitable as a cell cycle marker were undertaken. GFP-tagged *LmxDIP13* was expressed in wild type and *LmxMPK2* null mutant promastigotes. Localisation was punctate and found in singular or multiple spots

following a discrete line throughout the cell, consistent with the single microtubule extending through the cell. This was similar to the *T. brucei* homologue (Price *et al.*, 2012). No difference in general localisation was observed between wild type and *LmxMPK2* null mutants expressing GFP-LmxDIP13. However, the percentage of cells showing GFP-LmxDIP13 at the anterior end of the cell increased from 6% to at least 20%. Although the nature of the relationship remains uncertain.

Chapter 4

Characterisation of recombinant LmxMPK2

4.1 Introduction

The phosphorylation states of LmxMPK2 were unknown when this project was started. Attempts to find phosphorylation of LmxMPK2 *in vivo* using mass spectrometry proved unsuccessful, as the protein could not be detected in promastigotes and amastigotes (Rosenqvist, PhD Thesis, 2011). New data however, found that *L. donovani* MPK2 was phosphorylated on the tyrosine residue of the TDY motif (Y-176) in amastigotes. A serine residue was also phosphorylated at S-169. The phosphorylation of the TDY motif was found to be exclusive to the amastigotes (Tsigankov *et al.*, 2013).

Work to dephosphorylate LmxMPK1 using commercial λ -phosphatase was inconsistent. In order to successfully and consistently produce dephosphorylated recombinant kinase a co-expression plasmid where a kinase is co-expressed with a phosphatase was developed (McAlear, PhD Thesis, 2012). Human PTP1B, a tyrosine phosphatase, and the bacteriophage λ -phosphatase, a dual-specificity phosphatase, were selected for the system and should allow a comparison of the effect of differential phosphorylation of the kinase. The system was applied to this project with the aim to provide insight into the regulation of LmxMPK2. In order to show activity was due to LmxMPK2, an enzymatically inactive version of the kinase had been generated where a highly conserved lysine residue essential to kinase activity was mutated to a methionine residue (K42M) (Wiese unpublished). Immunoblots and autoradiographs in this section were selected as the best image from a minimum of three repeats. All are representative of a visual assessment and provide an accurate illustration of each investigation.

4.2 Results

4.2.1 Generation of LmxMPK2 expression plasmids

The novel dephosphorylation of LmxMPK2 required the co-expression of a phosphatase with LmxMPK2 on a single plasmid. This would allow the phosphatase to dephosphorylate the kinase during the expression of the plasmid in bacterial cells, with the ultimate aim of purifying dephosphorylated kinase. Plasmids encoding PTP1B (p-ampR-PTP1B) and λ -phosphatase were provided by Prof David Barford (ICR, London, UK) and were previously used to generate pJC-LmxMPK1-3HA- λ -phosphatase and pJC-LmxMPK1-3HA-PTP1B, respectively (McAler, 2012). The plasmids pJC-LmxMPK2 and pGEX-LmxMPK2 also pre-dated the beginning of the project.

pJC-LmxMPK1-3HA- λ -phosphatase was cleaved using *NcoI* and *HindIII* yielding a 3151 bp fragment, which was ligated with the 1441 bp fragment released following digestion of pJC-LmxMPK2 using the same enzymes. This produced the plasmid pJC-LmxMPK2-3HA- λ -phosphatase. Similarly, pJC-LmxMPK1-3HA-PTP1B was cleaved using *NcoI* and *NotI* yielding a 3144 bp fragment, which was ligated with the 1448 bp fragment released following digestion of pJC-LmxMPK2 using the same enzymes. This produced the plasmid pJC-LmxMPK2-3HA-PTP1B.

The enzymatically inactive LmxMPK2K42M was generated by cleavage of pJC1EH2MPK2 using *AscI* and *NheI* yielding a 3580bp fragment. This fragment was ligated with the 1012bp fragment released following digestion of pGEX-KG1LmxMPK2KM using *AscI* and *NheI* producing the plasmid pJC-LmxMPK2KM.

4.2.2 Recombinant co-expression and affinity purification of

LmxMPK2

The newly generated plasmids pJC-LmxMPK2-PTP1B, pJCLmxMPK2- λ -phosphatase and pJC-LmxMPK2K42M were used in an *E. coli* expression and purification system to confirm protein production. pGEX-KG-LmxMPK2 (GST-tag) and pJC-LmxMPK2 (His-tag) existed prior to this project but had only been tested for expression and so they were also included. The SDS-PAGE gel was Coomassie-stained to visualise the protein (figure 4.1).

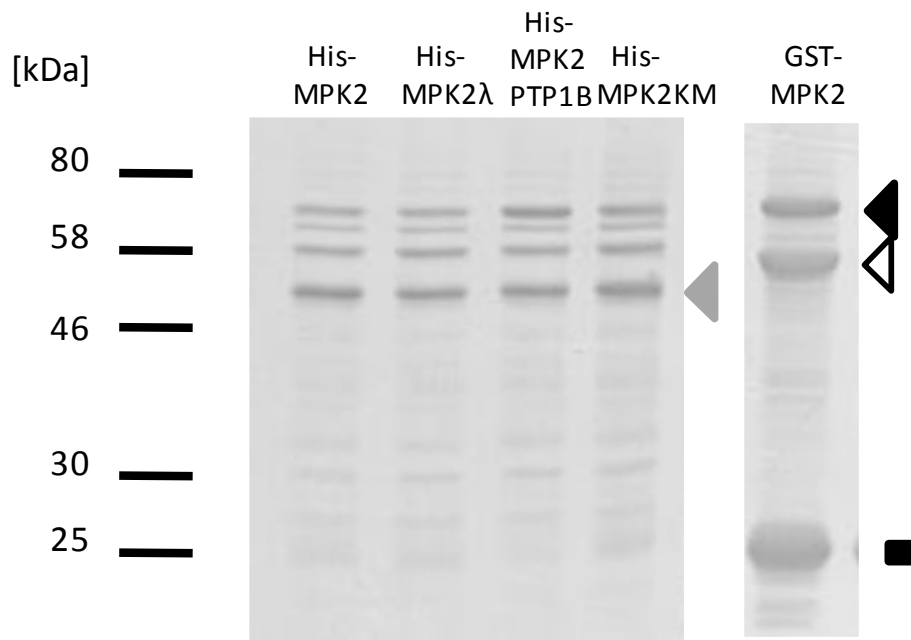


Figure 4.1. Coomassie-stained gel of recombinant GST-LmxMPK2 and various His-LmxMPK2 versions.

Differently tagged recombinant LmxMPK2 visually quantified using SDS-PAGE and Coomassie staining.

Left panel – various His-LmxMPK2; right panel – GST-LmxMPK2. (◄) GST-LmxMPK2; (◄) His-LmxMPK2; (◄) MPK2 (truncated at the C-term?); (■) GST-tag. Molecular masses of standard proteins are indicated in kDa.

The recombinant expression and purification of all proteins was successful (Figure 4.1). Standard SDS-PAGE separation followed by Coomassie staining showed distinct protein bands at 52 kDa in lanes 1-4, consistent with the His-tag fusion protein, and 78 kDa (lane 5) consistent with a GST-tag fusion protein. However, figure 4.1 also reveals two additional distinct bands in the separation of GST-LmxMPK2; the sizes roughly match untagged LmxMPK2 (52 kDa) and the GST-tag (26 kDa). Other proteins were also present in the His-LmxMPK2 preparations, likely to be of bacterial origin. All hexahistidine-tagged preparations showed equal expression levels but slightly lower expression than the GST-LmxMPK2.

4.2.3 Evaluation of LmxMPK2 bands on SDS-PA gels

GST-LmxMPK2 was able to phosphorylate the generic kinase substrate myelin basic protein (MBP) without showing autophosphorylation as seen in the case of His-LmxMPK2. To test whether any of the additional bands in the GST-LmxMPK2 preparation is a proteolytically processed kinase which might contribute to kinase activity His-LmxMPK2 and GST-LmxMPK2 were subjected to immunoblot analysis as detailed in chapter 2.2.15 using the anti-LmxMPK2 (C-term) polyclonal rabbit antiserum.

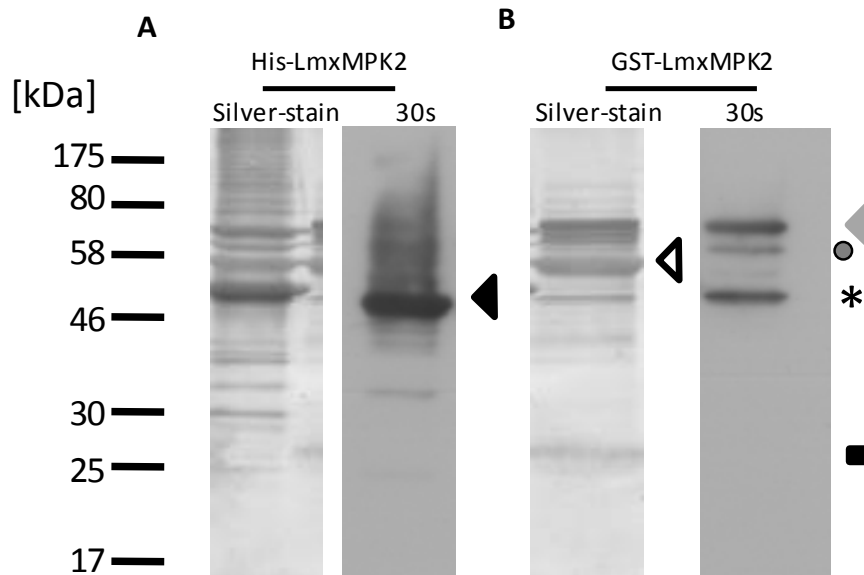


Figure 4.2. Immunoblot of differently tagged LmxMPK2 using anti-LmxMPK2 (C-term) polyclonal antiserum

Immunoblot identifying LmxMPK2 protein on SDS-PA gels and displaying comparison of MPK2 expression in recombinant (A) His-LmxMPK2 and (B) GST-LmxMPK2.

Left panels, Silver-stained gels; right panels, immunoblot probed with the polyclonal anti-LmxMPK2 antiserum after 30s exposure. (◄) His-LmxMPK2; (◄) GST-LmxMPK2; (*) LmxMPK2; (●) GST-LmxMPK2 cleavage product (GST-tag); (◄) GST-LmxMPK2 cleavage product (C-term of kinase); (■) GST-tag. Molecular masses of standard proteins are indicated in kDa.

In all assays containing GST-LmxMPK2, multiple bands were present. It was thought the band around 78 kDa was GST-LmxMPK2 (grey arrow), and the two further distinctive bands at approximately 52 kDa (black star) and 25 kDa (black rectangle) were LmxMPK2 (with the GST-tag cleaved) and the cleaved GST-tag, respectively. In order to show this was the case His-LmxMPK2 and GST-LmxMPK2 were subjected to immunoblot analysis with a polyclonal anti-LmxMPK2 antiserum against a C-terminal peptide of the kinase (figure 4.2). As expected, a strong and distinct signal was detected at approximately 52 kDa for the His-LmxMPK2 (lane 1'). Three bands were produced in the case of the GST-LmxMPK2 (lane 2'). In addition to the expected band at 78 kDa (indicating the GST-tagged LmxMPK2), a slightly lower band at around 65-70 kDa (grey circle) was detected and another band at around 52 kDa. Silver-staining of SDS-PA gels is a more sensitive method for protein detection than Coomassie-staining and was applied to increase the visibility of the protein band at 52 kDa in lane 2. The intense band observed around 56 kDa (black outline arrow) on the silver-stain gel did not react with the antiserum.

4.2.4 Optimisation of kinase assay conditions

Because no optimisation of the reaction conditions had been carried out for any LmxMPK2 construct yet this was done for His-LmxMPK2, His-LmxMPK2/PTP1B and His-LmxMPK2/ λ -phosphatase in this project. As with most *Leishmania* MAP kinases, the substrate for LmxMPK2 is currently unknown. In order to assess the phosphotransferase activity of the kinase, dephosphorylated myelin basic protein (MBP) was used as a model substrate.

Radiometric assays were carried out at 34°C under standard kinase assay conditions using equal amounts of purified LmxMPK2 to show clear and reproducible bands on a Coomassie-stained gel (approximately 1 μ g).

All results in this section are of kinase assays carried out simultaneously with radiation from a single stock to ensure equal levels of radioactive activity in each assay. Results shown are representative of three repeats.

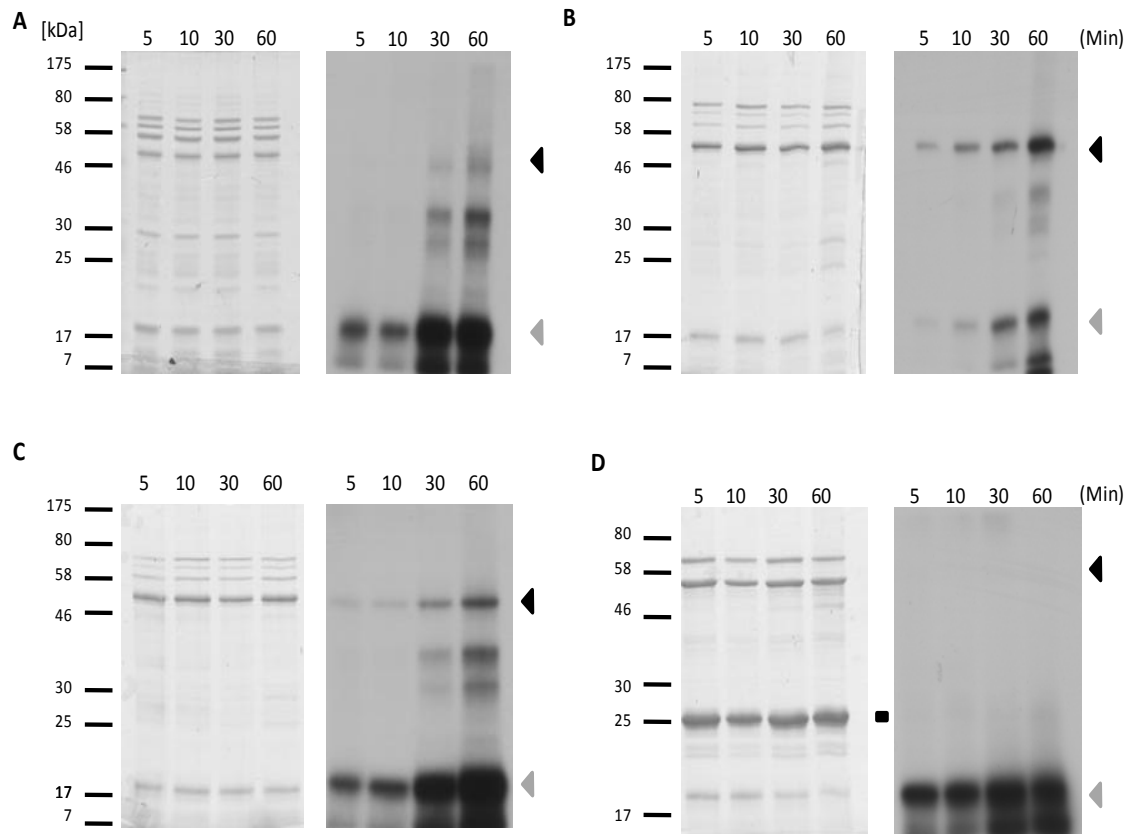


Figure 4.3. Kinase assays of different LmxMPK2 fusion proteins in standard kinase buffer.

Autophosphorylation and substrate phosphorylation of (A) His-LmxMPK2; (B) His-LmxMPK2 co-expressed with λ -phosphatase; (C) His-LmxMPK2 co-expressed with PTP-1B; (D) GST-LmxMPK2 assessed over 60 min in standard kinase assay buffer.

Left panels - Coomassie-stained gels; right panels - autoradiograph after 20 hours exposure. Assay conditions: (100 mM NaCl, 10 mM Mg^{2+} , 2 mM Mn^{2+} , 5 μ g MBP and 1 mM ATP containing 5 μ Ci γ - ^{32}P -ATP, 34°C incubation). (◄) LmxMPK2; (◄) MBP; (■) GST-tag. Molecular masses of standard proteins are indicated in kDa.

Figure 4.3 illustrates the assessment of LmxMPK2 phosphotransferase activity in a standard kinase reaction buffer prior to optimisation.

The phosphotransferase activity of singly expressed His-LmxMPK2 after incubation with radiolabelled ATP is shown in figure 4.3 A. Phosphorylation of MBP was evident after 5 min incubation with further phosphorylation occurring until 30 min when it appeared to plateau. Substrate phosphorylation commenced earlier than autophosphorylation, which began after approximately 30 min incubation.

Phosphotransferase activity of His-LmxMPK2 co-expressed with λ -phosphatase was analysed in the same manner (figure 4.3 B). Autophosphorylation and MBP phosphorylation was evident after 5 min incubation suggesting they occurred simultaneously unlike in the singly expressed His-LmxMPK2. MBP phosphorylation was weak at 5 min but gradually increased up to 60 min. The autophosphorylation also increased with longer incubation.

His-LmxMPK2 co-expressed with PTP1B displayed similar substrate phosphorylation activity as the singly expressed His-LmxMPK2 where MBP phosphorylation began at 5 min and prior to autophosphorylation (figure 4.3 C). The weak signal at 5 min suggests autophosphorylation began later. The phosphorylation of MBP continued to increase with increasing incubation time. Unlike in the singly expressed His-LmxMPK2, the PTP1B co-expressed His-LmxMPK2 began autophosphorylation after 5 min incubation (although only weakly) and increased over the 60 min incubation.

The activity of GST-LmxMPK2 was in complete contrast with all versions of His-LmxMPK2 as no autophosphorylation was present after any length of incubation (figure 4.3 D). However, it showed as strong a phosphorylation of MBP as His-LmxMPK2. The phosphorylation of MBP increased with longer incubation.

4.2.4.1 Optimisation of pH in kinase assay

The pH optimum was the first component of assay conditions investigated. A radiometric assay was carried out using equal amounts of purified LmxMPK2 to show a clear reproducible band on a Coomassie-stained gel (approximately 1µg) incubated at 34°C under standard ion and temperature conditions (figure 4.4).

All results in this section are of kinase assays carried out simultaneously with radiation from a single stock to ensure equal levels of radioactive activity in each assay. Results shown are representative of three repeats.

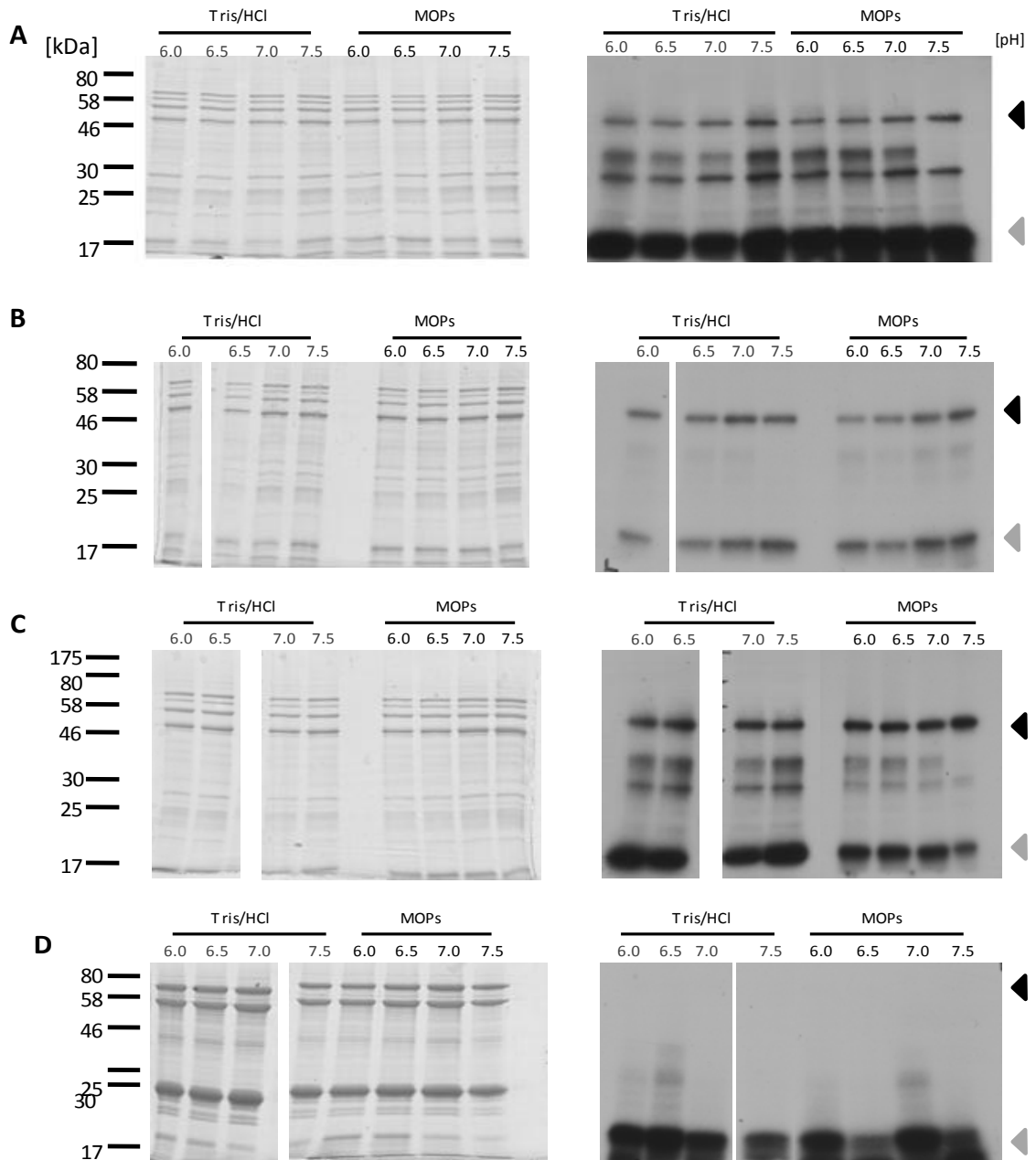


Figure 4.4. Kinase assays of different LmxMPK2 fusion proteins under different buffer and pH conditions.

Optimisation of buffer and pH for LmxMPK2 kinase assays. Autophosphorylation and substrate phosphorylation of (A) His-LmxMPK2; (B) His-LmxMPK2 co-expressed with λ -phosphatase; (C) His-LmxMPK2 co-expressed with PTP-1B; (D) GST-LmxMPK2 assessed after 60 min with varying buffers (Tris/HCl and MOPs) at varying pH.

Left panels - Coomassie-stained gels; right panels - autoradiographs after 20 hours exposure. (◄) LmxMPK2; (◄) MBP; (■) GST-tag. Molecular masses of standard proteins are indicated in kDa.

Singly expressed His-LmxMPK2 exhibited no substantial differences in the various buffers for either the autophosphorylation or MBP phosphorylation (figure 4.4 A). However, the phosphorylation of a co-purified protein of approximately 37 kDa (and likely of bacterial origin) appeared to be inhibited by MOPS pH 7.5 (lane 8). Hence, this buffer was not considered any further (reasons to be discussed later).

Similarly to the singly expressed His-LmxMPK2, His-LmxMPK2 co-expressed with λ -phosphatase displayed no substantial difference in phosphotransferase activity between the various buffers (figure 4.4 B). However, λ -phosphatase co-expressed His-LmxMPK2 appeared to have reduced phosphotransferase activity in comparison to singly expressed His-LmxMPK2. Incorporation of radiolabel into MBP was considerably lower for all pH when co-expressed with λ -phosphatase. Moreover, the additional bands around 30-40 kDa were hardly detectable.

Autophosphorylation and MBP phosphorylation of His-LmxMPK2 co-expressed with PTP1B was similar in all buffers (figure 4.4 C) and resembled that of the singly expressed His-LmxMPK2. Phosphorylation of a co-purified protein at approximately 37 kDa was also found to disappear in MOPS pH 7.5 (lane 8).

Singly expressed GST-LmxMPK2 displayed no autophosphorylation in any buffer (figure 4.4 D), which was to be expected as no autophosphorylation had been observed in earlier experiments. MBP phosphorylation varied between the various buffers and pH. MOPS pH 7.0 and Tris/HCl pH 6.5-7.0 appeared to result in highest activity.

Substrate phosphorylation appeared to be fairly consistent across the various His-tagged kinases. However, GST-LmxMPK2 did exhibit differences in MBP phosphorylation. The autoradiographs show many potentially suitable buffers for future kinase assays but Tris/HCl pH 7.0 was finally chosen due to slight elevation of autophosphorylation and it being the most universal buffer for both His-LmxMPK2 and GST-LmxMPK2.

4.2.4.2 Optimisation of ion concentration in kinase assay

Subsequent to establishing the best buffer and pH for optimal activity as Tris/HCl pH 7.0, a second round of radiometric kinase assays was carried out to assess the optimal ion concentration.

A radiometric assay was carried out using equal amounts of purified LmxMPK2 to show a clear reproducible band on a Coomassie-stained gel (approximately 1 μ g) incubated at 34°C under optimized pH and temperature conditions for 1 hour (figure 4.5).

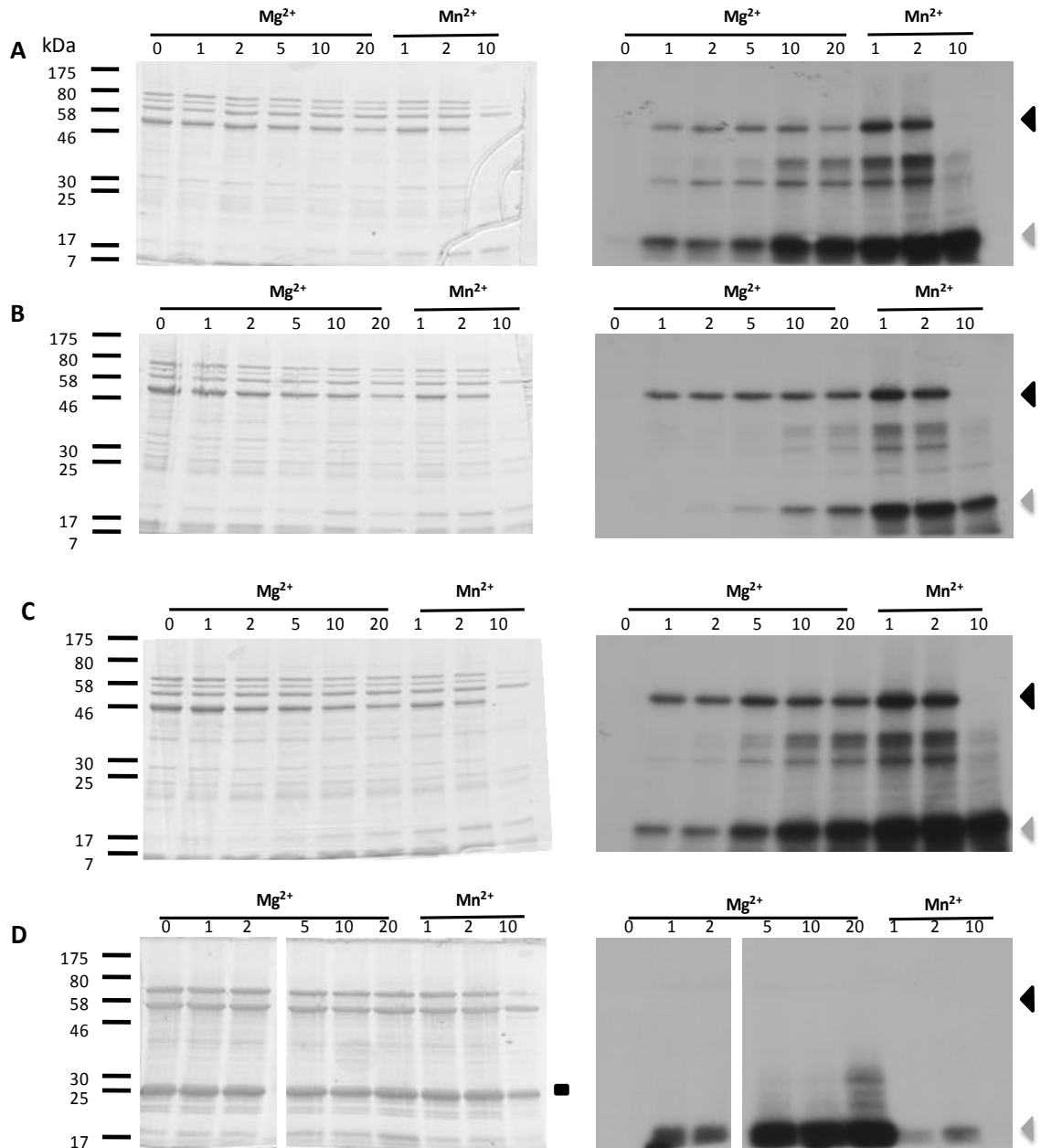


Figure 4.5. Kinase assays of different LmxMPK2 fusion proteins at varying ion concentrations.

Optimisation of ion concentration for LmxMPK2 kinase assays. Autophosphorylation and substrate phosphorylation of (A) His-LmxMPK2; (B) His-LmxMPK2 co-expressed with λ -phosphatase; (C) His-LmxMPK2 co-expressed with PTP-1B; (D) GST-LmxMPK2 assessed after 60 min with varying ions (Mg^{2+} and Mn^{2+}) at varying concentrations.

Left panels - Coomassie-stained gels; right panels - autoradiographs after 20 hours exposure. (◄) LmxMPK2; (◄) MBP; (■) GST-tag. Molecular masses of standard proteins are indicated in kDa.

The activity of singly expressed His-LmxMPK2 in Tris/HCl pH 7.0 with varying ion concentrations was assessed (figure 4.5 A). Lanes 1-6 show increasing Mg^{2+} concentration was associated with increased autophosphorylation and MBP phosphorylation activity. Kinase activity increased substantially in the presence of Mn^{2+} (lanes 7-9). Autophosphorylation and MBP phosphorylation increased further in the presence of 1-2 mM Mn^{2+} (lanes 7-8), however His-LmxMPK2 appeared to no longer be present in 10 mM Mn^{2+} and no autophosphorylation was found (lane 9). Despite the apparent lack of His-LmxMPK2, MBP phosphorylation was still detectable – signal at 17 kDa.

The phosphotransferase activity of His-LmxMPK2 co-expressed with λ -phosphatase was assessed (figure 4.5 B). Similar to the singly expressed His-LmxMPK2, lanes 1-6 show that increasing concentrations of Mg^{2+} increased the activity of the kinase with increasing signal intensity of the bands for MBP phosphorylation. As before, kinase activity substantially increased in the presence of Mn^{2+} (lanes 7-8), although at high concentrations (10 mM) no kinase was detectable on the gel. This also did not affect the ability of the kinase to phosphorylate MBP as a strong band is exhibited at 17 kDa (lane 9).

The phosphotransferase activity of His-LmxMPK2 co-expressed with PTP1B was also assessed in the same way (figure 4.5 C). Similar to the singly expressed His-LmxMPK2 and λ -phosphatase co-expressed His-LmxMPK2, increasing concentrations of Mg^{2+} increased the band intensity for both autophosphorylation and MBP phosphorylation (lanes 1-6). Activity of the kinase also increases considerably in the presence of Mn^{2+} - consistent with the other His-tagged versions of the kinase. Strong autophosphorylation and MBP phosphorylation is shown for 1-2 mM Mn^{2+} (lanes 7-8). As with the other His-tagged kinases, no His-LmxMPK2 was observed on the gel at 10 mM (lane 9) yet this did not affect the kinase's ability to phosphorylate MBP.

Singly expressed GST-LmxMPK2 phosphotransferase activity was also assessed (figure 4.5 D). No autophosphorylation occurred in any lane. Low concentrations of Mg^{2+} were

found to be unsuitable as very little MBP phosphorylation occurred. Strong MBP phosphorylation occurred in lanes 4-6 with no discernible difference between the concentrations (5-20 mM). Weak to no phosphotransferase activity occurred in buffers containing any concentration of Mn^{2+} .

The autophosphorylation of the His-tagged kinases increased as the Mg^{2+} concentration increased however they were most active in buffers containing Mn^{2+} . The maximal phosphotransferase activity for LmxMPK2 was also dependent upon Mn^{2+} . Despite GST-LmxMPK2 preferring Mg^{2+} (maximum activity at approximately 10 mM Mg^{2+}), 2 mM Mn^{2+} was chosen as the optimal ion for the kinase reaction buffer. Future assays would primarily focus on the activity of His-LmxMPK2.

4.2.4.3 Optimisation of incubation time for kinase assay

Having optimised the buffer (Tris/HCl pH 7.0, 100 mM NaCl, 2 mM Mn^{2+}) the optimal incubation time for LmxMPK2 could be examined. The pH optimum was first determined. A radiometric assay was carried out using equal amounts of purified LmxMPK2 to show a clear reproducible band on a Coomassie-stained gel (approximately 1 μ g) incubated at 34°C under optimized pH and ion concentrations for varying lengths of time (figure 4.6).

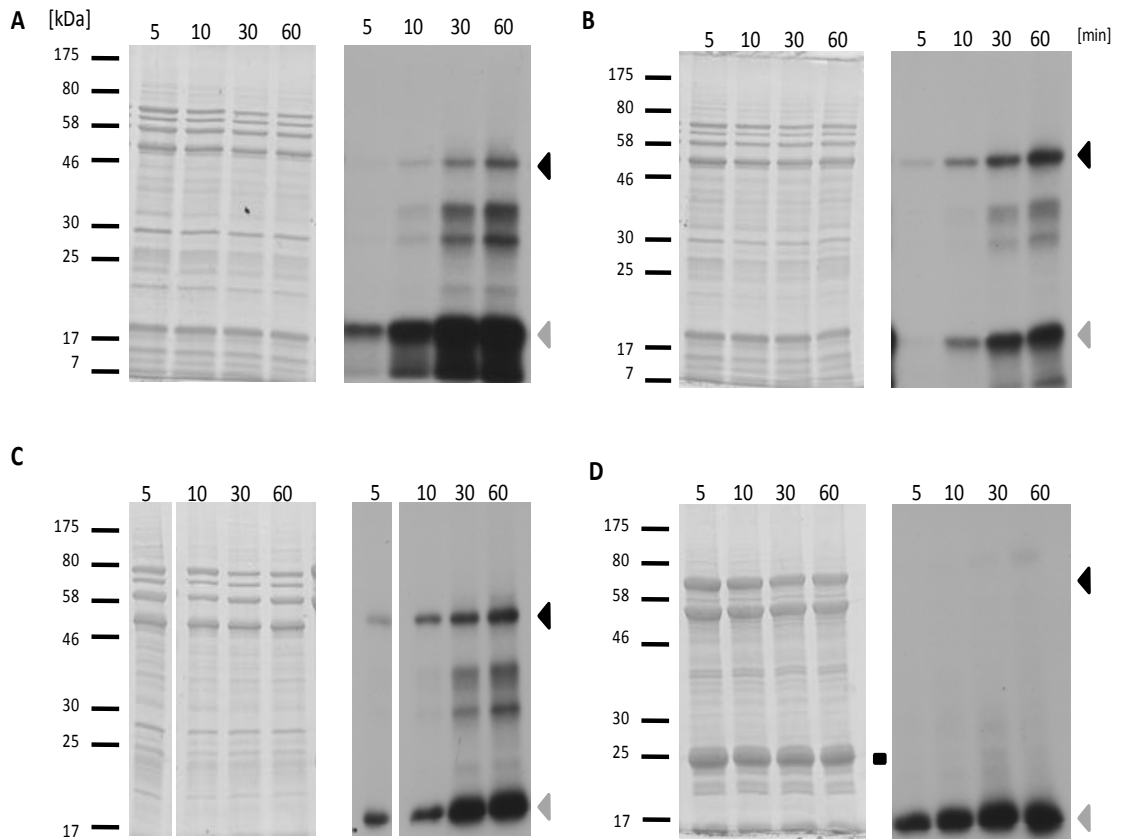


Figure 4.6. Kinase assays of different LmxMPK2 fusion proteins in an optimised buffer.

Autophosphorylation and substrate phosphorylation of (A) His-LmxMPK2; (B) His-LmxMPK2 co-expressed with λ -phosphatase; (C) His-LmxMPK2 co-expressed with PTP-1B; (D) GST-LmxMPK2 assessed over the course of 60 min in optimised buffer.

Left panels - Coomassie-stained gels; right panels - autoradiographs after 3 hours exposure. Assay conditions: (50 mM Tris/HCl pH 7.0, 100 mM NaCl, 2 mM Mn^{2+} , 5 μ g MBP). (\blacktriangle) LmxMPK2; (\blacktriangleleft) MBP; (\blacksquare) GST-tag. Molecular masses of standard proteins are indicated in kDa.

Singly expressed His-LmxMPK2 phosphorylation of MBP is evident after 5 min incubation with further phosphorylation occurring until 30 min, after which it appeared to plateau (figure 4.6 A). Substrate phosphorylation occurred earlier than autophosphorylation, which began after approximately 10 min incubation. Both the autophosphorylation and the MBP phosphorylation appeared to be stronger in the optimised reaction buffer compared to the standard reaction buffer in figure 4.3 A.

The phosphotransferase activity of His-LmxMPK2 co-expressed with λ -phosphatase was assessed in the same manner. Weak autophosphorylation was evident after 5 min incubation and increased with further incubation (figure 4.6 B). A slight delay in MBP phosphorylation was observed, with phosphorylation beginning after approximately 10 min incubation. The phosphorylation of MBP increased with longer incubation. As with the singly expressed His-LmxMPK2, the autophosphorylation and phosphotransferase activity of λ -phosphatase co-expressed His-LmxMPK2 were elevated in the optimised reaction buffer compared to the standard reaction buffer in figure 4.3 B.

Weak autophosphorylation was evident after 5 min incubation and gradually increased over the 60 min incubation for His-LmxMPK2 co-expressed with PTP1B (figure 4.6 C). Stronger phosphorylation of MBP at 5 min suggests phosphotransferase activity begins earlier than autophosphorylation. MBP phosphorylation increased with further incubation. The autophosphorylation activity of PTP1B co-expressed His-LmxMPK2 increased in the optimised reaction buffer, however the phosphotransferase activity remained the same.

As found in previous kinase assays, GST-LmxMPK2 exhibited no autophosphorylation activity (figure 4.6 D). Despite showing a high degree of phosphotransferase activity, the MBP phosphorylation appeared to be weaker in the optimised kinase buffer than in the standard kinase buffer shown in figure 4.3 D. This was likely due to this protein's dependence on Mg^{2+} (figure 4.5 D).

4.2.5 Assessment of LmxMPK2 activity

It is generally accepted that phosphorylation of both threonine (T) and tyrosine (Y) residues of the conserved TXY motif by a dual-specificity MAPK kinase is required for full activation of a MAP kinase. As mentioned in chapter 1.3, there are several differences between signalling in higher eukaryotes and *Leishmania* (i.e. some components have not been identified in *Leishmania*) (Parsons and Ruben, 2000). It is likely that the regulatory mechanisms are related but not exactly the same. Therefore, the change in phosphorylation state of tyrosine residues and threonine residues of the purified recombinant LmxMPK2 was assessed using dephosphorylated enzymes in kinase assays.

4.2.5.1 Assessment of tyrosine phosphorylation of phosphatase co-expressed protein

The phosphorylation of tyrosine residues in LmxMPK2 was assessed using phosphatase co-expressed His-LmxMPK2 and the monoclonal anti-phosphotyrosine antibody 4G10 (Bernhard Fleischer, BNI, Hamburg) in immunoblot analyses. Kinases assays were carried out as detailed in chapter 2.2.17 followed by immunoblot analysis as detailed in chapter 2.2.15.

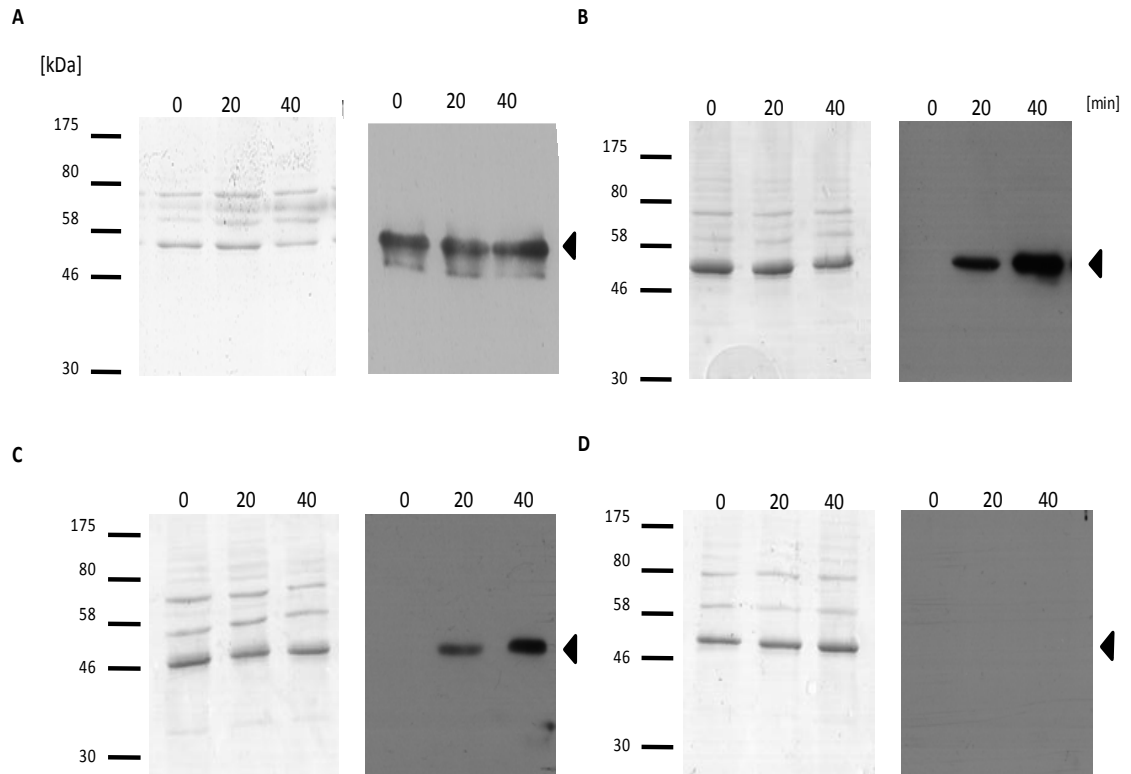


Figure 4.7. Immunoblot assessing tyrosine phosphorylation using different His-LmxMPK2 fusion proteins in autophosphorylation assays.

Immunoblot assessing tyrosine autophosphorylation of (A) His-LmxMPK2; (B) His-LmxMPK2 co-expressed with λ -phosphatase; (C) His-LmxMPK2 co-expressed with PTP-1B; (D) His-LmxMPK2KM over the course of 60 minutes, detected using monoclonal antibody 4G10.

Left panels - Coomassie-stained gels; right panels - immunoblots after 2 minute exposure. (◄) His-LmxMPK2.

Singly expressed His-LmxMPK2 as purified from *E. coli* (0 min, no ATP) appeared to be fully phosphorylated on tyrosine residues i.e. no further increase in band intensity with increasing time points (20 and 40 min) after incubation with ATP (figure 4.7 A).

The phosphotransferase activity of His-LmxMPK2 co-expressed with C-terminally tagged λ -phosphatase (figure 4.7 B) and LmxMPK2 co-expressed with N-terminally tagged PTP1B (figure 4.7 C) as purified from *E. coli* (0 min, no ATP) and increasing time points (20 and 40 min) after incubation with ATP was assessed in the same way. Both figures 28 B and 28 C show complete dephosphorylation of tyrosine when purified from *E. coli*. However, it did not appear to affect the activity of the kinase as increasing autophosphorylation on tyrosine was observed (20-40 min) for both phosphatase co-expressed kinases.

No phosphotransferase activity of His-LmxMPK2KM was observed (figure 4.7 D). This was expected as the mutation of lysine to a methionine in the ATP binding site renders the kinase unable to accept ATP.

4.2.5.2 Assessment of threonine phosphorylation of co-expressed proteins

The phosphorylation of threonine residues in LmxMPK2 was assessed using phosphatase co-expressed His-LmxMPK2 and the polyclonal anti-phosphothreonine antibody 71-8200 (Invitrogen, UK) in immunoblot analyses. Kinase assays were carried out as detailed in chapter 2.2.17 followed by immunoblot analysis as detailed in chapter 2.2.15.

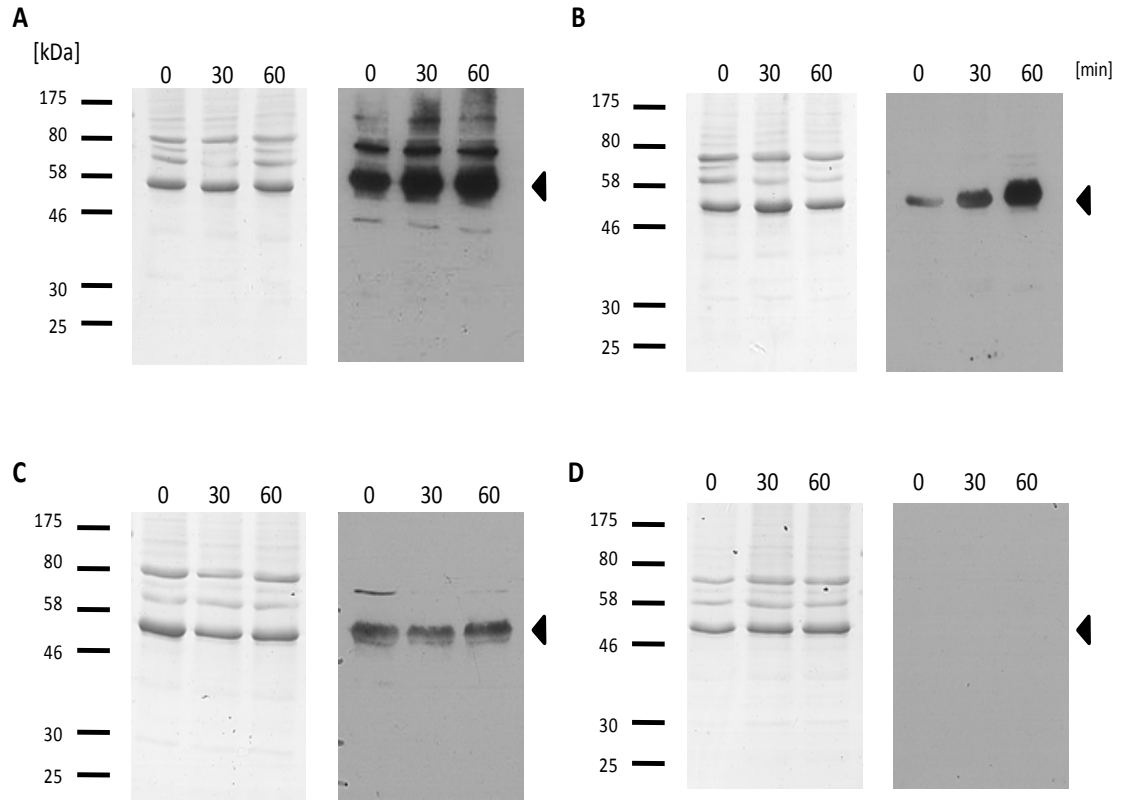


Figure 4.8. Immunoblot assessing threonine phosphorylation using different His-LmxMPK2 fusion proteins in autophosphorylation assay.

Threonine autophosphorylation of (A) His-LmxMPK2; (B) His-LmxMPK2 co-expressed with λ -phosphatase; (C) His-LmxMPK2 co-expressed with PTP1B; (D) His-LmxMPK2KM over the course of 60 min.

Left panels - Coomassie-stained gels; right panels - immunoblots after 2 min exposure.

(◄) His-LmxMPK2. Molecular masses of standard proteins are indicated in kDa.

Singly expressed His-LmxMPK2 as purified from *E. coli* (0 min, no ATP) displayed full phosphorylation on threonine residues and later time points (20 and 40 min) of incubation with ATP showed no further autophosphorylation (figure 4.8 A).

Following purification from *E. coli* His-LmxMPK2 co-expressed with λ -phosphatase exhibited partial dephosphorylation of threonine residues (figure 4.8 B). However, further autophosphorylation of threonine residues was observed after incubation with ATP.

His-LmxMPK2 co-expressed with N-terminally tagged PTP1B as purified from *E. coli* and further incubation with ATP (29 C) findings were similar to the singly expressed His-LmxMPK2 (29 A). The kinase appeared fully phosphorylated on threonine residues when purified from *E. coli* and no additional autophosphorylation occurred after incubation with ATP.

As expected, no phosphorylation on threonine was observed for His-LmxMPK2KM (figure 4.8 D).

4.2.5.3 Assessment of phosphotransferase activity of co-expressed proteins by pre-incubation kinase assays

Following expression of His-LmxMPK2 and His-LmxMPK2 co-expressed with phosphatase, kinase assays were carried out to determine the effects of autophosphorylation on phosphotransferase activity of LmxMPK2. For most kinases, dephosphorylation is used to inactivate the kinase. Hence, it was expected to find lower substrate phosphorylation activity in a kinase preparation exhibiting less autophosphorylation. However, work on LmxMPK1 suggested that extended incubation with ATP led to a decrease of further autophosphorylation of the kinase indicating saturation (as expected) but also a decrease in the ability to phosphorylate MBP, which was rather unexpected. As LmxMPK1 and LmxMPK2 are members of the same family branch, LmxMPK2 was also subjected to this type of “pre-incubation” assay.

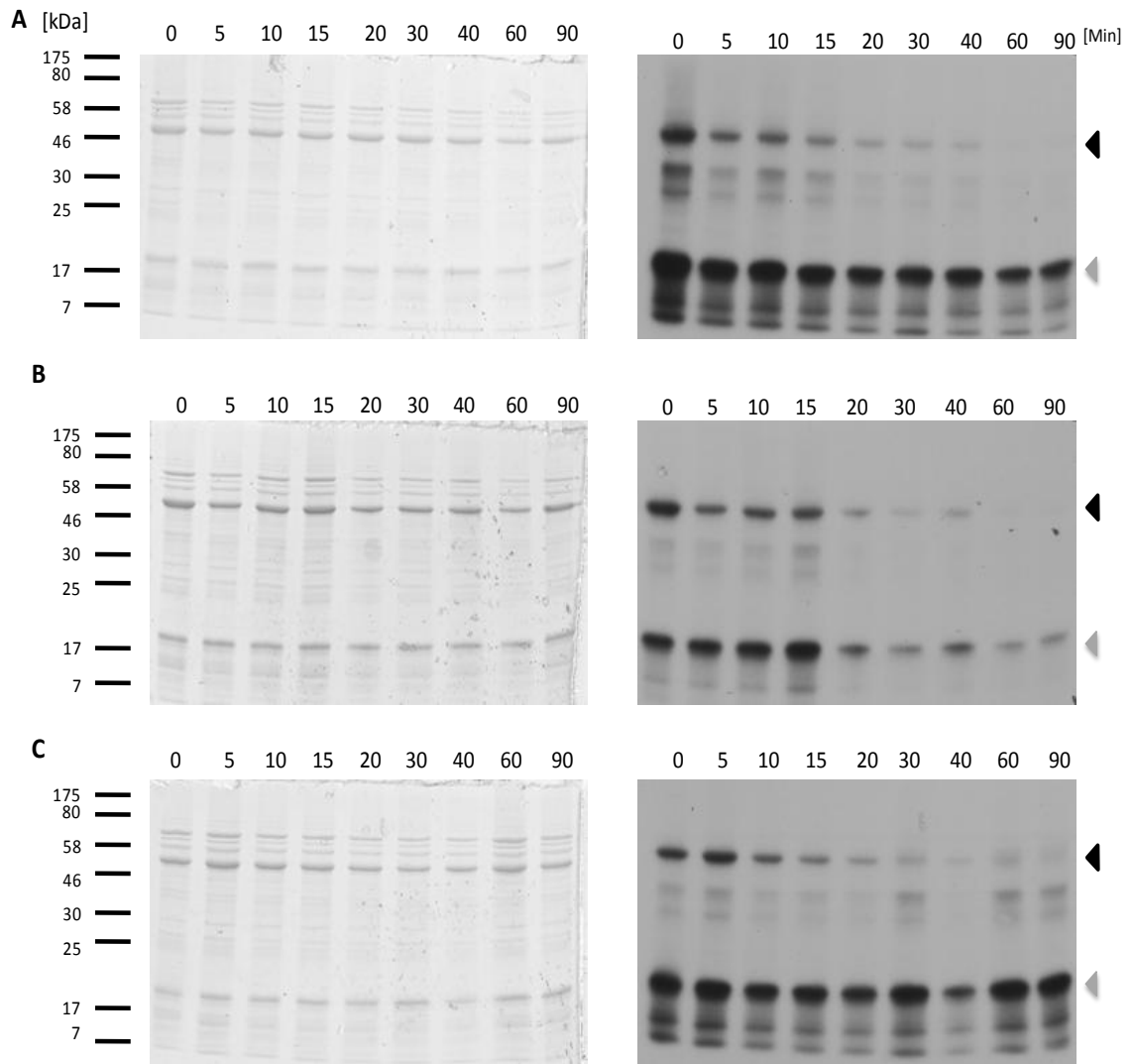


Figure 4.9. Pre-incubation kinase assay with different His-LmxMPK2 fusion proteins

Autophosphorylation and substrate phosphorylation of various LmxMPK2 protein pre-incubated for up to 90 minutes in the absence of radiolabel prior to radiometric assay. A, assay with His-LmxMPK2; B, assay with His-LmxMPK2 co-expressed with λ -phosphatase; C, assay with His-LmxMPK2 co-expressed with PTP-1B.

Left panels - Coomassie-stained gels; right panels - autoradiographs after 3 hours exposure. (◄) LmxMPK2, (◄) MBP. Molecular masses of standard proteins are indicated in kDa.

The phosphotransferase activity of LmxMPK2 after increasing pre-incubation time with unlabelled ATP was assessed using radiometric kinase assays (figure 4.9).

Singly expressed His-LmxMPK2 phosphotransferase activity was assessed after pre-incubation with “cold” ATP followed by a 10 min incubation with γ -³²P-ATP (figure 4.9 A). As pre-incubation time was increased, apparent autophosphorylation when incubated with radiolabelled ATP gradually decreased. No further autophosphorylation was observed after 60 min pre-incubation. MBP phosphorylation slightly decreased after extended pre-incubation, although it did not appear to be dramatically reduced and remained fairly stable.

The phosphotransferase activity of His-LmxMPK2 co-expressed with λ -phosphatase was assessed in the same manner (figure 4.9 B). As pre-incubation time increased, apparent autophosphorylation after incubation with radiolabelled ATP gradually decreased. As with singly expressed His-LmxMPK2, no further autophosphorylation was observed after 60 min pre-incubation. His-LmxMPK2 co-expression with λ -phosphatase substantially affected the phosphotransferase activity of the kinase. It was found that prolonged pre-incubation decreased the MBP phosphorylation and after 20 min pre-incubation there was a significant drop in MBP phosphorylation.

As pre-incubation time increased, apparent autophosphorylation of His-LmxMPK2 co-expressed with PTP1B when incubated with radiolabelled ATP gradually decreased (figure 4.9 C). However, unlike the singly expressed His-LmxMPK2 and the λ -phosphatase co-expressed His-LmxMPK2, low levels of autophosphorylation were observed at 60 and 90 min pre-incubation. MBP phosphorylation slightly decreased after extended pre-incubation, although it did not appear to be dramatically reduced and remains fairly stable, similar to singly expressed His-LmxMPK2.

4.2.5.4 Evaluation of the effect of the tag on LmxMPK2 (His vs. GST and cis/trans phosphorylation)

Previous assays showed LmxMPK2 was capable of autophosphorylation. However, this was only the case for His-LmxMPK2 and GST-LmxMPK2 did not conform to these findings (figure 4.6). Immunoblot analyses using the anti-phosphotyrosine antibody 4G10 or the polyclonal anti-phosphothreonine antibody assessing phosphorylation on tyrosine residues and threonine residues were performed to confirm the findings shown in figure 4.10.

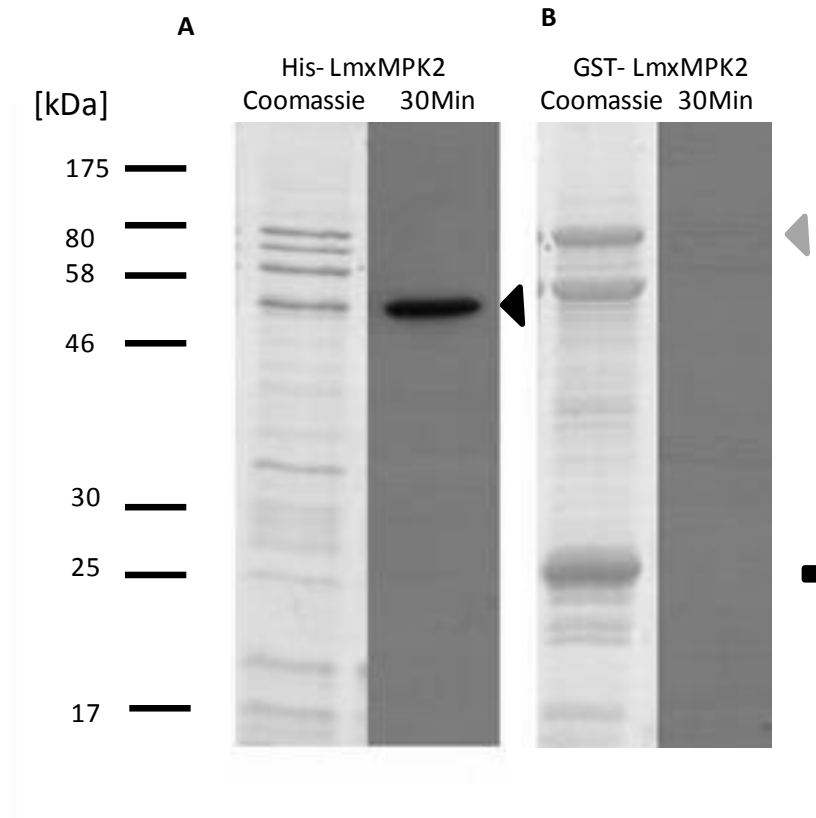


Figure 4.10 A. Immunoblot assessing the effect of His- and GST-tags on autophosphorylation of LmxMPK2 as isolated from *E. coli* using the anti-phosphotyrosine monoclonal antibody 4G10.

Tyrosine phosphorylation of A; His-LmxMPK2, and B; GST-LmxMPK2.

Left panels - Coomassie-stained gels; right panels - immunoblots after 2 minutes exposure using ECL. (◄) His-LmxMPK2; (◄) GST-LmxMPK2; (■) GST-tag. Molecular masses of standard proteins are indicated in kDa.

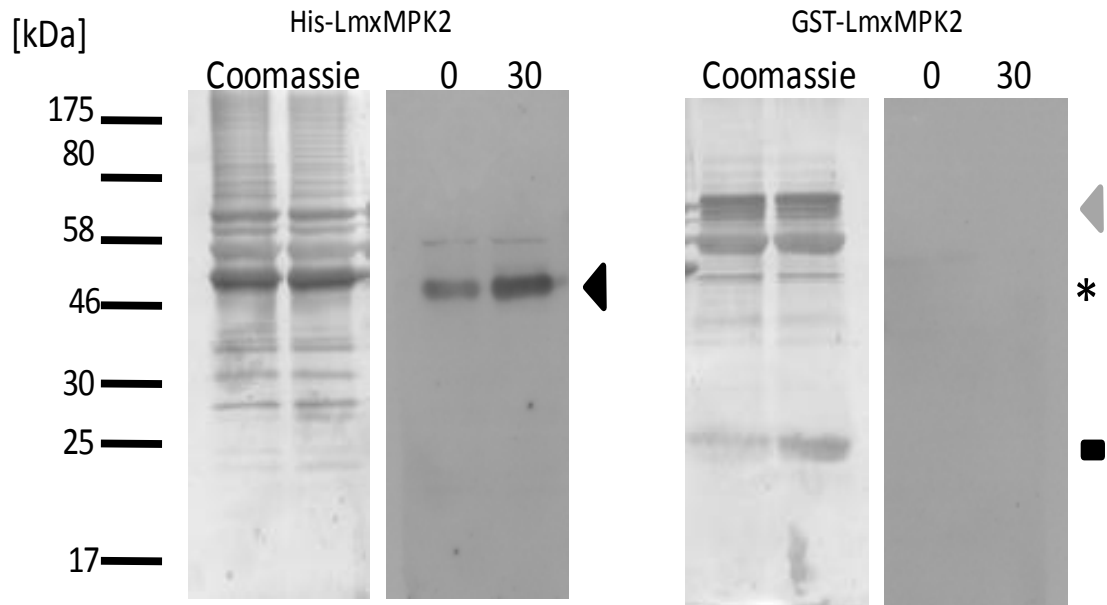


Figure 4.10 B. Immunoblot assessing the effect of two tags on auto-phosphorylation of LmxMPK2 using the anti-phosphothreonine polyclonal antibody.

Threonine phosphorylation of A; His-LmxMPK2, and B; GST-LmxMPK2.

Left panels - Coomassie-stained gels; right panels - immunoblots after 2 minutes exposure using ECL. (◄) His-LmxMPK2; (◄) GST-LmxMPK2; (■) GST-tag. Molecular masses of standard proteins are indicated in kDa.

Clear phosphorylation of tyrosine residues was observed at 52 kDa in lane 1' (His-LmxMPK2) (figure 4.10 A). However, GST-LmxMPK2 showed no phosphorylation of tyrosine residues (lane 2') when purified from *E. coli*. GST-LmxMPK2 was unable to autophosphorylate on tyrosine (figure 4.10 A).

As with the tyrosine immunoblot, clear phosphorylation of threonine residues was observed at 52 kDa in lane 1' (His-LmxMPK2) following purification from *E. coli* (figure 4.10 B). A small increase in band intensity was observed after 30 min incubation with ATP (lane 2'). However, GST-LmxMPK2 showed no phosphorylation of threonine residues (lane 3') when purified from *E. coli* or after 30 min incubation with ATP (lane 4'). Thus, confirming GST-LmxMPK2 was unable to autophosphorylate (figure 4.10 B).

To gain insight as to why GST-tagged kinase could not autophosphorylate, yet the His-tagged kinase could, the mechanism of autophosphorylation was investigated (i.e. cis-versus trans-phosphorylation). In order to determine the mechanism of autophosphorylation His-LmxMPK2, His-LmxMPK2KM and GST-LmxMPK2 were expressed and purified. While still bound to Co^{2+} beads, approximately 1 μg His-LmxMPK2 (singly expressed) was incubated with non-radiolabelled ATP for 60 min at 34°C with end-over-end rotation in a total volume of 50 μl . The beads containing kinase were sedimented and the supernatant was carefully removed. The kinase was then incubated with either eluted His-LmxMPK2KM or eluted GST-LmxMPK2 in the presence of radiolabelled ATP for 60 min at 34°C with end-over-end rotation in a total volume of 50 μl . The beads carrying His-LmxMPK2 were sedimented as before, this time transferring the supernatant to a fresh tube (discarding the beads containing His-LmxMPK2). Sixty minute incubation of singly expressed His-LmxMPK2 (on beads), eluted His-LmxMPK2KM and eluted GST-LmxMPK2 alone acted as controls. Twenty-five μl of each assay were separated by SDS-PAGE, Coomassie-stained then exposed to X-ray film at -80°C.

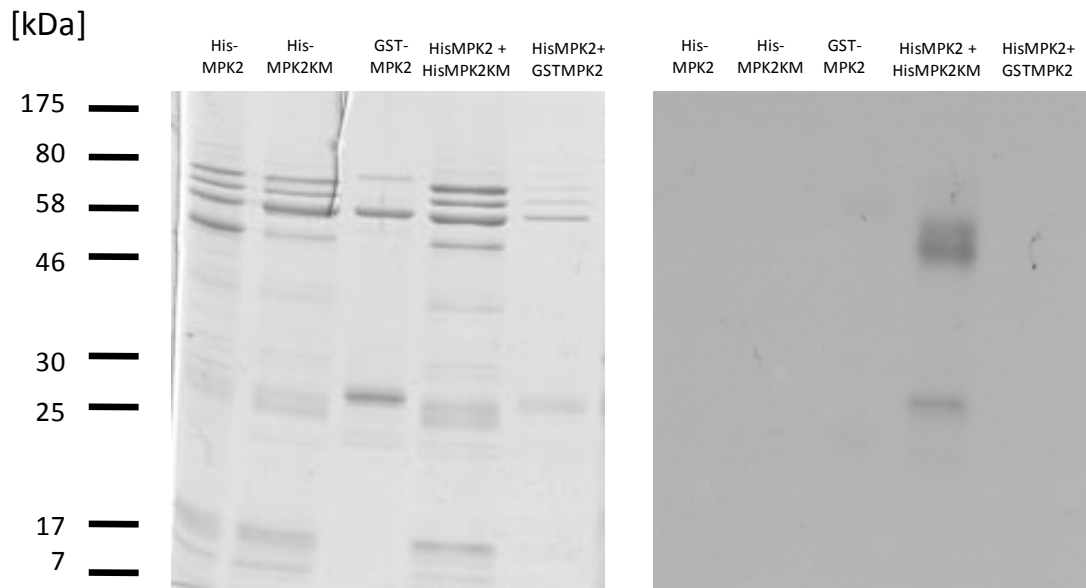


Figure 4.11. Assessment of LmxMPK2 autophosphorylation mechanism.

Lanes 1, His-LmxMPK2 pre-incubated with ATP under kinase assay conditions for 60 min (fully autophosphorylated); lanes 2, His-LmxMPK2KM; lanes 3, GST-LmxMPK2; lanes 4, His-LmxMPK2KM after incubation with immobilised fully autophosphorylated His-LmxMPK2; lanes 5, GST-LmxMPK2 after incubation with immobilised fully autophosphorylated His-LmxMPK2.

Left panel - Coomassie-stained gel; right panel - autoradiograph after 20 hours exposure. (◄) His-LmxMPK2; (◄) GST-LmxMPK2. Molecular masses of standard proteins are indicated in kDa

To assess the autophosphorylation mechanism of LmxMPK2, singly expressed His-LmxMPK2 was pre-incubated with non-radiolabelled ATP for 1 hour before being used in the kinase assay with either His-LmxMPK2KM or GST-LmxMPK2 (figure 4.11). Previous results showed His-LmxMPK2 would no longer autophosphorylate but would retain good phosphotransferase activity after this time (figure 4.9).

Singly expressed His-LmxMPK2 was pre-incubated with non-radiolabelled ATP, then after removal of the supernatant, incubated for a further 1 hour in the presence of radiolabel (lane 1). This acted as a control to show any observed phosphorylation of either His-LmxMPK2KM or GST-LmxMPK2 is not due to His-LmxMPK2 autophosphorylation. As expected no phosphorylation occurred.

Similarly, singly expressed His-LmxMPK2KM and GST-LmxMPK2 were incubated independently for 1 hour in the presence of radiolabel (lanes 2 and 3 respectively). These were also controls to show that they were unable to autophosphorylate in the absence of His-LmxMPK2. No phosphorylation can be seen in either lane.

His-LmxMPK2 was pre-incubated in the absence of radiolabelled ATP, then incubated with His-LmxMPK2KM in the presence of γ -³²P-ATP. The supernatant containing eluted His-LmxMPK2KM was subsequently transferred into a fresh tube and used for SDS-PAGE in order to isolate only His-LmxMPK2KM. Phosphorylation was observed at 52 kDa in accordance with the molecular mass of His-LmxMPK2KM (lane 4).

Investigation into the phosphotransferase mechanism of LmxMPK2 using GST-LmxMPK2 was performed in the same manner as His-LmxMPK2KM. No phosphorylation of GST-LmxMPK2 could be observed (lane 5). Trans-phosphorylation was observed for the His-LmxMPK2KM and no phosphorylation at all was observed for GST-LmxMPK2.

4.3 Discussion

In order to show this was the case His-LmxMPK2 and GST-LmxMPK2 were subjected to immunoblot analysis using the polyclonal anti-LmxMPK2 (C-terminus) antiserum (figure 4.2). His-LmxMPK2 acted as a positive control. A strong, distinct band was observed at ~52 kDa, consistent with His-LmxMPK2 (lane 1'). Three distinct bands were produced by the antiserum for the GST-LmxMPK2 (lane 2'); the expected band at 78 kDa showing the presence of the GST-tagged LmxMPK2, the other expected band at 52 kDa showing potentially cleaved LmxMPK2 and an unexpected band at 65-70 kDa. The intense band at around 56 kDa on the SDS-PA gel (lane 2) had earlier been assumed to be LmxMPK2 but on closer inspection and using a more sensitive staining technique, the band appeared to be slightly high. This was supported by the lack of reactivity of the band with the anti-LmxMPK2 antiserum. Recently, phosphorylation sites have been found in the C-terminus of LmxMPK2 (Rosenqvist and Wiese, unpublished). It is possible that C-terminally truncated kinase is active lacking the phosphorylated sites and able to phosphorylate MBP. The kinase lacking regions of the C-terminus would therefore lack the epitope recognised by the polyclonal antiserum. After Coomassie-staining, the potentially cleaved LmxMPK2 was only just visible on the SDS-PA gel, thus a more sensitive method of protein detection was used. After silver-staining, the protein corresponding to the signal at 52 kDa was more apparent (lane 2). Unexpectedly, the band visible at 65-70 kDa reacted with the LmxMPK2 antiserum suggesting partial cleavage of the GST-tag. It is a possibility that the GST-tag is cleaved by a protease from within the *E. coli* during the purification process. A possible way of assessing this in the future would be to use the whole cell lysates in a similar immunoblot to determine whether cleavage had occurred within *E. coli*. The GST-tag at 26 kDa was visible on the gel but did not react with the antiserum which was to be expected and showed the specificity of the antiserum.

As a prerequisite for the biochemical characterisation of LmxMPK2, the reaction conditions for the kinase assay were optimised with regard to pH, ion concentration and duration. Although MOPS is commonly used in kinase buffers (McAlear, PhD Thesis, 2012; John von Freyend, 2010b) the effects seen with LmxMPK2 at pH 7.5 resulted in

its exclusion (figure 4.4). LmxMPK2 showed good auto- and substrate phosphorylation in MOPS pH 7.5 however, the phosphorylation of a co-purified protein (bacterial origin) was ablated in this buffer (lane 8). While the phosphorylation of this unknown protein is not important for this assay or the understanding of LmxMPK2 activity, the MOPS pH 7.5 is inhibitory to the phosphorylation of an unknown protein. The LmxMPK2 in a pH 7.5 MOPS buffer shows a deficiency in its ability to phosphorylate potential substrates. Thus, when looking for new substrates the buffer would not be a good choice. Optimal activity in terms of both autophosphorylation and substrate phosphorylation occurred at pH 7.0 in Tris/HCl (figure 4.4). This is concurrent with many of the other *Leishmania* MAP kinases investigated to date which show maximum activity at near neutral pH (McAleer, Thesis, 2012; John von Freyend, 2010b; Erdmann, Thesis, 2009) and is also in accordance with *Leishmania* cytosolic pH which is kept at pH 6.4 to pH 7.5 (Zilberstein and Shapira, 1994). All kinases require an essential divalent metal cation for the proper co-ordination of the phosphoryl group of ATP for their activity (Tian *et al.*, 2002; Matte *et al.*, 1998). The cations are known to be specific for their binding sites thus LmxMPK2 may be able to bind both Mn^{2+} and Mg^{2+} however, Mn^{2+} appears to allow for better co-ordination of the phosphoryl groups of ATP (figure 4.5). This is in accordance with many of the *Leishmania* MAP kinases including LmxMPK1, LmxMPK3 and LmxMPK4 (McAleer, Thesis, 2012; Erdmann, Thesis, 2009; John von Freyend, Thesis, 2010). His-LmxMPK2 is a manganese-dependent kinase preferring Mn^{2+} over Mg^{2+} (figure 4.5). Oddly, the GST-LmxMPK2 appeared to favour Mg^{2+} but as the focus of this work was the activity of His-LmxMPK2, 2 mM Mn^{2+} was selected as the optimal ion concentration. Although the only the difference between the His-LmxMPK2 and GST-LmxMPK2 is the different tags, it is possible that the much larger GST-tag makes it difficult to accept the larger Mn^{2+} ion, thus reducing its activity. No kinase appeared to be present in lane 9 (10 mM Mn^{2+}) and therefore no autophosphorylation was detectable (lane 9, right panel). However, MBP phosphorylation did occur suggesting the presence of LmxMPK2 in the assay. This is possibly due to the high salt concentration in the buffer precipitating and sedimenting the kinase during the boiling/centrifugation stage. Mn^{2+} has previously been used to precipitate lipoproteins using high concentrations and pH over 5.5 (Rulz-Albusac *et al.*, 1988). Mn^{2+} is far less abundant in a cell than Mg^{2+} and therefore 10 mM

Mn^{2+} would constitute a high concentration in the assay resulting in a similar precipitating effect. This would account for the absence of kinase from the SDS-PA gels (and therefore lack of visible autophosphorylation) but result in the presence (possibly due to small size) of a phosphorylated substrate. GST-LmxMPK2 did not autophosphorylate at all but nevertheless was found to have increasing phosphotransferase activity over the 40 min incubation and plateau at 60 min (figure 4.6 D) as was seen for the His-tagged version. Thus, the inability of the GST-LmxMPK2 to autophosphorylate must be due to the only differentiating factor between the two versions – the large GST tag.

4.3.1.1 Phosphorylation and activity of LmxMPK2

In higher eukaryotes, MAP kinase activity is modulated by phosphorylation of threonine and tyrosine of the TXY motif in the activation lip, thus ideally dephosphorylated kinase is required to investigate the autophosphorylation and substrate phosphorylation dynamics. As previously discussed, work to produce dephosphorylated kinase entailed incubating the kinase with various commercially available phosphatases *in vitro*. Unfortunately, there were several problems associated with this method of dephosphorylation, for instance, it requires large quantities and concentrations of the phosphatases even with minimal kinase being utilised during long incubation times. The inconsistency and expense involved made this method unfeasible. The generation of LmxMPK2 co-expressed with the dual specificity λ -phosphatase and the human Protein-Tyrosine Phosphatase 1B (PTP1B) constituted a more appealing approach, which allowed the phosphatases to keep His-LmxMPK2 in a dephosphorylated state within the bacterial cell allowing for analysis of autophosphorylation of the purified kinase under defined conditions.

Mass spectrometry could not detect LmxMPK2 in amastigote and promastigote cell lysates (Rosenqvist, PhD Thesis, 2011), leaving the *in vivo* phosphorylation status unknown. However, the *T. brucei* homologue was found to be phosphorylated on the tyrosine residue of the TDY motif in procyclics (Nett *et al.*, 2009), therefore it was

considered likely for LmxMPK2 to also be phosphorylated on the tyrosine residue of the TDY motif. More recently, the phosphorylation states of MPK2 have been identified in *L. donovani* using mass spectrometry. *L. donovani* MPK2 was found to be phosphorylated on the tyrosine residue (Y-176) of the TDY motif as well as a serine residue (S-169). Although, this phosphorylation was discovered to be exclusive to the amastigote stage (Tsigankov *et al.*, 2013). Following purification of His-LmxMPK2 either singly expressed or co-expressed with (differentially tagged) phosphatase and the LmxMPK2KM mutant, the tyrosine phosphorylation was assessed using the anti-phosphotyrosine monoclonal antibody, 4G10. Singly expressed His-LmxMPK2 was found to be tyrosine-phosphorylated when purified from *E. coli* (figure 4.7 A) as seen for the *T. brucei* homologue. Both His-LmxMPK2s co-expressed with either λ -phosphatase or the PTP1B were completely dephosphorylated on tyrosine residues when purified from *E. coli* (figure 4.7 B and C, lanes 1). However, dephosphorylation did not eliminate kinase activity, which often requires the presence of a scaffold protein for autophosphorylation to occur (Roskoski, 2012; Bhattacharyya *et al.*, 2006). In fact, phosphorylation of tyrosine recurred subsequent to incubation with ATP (figure 4.7 B and C, lanes 2 & 3). As expected, the mutation of lysine (K42) to methionine (His-LmxMPK2KM) completely eliminated kinase activity (figure 4.7 D) and proved any phosphotransferase activity to be due to LmxMPK2 and not a kinase from the bacterial expression system.

The kinase was subjected to a second immunoblot, this time assessing the threonine phosphorylation using the anti-phosphothreonine polyclonal antibody 71-8200 (Invitrogen, UK). Singly expressed His-LmxMPK2 was phosphorylated on threonine residues when purified from *E. coli* (figure 4.8 A). His-LmxMPK2 co-expressed with λ -phosphatase was expected to be completely dephosphorylated when purified from *E. coli*. Some dephosphorylation appeared to have occurred, however, it was not possible to completely dephosphorylate all threonine residues (figure 4.8 B) suggesting threonine may play a pivotal role in LmxMPK2 activity. His-LmxMPK2 co-expressed with PTP1B did not dephosphorylate threonine residues at all (figure 4.8 C) – as expected. No threonine phosphorylation was observed in the His-LmxMPK2KM corroborating the elimination of kinase activity (figure 4.8 D). While it was discovered that

LmxMPK2 was capable of autophosphorylating on threonine and tyrosine residues, the localisation of these phosphorylation sites currently remain unknown.

To assess the effect of the autophosphorylation on the substrate phosphorylation activity of LmxMPK2, the kinase activity was investigated at different states of autophosphorylation starting with completely dephosphorylated kinase to a fully phosphorylated enzyme. This was achieved in a pre-incubation kinase assay. The kinase was incubated with non-radiolabelled ATP for varying lengths of time followed by replacement of the assay solution (more specifically the ATP) with MBP and γ - ^{32}P -ATP in an optimised kinase buffer and incubation for 10 minutes (regardless of pre-incubation time). It had been observed that extended intramolecular autophosphorylation of LmxMPK1 resulted in slower substrate phosphorylation kinetics (McAleer, PhD Thesis, 2012). As LmxMPK1 is the closest related kinase to LmxMPK2, sharing a branch of the phylogenetic tree (figure 1.8b), this hypothesis was also applied to LmxMPK2.

Singly expressed His-LmxMPK2 loosely fits this hypothesis (figure 4.9 A). LmxMPK2 autophosphorylation during the 10 minutes incubation in the presence of γ - ^{32}P -ATP steadily decreased as the pre-incubation time increased (due to more non-radio-labelled phosphate being incorporated as the pre-incubation time increased). No further autophosphorylation was detectable after 60 min pre-incubation, with other words, the kinase is fully autophosphorylated. The MBP phosphorylation slightly decreased between 0-20 minutes pre-incubation but then remained steady thereafter.

Kinase activity of His-LmxMPK2 co-expressed with λ -phosphatase is significantly affected by the dephosphorylation of threonine residues (figure 4.9 B). The autophosphorylation of His-LmxMPK2 steadily decreased during the 10 min incubation in the presence of γ - ^{32}P -ATP as the pre-incubation time increased. A decrease observed at 20 min is due to the drop in kinase amount as shown by the SDS-PA gel. No further autophosphorylation is detectable after 60 min pre-incubation. However, the kinase

exhibits reduced phosphotransferase activity with regard to MBP phosphorylation also decreasing significantly over the 90 min pre-incubation.

His-LmxMPK2 co-expressed with PTP1B behaves in a similar fashion as the singly expressed His-LmxMPK2. The autophosphorylation of His-LmxMPK2 decreased as the pre-incubation time increased, although unlike the singly expressed His-LmxMPK2 low levels of further autophosphorylation are still detectable at 60 and 90 min pre-incubation (figure 4.9 C). The MBP phosphorylation is lower than that of MBP phosphorylated by singly expressed kinase but it follows the same pattern – a slight decrease in phosphorylation between 0 and 20 min then a steady rate following extended incubation.

LmxMPK2 appears to be an unusual kinase as it retains the ability to autophosphorylate and subsequently phosphorylate a substrate (MBP) following dephosphorylation. It appears that phosphorylation of LmxMPK2 is important for kinase activity as dephosphorylation of the kinase by dual-specific phosphatase (λ -phosphatase) results in slower or delayed substrate phosphorylation compared to the singly expressed kinase (figure 4.6). It was possible to fully dephosphorylate tyrosine residues (figure 4.7) of His-LmxMPK2 and maintain active kinase. However, it was not possible to completely dephosphorylate threonine residues (figure 4.8) of His-LmxMPK2; this coupled with the significantly reduced phosphotransferase activity suggests that tyrosine phosphorylation is not important in the activation of LmxMPK2 kinase activity *in vitro*.

Since no difference in substrate phosphorylation between His-LmxMPK2 and His-LmxMPK2 co-expressed with PTP1B was observed, it can be assumed that phosphorylation on tyrosine does not influence substrate phosphorylation and phosphorylation of threonine alone is sufficient for kinase activity. It appeared that partial dephosphorylation of phosphothreonine was sufficient to prevent substrate phosphorylation (figure 4.6 B, lane 1). However, after recurring autophosphorylation substrate phosphorylation resumed (figure 4.6B, lanes 2-4). It remains unclear whether

the missing phosphothreonine is located in the TDY motif of the phosphorylation lip or somewhere else in the molecule regulating kinase activity, like for instance in *Leishmania* MPK10 where the C-terminus is phosphorylated and involved in the regulation of kinase activity (Horjales *et al.*, 2012). This and the apparent lack of importance of the phosphotyrosine in the TXY motif is different to the activation mechanism of most MAP kinases in higher eukaryotes which require phosphorylation of both threonine and tyrosine of the activation lip for a fully activated kinase (Roskoski *et al.*, 2012; Pearson *et al.*, 2001). However, an investigation into the mammalian T-cell antigen receptor signalling pathway was found to follow an alternative activation of p38 α bypassing the classical MAPK cascade. Monophosphorylation of Thr-180 led to an active kinase, albeit less active than dual-phosphorylated kinase on Thr-180 and Tyr-182. Tyr-182 was suggested to enhance the activity and play a role in determining specificity (Mittelstadt *et al.*, 2009). Similarly, the dual-specificity kinase weel appeared to be phosphorylated on tyrosine residues only when interacting with its specific, physiological substrates (i.e. Cdc2) (Wu and Russel, 1993). This could be partially true for LmxMPK2 as PTP1B co-expressed His-LmxMPK2 remained active but with slightly lower substrate phosphorylation than that of the singly expressed kinase. If the specific substrate (currently unknown) were used in place of a model substrate (MBP) an increase in phosphotransferase activity may occur. Similar results were found for the yeast MAP kinase Hog1, where phosphorylation on Tyr-178 of the activation lip was not important for the activation of the kinase (Bell and Engelberg, 2003). It was also suggested that autophosphorylation of this tyrosine residue acted as an inactivation mechanism (Bell and Engelberg, 2003). The results also (partially) support the hypothesis that extended autophosphorylation leads to a less active kinase, as prolonged incubation with ATP did lead to a reduction in MBP phosphorylation (albeit, not a hugely significant reduction).

4.3.1.2 Autophosphorylation mechanism of LmxMPK2

The differently tagged versions of LmxMPK2 (His-LmxMPK2 and GST-LmxMPK2) exhibited a substantial difference in the buffer optimisation assays. Only His-LmxMPK2 but not GST-LmxMPK2 had the ability to autophosphorylate. This might be

due to the large GST-tag sterically hindering autophosphorylation. Both versions of the kinase were subjected to an anti-phosphotyrosine immunoblot using the monoclonal antibody 4G10 (figure 4.10 A). As expected, His-LmxMPK2 was phosphorylated on tyrosine when purified from *E. coli*, while no tyrosine phosphorylation was detected for GST-LmxMPK2. Although unusual, this was not entirely unexpected as it was discussed previously (4.3.1.2) that tyrosine phosphorylation may not be required for the activity of LmxMPK2. However, it is widely accepted that threonine phosphorylation is essential for the activity of typical and atypical MAP kinases (John von Freyend *et al.*, 2012; Roskoski *et al.*, 2012; Bell and Engelberg, 2003). Therefore, when subjected to an anti-phosphothreonine immunoblot using the polyclonal antibody 71-8200 (Invitrogen, UK), it was anticipated that phosphorylated threonine residues would be detected for both His-LmxMPK2 and GST-LmxMPK2 when purified from *E. coli* (figure 4.10 B). His-LmxMPK2 was phosphorylated on threonine when purified from *E. coli* with further threonine autophosphorylation after 30 min incubation. Surprisingly, GST-LmxMPK2 was not phosphorylated on threonine when purified and also was unable to autophosphorylate on threonine after 30 min incubation with ATP. It is likely that no autophosphorylation is required for the activity of LmxMPK2 as there is no evidence for phosphothreonine, phosphotyrosine or any discernible incorporation of radiolabel into LmxMPK2 in kinase assays. This together with the additional strong band in the GST-LmxMPK2 suggests that the GST-tag hinders autophosphorylation, possibly preventing the interaction of two kinase monomers.

An investigation into the autophosphorylation mechanism of LmxMPK2 was carried out using radiometric assays. No autophosphorylation was present for the pre-incubated His-LmxMPK2 alone (figure 4.11, lanes 1) proving the suitability of the 60 min pre-incubation to guarantee full autophosphorylation. His-LmxMPK2KM alone (lanes 2) and GST-LmxMPK2 alone (lanes 3) also showed no autophosphorylation, corroborating previous results and confirming any observed phosphorylation was due to phosphorylation by active His-LmxMPK2. A phosphorylation signal was detected for His-LmxMPK2KM (after incubation with pre-incubated His-LmxMPK2) (lanes 4), however no phosphorylation was detected for GST-LmxMPK2 (after incubation with pre-incubated His-LmxMPK2) (lanes 5). These data are consistent with the necessity of

two LmxMPK2 molecules to be present for the autophosphorylation of the kinase in an intermolecular trans-phosphorylation reaction. From this work it is unclear whether the inability of His-LmxMPK2 to phosphorylate GST-LmxMPK2 is due to the large GST-tag blocking the phosphorylation site for autophosphorylation.

The requirement of LmxMPK2 to be phosphorylated for kinase activity does not necessarily translate to autophosphorylation activity (as discussed in 4.3.1.2) as the GST-LmxMPK2 phosphorylates MBP without exhibiting any apparent autophosphorylation (figure 4.6 D). LmxMPK2 could be phosphorylated by proteins coming from *E. coli* during the expression and purification stages or it could simply be phosphorylation (of residues not the TDY motif) hidden by the large GST-tag. Ideally, this would be confirmed by mass spectrometry which is a far more sensitive method for detection (although not all peptides can be detected). This experiment exceeded the given time frame of this work and will have to be part of future projects.

LmxMPK2 is an important kinase in the survival of amastigotes and was shown to contribute to the proliferation of promastigotes and regulation of the microtubules involved. LmxMPK2 has been found to be an unusual kinase which is not reliant on phosphorylation (either via an activating protein or autophosphorylation) *in vitro* for activity and readily phosphorylates MBP.

It was shown that LmjMPK2 null mutant parasites exhibited reduced SB(III) uptake and increased resistance, suggesting the absence of phosphorylation of LmjAQP1 resulted in decreased SB(III) uptake. In the add-back, this channel became stabilised (Mandal *et al.*, 2012). Although no evidence suggests LmjAQP1 is directly phosphorylated by LmxMPK2, there does appear to be a link between the two. LmjAQP1 resides in the flagellum of promastigotes, phosphorylation leads to increased levels and distribution over the surface of the entire cell (Mandal *et al.*, 2012). The potential stage specific nature of the LmjAQP1 (possibly phosphorylated in metacyclic) would correlate with the abnormal phenotypes. If the spiked posterior end phenotypes were re-categorised as metacyclic promastigotes then the diffuse green observed in the cells could be due to close association with AQP1 regulation either directly or indirectly. Although, it is not

possible to tell from these experiments the depth at which the LmxMPK2-GFP is found, it is a possibility that the LmxMPK2 associated closely to the inner surface of the cell and toward the anterior end – similar to the localisation of AQP1. Despite the lack of evidence as AQP1 as the substrate for LmxMPK2, this provides a good basis and narrowing possibilities in the search for LmxMPK2's substrate.

4.3.2 LmxDIP13 subcellular localisation

DIP13 is a small coiled protein first discovered in the flagellated green algae *Chlamydomonas reinhardtii*. It has been shown to associate with microtubule structures and play a role in cell division (Pfannenschmid *et al.*, 2003). An orthologue exists in *T. brucei* which appeared cell cycle stage dependent (Price *et al.*, 2012), it was thought that DIP13 could act as a putative marker protein for cell cycle stages in *L. mexicana*

GFP-tagged LmxDIP13 was transfected into wild type and *LmxMPK2* *-/-* null mutant *L. mexicana*. After confirming that all clones generated expressed GFP-LmxDIP13 (figure 33), an unexpected band was detected by the anti-GFP antibody in lanes 1-6 at 26 kDa – the approximate size of the GFP-tag. It is possible this additional band is observed due to cleavage of the tag. Although it is not clear how this might occur, it is not unique to this fusion protein. Similar results have been observed in fusion proteins such as GFP-PINK1 (Beilina *et al.*, 2005). It is also possible that association with microtubules may leave LmxDIP13 susceptible to regular degradation releasing free GFP into the cell. The localisation of GFP-LmxDIP13 within the wild type *L. mexicana* and the *LmxMPK2* null background *L. mexicana* was found to be similar, showing single spots (at the anterior, posterior or mid cell) or multiple spots (figure 16, Figure 17). LmxMPK2 dephosphorylation and activity

4.3.2.1 Generation, expression and optimisation

Prior to the beginning of this project, His-LmxMPK2 and GST-LmxMPK2 had both been successfully expressed and purified in an *E. coli* expression system, however, no optimisation of kinase assay conditions had been carried out. Previous attempts to

produce entirely dephosphorylated kinases *in vitro* using commercially available λ -phosphatase have proved inconsistent and expensive (McAleer, PhD Thesis, 2012). As part of a novel system to produce dephosphorylated kinase, plasmids encoding His-LmxMPK2 and either Bacteriophage λ -phosphatase or Human PTP1B were generated. The phosphatases were expressed with triple-HA tags at their N- or C-termini in order to detect and/or purify them if required. PTP1B was found to be most effective (in terms of kinase dephosphorylation) when tagged at the N-terminus and λ -phosphatase tagged at the C-terminus (McAleer, PhD Thesis, 2012). In addition to the phosphatase co-expressed LmxMPK2, an enzymatically inactive kinase was generated as a negative control. This was achieved by replacing the highly conserved lysine residue of subdomain II (K42) by a methionine residue, generating His-LmxMPK2KM. The lysine residue is essential for kinase activity as it plays an important role for the orientation of the α - or β -phosphoryl group of ATP for catalysis (Carrera *et al.*, 1993). It had been observed that GST-LmxMPK2 consistently produced multiple bands on Coomassie-stained SDS-PA gels: a band at 78 kDa corresponding to GST-tagged LmxMPK2, a band at 26 kDa – assumed to be the cleaved GST-tag – and a band at around 52-56 kDa assumed to be LmxMPK2 without the GST-tag. Dephosphorylation of recombinant

4.3.3 Summary

The localisation and possible role of LmxMPK2 within the parasite was carried out as part of these investigations. However, the mechanism of activation and phosphorylation states of the kinase were previously unknown. This constituted the focus of the investigations in this chapter.

Optimisation of the assay conditions were first carried out. Tris/HCl pH 7.0 and 2 mM Mn^{2+} with incubation at 34°C was determined to be the most suitable conditions for further analysis of LmxMPK2. Dephosphorylated recombinant LmxMPK2 was successfully generated using a novel phosphatase co-expression system. This was then used in kinase assays to determine the role of phosphorylation in regulating kinase activity. Complete dephosphorylation of tyrosine residues had no impact on the ability of LmxMPK2 to phosphorylate the generic kinase substrate myelin basic protein (MBP) yet the kinase retained the ability to autophosphorylate. However, only incomplete dephosphorylation of threonine (also dephosphorylating tyrosine and serine) using λ -phosphatase was achieved causing a significant reduction of the ability of LmxMPK2 to phosphorylate MBP. LmxMPK2 appears to be an unusual kinase whose activation mechanism varies from that of higher eukaryotes. Tyrosine appears not to be important for the phosphorylation of the generic substrate MBP but may be involved with directing specific substrate interactions as with other unusual kinases found in yeast (of course the natural substrate for LmxMPK2 would have to be identified to test this hypothesis). Additionally, the site of tyrosine phosphorylation remains unclear. Investigations into the regulation of kinase activity focused on His-tagged recombinant LmxMPK2. Early optimisation work included a GST-tagged version which revealed an inability to autophosphorylate possibly due to the large tag blocking intermolecular phosphorylation. However, it appeared that autophosphorylation of LmxMPK2 *in vitro* does not influence substrate phosphorylation. The mechanism of LmxMPK2 phosphorylation was examined and discovered that autophosphorylation of LmxMPK2 was by trans-phosphorylation (requiring two molecules).

Chapter 5

Characterisation of recombinant LmxGSK3- β

5.1 Introduction

Prior to commencement of this project attempts to delete *LmxGSK3- β* had failed. However, it was discovered that the addition of a copy of the gene on a plasmid made it possible to delete *LmxGSK3- β* from the genome. Through the use of mouse infection studies and PCR it was determined that *LmxGSK3- β* was essential to both life stages of *Leishmania mexicana* and therefore represented an ideal drug target (Munro, Honours Thesis, 2009).

GSK3 has been shown to be a highly active and versatile enzyme involved in multiple different cellular processes (Ojo *et al.*, 2011; Phukan *et al.*, 2010). The dysregulation of which is involved in several human illnesses such as diabetes mellitus, Alzheimer's dementia, osteoporosis and atherosclerosis (Wang *et al.*, 2011; Ojo *et al.*, 2008). It is therefore understandable that GSK3 has been the subject of a lot of research in human disease since the 1980's. More recently, it has been identified as a potential target for the treatment of human African trypanosomiasis and leishmaniasis (Xingi *et al.*, 2009; Ojo *et al.*, 2008). Previous work within the group has provided evidence to support the importance of LmxGSK3- β within the parasite (and therefore as an important drug target). Work to generate LmxGSK3- β genomic null mutant *L. mexicana* failed, and was only possible using a plasmid carrying the gene in trans (Δ LmxGSK3- β -/- + pLmxGSK3- β) (Bleicher and Wiese, unpublished). Grown in Balb/c mice for 13 weeks in the absence of antibiotic pressure, the Δ LmxGSK3- β + LmxGSK3- β *L. mexicana* were unable to lose the plasmid proving *LmxGSK3- β* to be essential (Munro, Bachelor's Thesis, 2009). As LmxGSK3- β is expected to phosphorylate a multitude of substrate proteins, its inhibition would affect multiple cellular processes and could lead to cell death while reducing the chance of redundancy mechanisms compensating within the cell.

The phosphatase co-expression system used for LmxMPK2 (and LmxMPK1) (McAler, PhD Thesis, 2012) was applied to this project with the aim of providing insight into the activity of LmxGSK3- β . When measuring kinase activity in an *in vitro* kinase assay, it is important to ensure that the measured activity is not due to other proteins from the expression system, therefore the enzymatically inactive LmxGSK3- β KM was included. GSK3- β is known to be constitutively phosphorylated on the Tyr-186 (Tsigankov *et al.*, 2013). Since LmxGSK3- β possesses a highly conserved catalytic domain, it is anticipated that the activation mechanism will remain the same as the human homologue and rely on negative regulation. Immunoblots and autoradiographs in this section were selected as the best image from a minimum of three repeats. All are representative of a visual assessment and provide an accurate illustration of each investigation.

A library of natural compounds owned by Strathclyde's Institute for Drug Research (SIDR) was used to screen for inhibitors of LmxGSK3- β . Malabaricone compounds were identified as potential inhibitors, isolated from *Myristica* plants. Malabaricones had already been shown to possess anti-leishmanial properties (Kang *et al.*, 2012; Sen *et al.*, 2007). Malabaricone B and Malabaricone C were selected for screening against LmxGSK3- β . The successful establishment of inhibitor screening using enzymes as targets requires the recombinant expression of high quantities of an active protein. Fortunately, LmxGSK3- β expresses well and yields high quantities of protein. Unfortunately, activity diminishes quickly when kept refrigerated. The suitability of LmxGSK3- β to be frozen was investigated and found to be feasible. However, it was noted that LmxGSK3- β could not be kept frozen indefinitely as activity was lost after 6 months at -80°C (results not shown).

5.2 Results

5.2.1 Generation of various LmxGSK3- β expression plasmids

As a constitutively active kinase, it was anticipated that LmxGSK3- β would be very difficult to dephosphorylate using conventional methods. Therefore, the novel approach of co-expressing the kinase with a phosphatase in the *E.coli* expression system was identified as an ideal way to dephosphorylate LmxGSK3- β and identify its activation mechanism. This method, previously tested with LmxMPK1 and LmxMPK2 (in this thesis) had shown excellent results and would allow the phosphatase to dephosphorylate the kinase during the expression of the plasmid in bacterial cells. Plasmids carrying both LmxGSK3- β and a phosphatase (either PTP1B or λ -phosphatase) were generated to fully dephosphorylate the kinase

5.2.2 Assessment of LmxGSK3- β activity

5.2.2.1 Assessment of tyrosine phosphorylation

The activation mechanism of human GSK3- β is well documented, however, the activation mechanism of the *Leishmania* orthologue LmxGSK3- β is currently unknown. Tyrosine phosphorylation was first assessed using phosphatase co-expressed His-LmxMPK2 and the monoclonal anti-phosphotyrosine 4G10 (Bernhard Fleischer, BNI, Hamburg) in immunoblot analyses. Kinase assays were carried out as detailed in chapter 2.2.17 followed by immunoblot analysis as detailed in chapter 2.2.15.

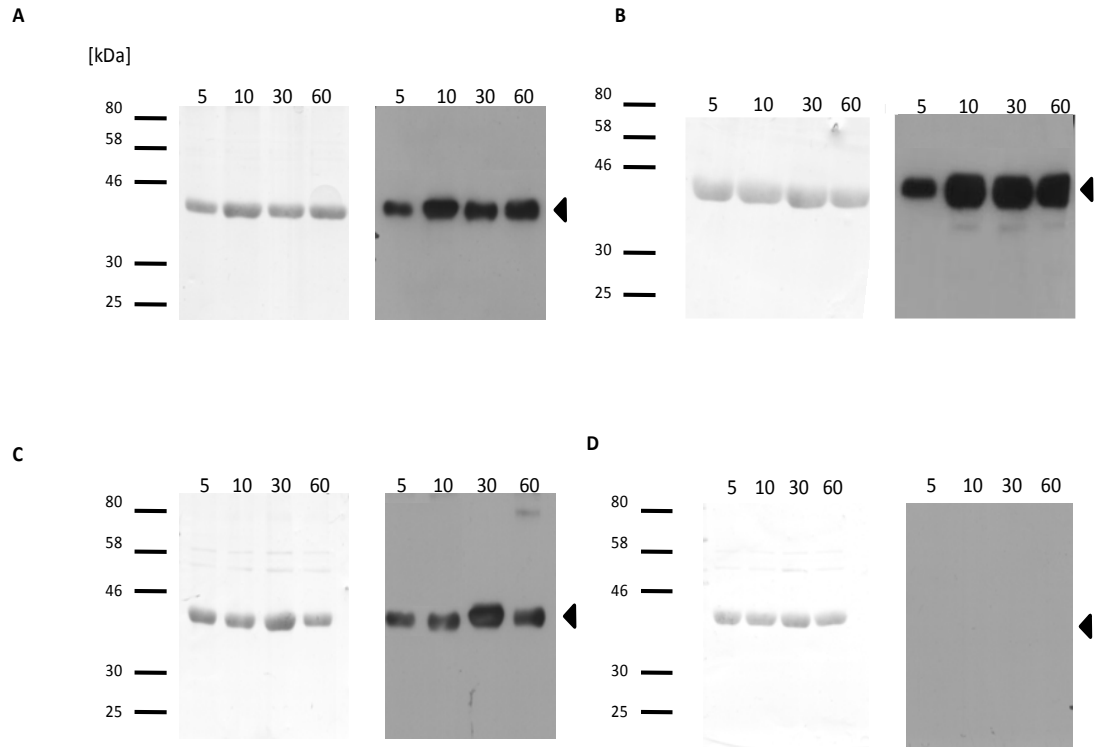


Figure 5.1. Immunoblot assessing tyrosine phosphorylation of singly and co-expressed LmxGSK3- β and LmxGSK3- β KM.

Tyrosine autophosphorylation of (A) His-LmxGSK3- β ; (B) His-LmxGSK3- β co-expressed with λ -phosphatase; (C) His-LmxGSK3- β co-expressed with PTP1B; (D) His-LmxGSK3- β KM over the course of 60 min.

Left panels, Coomassie-stained gels; right panels, immunoblots after 2 min exposure. (◄) His-LmxGSK3- β . Molecular masses of standard proteins are indicated in kDa.

Tyrosine phosphorylation of singly expressed LmxGSK3- β as purified from *E. coli* (0 min, no ATP) and increasing time points (10-60) after incubation with ATP was assessed using mAb 4G10 (figure 5.1 A). LmxGSK3- β was shown to be fully phosphorylated on tyrosine residues when purified from *E. coli*. There appeared to be an increase in tyrosine phosphorylation between 0 min and 5 min incubation but this was most likely due to the higher amount of protein present in lane 2.

LmxGSK3- β co-expressed with C-terminally HA-tagged λ -phosphatase (figure 5.1 B) or N-terminally HA-tagged PTP1B (figure 5.1 C) was purified from *E. coli* and further incubated with ATP to assess tyrosine phosphorylation. LmxGSK3- β co-expressed with λ -phosphatase showed lower phosphorylation of tyrosine residues when purified from *E. coli*, however, further autophosphorylation of tyrosine residues is observed after incubation with ATP. PTP1B co-expressed kinase findings were similar to the singly expressed LmxGSK3- β . The kinase appeared fully phosphorylated on tyrosine residues when purified from *E. coli* and no additional autophosphorylation occurred after incubation with ATP.

No tyrosine phosphorylation of His-LmxGSK3- β KM was observed (figure 5.1 D). This was expected as the mutation of lysine (K50) to a methionine in the ATP binding site renders the kinase unable to accept ATP.

5.2.2.2 Assessment of threonine phosphorylation

Although very little dephosphorylation of tyrosine was observed in the presence of either phosphatase, threonine is known to play an important role in human GSK3- β . The phosphorylation of threonine residues in LmxGSK3- β was assessed using phosphatase co-expressed His- LmxGSK3- β and the polyclonal anti-phosphothreonine antibody 71-8200 (Invitrogen, UK) in immunoblot analyses. Kinase assays were carried out as detailed in chapter 2.2.17 followed by immunoblot analysis as detailed in chapter 2.2.15.

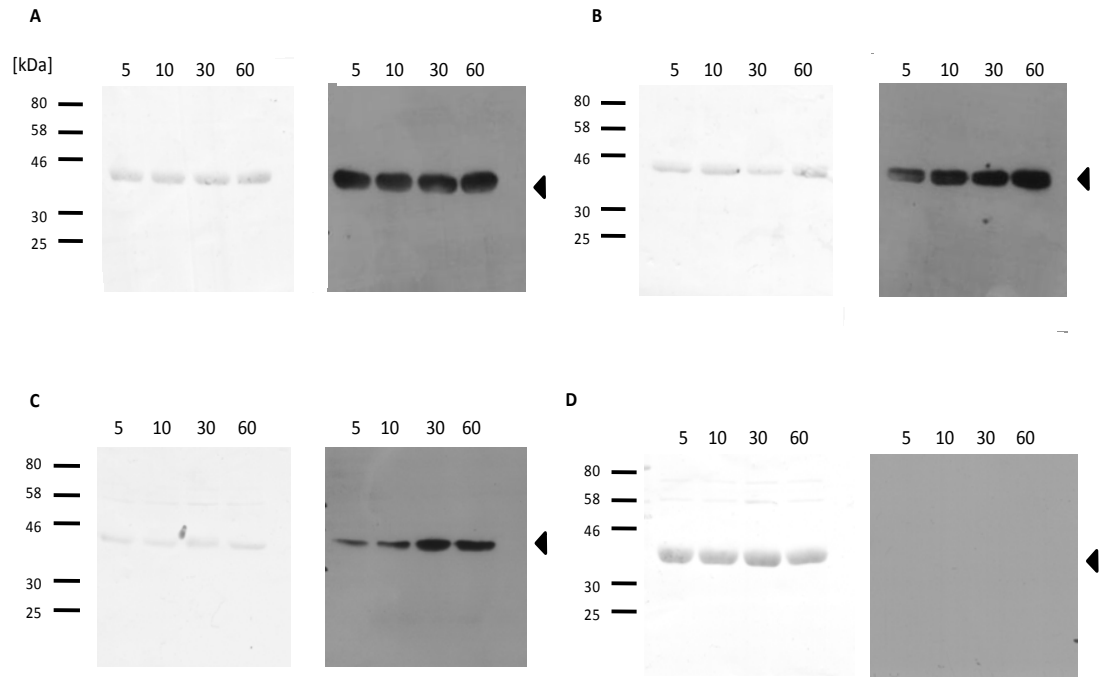


Figure 5.2. Immunoblot assessing threonine phosphorylation of singly and co-expressed LmxGSK3- β and LmxGSK3- β KM at varying time points.

Threonine autophosphorylation of (A) His-LmxGSK3- β ; (B) His-LmxGSK3- β co-expressed with λ -phosphatase; (C) His-LmxGSK3- β co-expressed with PTP1B; (D) His-LmxGSK3- β KM over the course of 60 min. Left panels, Coomassie-stained gels; right panels, immunoblots after 2 min exposure. (◄) His-LmxGSK3- β . Molecular masses of standard proteins are indicated in kDa.

Threonine phosphorylation of singly expressed LmxGSK3- β as purified from *E. coli* (0 min, no ATP) and increasing time points (10-60) of incubation with ATP was assessed using a polyclonal anti-threonine antibody (figure 5.2 A). LmxGSK3- β was shown to be fully phosphorylated on threonine residues when purified from *E. coli*. No further autophosphorylation on threonine residues occurred when incubated with ATP.

Threonine phosphorylation of LmxGSK3- β co-expressed with C-terminally HA-tagged λ -phosphatase (figure 5.2 B) or N-terminally HA-tagged PTP1B (figure 5.2 C) purified from *E. coli* and increasing time points of incubation with ATP was assessed using a polyclonal anti-threonine antibody. Co-expression of LmxGSK3- β with λ -phosphatase appeared to have a small reduction in threonine phosphorylation. After 5 min incubation with ATP, the kinase appeared to be fully phosphorylated and no further phosphorylation of threonine occurred. Whereas, kinase co-expressed with PTP1B appeared fully phosphorylated on threonine residues when purified from *E. coli* and no further autophosphorylation occurred when incubated with ATP. It was likely that the lower amount of protein on the gel accounts for the lower visible signal, rather than less phosphorylation of threonine residues.

As expected, no threonine phosphorylation of His-LmxGSK3- β KM was observed (figure 5.2 D). Confirmation that any signal produced was due to phosphorylation of threonine residues.

5.2.2.3 Assessment of phosphotransferase activity of LmxGSK3- β

Following expression of His-LmxGSK3- β and His-LmxGSK3- β co-expressed with phosphatase, it was that clear autophosphorylation activity is important to LmxGSK3- β activity as it was impossible to fully dephosphorylate the kinase and keep it in that state. Kinase assays were carried out to determine the phosphotransferase activity of LmxGSK3- β using short incubation periods.

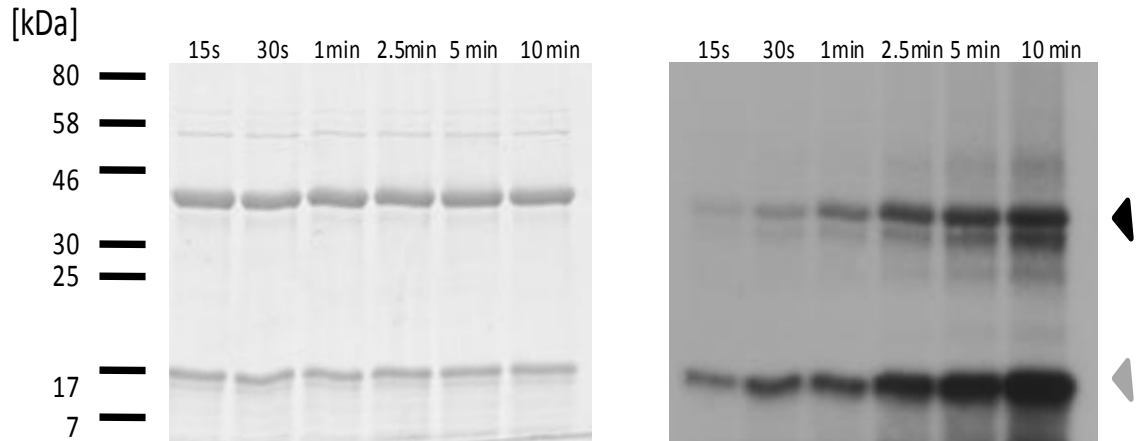


Figure 5.3. Kinase assay of His-LmxGSK3- β at 34°C.

Autophosphorylation and substrate phosphorylation of (A) His- LmxGSK3- β ; (B) His- LmxGSK3- β co-expressed with λ -phosphatase; (C) His- LmxGSK3- β co-expressed with PTP-1B; (D) GST- LmxGSK3- β assessed over the course of 10 min at 34°C.

Left panels, Coomassie-stained gels; right panels, autoradiographs after 18 hours exposure. (\blacktriangleleft) LmxMPK2; (\triangleleft) MBP; (\blacksquare) GST-tag. Molecular masses of standard proteins are indicated in kDa.

The phosphotransferase activity of LmxGSK3- β was assessed in an optimised kinase reaction buffer (50 mM Tris/HCl pH 7.0, 100 mM NaCl, 2 mM Mn²⁺) and incubated at 34°C (figure 5.3).

The autophosphorylation and substrate phosphorylation of singly expressed His-LmxGSK3- β began as early as 15 seconds (figure 5.3). The stronger MBP phosphorylation at 15 s suggests that substrate phosphorylation began earlier than autophosphorylation. Both autophosphorylation and MBP phosphorylation increased with further incubation.

LmxGSK3- β was shown to be highly active at early time points (figure 5.3). Due to the inability to dephosphorylate LmxGSK3- β using the phosphatases, kinase assays were carried out to determine the phosphotransferase activity of LmxGSK3- β using short incubation periods at low temperatures.

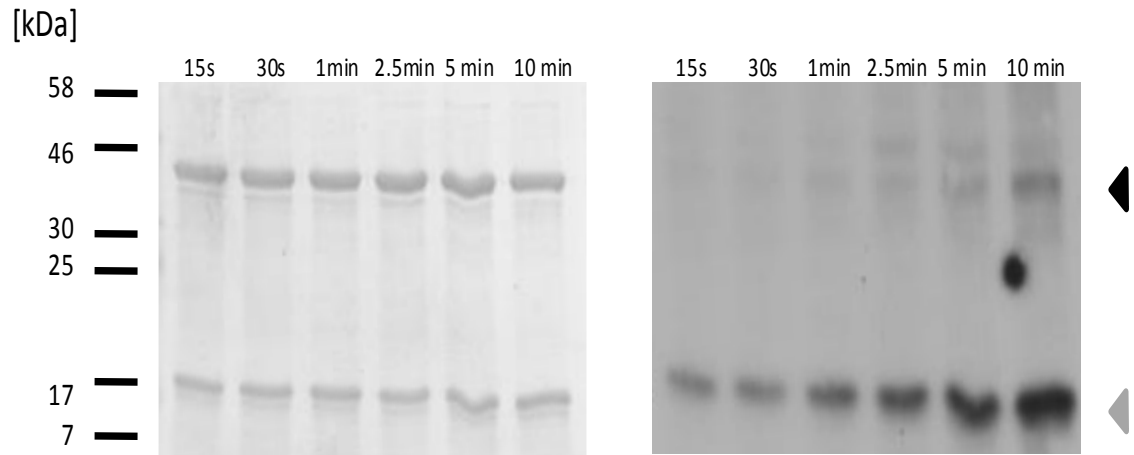


Figure 5.4. Kinase assay of His-LmxGSK3- β on ice.

Autophosphorylation and substrate phosphorylation of (A) His- LmxGSK3- β ; (B) His- LmxGSK3- β co-expressed with λ -phosphatase; (C) His- LmxGSK3- β co-expressed with PTP-1B; (D) GST- LmxGSK3- β assessed over the course of 10 min on ice.

Left panels, Coomassie-stained gels; right panels, autoradiographs after 18 hours exposure. (▲) LmxMPK2; (◄) MBP; (■) GST-tag. Molecular masses of standard proteins are indicated in kDa.

The phosphotransferase activity of LmxGSK3- β was assessed at a low temperature in an optimised kinase reaction buffer (50 mM Tris/HCl pH 7.0, 100 mM NaCl, 2 mM Mn^{2+}) which was incubated on ice (figure 5.4).

Very weak autophosphorylation of singly expressed His-LmxGSK3- β was observed after 2.5 min – 5 min incubation at 4°C, however, it was not until 10 min a definite signal was visible (figure 5.4). In contrast MBP phosphorylation was observed at 15 s, which suggests phosphotransferase activity began earlier than autophosphorylation. MBP phosphorylation increased with further incubation. Although weaker MBP phosphorylation was observed at 4°C than at 34°C as in figure 5.3, it is clear His-LmxGSK3- β was very active even at low temperatures.

5.2.3 Screening of novel compounds

The global impact of Leishmaniasis on human and animal health is becoming increasingly serious, which is only made worse by the lack of safe, effective and affordable treatments. The increasing resistance to current treatments has led to a huge push to understand the mechanisms by which *Leishmania* acquire resistance to antimony (Sen and Chatterjee, 2011). Although there are great advances in this field that fact remains that many of the treatments available are still highly toxic and/or too expensive for the majority of patients. Thus, it is imperative to find new, safe and affordable alternatives. One area which has attracted a lot of attention for potential new drugs is the 'natural products' development. Natural products are being screened for the presence of inhibitors of enzymes essential for replication, cell cycle regulation or production of virulence factors (Sen and Chatterjee, 2011).

The rind of the plant *Myristica malabarica* – also known as Bombay mace or false nutmeg is a commonly used spice in Indian cuisine which has attracted a lot of interest over the past few years. The activities of *M. malabarica* include hepatoprotective, anti-ulcerogenic, anti-cancer, anti-oxidant and anti-leishmanial (Kang *et al.*, 2012; Manna *et al.*, 2012). The pharmacological activities are attributed to the malabaricones (of which there are four - malabaricone A-D) which are phytoconstituents of *M. malabarica*. Malabaricone C exhibits potent anti-oxidant and anti-cancer activity, which may mediate anti-leishmanial activity in a similar way to miltefosine (a currently available anti-leishmanial and anti-cancer drug) (Manna *et al.*, 2012). *Myristica fragrans* has also been shown to possess similar pharmacological activities as *M. malabarica* (Chirathaworn *et al.*, 2007; Latha *et al.*, 2005).

Malabaricones were extracted from two sources *Myristica fatua* and *Myristica fragrans*, members of the *Myristicaceae* family (Igoli, J – University of Strathclyde). Malabaricones were extracted from *M. fatua* using a hexane extraction method over a silica gel column. This yielded pure Malabaricone B, here termed- MFHE 84-89

(*Myristica fatua* Hexane Extract fraction 84-89) and Malabaricone C (*Myristica fatua* Hexane Extract fraction 90-93). Malabaricones were extracted from the second source, *M. fragrans*, using an ethylacetate extraction over a silica gel column. Only pure Malabaricone C was extracted – NME 31-37 (Nutmeg Ethylacetate fraction 31-37). This could be due to Malabaricone B being less abundant in *M. fragrans* than in *M. fatua*. The crude extract (NME 1), all three pure compounds (MFHE 84-89, MFHE 90-93 and NME 31-37) and several fractions from the second extraction were used to test inhibition of LmxGSK3- β and for anti-leishmanial activity. The chemical structures of malabaricone B and malabaricone C are shown in figure 5.5.

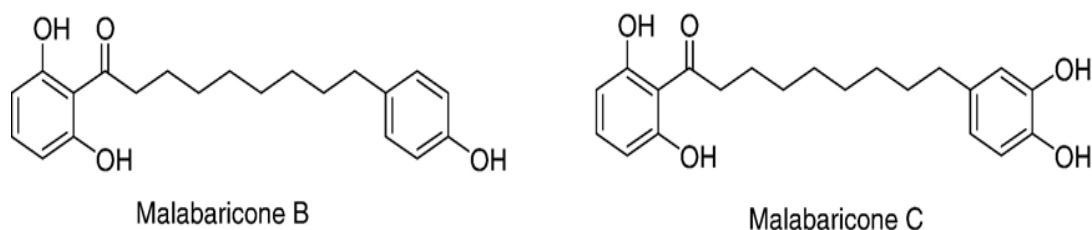


Figure 5.5. Chemical structures of Malabaricone B and Malabaricone C (Banerjee *et al.*, 2008).

5.2.3.1 Analysis of inhibition of LmxGSK3- β using the Kinase-Glo® system

Radiometric methods are the most commonly applied in *in vitro* kinase assays. However, despite being a universal kinase assay and excellent for protein characterisation it is not the most suitable method for inhibitor screening. It requires the use of radioisotopes, is difficult to perform and is expensive. Other assays have been developed such as fluorescence-based assays and anti-phospho amino acid antibody-based immunoassays. These all have the same drawbacks – they require special detection technology, they are expensive and have various experimental drawbacks such as interference with fluorescence or cross reactivity (Ma *et al.*, 2009).

The Kinase-Glo® luminescent kinase assay, available from Promega, quantifies the amount of ATP remaining in solution following a kinase reaction. This is based on measuring the intensity of luminescence generated by the mono-oxygenation of beetle luciferin by luciferase in the presence of Mg^{2+} , ATP and molecular oxygen (figure 5.6) (Baki *et al.*, 2007). The luciferase signal is proportional to the amount of ATP present and inversely correlated to kinase activity. As a homogeneous, non-radioactive kinase assay, it was chosen for inhibitor screening in this investigation. It has also been developed specifically for (human) GSK3- β and shown to be a robust and reproducible method for screening this highly active kinase (Baki *et al.*, 2007).

Kinase-Glo® assays were performed using black 96-well plates. The inhibitory activities were calculated as a percentage of maximal activity measured in the absence of inhibitor.

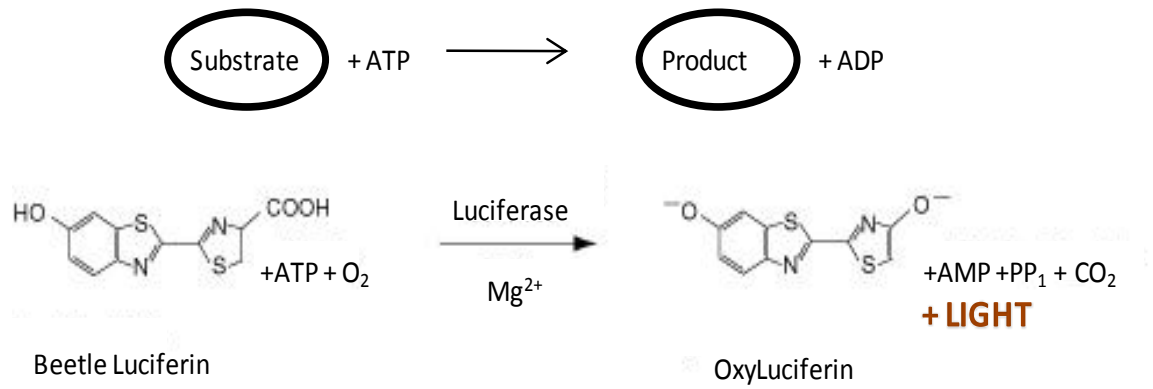


Figure 5.6. Assay principle of the Kinase-Glo® Assay (Adapted from Baki *et al.*, 2007).

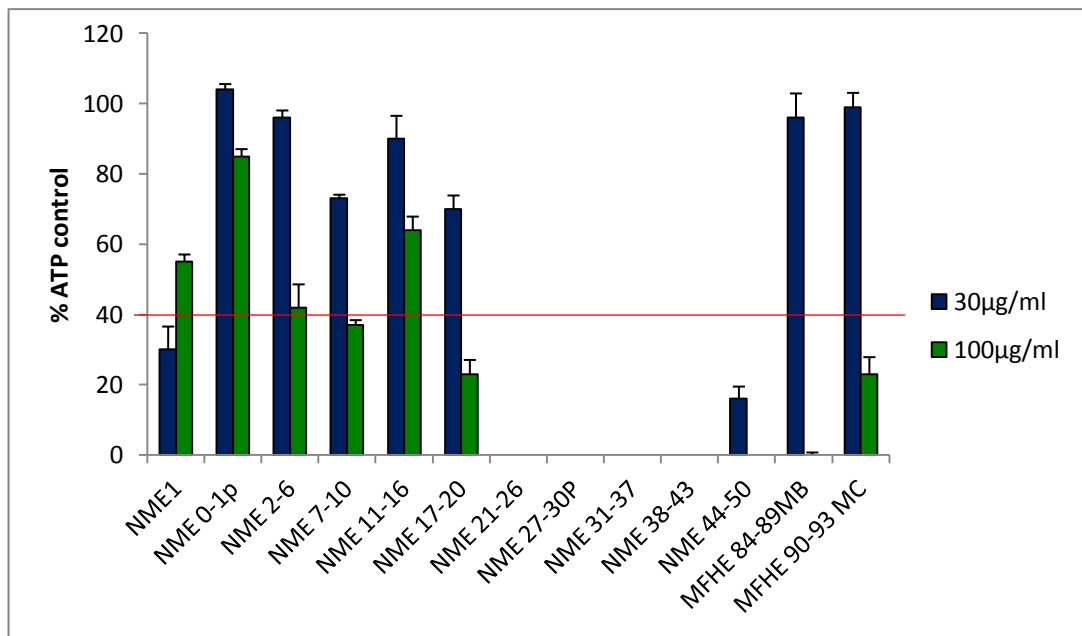


Figure 5.7. Inhibition of LmxGSK3-β using novel compounds in a Kinase-Glo® assay

Bar graphs showing the effects of pure or fractionated malabaricone compounds at different concentrations on the activity of LmxGSK3-β. Enzymatic activity of LmxGSK3-β determined using Kinase-Glo® assay. Each data point represents mean \pm SD value of three independent repeats.

Blue bars - 30 µg/ml; Green bars - 100 µg/ml. Maximum values less than red line deemed significant ($p < 0.05$) as determined by One-way ANOVA.

The extracted fractions and pure compounds were tested against LmxGSK3- β in a kinase-Glo® assay at two concentrations – 30 $\mu\text{g/ml}$ and 100 $\mu\text{g/ml}$ (figure 5.7). A total of 13 compounds were tested, five of these **NME 21-26**, **NME 27-30p**, **NME 31-37**, **NME 38-43**, NME 44-50, inhibited the activity of LmxGSK3- β by 50% or more at both 30 $\mu\text{g/ml}$ (blue bars) and 100 $\mu\text{g/ml}$ (green bars) compound concentration. Four of those completely ablated the activity of LmxGSK3- β at both compound concentrations (highlighted in bold). NME 44-50 did not completely ablate LmxGSK3- β activity however, it did show inhibition of greater than 75% in both concentrations. A further five compounds showed inhibition of 50% or greater of LmxGSK3- β activity at 100 $\mu\text{g/ml}$ only (green bars), this included both (early hexane extraction) pure compounds – **MFHE-84-89 MB** and **MFHE 90-93 MC** and three fractions (NME 2-6, NME7-10 and NME17-20). Inhibition of greater than 75% (i.e. 25% ATP control or lower) by these compounds is indicated in bold. All other compounds induced less than 50% inhibition (i.e. up to 100% ATP control) at both 30 $\mu\text{g/ml}$ and 100 $\mu\text{g/ml}$ and were therefore not considered important as LmxGSK3- β inhibitors.

5.2.3.2 Analysis of inhibition of LmxGSK3- β using a radiometric kinase assay

The inhibitor screen using the malabaricone compounds showed good inhibition of LmxGSK3- β . Studies suggest that the Kinase-Glo® assay is a reproducible and robust system for screening LmxGSK3- β (Baki et al, 2007), which was reflected in the kinase assays carried out here. However, as a fairly new system (with documented limitations) a radiometric kinase assay was carried out using the pure compounds (MFHE 84-89 MB and MFHE 90-93 MC) to confirm the results. Approximately 1 μg of recombinant LmxGSK3- β was incubated in optimised kinase buffer with 5 μg MBP, varying concentration inhibitor or 1% DMSO control and 5 μl 1 mM ATP containing 5 μCi γ - ^{32}P -ATP (6000 Ci/mmol) for 60 minutes at 34°C with end-over-end rotation in a total volume of 50 μl . The reaction was stopped by the addition of 12.5 μl SSB/DDT, heating at 95°C for 10 minutes then placing on ice. Twenty-five μl of each assay were separated by SDS-PAGE, Coomassie-stained then exposed to X-ray film at -80°C.

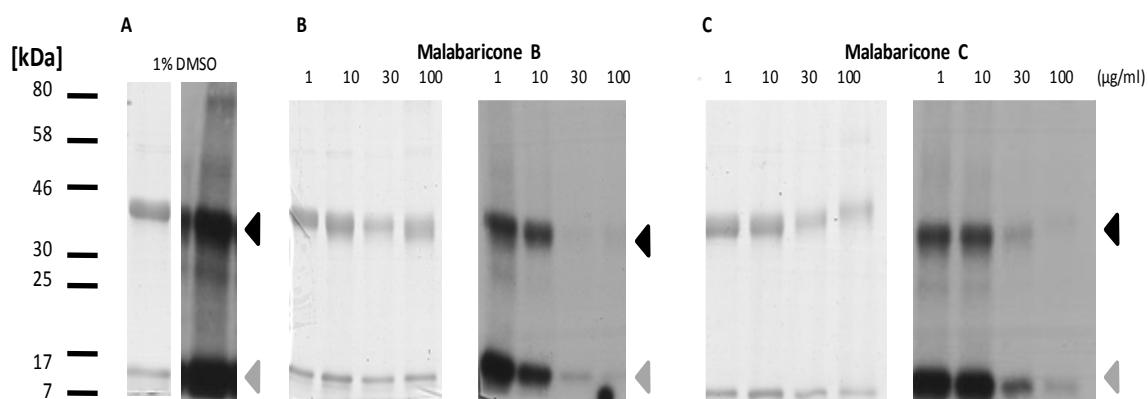


Figure 5.8. Inhibition of LmxGSK3- β using novel compounds

Left panels, Coomassie-stained gels; right panels, kinase assay after 3 hours exposure

Autophosphorylation and substrate phosphorylation of LmxGSK3- β when incubated with (A) 1% DMSO; (B) 1-100 μ g/ml Malabaricone B (MFHE 84-89 MB); (C) 1-100 μ g/ml Malabaricone C (MFHE 90-93 MC).

(◄) His-LmxGSK3- β ; (◄) MBP. Molecular masses of standard proteins are indicated in kDa.

The effects of pure compounds malabaricone B and malabaricone C on His-LmxGSK3- β were assessed in a radiometric assay (figure 5.8).

A 1% DMSO control was included to show any potential decrease in His-LmxGSK3- β activity was actually due to the malabaricones and not the DMSO content of the inhibitor solutions (figure 5.8 A). Strong autophosphorylation and phosphorylation of MBP were observed (lane 1).

Malabaricone B appeared to have reduced the autophosphorylation activity as well as the substrate phosphorylation activity of the His-LmxGSK3- β (figure 5.8 B). At low concentrations of the inhibitor (1 $\mu\text{g/ml}$ and 10 $\mu\text{g/ml}$) a reduction of autophosphorylation and MBP phosphorylation occurred, however, this was not a significant reduction compared to the DMSO control (figure 5.8 A) and clear bands were observed for both (lane 2 and 3). Increasing the inhibitor concentration to 30 $\mu\text{g/ml}$ showed a drastic reduction in activity with no autophosphorylation and substantially diminished MBP phosphorylation (lane 4). Almost no phosphotransferase activity was observed when 100 $\mu\text{g/ml}$ malabaricone B was used against His-LmxGSK3- β (lane 5).

As with malabaricone B, it was found that increasing the concentration of malabaricone C also led to the reduction of His-LmxGSK3- β phosphotransferase activity (figure 5.8 C). Low concentrations of the inhibitor, 1 $\mu\text{g/ml}$ and 10 $\mu\text{g/ml}$, appeared to lead to a slight but not substantial reduction in kinase activity when compared to the DMSO control (lane 1). When incubated with 30 $\mu\text{g/ml}$ malabaricone C, His-LmxGSK3- β exhibited significant reduction in autophosphorylation and MBP phosphorylation compared to 30 $\mu\text{g/ml}$ malabaricone B. However, despite the lower protein amounts in figure 5.7 C, lane 4 than in figure 5.7 B, lane 4, there appeared to be a more intense phosphorylation for MBP. Also, phosphorylation of MBP was observed when assayed with 100 $\mu\text{g/ml}$ malabaricone C (lane 5) unlike with malabaricone B (figure 5.8 B lane 5).

5.2.3.3 Analysis of inhibition of *L. mexicana* promastigotes using Alamar blue

Following on from the promising results with inhibition of LmxGSK3- β in the Kinase-Glo® assay (figure 5.7) and the radiometric kinase assay (figure 5.8), the plant fractions and pure compounds (malabaricone B and malabaricone C) were used against *L. mexicana* promastigotes in an Alamar blue assay to determine anti-leishmanial activity of the compounds. The effects of various fractions and pure Malabaricone C on *L. mexicana* promastigotes is shown in figure 5.9 and are representative of three biological repeats.

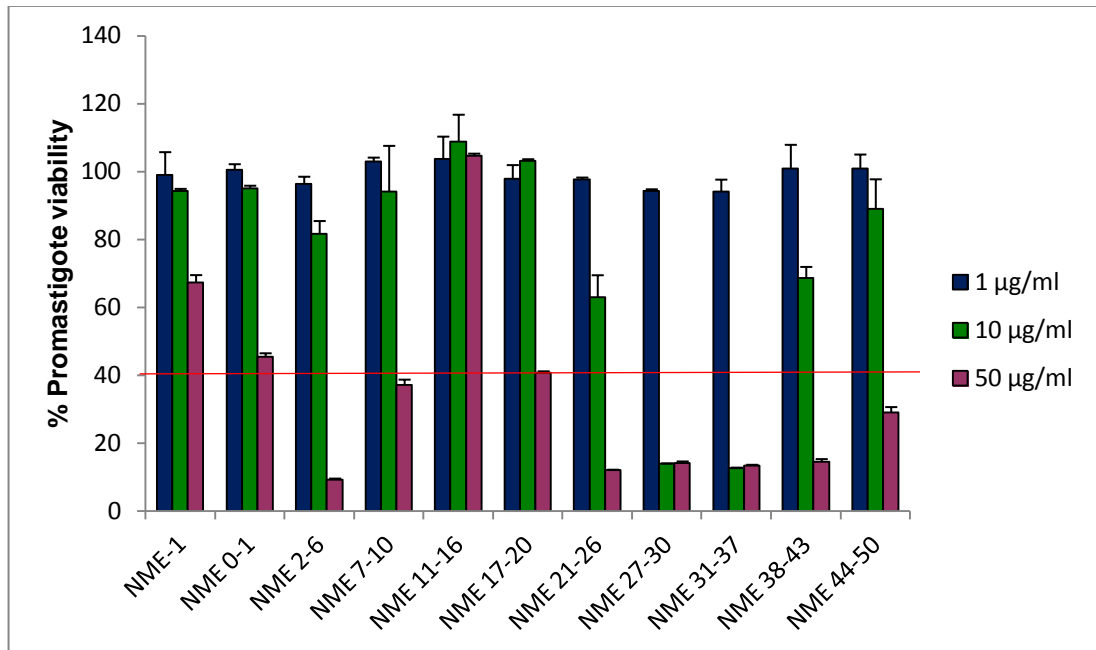


Figure 5.9. Effects of pure and fractionated malabaricones on growth of *Leishmania mexicana* promastigotes *in vitro*.

Viability of *L. mexicana* promastigotes incubated with malabaricone fractions and pure compound (NME 27-30 and NME31-37) was quantified by an Alamar Blue assay. Each data point represents mean \pm SD value of three independent repeats.

Blue bars - 1 μ g/ml; green bars - 10 μ g/ml; purple bars - 50 μ g/ml. Maximum values lower than red line deemed significant ($p < 0.05$) as determined by One-way ANOVA.

A selection of fractions which had shown inhibition of LmxGSK3- β in the Kinase-Glo assay® (figure 5.7) were tested against promastigotes at various concentrations in an Alamar blue assay (figure 5.9). Promastigotes grown in media without phenol red acted as a negative control which was used as the 100% growth comparison. Only newly produced fractions and pure Malabaricone C (NME 27-30 and NME 31-37) were included in this investigation. It had not been possible to extract pure Malabaricone B from *M. fragrans*, this is possibly due to Malabaricone B being less abundant in *M. fragrans* than in *M. fatua*.

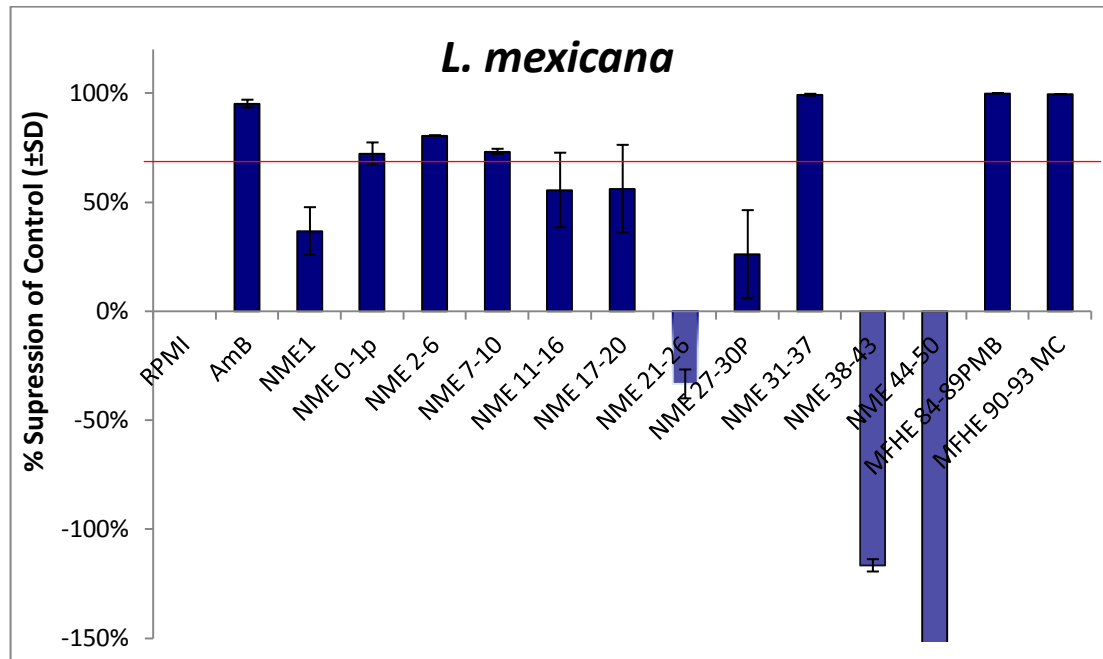
Eleven compounds were tested against *L. mexicana* promastigotes at three concentrations (1 $\mu\text{g/ml}$, 10 $\mu\text{g/ml}$ and 50 $\mu\text{g/ml}$) in a preliminary investigation. Nine compounds (NME 0-1, **NME 2-6**, NME 7-10, NME 17-20, **NME 21-26**, **NME 27-30**, **NME 31-37**, **NME 38-43**, NME 44-50) showed good inhibition of promastigote growth at 50 $\mu\text{g/ml}$ (purple bars) i.e. cell viability of less than 50%. Five of these showed cell viability of less than 20% (highlighted in bold). Only 2 fractions showed sufficient inhibition of *L. mexicana* promastigotes at concentrations less than 50 $\mu\text{g/ml}$ to be considered useful. Malabaricone C (NME 27-30 and NME 31-37) induced cell death at 10 $\mu\text{g/ml}$ (green bars) – cell viability was less than 20%. 1 $\mu\text{g/ml}$ (blue bars) appeared to be too low a concentration to cause substantial cell death with 94% cell viability being the lowest exhibited for any fraction.

5.2.3.4 Analysis of inhibition of *Leishmania* amastigotes using a luminescent system

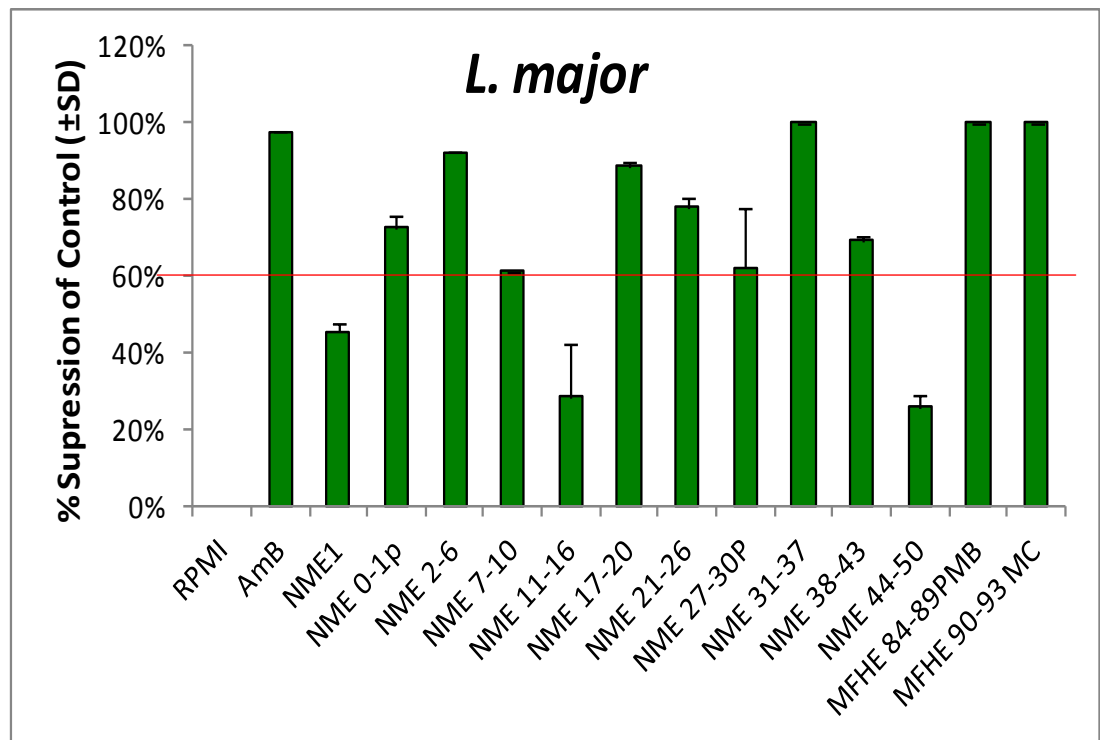
As some anti-leishmanial drugs only inhibit the amastigote stages, such as sodium stibogluconate (Ephros *et al.*, 1999), the compounds were also tested against the amastigote life stage of *L. mexicana*. Luminescent *L. mexicana*, *L. major* and *L. donovani* had previously been generated (Alsaadi *et al.*, 2012) and were utilised to test the compounds. Bone marrow macrophages harvested from mice were seeded on black 96 well plates and infected with luminescent promastigotes after 24 hours then incubated at 34°C (*L. mexicana*, *L. major*) or 37°C (*L. donovani*) for a further 24 hours.

Following incubation for 24 h, the pre-diluted compounds were added directly to the plate and incubated as before. After the final incubation, luciferin was added to the plates and read in the IVIS (*in vivo* imager). This was followed by a manual infection count of the macrophages in order to confirm the luminescent results (results not shown). Results are representative of three biological repeats.

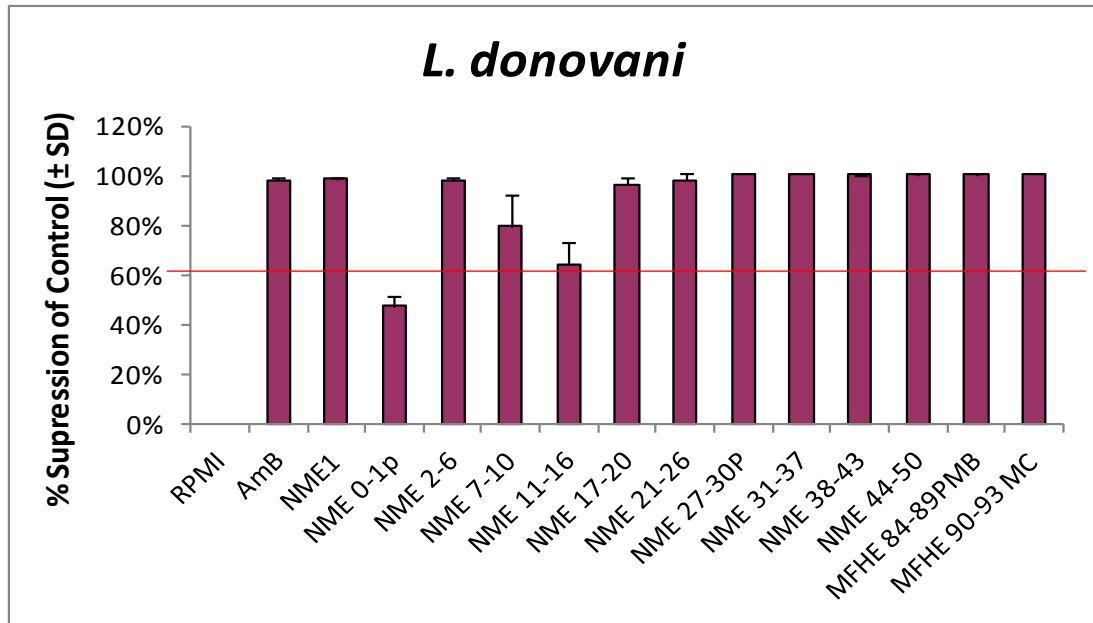
A



B



C



D

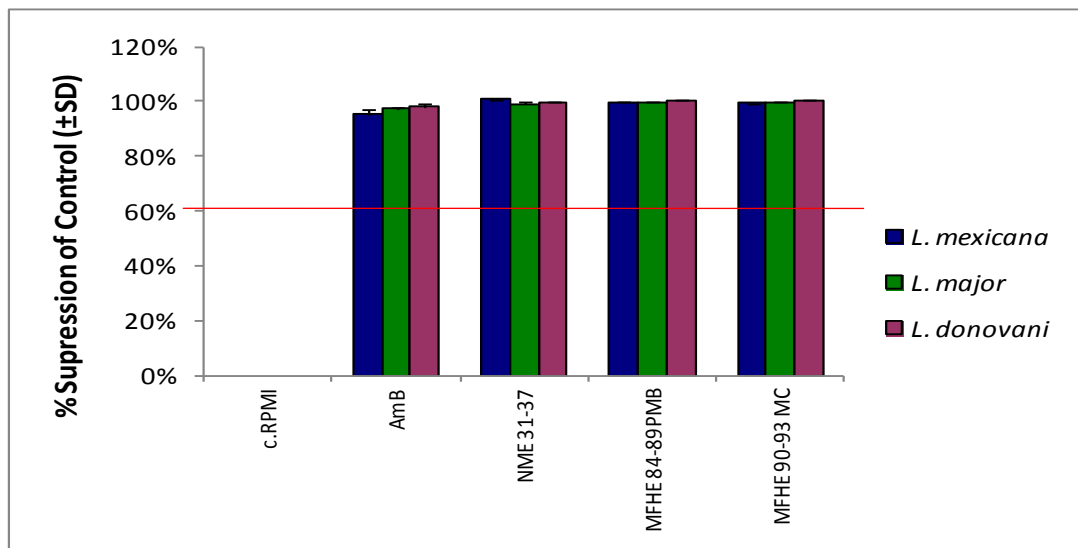


Figure 5.10. Effects of pure Malabaricones on intracellular *Leishmania*.

Bar graph showing the effects of pure or fractionated Malabaricone compounds on the growth of intracellular luciferase expressing *Leishmania* amastigotes. Viability of *Leishmania* amastigotes was determined using luciferase expression as a marker for growth. Each data point represents mean \pm SD value of three independent repeats.

(A) Compounds at 30 μ g/ml tested on macrophage infected luciferase expressing *L. mexicana*; (B) compounds at 30 μ g/ml tested on macrophage infected luciferase expressing *L. major*; (C) compounds at 30 μ g/ml tested on macrophage infected luciferase expressing *L. donovani*; (D) overview of pure compounds at 30 μ g/ml tested on macrophage infected luciferase expressing *L. mexicana*, *L. major* and *L. donovani*. Blue bars, *L. mexicana*; green bars, *L. major*; purple bars, *L. donovani*. Maximum values higher than red line deemed significant ($p < 0.05$) as determined by One-way ANOVA.

Fractions which had shown promise in the previous assays (figure 5.7, Figure 5.8 and figure 5.9) and the pure compounds Malabaricone B (MFHE 84-89 MB) and Malabaricone C (MFHE 90-93 MC and NME 31-37) were tested against luminescent intracellular amastigotes (figure 5.10 A-D). RPMI alone acted as a negative control which was used as the 100% growth comparison. Amphotericin B was also included as a positive control showing reduced luminescence was directly correlated to cell death.

The effects of these compounds against luminescent *L. mexicana* were determined as shown in figure 5.10 A. As expected, the *L. mexicana* infected the macrophages and grew normally in the presence of RPMI alone – resulting in the basis (0% suppression) for analysis of inhibitors. Additionally, the amphotericin B also acted as expected, resulting in an almost 100% suppression of luminescence (cell death). Of the 13 compounds used to inhibit *L. mexicana*, nine showed 50% suppression of luminescence or greater - fractions NME 0-1p, **NME 2-6**, NME 7-10, NME 11-16, NME 17-20 and **NME 27-30p** and all three pure compounds **NME 31-37**, **MFHE 84-89 MB** and **MFHE 90-93 MC**. Five of these showed luminescence suppression of greater than 75% (highlighted in bold). The other four inhibitors did not produce significant suppression of luminescence and have not been considered useful. Interestingly, three of the compounds (NME 21-26, NME 38-43 and NME 44-50) which were deemed no use actually promoted *L. mexicana* growth with increased luminescence of up to 150%.

The compounds appeared to be slightly more potent when tested against *L. major* (figure 5.10 B). *L. major* proliferated normally in the presence of RPMI alone and exhibited 100% luminescence suppression in the presence of amphotericin B thus validating the controls. Of the 13 inhibitors tested, ten exhibited suppression of luminescence at 50% or greater. These included all three pure compounds **NME 31-37**, **MFHE 84-89 MB** and **MFHE 90-93 MC** and fractions NME 0-1p, **NME 2-6**, NME 7-10, **NME 17-20**, **NME 21-26**, NME 27-30p, NME 38-43. Six of these showed luminescence suppression of greater than 75% (highlighted in bold). The other three compounds did not produce significant suppression of luminescence and have not been considered useful. No fractions appeared to increase *L. major* growth as with *L. mexicana* in figure 5.10 A.

The compounds were also tested against luminescent *L. donovani* (figure 5.10 C) and demonstrated good inhibition across the board. Of the 13 inhibitors tested, twelve exhibited suppression of luminescence at 50% or greater, these included all three pure compounds **NME 31-37**, **MFHE 84-89 MB** and **MFHE 90-93 MC** and fractions **NME 1**, **NME 2-6**, **NME 7-10**, NME 11-16, **NME 17-20**, **NME 21-26**, **NME 27-30p**, **NME 38-43** and **NME 44-50**. Eleven of these showed luminescence suppression of greater than 75% (highlighted in bold). Only one compound was considered of no use (NME 0-1p). As before, *L. donovani* thrived in the presence of RPMI alone and the addition of amphotericin B was entirely detrimental (100% luminescence suppression).

A direct comparison of the pure compounds (NME 31-37, MFHE 84-89 MB and MFHE 90-93 MC) effects on *L. mexicana*, *L. major* and *L. donovani* was graphed (figure 5.10 D). Both the Malabaricone B (MFHE 84-89 MB) and Malabaricone C (NME 31-37 and MFHE 90-93 MC) show excellent inhibition of all three strains of *Leishmania* and is as effective as amphotericin B (a currently available treatment of leishmaniasis). All strains were infective and proliferating normally in the presence of RPMI alone.

5.3 Discussion

5.3.1 LmxGSK3- β by co-expression with phosphatases and analysis of kinase activity

Prior to the commencement of this project His-LmxGSK3- β had been generated and used in kinase buffer optimisation assays. The optimised buffer was used in all assays performed in this work. As previously discussed, post-translational modifications, including phosphorylations, are key in regulating various kinases. In order to investigate the autophosphorylation and substrate phosphorylation of His-LmxGSK3- β the phosphatase co-expression system was applied and phosphatase (λ -phosphatase and PTP1B) co-expression constructs with His-LmxGSK3- β were generated along with an enzymatically inactive version of the kinase, His-LmxGSK3- β K50M (generated as before – mutation of the essential lysine 50 to methionine).

The phosphatase co-expressing system provided an effective and consistent alternative to assaying in the presence of a phosphatase in investigations with LmxMPK1 (McAlear, PhD Thesis, 2012) and LmxMPK2 (shown in chapter 4). Despite its success with LmxMPK1 and LmxMPK2, the co-expression system failed to fully dephosphorylate His-LmxGSK3- β . This was not entirely unexpected as the catalytic domain of the kinase is highly conserved and the human orthologue known to be a constitutively active kinase would make it very difficult, if not impossible to fully dephosphorylate the kinase. The importance of GSK3- β in human and animal health and the constitutively active nature of the kinase along with the inability to dephosphorylate the kinase sparked an interest in its activity at low temperatures. It was hypothesised that LmxGSK3- β autophosphorylation occurred too quickly for effective dephosphorylation by the phosphatases during co-expression. A second radiometric time course assay was performed, this time investigating the activity of His-LmxGSK3- β at approximately 4°C. The experiment was set up as before, only this time rather than incubating at 34°C, the samples were incubated on ice. As was seen with the kinase assay at 34°C, substrate phosphorylation occurs first and a distinct band is obvious on the autoradiograph after just 15 seconds incubation on ice. The MBP phosphorylation

continues to increase over the 10 min incubation. In contrast, the autophosphorylation is not detected until around 2.5-5 min after incubation with γ -³²P-ATP. The activity of His-LmxGSK3- β while on ice could be a factor in the inability to completely dephosphorylate threonine or tyrosine residues as the kinase would be active and autophosphorylating during the purification process.

Nevertheless, the inability to completely dephosphorylate His-LmxGSK3- β using either phosphatase is consistent with the activity of GSK3- β in higher eukaryotes, where the kinase is known to be constitutively active under basal conditions (Wang *et al.*, 2011). The inability to completely dephosphorylate tyrosine residues is also consistent with GSK3- β in higher eukaryotes as the activity of GSK3- β is largely regulated by the phosphorylation state of a particular tyrosine residue (Tyr-216 in LmxGSK3- β and Tyr-279 in GSK3- α). This tyrosine is important for activity of the kinase and dephosphorylation has been shown to diminish kinase activity (Sayas *et al.*, 2006). In *Leishmania*, it has recently been shown that tyrosine plays an integral role in the activity of *Leishmania* GSK3. Phosphorylation of Tyr-186 was shown to be constitutively phosphorylated (Tsigankov *et al.*, 2013). The results from the experiments performed here and those obtained by mass spectrometry (Tsigankov *et al.*, 2013) demonstrate the regulation and activity of His-LmxGSK3- β to be consistent with its orthologues in higher eukaryotes.

In humans, one suggested activator of GSK3- β is the tyrosine kinase Pyk2 that (although GSK3- β is constitutively active) increases phosphotransferase activity through tyrosine phosphorylation in GSK3- β (Sayas *et al.*, 2006). However, there is significant evidence that phosphorylation of the tyrosine residue is actually due to autophosphorylation of GSK3- β on Tyr-216 (Cole *et al.*, 2004). This would account for the inability to dephosphorylate the tyrosine residues as they are essential to the fully activated kinase. Although there is low similarity between the human and *Leishmania* GSK3- β , the catalytic domains are highly conserved which is reflected by the activity of the kinase and consistency of these data with that of the human GSK3- β activity. The constitutively active nature of LmxGSK3- β suggests the kinase is far more likely regulated by inhibitory phosphorylation, as with human GSK3- β (Wang *et al.*, 2011; Phukan *et al.*, 2010; Fang *et al.*, 2000). Identification of a regulatory kinase would aid further analysis, since it is possible that specific interactions are required for the

regulation of LmxGSK3- β . The identification of the substrate(s) within *Leishmania* may also be a valuable tool in further analyses of LmxGSK3- β in providing insight into its specific roles in *Leishmania*. Ultimately, these investigations have shown the activation of LmxGSK3 conforms to the same activation mechanisms as the human orthologue GSK3, confirming our initial hypothesis.

5.3.2 Effects of novel compounds on LmxGSK3- β and *Leishmania* parasites

Myristica malabarica (also known as Bombay mace or false nutmeg) is a commonly used spice in Indian cooking. More recently, it has attracted a lot of attention in the science community due to the hepatoprotective, anti-ulcerogenic, anti-cancer, anti-oxidant and anti-leishmanial activity exhibited by malabaricone compounds extracted from this plant (Kang et al., 2012; Manna et al., 2012).

For these investigations, the natural compound Malabaricone C was extracted from two sources of *Myristica* plant; *Myristica fatua* (MFHE 90-93) and *Myristica fragrans* (NME 31-37), while Malabaricone B could only be extracted from *Myristica fatua* (MFHE 84-89). The effects of pure compounds Malabaricone B and Malabaricone C along with several fractions (pre-screened for biological relevance) were tested against LmxGSK3- β in a new system – the Kinase-Glo® assay. As the Kinase-Glo® assay was a fairly new system, the pure Malabaricone B and C (extracted from *M. fatua*) were also subjected to a radiometric kinase assay to confirm the results. Thirteen of the fractions and pure compounds were tested at two concentrations (30 $\mu\text{g/ml}$ and 100 $\mu\text{g/ml}$) in the Kinase-Glo® assay (figure 5.7). Five compounds completely ablated LmxGSK3- β activity at both concentrations with a further three showing excellent inhibition (greater than 75% compared to the ATP control) at one or both concentrations. The Malabaricone C (NME 31-37) extracted from *M. fragrans* completely ablated activity of LmxGSK3- β . However, the pure malabaricone compounds extracted from *M. fatua* Malabaricone B (MFHE 84-89 MB) and Malabaricone C (MFHE 90-93 MC) were only effective at 100 $\mu\text{g/ml}$ – completely diminishing activity but not 30 $\mu\text{g/ml}$ which did not affect kinase activity. This could be due to degradation of the Malabaricones extracted from the *M. fatua* which were extracted at an earlier date, dissolved in 1% DMSO and

remained frozen until required. Compound stability and storage investigations could be carried out to confirm this.

The pure malabaricone compounds are of most interest, therefore only these were selected for radiometric inhibition assays to verify the Kinase-Glo® results (MFHE 84-89 and MFHE 90-93). This time, instead of using only two concentrations the LmxGSK3- β was subjected to inhibitor at 1 $\mu\text{g/ml}$, 10 $\mu\text{g/ml}$, 30 $\mu\text{g/ml}$ and 100 $\mu\text{g/ml}$. A 1% DMSO control was included to show LmxGSK3- β activity in the presence of the solvent only (figure 5.8 A). A slight reduction in autophosphorylation and MBP phosphorylation was observed at 1 $\mu\text{g/ml}$ for both compounds compared to the DMSO control. Activity gradually diminished as Malabaricone B and Malabaricone C concentrations increased. Malabaricone B caused almost complete ablation of kinase activity at 30 $\mu\text{g/ml}$ and complete ablation at 100 $\mu\text{g/ml}$. Malabaricone C is less effective than malabaricone B and did not appear to diminish the kinase activity as well at 30 $\mu\text{g/ml}$ or 100 $\mu\text{g/ml}$ with MBP phosphorylation still present at 100 $\mu\text{g/ml}$. These results correlate to the observations made in the Kinase-Glo® assays. Malabaricone B has been shown to be a more effective inhibitor of LmxGSK3- β than Malabaricone C, however, the radiometric assay suggests Malabaricone B to be more effective at 30 $\mu\text{g/ml}$ than is observed in the Kinase-Glo® assay. This could be partially due to the excessive quantities of kinase used in the radiometric assay (upwards of 2 μg – visually assessed). Moreover, the Kinase-Glo® assay is quantitative (Baki *et al.*, 2007) while the radiometric assay is not and simply shows trends.

Only the pure compounds were tested in the radiometric assay, simply as a validation method to complement a new method. The nature of the Kinase-Glo® assay means it can result in false negatives due to ATP depletion by the kinase over prolonged incubation or interference from luciferase inhibitors (Glickman *et al.*, 2012). Therefore, it was deemed necessary to test all fractions and pure compounds in the *in vivo* assays against intracellular amastigotes. However, not all of these were used in an inhibition assay against the promastigotes for three reasons. I. Only the *M. fragrans* extracted Malabaricone C (NME 31-37) had an effect on LmxGSK3- β at both concentrations. II.

Some currently available anti-leishmanial drugs are only effective against the amastigote stage of the parasite (Ephros *et al.*, 1999). III. Targeting the amastigote stage of *Leishmania* (i.e. the host stage) is most important in the development of new drugs.

Eleven fractions were initially tested against *L. mexicana* promastigotes at three concentrations; 1 µg/ml, 10 µg/ml and 50 µg/ml. While several showed good anti-leishmanial activity at 50 µg/ml, only two exhibited excellent anti-leishmanial activity at 10 µg/ml or below (figure 5.9). The pure Malabaricone C (NME 31-37) and almost pure fraction NME 27-30 exhibited excellent anti-leishmanial activity resulting in over 80% cell death. These results are similar to other studies showing Malabaricone C to possess excellent anti-leishmanial properties (Sen *et al.*, 2007).

Leishmania mexicana promastigotes expressing firefly luciferase (provided by R. Williams, University of Strathclyde) were used to infect bone marrow macrophages for use in investigations into the susceptibility of amastigotes to malabaricone compounds. All fractions and pure malabaricone compounds were tested against the luciferase expressing intracellular amastigotes at a concentration of 30 µg/ml. Amphotericin B (one of the most effective anti-leishmanial treatments currently available) was included as a positive control and showed that diminished luminescence was correlated to cell death. RPMI alone acted as the baseline for 100% growth of parasites. Amphotericin B is a second line drug in the treatment of visceral and mucocutaneous leishmaniasis, it is also known to clear cutaneous infections (Tiuman *et al.*, 2011; Nelson *et al.*, 2006). It was therefore anticipated amphotericin B would induce widespread cell death in *L. mexicana*, *L. major* and *L. donovani*, this was reflected in the results (figure 5.10). The malabaricone fractions had varying levels of success with the different *Leishmania* species and unexpectedly, some fractions actually promoted parasite growth, increasing the luminescence signal compared to the RPMI control (figure 5.10). For instance, three fractions were found to increase *L. mexicana* growth but resulted in complete cell death when tested against *L. donovani* and exhibited a high level of inhibition of *L. major*. It is unclear why three fractions increased the growth the *L. mexicana*, since this effect is not seen with the pure compounds, it is possible that there may be a compound in the crude fraction which promotes *L. mexicana* growth but not *L. major* or *L. donovani*.

NMR spectroscopy of the sample could elucidate this. The pure malabaricone compounds were in complete contrast to the activities of the crude fractions. Malabaricone B (MFHE 84-89), Malabaricone C (MFHE 90-93) and Malabaricone C (NME 31-37) all exhibited powerful anti-leishmanial activities against all three species of *Leishmania* resulting in almost 100% cell death.

Although it is not clear what causes the diverse forms of the disease the species divergence is likely to be a factor (Peacock *et al.*, 2007). This often leads to different effective treatments for different species such as miltefosine which has an efficacy of 94-97% in *L. donovani* infected patients but only 60% in *L. mexicana* infected patients and 33% in *L. braziliensis* infections. It is also largely ineffective against *L. major* infections (Minodier and Parola, 2007). Nonetheless, proteins which exhibit a high degree of similarity across the species represent potential drug targets that could lead to effective treatments against multiple species of *Leishmania*. Furthermore, due to the lack of understanding of the actions of current treatments and mechanism of resistance, inhibition of a specific target is an attractive avenue (Sen and Chatterjee, 2011). LmxGSK3- β is highly conserved between the species resulting in it being an excellent drug target. Sen *et al.*, 2007 found Malabaricone B to be a more effective anti-leishmanial than Malabaricone C. However, those studies were in relation to promastigotes and were not reflected in these investigations. Malabaricone B and Malabaricone C were highly effective against *L. mexicana*, *L. major* and *L. donovani* at 30 $\mu\text{g/ml}$ causing almost complete cell death. This contributes to the hypothesis that malabaricone may inhibit LmxGSK3- β .

Taking the Kinase-Glo® and radiometric assay results into consideration with the anti-leishmanial activity of the malabaricones, it appears highly likely that the target is LmxGSK3- β . This suggests Malabaricone B and Malabaricone C are both inhibitors of LmxGSK3- β .

5.3.3 Summary

The phosphotransferase activity of LmxGSK3- β was assessed and an investigation into the inhibition by novel compounds was the focus of this study. Attempts to generate *LmxGSK3- β* null mutants were performed prior to this project (Bleicher and Wiese, unpublished). All attempts to generate a null mutant by replacing the two alleles of *LmxGSK3- β* using resistance conferring genes using homologous recombination failed. However, when providing a copy of the wild type *LmxGSK3- β* on a plasmid both alleles could be deleted. LmxGSK3- β was shown as essential to both life stages of *L. mexicana* suggesting it would be an ideal drug target. This could be further supported by the addition of selective inhibition studies. The Inhibitor sensitised LmxGSK3- β mutants would allow selective inhibition and mimic RNAi methods used in Trypanosomes.

The phosphatase co-expression system was applied to recombinant LmxGSK3- β . It was not possible to fully dephosphorylate LmxGSK3- β on either threonine or tyrosine. An assessment of LmxGSK3- β phosphotransferase activity at 34°C and 4°C revealed LmxGSK3- β to be constitutively active and continues to be active at low temperatures. The highly active nature of LmxGSK3- β , even at low temperatures, could account for the lack of dephosphorylation of the kinase. Activity of LmxGSK3- β is very similar to its human orthologue, which appears to require the phosphorylation of tyrosine (likely on the Y-216 equivalent in *L. mexicana*, Y-186) for full activity.

Natural compounds Malabaricone B and C were isolated from *Myristica* plants (*Myristica fatua* and *Myristica fragrans*) and used for screening against LmxGSK3- β . Two methods were employed to assess the inhibition of LmxGSK3- β ; the relatively new system Kinase-Glo® and the more conventional radiometric assay. Both confirmed Malabaricone B and C to inhibit LmxGSK3- β . Various fractions and the pure compounds were tested for inhibition of promastigotes and intracellular amastigotes. Inhibition of promastigotes by Malabaricone C extracted from *Myristica fragrans* (NME 31-37) induced over 80% cell death at 10 μ g/ml. In the inhibition of amastigotes, the pure malabaricone compounds proved to be as effective as Amphotericin B - a currently available treatment for leishmaniasis. Therefore, LmxGSK3- β is a target for the malabaricones, moreover, Malabaricone B and C possess potent anti-leishmanial activity and are very promising potential drugs.

Chapter 6

6.1 General Discussion

Leishmaniasis is a tropical disease affecting around 12 million people worldwide. Treatments have changed little in the past century and often patients are treated with increasingly ineffective and highly toxic drugs, thus highlighting the requirement for safer and more effective medication.

Protein kinases are key regulatory molecules, along with their antagonists – protein phosphatases, forming complex networks of mutually activating and silencing molecules in all eukaryotic cells. Phosphorylation is a common post-translational modification which can induce conformational changes in proteins generating or masking binding motifs. These changes can modulate the activity of an enzyme, binding properties, protein stability or change the subcellular localisation of a protein. Mitogen Activated Protein kinases are part of the CMGC group of kinases involved in cellular signal transduction and are essential in almost all eukaryotes. They play a central role in regulating proliferation, differentiation and apoptosis of cells. This class of protein has recently attracted a lot of attention as potential targets for treating a variety of human diseases, including leishmaniasis.

This thesis was concerned with the analysis of the two protein kinase homologues, LmxMPK2 and LmxGSK3- β , of *Leishmania mexicana*. Previous investigations had already identified LmxMPK2 and LmxGSK3- β as potential drug targets as LmxMPK2 was shown to be essential in amastigote, while LmxGSK3- β was shown to be essential in both promastigote and amastigote life stages.

Prior to beginning this project, *LmxMPK2* null mutants as well as genomic add back *L. mexicana* parasites had already been generated and confirmation of status carried out by immunoblot. Electron microscopy investigations had also been carried out, revealing multiple morphological abnormalities. Localisation studies using GFP-tagged LmxMPK2 revealed close localisation to the cell membrane. Similar localisation to that

of LmjAQP1 suggested a link between the two. Although, it is unlikely that LmjAQP1 is a direct substrate of LmxMPK2, it does provide a basis for the search for the LmxMPK2 substrate. An investigation to ascertain a relationship between LmxMPK2 and LmxDIP13 (Deflagellation Inducible Protein), a small coiled protein shown to associate with microtubules was carried out. No difference in general localisation was observed between wild type and *LmxMPK2* null mutants expressing GFP-LmxDIP13. However, the percentage of cells showing GFP-LmxDIP13 at the anterior end of the cell increased from 6% to at least 20% suggesting an interaction between LmxDIP13 and LmxMPK2. Despite this, the association between the two has not been elucidated. In addition to a potential relationship with LmxMPK2, LmxDIP13 was hypothesised to be a potential cell cycle marker in *Leishmania* due to an observation made by Price *et al.*, 2012, where it was noted that expression was limited to early mitotic stages of *T. brucei* development. Ultimately, no difference in localisation was observed and therefore it was discounted as a putative cell cycle marker for *Leishmania*.

Recombinant expression of LmxMPK2 resulted in an active enzyme already phosphorylated on tyrosine and threonine which is able to phosphorylate myelin basic protein (MBP) despite the absence of activation by a MAP kinase kinase. Co-expression with different phosphatases led to LmxMPK2 being fully dephosphorylated on tyrosine but not threonine residues. Despite full dephosphorylation of the tyrosine residues, LmxMPK2 retain the ability of tyrosine autophosphorylation and maintained substrate phosphorylation abilities. The inability to dephosphorylate LmxMPK2 on threonine suggests a deviation from normal MAP kinase activation mechanism where phosphorylation of both threonine and tyrosine on the TXY motif is required for full activation. Further works with the use of mass spectrometry would provide greater insight and better understanding of the activation mechanism of LmxMPK2 and the specific location of the activating phosphorylations.

While it appears a relationship does exist between LmxMPK2 and LmxDIP13, the actual association was determined in these investigations. LmxDIP13 was also deemed of no use as a putative cell cycle marker in *Leishmania*.

Investigations into the activation mechanism revealed LmxMPK2 to be an unusual MAP kinase which is able to autophosphorylate on threonine and tyrosine residues of unknown localisation without affecting the activity of the enzyme. Understanding fully how this essential kinase is regulated would allow for better drug design for the treatment of leishmaniasis.

Attempts to generate *LmxGSK3-β* null mutants were performed prior to this project (Bleicher and Wiese, unpublished). All attempts to generate a null mutant by replacing the two alleles of *LmxGSK3-β* using resistance conferring genes using homologous recombination failed. However, when providing a copy of the wild type *LmxGSK3-β* on a plasmid both alleles could be deleted. LmxGSK3-β was shown as essential to both life stages of *L. mexicana* suggesting it would be an ideal drug target. This could be further supported by the addition of selective inhibition studies.

The phosphatase co-expression system was applied to recombinant LmxGSK3-β. However, it was not possible to fully dephosphorylate LmxGSK3-β on either threonine or tyrosine. Activity of LmxGSK3-β was discovered to be similar to that of human GSK3-β. An assessment of LmxGSK3-β phosphotransferase activity at 34°C and 4°C revealed LmxGSK3-β to be highly active even at low temperatures. Through these investigations it is highly likely the activity of LmxGSK3-β is very similar to its human orthologue, which appears to require the phosphorylation of tyrosine (likely on the Y-216 equivalent in *L. mexicana*, Y-186) for full activity.

Natural compounds Malabaricone B and C were isolated from *Myristica* plants and used for screening against LmxGSK3-β. Radiometric assays and new method Kinase-Glo® carried out confirmed the inhibition of various fractions and pure malabaricone compounds on LmxGSK3-β. Inhibition of promastigotes by malabaricone C extracted from *Myristica fragrans* induced over 80% cell death at 10 µg/ml. The pure compounds proved just as effective in the inhibition of intracellular amastigotes as currently available leishmaniasis treatment, amphotericin B.. Both compounds were identified as inhibitors of LmxGSK3-β and possess potent anti-leishmanial activity. Further studies to determine EC50 values for the pure compounds are already underway.

Investigations to characterise the phosphorylation states and activity of LmxGSK3- β , it was revealed that LmxGSK3- β was a highly active kinase which could not be fully dephosphorylated in the co-expression system. Additionally, it is likely that it is constitutively active on the Tyr-186 and possesses the same activity as its human orthologue which is regulated by inhibitory phosphorylation.

The pure compounds Malabaricone B and Malabaricone C, extracted from *Myristica* plants proved to be effective inhibitors of LmxGSK3- β . Moreover, they provided potent anti-leishmanial activity of both life stages and are therefore deemed excellent candidates for future anti-leishmanial drugs.

7. References

- Agron, P. G., Reed, S. L., & Engel, J. N. (2005). An essential , putative MEK kinase of *Leishmania major*. *Molecular and Biochemical Parasitology*, *142*, 121–125.
- Alexander, J., Satoskar, A. R., & Russell, D. G. (1999). *Leishmania* species : models of intracellular parasitism. *Journal of Cell Science*, *3002*, 2993–3002.
- Alsaadi, M., Italia, J. L., Mullen, a B., Ravi Kumar, M. N. V, Candlish, a a, Williams, R. a M., Shaw, C. D., et al. (2012). The efficacy of aerosol treatment with non-ionic surfactant vesicles containing amphotericin B in rodent models of leishmaniasis and pulmonary aspergillosis infection. *Journal of Controlled Release*, *160*(3), 685–91.
- Alvar, J., Yactayo, S., & Bern, C. (2006). Leishmaniasis and poverty. *Trends in Parasitology*, *22*(12), 552-557.
- Ambit, A., Woods, K. L., Cull, B., Coombs, G. H., & Mottram, J. C. (2011). Morphological events during the cell cycle of *Leishmania major*. *Eukaryotic Cell*, *10*(11), 1429–38.
- Antoine, J., Prina, E., Lang, T., & Courret, N. (1998). The biogenesis and properties of the parasitophorous vacuoles that harbour *Leishmania* in murine macrophages. *Trends in Microbiology*, *6*(10), 392–401.
- Avruch, J. (2007). MAP kinase pathways : The first twenty years. *Biochimical Biophysics Acta*, *1773*(8), 1150–1160.
- Baki, A., Bielik, A., Molnár, L., Szendrei, G., & Keserü, G. M. (2007). A high throughput luminescent assay for glycogen synthase kinase-3beta inhibitors. *Assay and Drug Development Technologies*, *5*(1), 75–83.
- Banerjee, D., Bauri, A. K., Guha, R. K., Bandyopadhyay, S. K., & Chattopadhyay, S. (2008). Healing properties of malabaricone B and malabaricone C, against indomethacin-induced gastric ulceration and mechanism of action. *European Journal of Pharmacology*, *578*(2-3), 300–312.
- Barcinski, M. A., Schechtman, D., Quintao, L. G., Costa, D. D. E. A., Soares, L. R. B., Moreira, M. E. C., & Charlab, R. (1992). Granulocyte-Macrophage Colony-Stimulating Factor Increases the Infectivity of *Leishmania amazonensis* by Protecting Promastigotes from Heat-Induced Death. *Microbiology*, *60*(9), 3523–3527.
- Bates, P. A. (2007). Transmission of *Leishmania* metacyclic promastigotes by *phlebotomine* sand flies. *International Journal for Parasitology*, *37*, 1097–1106.

- Bates, P. A. (2008). *Leishmania* sand fly interaction : progress and challenges. *Current Opinion in Microbiology*, 11, 340–344.
- Beilina, A., Van Der Brug, M., Ahmad, R., Kesavapany, S., Miller, D. W., Petsko, G. a, & Cookson, M. R. (2005). Mutations in PTEN-induced putative kinase 1 associated with recessive parkinsonism have differential effects on protein stability. *Proceedings of the National Academy of Sciences of the United States of America*, 102(16), 5703–8.
- Bell, M., & Engelberg, D. (2003). Phosphorylation of Tyr-176 of the yeast MAPK Hog1/p38 is not vital for Hog1 biological activity. *The Journal of Biological Chemistry*, 278(17), 14603–6.
- Bengs, F., Scholz, A., Kuhn, D., & Wiese, M. (2005). LmxMPK9 , a mitogen-activated protein kinase homologue affects flagellar length in *Leishmania mexicana*. *Molecular Microbiology*, 55, 1606–1615.
- Berzunza-cruz, M., Bricaire, G., Suazo, N. S., & Pérez-montfort, R. (2009). PCR for identification of species causing American cutaneous leishmaniasis. *Parasitology Research*, 104, 691–699.
- Bhattacharyya, R. P., Reményi, A., Good, M. C., Bashor, C. J., Falick, A. M., & Lim, W. a. (2006). The Ste5 scaffold allosterically modulates signaling output of the yeast mating pathway. *Science*, 311(5762), 822–6.
- Bolhassani, A., Taheri, T., Taslimi, Y., Zamanilui, S., Zahedifard, F., Seyed, N., Torkashvand, F., et al. (2011). Fluorescent *Leishmania* species: development of stable GFP expression and its application for in vitro and in vivo studies. *Experimental Parasitology*, 127(3), 637–45.
- Braun, P., & Labaer, J. (2003). High throughput protein production for functional proteomics, *Trends in Biotechnology*, 21(9), 383–388.
- Bringaud, F., Vedrenne, C., Cuvillier, A., Parzy, D., Baltz, D., Tetaud, E., Pays, E., Venegas, J., Merlin, G., and Baltz, T. (1998) Conserved organization of genes in trypanosomatids. *Mol. Biochem. Parasitol.* 94 (2): 249
- Brumlik, M. J., Pandeswara, S., Ludwig, S. M., Murthy, K., & Curiel, T. J. (2011). Parasite mitogen-activated protein kinases as drug discovery targets to treat human protozoan pathogens. *Journal of Signal Transduction*, 2011, 1-16.
- Cargnello, M., & Roux, P. P. (2011). Activation and function of the MAPKs and their substrates, the MAPK-activated protein kinases. *Microbiology and Molecular Biology Reviews*, 75(1), 50–83.
- Carrera, A. N. A. C., Alexandrov, K., & Roberts, T. M. (1993). The conserved lysine of the catalytic domain of protein kinases is actively involved in the phosphotransfer reaction and not required for anchoring ATP. *Biochemistry*, 90, 442–446.

- Chirathaworn, C., Kongcharoensuntorn, W., Dechdougchan, T., Lowanitchapat, A., Sa-nguanmoo, P., & Poovorawan, Y. (2007). *Myristica fragrans* Houtt. methanolic extract induces apoptosis in a human leukemia cell line through SIRT1 mRNA downregulation. *Journal of the Medical Association of Thailand*, 90(11), 2422–8.
- Cohen, P. (2009). Targeting protein kinases for the development of anti-inflammatory drugs. *Current Opinion in Cell Biology*, 21, 317–324.
- Cole, A., Frame, S., & Cohen, P. (2004). Further evidence that the tyrosine phosphorylation of glycogen synthase kinase-3 (GSK3) in mammalian cells is an autophosphorylation event. *The Biochemical Journal*, 377, 249–55.
- Costa, S., Golim, M. D. A., Rossi-bergmann, B., Trindade, F., Costa, M., & Giorgio, S. (2011). Use of In Vivo and In Vitro Systems to Select *Leishmania amazonensis* Expressing Green Fluorescent Protein. *Korean Journal of Parasitology*, 49(4), 357–364.
- Croft, S. L., & Coombs, G. H. (2003). Leishmaniasis – current chemotherapy and recent advances in the search for novel drugs. *Trends in Parasitology*, 19(11), 502–508.
- Croft, S. L., Sundar, S., & Fairlamb, A. H. (2006). Drug Resistance in Leishmaniasis. *Clinical Microbiology Reviews*, 19(1), 111–126.
- Cruz, I., Nieto, J., Moreno, J., Cañavate, C., Desjeux, P., & Alvar, J. (2006). *Leishmania* / HIV co-infections in the second decade. *Indian Journal Of Medical Research*, 357–388.
- Dagger, F., Valdivieso, E., Marcano, A. K., & Ayesta, C. (2013). Regulatory volume decrease in *Leishmania mexicana*: effect of anti-microtubule drugs. *Memórias do Instituto Oswaldo Cruz*, 108(1), 84–90.
- Davis, R. J. (1993). The Mitogen-activated Protein Kinase Signal Transduction Pathway. *Biochemistry*, 268, 14553–14556.
- Desjeux, P. (2004). Leishmaniasis: current situation and new perspectives. *World Health*, 27, 305–318.
- Domenicali Pfister, D., Burkard, G., Morand, S., Renggli, C. K., Roditi, I., & Vassella, E. (2006). A Mitogen-activated protein kinase controls differentiation of bloodstream forms of *Trypanosoma brucei*. *Eukaryotic cell*, 5(7), 1126–35.
- Donovan, C. (1903). On the possibility of the occurrence of trypanosomiasis in India. *British Medical Journal*, 2 (2219), 79.
- Dorin-Semblat, D., Quashie, N., Halbert, J., Sicard, A., Doerig, C., Peat, E., Ranford-Cartwright, L., et al. (2007). Functional characterization of both MAP kinases of the human malaria parasite *Plasmodium falciparum* by reverse genetics. *Molecular microbiology*, 65(5), 1170–80.

- Dougall, A. M., Alexander, B., Holt, D. C., Harris, T., Sultan, A. H., Bates, P. a, Rose, K., et al. (2011). Evidence incriminating midges (Diptera: *Ceratopogonidae*) as potential vectors of *Leishmania* in Australia. *International journal for parasitology*, *41*(5), 571–9.
- Dumonteil, E., Jesus, R. M., & Javier, E. (2003). DNA vaccines induce partial protection against *Leishmania mexicana*. *Parasitology*, *21*, 2161–2168.
- Ephros, M., Bitnun, a, Shaked, P., Waldman, E., & Zilberstein, D. (1999). Stage-specific activity of pentavalent antimony against *Leishmania donovani* axenic amastigotes. *Antimicrobial Agents and Chemotherapy*, *43*(2), 278–82.
- Erdmann, M. (2009). LmxMPK3, a mitogen-activated protein kinase involved in length control of a eukaryotic flagellum. PhD Thesis. University of Hamburg, Germany.
- Erdmann, Maja, Scholz, A., Melzer, I. M., Schmetz, C., & Wiese, M. (2006). Interacting Protein Kinases Involved in the Regulation of Flagellar Length. *Molecular Biology of the Cell*, *17*, 2035–2045.
- Fang, X., Yu, S. X., Lu, Y., Bast, R. C., Woodgett, J. R., & Mills, G. B. (2000). Phosphorylation and inactivation of glycogen synthase kinase 3 by protein kinase A. *Proceedings of the National Academy of Sciences of the United States of America*, *97*(22), 11960–5.
- Francis, S. H., Busch, J. L., & Corbin, J. D. (2010). cGMP-Dependent Protein Kinases and cGMP Phosphodiesterases in Nitric Oxide and cGMP Action. *Pharmacological Reviews*, *62*(3), 525–563.
- Gibbs, C. S., & Zoller, M. J. (1991). Rational Scanning Mutagenesis of a Protein Kinase Identifies Functional Regions Involved in Catalysis and Substrate Interactions. *The Journal of Biological Chemistry*, *266*(14), 8923–8931.
- Glickman, J. F., Ph, D., & Mcgee, J. (2012). Assay Development for Protein Kinase Enzymes. *Assay Guide Manual*.
- Gramiccia, M., & Gradoni, L. (2005). The current status of zoonotic leishmaniases and approaches to disease control. *International Journal for Parasitology*, *35*, 1169–1180.
- Hammarton, T. C. (2007). Cell cycle regulation in *Trypanosoma brucei*. *Molecular and Biochemical Parasitology*, *153*(1), 1–8.
- Hanks, S. K. (2003). Genomic analysis of the eukaryotic protein kinase superfamily: a perspective. *Genome Biology*, *4*(111).
- Hanks, S. K., & Hunter, T. (1995). The eukaryotic protein kinase superfamily: (catalytic) domam structure and classification. *The FASEB Journal*, *9*(8), 576–596.

- Hermoso, T., Fishelson, Z., Becker, S. I., Hirschberg, K., & Jaffe, C. L. (1991). Leishmanial protein kinases phosphorylate of the complement system components. *EMBO Journal*, 10(13), 4061–4067.
- Hoarse, C. A., (1938). Early discoveries regarding the parasite of oriental sore. *Transactions of the Royal Society of Tropical Medicine and Hygiene*, 32 (1), 67-86.
- Horjales, S., Schmidt-arras, D., Limardo, R. R., Leclercq, O., Obal, G., Prina, E., Turjanski, A. G., et al. (2012). Article The Crystal Structure of the MAP Kinase LmaMPK10 from *Leishmania Major* Reveals Parasite-Specific Features and Regulatory Mechanisms. *Structure*, 20, 1–12.
- Hua, S., & Wang, C. C. (1997). Interferon- γ Activation of a Mitogen-activated Protein Kinase , KFR1 , in the Bloodstream Form of *Trypanosoma brucei*. *The Journal of Biological Chemistry*, 272(16), 10797–10803.
- Jeffrey, K. L., Rommel, C., & Mackay, C. R. (2007). Targeting dual-specificity phosphatases : manipulating MAP kinase signalling and immune responses. *Inflammation Research*, 6, 391–403.
- John von Freyend, S. (2010). Analysis of LmxMPK4 and LmxMPK6 , two mitogen-activated protein kinases of *Leishmania mexicana*. PhD Thesis. Department of Biology. University of Hamburg.
- John von Freyend, S., Rosenqvist, H., Fink, A., Melzer, I. M., Clos, J., Jensen, O. N., & Wiese, M. (2010). LmxMPK4, an essential mitogen-activated protein kinase of *Leishmania mexicana* is phosphorylated and activated by the STE7-like protein kinase LmxMCK5. *International journal for parasitology*, 40(8), 969–78.
- Johnson, S. A., & Hunter, T. (2005). Kinomics : methods for deciphering the kinome. *Nature methods*, 2(1), 17–25.
- Kamhawi, S. (2006). Phlebotomine sand flies and *Leishmania* parasites : friends or foes? *Trends in Parasitology*, 22(9), 439-445.
- Kang, J., Tae, N., Min, B. S., Choe, J., & Lee, J.-H. (2012). Malabaricone C suppresses lipopolysaccharide-induced inflammatory responses via inhibiting ROS-mediated Akt/IKK/NF- κ B signaling in murine macrophages. *International Immunopharmacology*, 14(3), 302–10.
- Kelly, P., & Baudry, T. (2012). Imported cutaneous leishmaniasis in a short-term traveler returning from Central Mali - The role of PCR. *Travel Medicine and Infectious Disease*, 10, 97–100.
- Kim, E. K., & Choi, E. (2010). Biochimica et Biophysica Acta Pathological roles of MAPK signaling pathways in human diseases. *BBA - Molecular Basis of Disease*, 1802(4), 396–405.

- Kolev, N. G., Tschudi, C., & Ullu, E. (2011). RNA Interference in Protozoan Parasites : Achievements and Challenges. *Eukaryotic Cell*, 10(9), 1156–1163.
- Krupa, A., Preethi, G., & Srinivasan, N. (2004). Structural Modes of Stabilization of Permissive Phosphorylation Sites in Protein Kinases : Distinct Strategies in Ser / Thr and Tyr Kinases. *Journal of Molecular Biology*, 339(5), 1025–1039.
- Kuhn, D., & Wiese, M. (2005). LmxPK4, a mitogen-activated protein kinase kinase homologue of *Leishmania mexicana* with a potential role in parasite differentiation. *Molecular Microbiology*, 56(5), 1169–1182.
- Kumari, S., Singh, S., Saha, B., & Paliwal, P. K. (2011). *Leishmania major* MAP kinase 10 is protective against experimental *L. major* infection. *Vaccine*, 29(48), 8783–8787
- Lainson, R., Shaw, J. J., Peters, W., & Killick-Kendrick, R. (1987). Evolution, classification and geographical distribution. The Leishmaniases in biology and medicine, 1, 1–120.
- Latha, P. G., Sindhu, P. G., Suja, S. R., Geetha, B. S., Pushpangadan, P., & Rajasekharan, S. (2005). Pharmacology and chemistry of *Myristica fragrans* Houtt – a review. *Journal of Spices and Aromatic Crops*, 14(2), 94–101.
- Laxman, S. and Beavo, J. A. (2007) Cyclic nucleotide signaling mechanisms in trypanosomes: possible targets for therapeutic agents. *Mol. Interv.* 7 (4): 203
- Leishman, W. B. (1903). ON THE POSSIBILITY OF THE OCCURRENCE OF TRYPANOSOMIASIS IN INDIA. *BMJ*, 1(2213), 1252–1254.
- Lichty, J. J., Malecki, J. L., Agnew, H. D., Michelson-Horowitz, D. J., & Tan, S. (2005). Comparison of affinity tags for protein purification. *Protein Expression and Purification*, 41(1), 98–105.
- Liu, D., Uzonna, J. E., & Bengoechea, J. A. (2012). The early interaction of *Leishmania* with macrophages and dendritic cells and its influence on the host immune response. *Microbiology*, 2, 1–8.
- Lye, L., Owens, K., Shi, H., Murta, S. M. F., Vieira, A. C., Turco, S. J., Tschudi, C., et al. (2010). Retention and Loss of RNA Interference Pathways in Trypanosomatid Protozoans. *Plos Pathogens*, 6(10), 1-13.
- Ma, H., Deacon, S., & Horiuchi, K. (2009). The challenge of selecting protein kinase assays for lead discovery optimization. *Expert Opinion in Drug Discovery*, 3(6), 607–621.
- Mandal, G., Sharma, M., Kruse, M., Sander-juelch, C., Munro, L. A., Wang, Y., Vilg, J. V., et al. (2012). Modulation of *Leishmania major* aquaglyceroporin activity by a mitogen-activated protein kinase. *Molecular Microbiology*, 85, 1204–1218.

- Manna, A., Saha, P., Sarkar, A., Mukhopadhyay, D., Bauri, A. K., Kumar, D., Das, P., et al. (2012). Malabaricone-A induces a redox imbalance that mediates apoptosis in U937 cell line. *PloS one*, 7(5), 1-11.
- Manning, G., Plowman, G. D., Hunter, T., & Sudarsanam, S. (2002). Evolution of protein kinase signaling from yeast to man. *Trends in Biochemical Sciences*, 27(10), 514–520.
- Manning, G., Whyte, D. B., Martinez, R., Hunter, T., & Sudarsanam, S. (2002). The Protein Kinase Complement of the Human Genome. *Science*, 298, 1912–1934.
- Matte, a, Tari, L. W., & Delbaere, L. T. (1998). How do kinases transfer phosphoryl groups? *Structure*, 6(4), 413–9.
- Mcaleer, P. P. (2012). Strathclyde Institute of Pharmacy and Biomedical Analysis of the regulation mechanism of LmxMPK1 , a *Leishmania mexicana* MAP kinase homologue. PhD Thesis. SIPBS. University of Strathclyde.
- Minodier, P., & Parola, P. (2007). Cutaneous leishmaniasis treatment. *Travel Medicine and Infectious Disease*, 5, 150–158.
- Miranda-saavedra, D., Stark, M. J. R., Packer, J. C., Vivares, C. P., Doerig, C., & Barton, G. J. (2007). The complement of protein kinases of the microsporidium *Encephalitozoon cuniculi* in relation to those of *Saccharomyces cerevisiae* and *Schizosaccharomyces pombe*. *BMC Genomics*, 21, 1–21.
- Mittelstadt, P. R., Yamaguchi, H., Appella, E., & Ashwell, J. D. (2009). T cell receptor-mediated activation of p38- α by mono-phosphorylation of the activation loop results in altered substrate specificity. *The Journal of Biological Chemistry*, 284(23), 15469–74.
- Mojtahedi, Z., Clos, J., & Kamali-sarvestani, E. (2008). *Leishmania major* : Identification of developmentally regulated proteins in procyclic and metacyclic promastigotes. *Experimental parasitology*, 119, 422–429.
- Morales, M. A., Pescher, P., & Spa, G. F. (2010). *Leishmania major* MPK7 Protein Kinase Activity Inhibits Intracellular Growth of the Pathogenic Amastigote Stage. *Eukaryotic Cell*, 9(1), 22–30.
- Morales, M. A., Renaud, O., Faigle, W., Shorte, S. L., & Spa, G. F. (2007). Over-expression of *Leishmania major* MAP kinases reveals stage-specific induction of phosphotransferase activity. *International Journal for Parasitology*, 37, 1187–1199.
- Munro, L. A. (2009). A study into the immune response induced by different *Leishmania mexicana* mutants. B.Sc Dissertation. SIPBS. University of Strathclyde.

- Murray, H. W., Berman, J. D., Davies, C. R., & Saravia, N. G. (2005). Advances in leishmaniasis. *The Lancet*, 366.
- Naula, C, Schuab, R., Leech, V., Melville, S., & Seebeck, T. (2001). Spontaneous dimerization and leucine-zipper induced activation of the recombinant catalytic domain of a new adenylyl cyclase of. *Molecular and Biochemical Parasitology*, 112, 19 – 28.
- Naula, Christina, Parsons, M., & Mottram, J. C. (2005). Protein kinases as drug targets in trypanosomes and *Leishmania*. *Infection*, 1754, 151 – 159.
- Nelson, K. G., Bishop, J. V, Ryan, R. O., & Titus, R. (2006). Nanodisk-Associated Amphotericin B Clears *Leishmania major* Cutaneous Infection in Susceptible BALB / c Mice. *Antimicrobial Agents and Chemotherapy*, 50(4), 1238–1244.
- Nett, I. R. E., Davidson, L., Lamont, D., & Ferguson, M. a J. (2009). Identification and specific localization of tyrosine-phosphorylated proteins in *Trypanosoma brucei*. *Eukaryotic Cell*, 8(4), 617–26.
- Nett, I. R. E., Martin, D. M. a, Miranda-Saavedra, D., Lamont, D., Barber, J. D., Mehlert, A., & Ferguson, M. a J. (2009a). The phosphoproteome of bloodstream form *Trypanosoma brucei*, causative agent of African sleeping sickness. *Molecular & cellular proteomics : MCP*, 8(7), 1527–38.
- Neuber, H. (2008). Leishmaniasis. *The Americas*, 754–765.
- Nolan, D. P., Revelard, P., & Pays, E. (1994). Overexpression and Characterization of a Gene for a Ca^{2+} -ATPase of the Endoplasmic Reticulum in *Trypanosoma brucei*. *The Journal of Biological Chemistry*, 269(42), 26045–26051.
- Nozaki, T., Toh-e A, Fujii, M., Yagisawa, H., Nakazawa, M., and Takeuchi, T. (1999) Cloning and characterization of a gene encoding phosphatidyl inositol-specific phospholipase C from *Trypanosoma cruzi*. *Mol. Biochem. Parasitol.* 102 (2): 283
- Ojo, K. K., Arakaki, T. L., Napuli, A. J., Inampudi, K. K., Keyloun, K. R., Zhang, L., Hol, W. G. J., et al. (2011). Structure determination of glycogen synthase kinase-3 from *Leishmania major* and comparative inhibitor structure-activity relationships with *Trypanosoma brucei* GSK-3. *Molecular and Biochemical Parasitology*, 176(2), 98–108.
- Ojo, K. K., Gillespie, J. R., Riechers, A. J., Napuli, A. J., Verlinde, C. L. M. J., Buckner, F. S., Gelb, M. H., et al. (2008). Glycogen synthase kinase 3 is a potential drug target for African trypanosomiasis therapy. *Antimicrobial Agents and Chemotherapy*, 52(10), 3710–7.
- Olivier, M., & Gregory, D. J. (2005). Subversion Mechanisms by Which *Leishmania* Parasites Can Escape the Host Immune Response: a Signalling Point of View. *Clinical Microbiology Reviews*, 18(2), 293–305.

- Parsons, M., & Ruben, L. (2000). Pathways Involved in Environmental Sensing in Trypanosomatids. *Parasitology*, *16*(2), 449–454.
- Parsons, Marilyn, Worthey, E. A., Ward, P. N., & Mottram, J. C. (2005). Comparative analysis of the kinomes of three pathogenic trypanosomatids: *Leishmania major*, *Trypanosoma brucei* and *Trypanosoma cruzi*. *BMC Genomics*, *19*, 1–19.
- Pavli, A., & Maltezou, H. C. (2010). International Journal of Infectious Diseases Leishmaniasis, an emerging infection in travellers. *International Journal of Infectious Diseases*, *14*(12), e1032–e1039.
- Peacock, C. S., Seeger, K., Harris, D., Murphy, L., Ruiz, J. C., Quail, M. a, Peters, N., et al. (2007). Comparative genomic analysis of three *Leishmania* species that cause diverse human disease. *Nature genetics*, *39*(7), 839–47.
- Pearson, G., Robinson, F., Gibson, T. B., Xu, B., Karandikar, M., Berman, K., & Cobb, M. H. (2001). Mitogen-Activated Protein (MAP) Kinase Pathways: Regulation and Physiological Functions. *Endocrine Reviews*, *22*(2), 153–183.
- Perdiz, D., Mackeh, R., Poüs, C., & Baillet, A. (2011). The ins and outs of tubulin acetylation: more than just a post-translational modification? *Cellular Signalling*, *23*(5), 763–71.
- Pfannenschmid, F. (2003). *Chlamydomonas* DIP13 and human NA14: a new class of proteins associated with microtubule structures is involved in cell division. *Journal of Cell Science*, *116*(8), 1449–1462.
- Phukan, S., Babu, V. S., Kannoji, a, Hariharan, R., & Balaji, V. N. (2010). GSK3beta: role in therapeutic landscape and development of modulators. *British Journal of Pharmacology*, *160*(1), 1–19.
- Price, H. P., Hodgkinson, M. R., Curwen, R. S., MacLean, L. M., Brannigan, J. a, Carrington, M., Smith, B. a, et al. (2012). The orthologue of Sjögren’s syndrome nuclear autoantigen 1 (SSNA1) in *Trypanosoma brucei* is an immunogenic self-assembling molecule. *PloS one*, *7*(2), e31842.
- Robinson, D. R., Sherwin, T., Ploubidou, a, Byard, E. H., & Gull, K. (1995). Microtubule polarity and dynamics in the control of organelle positioning, segregation, and cytokinesis in the *trypanosome* cell cycle. *The Journal of cell biology*, *128*(6), 1163–72.
- Rogers, M. E., Ilg, T., Nikolaev, A. V, Ferguson, M. A. J., & Paul, A. (2004). Transmission of cutaneous leishmaniasis by sand flies is enhanced by regurgitation of fPPG. *Nature*, *430*(6998), 463–467.
- Rose, K., Curtis, J., Baldwin, T., Mathis, A., Kumar, B., Sakhianandeswaren, A., Spurck, T., et al. (2004). Cutaneous leishmaniasis in red kangaroos: isolation and

- characterisation of the causative organisms. *International Journal for Parasitology*, 34, 655–664.
- Rosenqvist, H. (2011) *Leishmania mexicana* phosphoproteomics. PhD Thesis. SIPBS. University of Strathclyde.
- Roskoski Jnr, R. (2012). ERK1 / 2 MAP kinases : Structure, function , and regulation. *Pharmacological Research*, 66(2), 105–143.
- Rotureau, B., Morales, M. A., Bastin, P., & Späth, G. F. (2009). Microreview: The flagellum – mitogen-activated protein kinase connection in Trypanosomatids: a key sensory role in parasite signalling and development? *Cellular Microbiology*, 11, 710–718.
- Rulz-Albusac, J. M., Velazquez, E., & Montes, A. (1988). Differential Precipitation of Isolated Human Plasma Lipoproteins with Heparin and Manganese Chloride. *Clinical Chemistry*, 34(2), 240–243.
- Sádlová, J., & Volf, P. (2009). Peritrophic matrix of *Phlebotomus duboscqi* and its kinetics during *Leishmania major* development. *Cell and Tissue Research*, 337, 313–325.
- Salman, S. M., Rubeiz, N. G., & Kibbi, A. G. (1999). Cutaneous leishmaniasis: clinical features and diagnosis. *Clinical Dermatology*, 17(3), 291–296.
- Sarkar, A., Aga, E., Bussmeyer, U., Bhattacharyya, A., Möller, S., Hellberg, L., Behnen, M., et al. (2012). Infection of neutrophil granulocytes with *Leishmania major* activates ERK 1 / 2 and modulates multiple apoptotic pathways to inhibit apoptosis. *Medical Microbiology and Immunology*.
- Sayas, C. L., Ariaens, A., Ponsioen, B., & Moolenaar, W. H. (2006). GSK-3 Is Activated by the Tyrosine Kinase Pyk2 during LPA 1 -mediated Neurite Retraction. *Molecular Biology of the Cell*, 17, 1834–1844.
- Schoppmeier, J., Mages, W., & Lechtreck, K.-F. (2005). GFP as a tool for the analysis of proteins in the flagellar basal apparatus of *Chlamydomonas*. *Cell Motility and the Cytoskeleton*, 61(4), 189–200.
- Seebeck, T., Gong, K., Kunz, S., Schaub, R., Shalaby, T., & Zoraghi, R. (2001). cAMP signalling in *Trypanosoma brucei*. *International Journal for Parasitology*, 31, 491–498.
- Sen, R., Bauri, A. K., Chattopadhyay, S., & Chatterjee, M. (2007). Antipromastigote Activity of the Malabaricones of *Myristica malabarica* (*Rampatri*). *Phytotherapy Research*, 21, 592–595.

- Sen, R., & Chatterjee, M. (2011). Plant derived therapeutics for the treatment of Leishmaniasis. *Phytomedicine: International Journal of Phytotherapy and Phytopharmacology*, 18(12), 1056–69.
- Shio, M. T., Hassani, K., Isnard, A., Ralph, B., Contreras, I., Gomez, M. A., Abudayyeh, I., et al. (2012). Host Cell Signalling and *Leishmania* Mechanisms of Evasion. *Journal of Tropical Medicine*, 2012.
- Shiu, S., Karlowski, W. M., Pan, R., Tzeng, Y., Mayer, K. F. X., & Li, W. (2004). Comparative Analysis of the Receptor-Like Kinase Family in Arabidopsis and Rice. *The Plant Cell*, 16, 1220–1234.
- Singh, N., Kumar, M., & Singh, R. K. (2012). Leishmaniasis: Current status of available drugs and new potential drug targets. *Asian Pacific Journal of Tropical Medicine*, 5(6), 485–497.
- Solbach, W., & Laskay, T. (2000). The host response to *Leishmania* infection. *Advances in Immunology*, 74.
- Terpe, K. (2003). Overview of tag protein fusions: from molecular and biochemical fundamentals to commercial systems. *Applied Microbiology and Biotechnology*, 60(5), 523–33.
- Tian, G., Kane, L. S., Holmes, W. D., & Davis, S. T. (2002). Modulation of cyclin-dependent kinase 4 by binding of magnesium (II) and manganese (II). *Biophysical Chemistry*, 95(1), 79–90.
- Tiuman, T. S., Santos, A. O., Dias, B. P., & Nakamura, C. V. (2011). Recent advances in leishmaniasis treatment. *International Journal of Infectious Disease*, 15, 525–532.
- Tsigankov, P., Gherardini, P. F., Helmer-Citterich, M., Späth, G. F., & Zilberstein, D. (2013). Phosphoproteomic analysis of differentiating *Leishmania* parasites reveals a unique stage-specific phosphorylation motif. *Journal of Proteome Research*, 12(7), 3405–12.
- Wang, H., Brown, J., & Martin, M. (2011). Glycogen synthase kinase 3: a point of convergence for the host inflammatory response. *Cytokine*, 53(2), 130–40.
- Wheeler, R. J., Gluenz, E., & Gull, K. (2011). The cell cycle of *Leishmania*: morphogenetic events and their implications for parasite biology. *Molecular Microbiology*, 79, 647–662.
- Wiese, M. (1998). A mitogen-activated protein (MAP) kinase homologue of *Leishmania mexicana* is essential for parasite survival in the infected host. *The EMBO journal*, 17(9), 2619–2628.

- Wiese, M. (2007). *Leishmania* MAP kinases--familiar proteins in an unusual context. *International Journal for Parasitology*, 37(10), 1053–62.
- Wiese, M., Wang, Q., & Go, I. (2003). Identification of mitogen-activated protein kinase homologues from *Leishmania mexicana*. *International Journal for Parasitology*, 33, 1577–1587.
- Weise, F., Stierhof, Y. D., Kühn, C., Wiese, M., & Overath, P. (2000). Distribution of GPI-anchored proteins in the protozoan parasite *Leishmania*, based on an improved ultrastructural description using high-pressure frozen cells. *Journal of cell science*, 113, 4587–603.
- Wu, L., & Russell, P. (1993). Nim1 kinase promotes mitosis by inactivating Wee1 tyrosine kinase. *Nature*, 363(6431), 738–41.
- Xingi, E., Smirlis, D., Myrianthopoulos, V., Magiatis, P., Grant, K. M., Meijer, L., Mikros, E., et al. (2009). 6-Br-5methylindirubin-3'oxime (5-Me-6-BIO) targeting the leishmanial glycogen synthase kinase-3 (GSK-3) short form affects cell-cycle progression and induces apoptosis-like death: exploitation of GSK-3 for treating leishmaniasis. *International Journal for Parasitology*, 39(12), 1289–303.
- Zhou, C., Yang, Y., & Jong, A. Y. (1990). Mini-prep in ten minutes. *BioTechniques*, 8(2), 172-3.
- Zilberstein, D., Blumenfeld, N., Liveanu, V., Gepstein, A., & Jaffe, C. L. (1991). Growth at acidic pH induces an amastigote stage-specific protein in *Leishmania* promastigotes. *Molecular and Biochemical Parasitology*, 45(1), 175–8.

8. Appendix

8.1 LmxMPK2

8.1.1 Genetic sequence of *LmxMPK2* (Genbank: CAC07956) (Acc no: LmxM.36.0720)

ATGTCGGCCGAAATCGAGTCGCATATTCTGAAGAAGTATGAGATTCAAACACAGCTAGGC
 CAGGGTGCCTACGGCATTGTGTGGCGGCCCTGGAGCGCAAGCACAAACCGCGTTCGTTGCCG
 CTCAAGAAAATTTACGATGCCTTCCAAAACCTCGACCGATGCGCAGCGCACCTTCCGCGAG
 ATCATGTTTCTGCACCGGCTGCACCACCCGAACATCATCCGGCTGCTGCATGTCCATCGC
 GCCTTCAACGATCGCGACATATACTGGTCTTTCGAATACATGGAGACCGACCTTCATGTG
 GTGATTAGGGCAAATATCTTGGAGGGAATCCACAAACAGTTTATCATTACCAGTTGCTC
 AAGACGATGAAGTTTCTGCATTCTGCCGAGATTCTTACCCTGACATGAAGCCAAGCAAT
 CTGCTCGTAAACAGCGACTGCACGATGAAGGTGGCTGACTTCGGTCTCGCGCGCTCTATC
 CTGTCCCTTGAGGGCGAGCAGGCGTCGCGGCCGGTGTAAACGGACTACATTGGCAGACGG
 TGGTACCGCCCCGCCGAGATTTTGTCTCGGCTCGACACGATACACTAAGGGCGTGGATATG
 TGGTCAGTGGGCTGCATTCTTGGAGAGTTGATGCTGGGCAAGCCCATGTTTCCCGGCCGC
 TCCACCACGAACCAGCTGGAGCTGATTTGCAGCGTGACGGGCATGCCCTCCGCGGCGGAT
 GTGGCAGCCACCAACTCGCAGTTCGCCAACGCGATGCTTCGCGACATTCACTGCGCACAC
 CGACGCACGTTTCGCTGAGCTGCTGCCAAGCGCTTCCGCGGATGCGCTGAACCTAATTGAG
 CGCCTTATGTGTTTCAACCCAAACCGTCGCTTGTCTGCCGCGAGGCTCTGGAACACCCC
 TACGTCGCTGCCTTTTACCCTCTGACGACGAACCGGTGGCACCCGAACCCATCACCGTT
 TCTCTCCCTGACAGCCAGCGTTTGCCTTGGCCAAGTACAGAGACGCCATCTACGAGCAA
 ATCGCCTCGCTGCGCCGTATCTCCACATCCACCGATCATCGGCATCGCGCGGAGCGACAT
 GGGCCCGGGCCACCGCTAGCCGCAAGACGTCCGCCAGCGGGCGGGAGGCGCTGCTGGC
 GGCTCTCGAGGTGGCACCGGGACATCTGGGGCCACGCGACCCGCCACGAGCTGCAGCAGC
 AGCACCGCCGCACGGGCGGCTCCGACGCGCAGTGTGTAAAGCCCACCTCGACTAGTGGAG
 GTCAACGAATCATCATCTTCAAGGCGTACGGGCGTCCCGGCTTCCGCTCGGTAGCGTCT
 ACCAGCTCTGGTCTGGAAAGCAGACCCGTCGAGCGTGAGGCAGCGGTGCGCAAATGA

Sequence length: 1377 bp

8.1.2 Amino acid sequence LmxMPK2

MSAEIESHILKKYEIQTLGQGAYGIVWRALERKHNRVVALKKIYDAFQNSTDAQRTFRE
 IMFLHRLHHPNIIRLLHVHRAFNDRIYLVFEYMETDLHVVIRANILEGIHKQFIYQLL
 KTMKFLHSAEILHRDMKPSNLLVNSDCTMKVADDFGLARSILSLEGEQASRPVLTDIATR
 WYRPEIILLGSTRYTKGVDMWSVGCILGELMLGKPMFPGRSTTNQLELICSVTGMPAAD
 VAATNSQFANAMLRDIHCAHRRTFAELLPSASADALNLIERLMCFNPNRRLSAAEALHP
 YVAAFHRPDDEPVAPEPITVSLPDSQRLPLAKYRDAIYEQIASLRRISTSTDHRHRAERH
 GAGGTASRKTSASGGGAAGGSRGGTGTSGATRPATSCSSSTAARAAPQRSVVKPTSTSG
 VNESSSKAYGRPGFRSVASTSSGLESRPVEREA AVRK

Sequence length: 458 aa

MW: 52 kDa

pI: 9.92

8.2 LmxDIP13

8.2.1 Genetic sequence of *LmxDIP13* (Acc No: LmxM.33.4540)

ATGGCTGCGCTCGGGTCCGATGTGCAGGCCACCAGTGTGCGAGCTGGTGTCTGTGATTGAG
 AAAATGAAGGAGCGCAAGACGTTGCTTGAAGAGCAAATCTCTGCCGAGGAGACTGAGTAC
 GAGGGTGTGCTAGCCGAAGTGCGGGCTATGCAGGAGCGACTTGCCGCCCTGAAGGACAGT
 CTCGCGAAGAAGCAGGCGGTGCGAGCGGACTTGGAGCGAACCATATCGGAGACGTACTCG
 GCGTTCAAGAGTATCCTAGACGCCTCCAAGAAGCTACTCTCCACCGCCAAGGAAGAGTCA
 TCGGCGCTCAAGGCGCAGATAAACTGA

Sequence length: 327 bp

8.2.2 Amino acid sequence of LmxDIP13

MAALGSDVQATSVELVSVIEKMKERKTLLEEQISAEETEYEGVLAEVRAMQERLAALKDS
 LAKKQAVRADLERTISETYSAFKSI LDASKKLLSTAKEESSALKAQIN

Sequence Length: 108 aa

MW: 11.8 kDa

pI: 4.8

8.3 LmxGSK3-β

8.3.1 Genetic sequence of *LmxGSK3-β* (Acc No: LmxM.18.0270)

ATGTGCGCTCAACGCTGCCGATGCTGCGGACGAGCGAAGTCGCAAGGAGATGGACCGGTTCC
 CTGGTGGAAACGCATGGCTGGGCAGGGTACATTCGGCACTGTGCAACTGGGGAAGGAGAAG
 TCCACAGGCATGAGCGTGGCGATCAAGAAGGTTATCCAAGACCCGCGCTTCCGCAACCGC
 GAGCTGCAGATCATGCAGGACCTTGCCGTGCTGCACCACCCCAACATCGTGCAGCTCCAG
 AGTACTTCTACACCCTGGGTGAGCGCGACCCGCCGACATCTACCTCAATGTCTGTGATG
 GAGTACGTGCCGGATACGCTGCACCGCTGCTGCCGCAACTACTACCGCCGTC AAGTGGCG
 CCACCGCCGATCCTGATCAAGGTCTTTCTTTTTTCAGCTGATCCGAAGTATCGGGTGTCTTG
 CACCTGCCCTCCGTAAACGTGTGCCACCGCGACATCAAGCCACACAACGTGCTCGTCAAC
 GAGGCGGAAGGCACCCTGAAGCTGTGCGATTTTGGCAGTGCGAAGAAACTCTCGCCGTCC
 GAGCCAAACGTGGCATAACATCTGCTCTCGTTACTACCGCGCCCCTGAGCTCATCTTTGGT
 AACCAGCATTACACGACCTCGGTGACATCTGGTCGGTGGGGTGTATCTTCGCTGAGATG
 ATGCTTGGCGAGCCCATCTTCCGCGGCGATAACAGCGCCGGCCAGCTGCACGAAATTGTG
 CGCGTGTCTCGGCTGCCCTCGCGGAGGTGCTGCGTAAGCTGAATCCGTCGCACACGGAC
 GTGGATCTGTACAATAGCAAGGGCATCCCGTGGAGCACCGTTTTCTGTGACCACTCACTG
 AAGGACGCCAAGGAGGCGTACGATCTTCTTAGTGCCCTGCTGCAGTACTTGCCGGAGGAT
 CGCATGAAGCCTTACGAAGCACTGTGCCACCCGTACTTTGACGAGCTTCACGACTCCGCC
 ACGAAACTGCCGAATCACAAGAATCTCCCGGAAGACCTCTTTGCTTCTTGCCGAGCGAG
 ATTGAGGTGATGAGCGAAGCGCAGAAGGCCAAGCTGGTTCGCAAGTAA

Sequence length: 1068 bp

8.3.2 Amino acid sequence of LmxGSK3- β

MSLNAADAADERSRKEMDRFLVERMAGQGTFGTVQLGKEKSTGMSVAIKKVIQDPRFRNR
 ELQIMQDLAVLHHPNIVQLQSYFYTLGERDRRDIYLNVMVEYVPTLHRCRNYYRRQVA
 PPPILIKVFLFQLIRSIGCLHLPVNVCHRDIKPHNVLVNEAEGTLKLCDFGSAKKLSPS
 EPNVAYICSRYYRAPELIFGNQHYTTSDVIWSVGCIFAEMMLGEPIFRGDNSAGQLHEIV
 RVLGCPSREVLRLKLNPSHTDVDLYNSKGI PWSTVFCDHSLKDAKEAYDLLSALLQYLPED
 RMKPYEALCHPYFDELHDSATKLPNHKNLPEDLFRFLPSEIEVMSEAQKAKLVRK

Sequence length: 355 aa

MW: 40.7 kDa

pI: 7.75

8.4 Phosphatases

8.4.1 Genetic sequence of PTP1B (Acc no. M33689)

ATGGAGATGGAAAAGGAGTTCGAGCAGATCGACAAGTCCGGGAGCTGGGCGGCCATTTACC
 AGGATATCCGACATGAAGCCAGTGACTTCCCATGTAGAGTGGCCAAGCTTCCTAAGAACAA
 AAACCGAAATAGGTACAGAGACGTCAGTCCCTTTGACCATAGTTCGGATTAAGTACATCAA
 GAAGATAATGACTATATCAACGCTAGTTTTGATAAAAAATGGAAGAAGCCCAAAGGAGTTACA
 TTCTTACCCAGGGCCCTTTGCCTAACACATGCGGTCACTTTTGGGAGATGGTGTGGGAGCA
 GAAAAGCAGGGGTGTCGTCATGCTCAACAGAGTGATGGAGAAAGGTTTCGTTAAAAATGCGCA
 CAATACTGGCCACAAAAAGAAGAAAAAGAGATGATCTTTGAAGACACAAAATTTGAAATTAA
 CATTGATCTCTGAAGATATCAAGTCATATTATACAGTGCACAGCTAGAATTTGGAAAACCT
 TACAACCCAAGAAACTCGAGAGATCTTACATTTCCACTATACCACATGGCCTGACTTTGGA
 GTCCCTGAATCACCAGCCTCATTCTTGAACCTTTCTTTTCAAAGTCCGAGAGTCAGGGTCAC
 TCAGCCCGGAGCACGGGCCCCGTTGTGGTGCAGTGCAGGCATCGGCAGGTCTGGAAC
 CTTCTGTCTGGCTGATACCTGCCTCTTGCTGATGGACAAGAGGAAAAGACCCCTTCTCCGTT
 GATATCAAGAAAGTGCTGTTAGAAATGAGGAAGTTTCGGATGGGGCTGATCCAGACAGCCG
 ACCAGCTGCGCTTCTCCTACCTGGCTGTGATCGAAGGTGCCAAATTCATCATGGGGGACTC
 TTCCGTGCAGGATCAGTGGAAGGAGCTTTCCACGAGGACCTGGAGCCCCACCCGAGCAT
 ATCCCCCACCTCCCCGGCCACCCAAACGAATCCTGGAGCCACACAATGGGAAATGCAGGG
 AGTTCTTCCCAAATCACCAGTGGGTGAAGGAAGAGACCCAGGAGGATAAAGACTGCCCCAT
 CAAGGAAGAAAAAGGAAGCCCCTTAAATGCCGCACCCTACGGCATCGAAAGCATGAGTCAA
 GACACTGAAGTTAGAAGTCGGGTGCTGGGGGGAAGTCTTCGAGGTGCCAGGCTGCCCTCCC
 CAGCCAAAGGGGAGCCGTCACTGCCCGAGAAGGACGAGGACCATGCACTGAGTTACTGGAA
 GCCCTTCTGGTCAACATGTGCGTGGCTACGGTCTCACGGCCGGCGCTTACCTCTGCTAC
 AGGTTCTGTTCAACAGCAACACATAG

Sequence length: 1308 aa

8.4.2 Amino acid sequence of PTP1B

MEMEKEFEQIDKSGSWAAIYQDIRHEASDFPCRVAKLPKNKNRNRVYRDVSPFDHSRIKLH
 QEDNDYINASLIKMEEAQRSYILTQGPLPNTCGHFWEMVWEQKSRGVVMLNRVMEKGLK
 CAQYWPQKEEKEMIFEDTNLKLTLISEDIKSYYTVRQLELENLTTQETREILHFHYTTWP
 DFGVPESPASFLNFLFKVRESGSLSPHEGPPVVVHCSAGIGRSGTFCLADTCLLLMDKRKD
 PSSVDIKKVLLEMRKFRMGLIQTADQLRFSYLAVIEGAKFIMGDSSVQDQWKELSHEDLE
 PPPEHI PPPRPPKRILEPHNGKCREFFPNHQWVKEETQEDKDCPIKEEKGSPLNAAAPYG
 IESMSQDTEVRSRVVGGSLRGAQAASPAKGEPSLPEKDEDHALSYWKPFVNMCVATVLT
 AGAYLCYRFLFNSNT

Sequence length: 435 aa

MW: 49.9 kDa

pI: 5.88

8.4.3 Genetic sequence of λ -phosphatase (Acc No: J02459, ORF: 43224-43889 bp)

ATGCGCTATTACGAAAAAATTGATGGCAGCAAATACCGAAAATATTTGGGTAGTTGGCGATC
 TGCACGGATGCTACACGAACCTGATGAACAAACTGGATACGATTGGATTCGACAACAAAAA
 AGACCTGCTTATCTCGGTGGGCGATTTGGTTGATCGTGGTGCAGAGAACGTTGAATGCCTG
 GAATTAATCACATTCCCCTGGTTCAGAGCTGTACGTGGAAACCATGAGCAAATGATGATTG
 ATGGCTTATCAGAGCGTGGAAACGTTAATCACTGGCTGCTTAATGGCGGTGGCTGGTTCTT
 TAATCTCGATTACGACAAAAGAAATTCTGGCTAAAGCTCTTGCCATAAAGCAGATGAACCT
 CCGTTAATCATCGAACTGGTGAGCAAAGATAAAAAATATGTTATCTGCCACGCCGATTATC
 CCTTTGACGAATACGAGTTTGGAAAGCCAGTTGATCATCAGCAGGTAATCTGGAAACCGCGA
 ACGAATCAGCAACTCACAAAACGGGATCGTGAAAGAAATCAAAGGCGCGGACACGTTTCATC
 TTTGGTCATACGCCAGCAGTGAAACCACTCAAGTTTGCCAACCAAATGTATATCGATACCG
 GCGCAGTGTTCTGCGGAAACCTAACATTGATTTCAGGTACAGGGAGAAGGCGCATGA

Sequence length: 666 aa

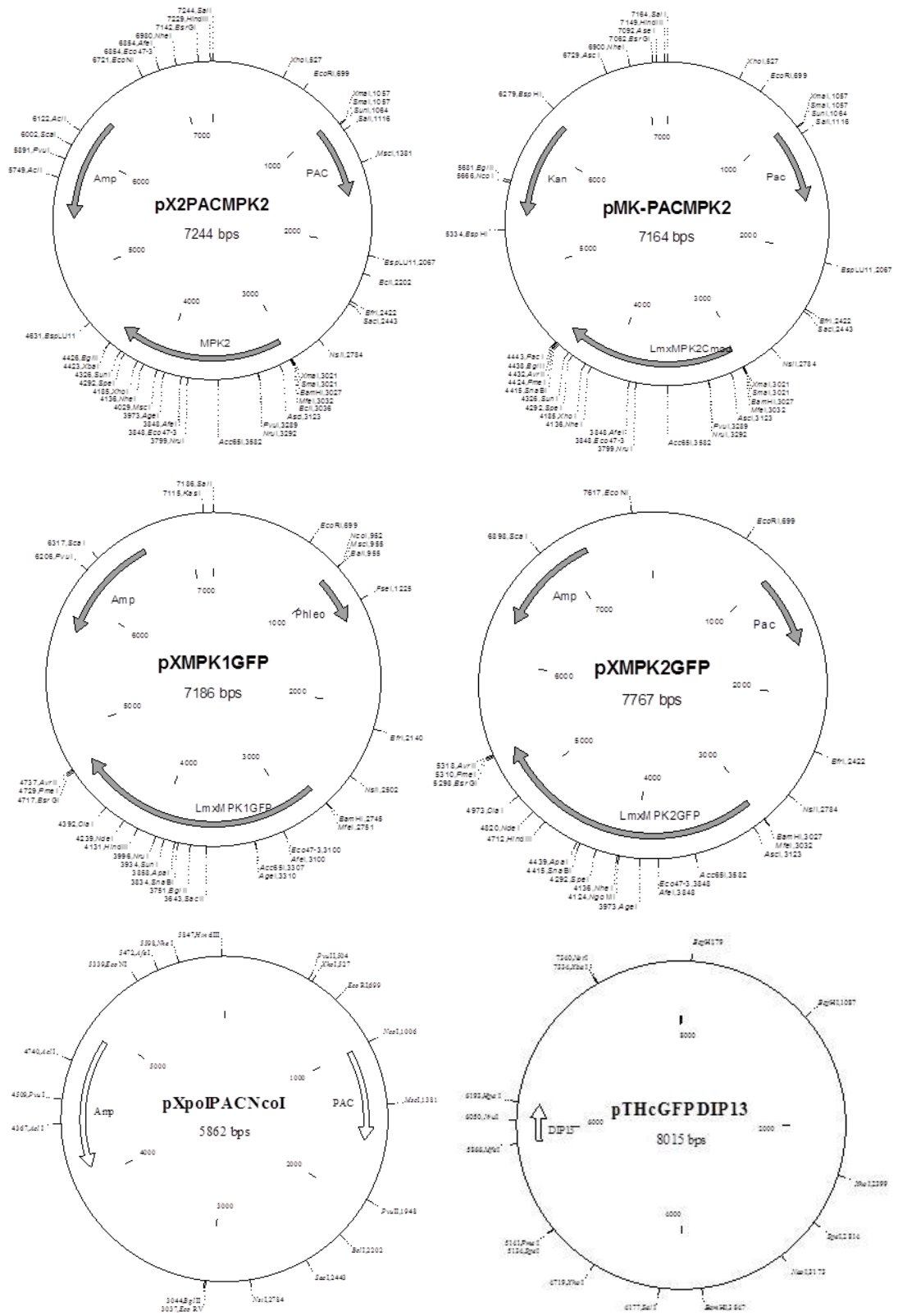
8.4.4 Amino acid sequence of λ -phosphatase

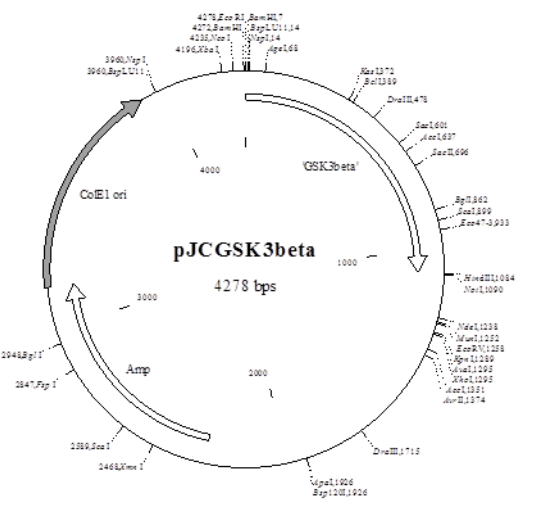
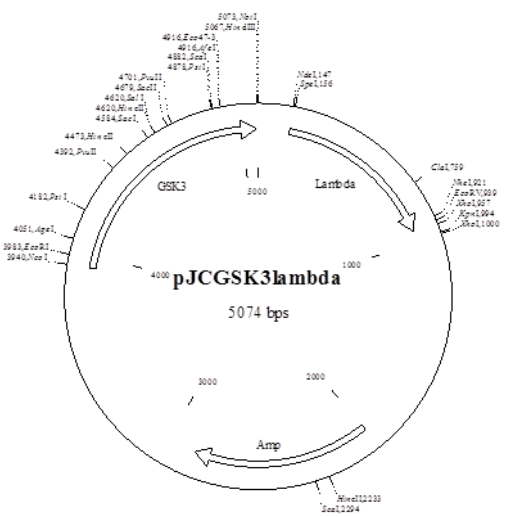
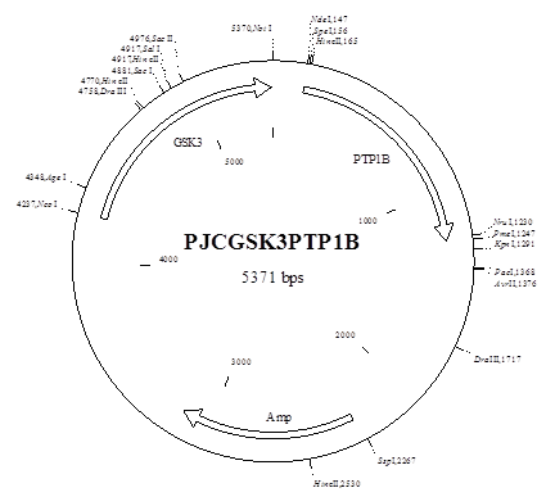
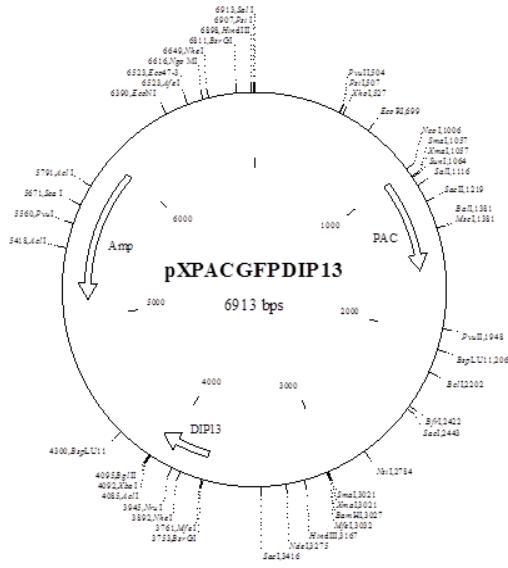
MRYYEKIDGSKYRNIWVVGDLHGCTNLMNKLDITIGFDNKKDLLISVGDIVDRGAENVEC
 LELITFPWFRAVRGNHEQMMIDGLSERGNVNHLLNNGGWFFNLDYDKEILAKALAHKAD
 ELPLIIELVSKDKKYVICHADYPFDEYEFGKPVVDHQQVIWNRERISNSQNGIVKEIKGAD
 TFIIFGHTPAVKPLKFANQMYIDTGAVFCGNLTLIQVQGEA

Sequence length: 221 aa

MW: 25.2 kDa

pI: 5.49





Acknowledgments

First and foremost, I would like to thank my supervisor Dr Martin Wiese not only for giving me the opportunity to carry out my PhD but also for your support, guidance, and patience throughout the project. They were invaluable to the success of this PhD. Thanks to the Deutsche Forschungsgemeinschaft (DFG - WI2044/5-1) and the Strathclyde Institute of Pharmacy and Biomedical Sciences for funding this project.

I would also like to thank Dr Chris Carter for teaching me mammalian cell harvest, culture and infection which were essential for the drug screening aspect of this work. Thanks to Dr John Igoli and Professor Alexander Gray for purification of the Malabaricones. A note of thanks is due to Dr Roderick Williams for generation of the luminescent parasites used in the screening project. Also, thanks to Thomas, Lucy and Simon for help with some experiments. A special thank you is due to Louise Young for all her help with the LmxGSK3- β screening work, as well as some good chats along the way.

I was extremely fortunate to have the company of Patrick McAleer for the first two years of my PhD. We have had some great times and he managed to keep up with my occasionally round about thoughts. Thanks for proofreading this! Thanks also to Heidi Rosenqvist, Simona John von Freyend and Nadja Bleicher who provided helpful tips and insight and some excellent discussions (even if we did not work together long – or at all!).

For my final year, I was grateful to have the company of Stubear (Stuart Woods) who provided me with gossip by the proverbial water cooler and Shaw (Craig Shaw) who helped me decipher notes taken while learning from Chris; you both kept me sane! Jana Hiltner my office buddy also provided excellent early morning chats – always a good way to start the day. A mention also goes to past and present members of Lab 253/HW601 who I shared the daily highs and lows of a PhD with. In particular, I would like to thank Bharath, Sara, Caroline, Chris, Anto, Selina, Adrienne, Gayle, Jenny, Lewis, Richard and Flo. You have all made the last three years more enjoyable.

Last but not least, I would like to thank my family for their support and encouragement over the past three years. I couldn't have done it without you! To my older sister Lynn: this concludes the race.